

Distribution Agreement

In presenting this thesis or dissertation as a partial fulfillment of the requirements for an advanced degree from Emory University, I hereby grant to Emory University and its agents the non-exclusive license to archive, make accessible, and display my thesis or dissertation in whole or in part in all forms of media, now or hereafter known, including display on the world wide web. I understand that I may select some access restrictions as part of the online submission of this thesis or dissertation. I retain all ownership rights to the copyright of the thesis or dissertation. I also retain the right to use in future works (such as articles or books) all or part of this thesis or dissertation.

Signature:

Weiwei Guo

Date

**Polyoxometalate-based Catalysts for Toxic Compound
Decontamination and Solar Energy Conversion**

By

Weiwei Guo
Doctor of Philosophy

Chemistry

Craig L. Hill, Ph.D.
Advisor

Tianquan Lian, Ph.D.
Committee Member

Chris Scarborough, Ph.D.
Committee Member

Accepted:

Lisa A. Tedesco, Ph.D.
Dean of the James T. Laney School of Graduate Studies

Date

**Polyoxometalate-based Catalysts for Toxic Compound
Decontamination and Solar Energy Conversion**

By

Weiwei Guo
B.S. University of Science and Technology of China, 2011

Advisor: Craig L. Hill

An Abstract of
A dissertation submitted to the Faculty of the James T. Laney School of
Graduate Studies of Emory University in partial fulfillment of the
requirements for the degree of
Doctor of Philosophy in Chemistry

2016

Abstract

Polyoxometalate-based Catalysts for Toxic Compound Decontamination and Solar Energy Conversion

By Weiwei Guo

Polyoxometalates (POMs) have been attracting interest from researchers in the fields of Inorganic Chemistry, Physical Chemistry, Biomolecular Chemistry, etc. Their unique structures and properties render them versatile and facilitate applications in medicine, magnetism, electrochemistry, photochemistry and catalysis. In particular, toxic compound (chemical warfare agents (CWAs) and toxic industrial compounds (TICs)) decontamination and solar energy conversion by POM-based materials have becoming promising and important research areas that deserve much attention. The focus of this thesis is to explore the structural features of POMs, to develop POM-based materials and to investigate their applications in toxic compound decontamination and solar energy conversion.

The first part of this thesis gives a general introduction on the history, structures, properties and applications of POMs. The second part reports the synthesis, structures, and reactivity of different types of POMs in the destruction of TICs and CWAs. Three tetra-*n*-butylammonium (TBA) salts of polyvanadotungstates, [*n*-Bu₄N]₆[PW₉V₃O₄₀] (**PW₉V₃**), [*n*-Bu₄N]₅H₂PW₈V₄O₄₀ (**PW₈V₄**), [*n*-Bu₄N]₄H₅PW₆V₆O₄₀·20H₂O (**PW₆V₆**) are discussed in detail. These vanadium-substituted Keggin type POMs show effective activity for the aerobic oxidation of formaldehyde (a major TIC and human-environment carcinogen) to formic acid under ambient conditions. Moreover, two types of POMs have also been developed for the removal of CWAs and/or their simulants. Specifically, a layered manganese(IV)-containing heteropolyvanadate with a 1:14 Stoichiometry, K₄Li₂[MnV₁₄O₄₀]·21H₂O has been prepared. Its catalytic activity for oxidative removal of 2-chloroethyl ethyl sulfide (a mustard simulant) is discussed. The second type of POM developed for decontamination of CWAs and their simulants is the new one-dimensional polymeric polyniobate (P-PONb), K₁₂[Ti₂O₂][GeNb₁₂O₄₀]·19H₂O (**KGeNb**). The complex has been applied to the decontamination of a wide range of CWAs and their simulants under mild conditions and in the dark. The third part of this dissertation addresses the use of POM-based materials in photocatalytic hydrogen evolution reactions. The structures, characterizations and catalytic hydrogen generation activities of a new tri-nickel-containing Wells-Dawson POM, [Ni₃(OH)₃(H₂O)₃P₂W₁₆O₅₉]⁹⁻ and a new hybrid material that combines POMs, Pt nanoparticles (NPs) and MOFs are investigated.

**Polyoxometalate-based Catalysts for Toxic Compound
Decontamination and Solar Energy Conversion**

By

Weiwei Guo
B.S. University of Science and Technology of China, 2011

Advisor: Craig L. Hill

A dissertation submitted to the Faculty of the James T. Laney School of
Graduate Studies of Emory University in partial fulfillment of the
requirements for the degree of
Doctor of Philosophy in Chemistry

2016

Acknowledgement

During the past five years as a graduate student in the Department of Chemistry at Emory University, I learn not only to conduct research but also to enjoy every aspect of life. I am grateful to all who accompanied me and guided me over the years. First, I would like to thank my advisor, Dr. Craig Hill. I will never forget his patient guidance, unconditional support, constant encouragement and invaluable advice. He has taught me the crucial importance of thinking creatively and being careful in conducting research. He not only walked me through the difficulties in research but also the obstacles in life.

I want to thank my graduate research committee members, Dr. Tianquan Lian and Dr. Chris Scarborough. They gave precious advice, encouragement and continual support to my research and my career development. I also want to thank Dr. Cora MacBeth who interviewed me five years ago and gave me the opportunity to study at Emory.

I am very grateful to all of the previous and current Hill group members. I would like to thank Dr. Hongjin Lv for his instructive advice and suggestions on many of my research projects, Dr. Zhen Luo for his unconditional guidance, Dr. Yurii Geletii for his knowledgeable advice and critiques, Mr. Kevin Sullivan for his help in many measurements and experiments, Dr. Guibo Zhu who helped on my research and talked me through a lot of hard time in life, etc. My gratitude goes to every group member: Dr. Chongchao Zhao, Dr. James Vickers, Dr. Elliot Glass, Sarah Lauinger, Juncheng Yang, Mooeung Kim, Yimu Hu, Ben Yin, Daniel Collins-Wildman, Marika Wieliczko, Dr. Yingnan Chi, Dr. Yuanzhe Gao, Je Seong Lee, Rocky Li, Azam Aliakbari Sefiddarbuni and others I have known in the Hill group.

I would also like to thank Dr. Djamaladdin G. Musaev who is one of our computational collaborators, and my collaborators at Virginia Tech, Edgewood Chemical Biological Center, Brookhaven National Laboratory, etc.

I am thankful to Leslie Chauvin and Ann Dasher. Their strong organizational and consulting skills help me prepare all important paperwork and forms needed for research meetings as well as for graduation. I truly appreciate Dr. John Bacsá for his long time help and support on crystallographic measurements. My thanks also goes to Dr. Shaoxiong Wu and Dr. Bing Wang for their help in collecting NMR data. I am grateful to all of my colleagues and friends who helped me a lot when I lost all of my belongings during a fire.

Last but not least, I thank my parents, my sister, and my husband. My parents give me unconditional love and support the past 27 years. They encourage me to work hard and to see a different world on the other side of earth even though they really want me to accompany them. My sister, Wenwen Guo, is four years older than me, but she is more like a friend. My husband, Yueqin Zheng, would always love me and support me. I feel so blessed to be my parents' daughter, to be Wenwen's younger sister, and to be Yueqin's wife.

Table of Contents

Chapter 1 Introduction: Overview of the Structures, Properties and Applications of Polyoxometalates in Toxic Compound Decontamination and Solar Energy Conversion.....	1
1.1 General Structures of POMs	2
1.2 Catalytic Properties of POMs in Toxic Compound Decontamination.....	7
1.2.1 Air-based oxidation of organic compounds by POMs.....	7
1.2.2 The use of POMs in the decontamination of toxic compounds	9
1.3 The use of POMs in solar energy conversion	12
1.4 Goal of this work and outline	14
References	16
Chapter 2 Polyvanadotungstates for Aerobic Oxidation of Formaldehyde under ambient conditions.....	26
2.1 Introduction	27
2.2 Experimental	29
2.2.1 General Methods and Materials	29
2.2.2 Preparation of Catalysts	30
2.2.3 Preparation of $[n\text{-Bu}_4\text{N}]_5[\text{W}_3\text{V}_3\text{O}_{19}]$, $[n\text{-Bu}_4\text{N}]_3\text{H}_3\text{V}_{10}\text{O}_{28}$, $[n\text{-Bu}_4\text{N}]_7\text{SiW}_9\text{V}_3\text{O}_{40}$, $[n\text{-Bu}_4\text{N}]_9\text{P}_2\text{W}_{15}\text{V}_3\text{O}_{62}$, $[n\text{-Bu}_4\text{N}]_5\text{PW}_{11}\text{CoO}_{39}$ and $[n\text{-Bu}_4\text{N}]_4[\text{SiW}_{11}\text{Ce}^{\text{IV}}\text{O}_{39}]$	31
2.2.4 Preparation of Internal Standard Acetone-2,4-DNP-Hydrazone Solution.....	32
2.2.5 Catalytic Aerobic Oxidative Removal of Formaldehyde.....	32
2.3 Results and Discussion.....	33
2.3.1 Syntheses and characterization of catalysts	33
2.3.2 Catalytic Aerobic Oxidative Removal of Formaldehyde.....	38

2.3.3 Comparison of supported noble metal and POM catalysts for aerobic formaldehyde oxidation.	45
2.3.4 Catalyst stability and reusability.	48
2.4 Conclusions	50
References	51
Chapter 3 A Manganese(IV)-containing Heteropolyvanadate for Oxidative Removal of 2-Chloroethyl Ethyl Sulfide.	58
3.1 Introduction	59
3.2 Experimental	60
3.2.1 General Methods and Materials	60
3.2.2 Synthesis of $K_4Li_2[MnV_{14}O_{40}] \cdot 21H_2O$	61
3.2.3 X-ray Crystallography.....	61
3.2.4 Magnetochemical Characterization.....	64
3.2.5 Catalytic Oxidation of 2-Chloroethyl Ethyl Sulfide (CEES).....	64
3.3 Results and Discussion.....	64
3.3.1 Synthesis and Structure	64
3.3.2 Characterization.	67
3.3.3 Magnetic Properties.	69
3.3.4 Catalytic Properties.	72
3.4 Conclusions	74
References	75
Chapter 4 Heteropolyniobates for Liquid- and Gas-Phase Decontamination of Chemical Warfare Agents.....	79
4.1 Introduction	80
4.2 Experimental	81

4.2.1 General Methods and Materials	81
4.2.2 Synthesis of a new polymeric polyniobate, KGeNb	81
4.2.3 X-ray Crystallography.....	82
4.2.4 Degradation of DMMP by KSiNb and KGeNb	84
4.2.5 Degradation of DECP by KSiNb and KGeNb	84
4.2.6 Degradation of live agent (GD) by KSiNb	84
4.2.7 Gas Phase Adsorptive Degradation of Live Agents (GB and HD) on KSiNb and KGeNb	85
4.2.8 Computational Studies.	85
4.3 Results and Discussion.....	86
4.3.1 Synthesis and structure of KGeNb	86
4.3.2 Decontamination of chemical warfare agents and simulants by KGeNb	88
4.3.3 Computational studies.....	102
4.4 Conclusions	103
References.....	104
Chapter 5 Di- and Trinickel Polyoxometalates for Photocatalytic Hydrogen Evolution	109
5.1 Introduction	110
5.2 Experimental	112
5.2.1 General Methods and Materials	112
5.2.2 Synthesis of $\text{Na}_8\text{Li}_{12}[\text{Ni}_2(\text{P}_2\text{W}_{15}\text{O}_{56})_2] \cdot 74\text{H}_2\text{O}$	112
5.2.3 Synthesis of $\text{Na}_4\text{Li}_5[\text{Ni}_3(\text{OH})_3(\text{H}_2\text{O})_3\text{P}_2\text{W}_{16}\text{O}_{59}] \cdot 48\text{H}_2\text{O}$	113
5.2.4 Synthesis of TBANi_2 and TBANi_3	113
5.2.5 X-ray Crystallography.....	116
5.2.6 Photocatalytic experimental processes.....	116

5.3 Results and Discussion.....	117
5.3.1 Syntheses.....	117
5.3.2 Structures and Characterizations.....	118
5.3.3 Photocatalytic hydrogen evolution.....	125
5.3.4 Correlation between POM structure and hydrogen evolution activity.....	129
5.4 Conclusions	129
References	130
Chapter 6 A Hybrid Nanocomposite of Polyoxometalates, Pt Nanoparticles and Metal-Organic Frameworks for Synergistic Hydrogen Evolution.....	134
6.1 Introduction	135
6.2 Experimental	136
6.2.1 General Methods and Materials	136
6.2.2 Synthesis of NH ₂ -MIL-53.....	138
6.2.3 Synthesis of POM-Pt NPs@NH ₂ -MIL-53 (PNPMOF).....	138
6.2.4 Synthesis of POM-Pt NPs@NH ₂ -silica	138
6.2.5 Photocatalytic experimental processes.....	138
6.2.6 Recycle and Reuse	139
6.3 Results and Discussion.....	139
6.3.1 Synthesis and characterization of PNPMOF	139
6.3.2 Photocatalytic hydrogen evolution.....	147
6.4 Conclusions	156
References	156
Chapter 7 Conclusions and Future Outlook	163

List of Figures

- Figure 1-1.** X-ray crystal structures of representative plenary and lacunary polytungstates as well as the assembly of some TMSPs.4
- Figure 1-2.** (a) Polyhedral representation of the X-ray crystal structure of $[V_{10}O_{28}H_3]^{3-}$, (b) coordination of alkoxy group with hexavanadate in $[V_6^V O_{13}[(OCH_2)_3CH_3]_2]^{2-}$ and (c) coordination of alkoxy groups with hexavanadate in $[V_6^V V_5^{IV} O_7(OH)_3[(OCH_2)_3CH_3]_3]^-$ 5
- Figure 1-3.** X-ray crystal structures of (a) $[Nb_6O_{19}]^{8-}$, (b) $[H_2Si_4Nb_{16}O_{56}]^{14-}$, (c) $[PNb_{12}O_{40}(VO)_6]^{3-}$ and (d) $[Nb_{24}O_{72}H_9]^{15-}$ 7
- Figure 1-4.** Left: Polyhedral representation of $PMo_{10}V_2O_{40}^{5-}$. Right: The general two-step mechanism for POM-catalyzed O_2 -based oxidations of organic compounds.9
- Figure 1-5.** X-ray crystal structures of $[Cu_3(C_9H_3O_6)_2]_4 [\{ (CH_3)_4N \}_4 CuPW_{11}O_{39}H]$ and $H_3[(Cu_4Cl)_3(C_9H_3O_6)_8]_2[PW_{12}O_{40}]_3(C_4H_{12}N)_6 \cdot 3H_2O$. One of the large pores in MOFs containing the pink and purple Keggin-type POM is shown.11
- Figure 2-1.** Thermogravimetric analysis of (a) PW_9V_3 , (b) PW_8V_4 and (c) PW_6V_6 .34
- Figure 2-2.** Representative polyhedral representations of the vanadium-substituted Keggin-type polyvanadotungstates of (a) PW_9V_3 , (b) PW_8V_4 and (c) PW_6V_6 based on X-ray crystal structures of the parent Keggin POMs...35
- Figure 2-3.** ^{31}P NMR of (a) PW_9V_3 , (b) PW_8V_4 and (c) PW_6V_6 with respect to 85% H_3PO_4 (0 ppm)36
- Figure 2-4.** FT-IR spectra of PW_9V_3 , PW_8V_4 and PW_6V_6 37
- Figure 2-5.** Normalized UV-vis absorption spectra of PW_9V_3 , PW_8V_4 , and PW_6V_6 . Conditions: 0.5 mM in 100% acetonitrile.38

Figure 2-6. (a) Time profile of formaldehyde consumption catalyzed by PW₉V₃ , PW₈V₄ , PW₆V₆ and blank in DMA/H ₂ O (v/v = 20/1). (b) The formaldehyde DNP-hydrazone peaks as detected by GC at various time points over 120 h using PW₉V₃ as the catalyst in DMA/H ₂ O (v/v = 20/1).	42
Figure 2-7. (a) Initial rate of formaldehyde oxidation as a function of the initial reactant concentration ([PW₉V₃] = 3.8 mM); (b) initial rate of formaldehyde oxidation as a function of the initial catalyst (PW₉V₃) concentration ([CH₂O] = 0.52 M)	43
Figure 2-8. Time profile of formaldehyde consumption catalyzed by PW₉V₃ under 1 atm oxygen and under 1 atm of air in DMA/H ₂ O (v/v = 20/1) at ambient temperature	44
Figure 2-9. Time profile of formaldehyde consumption catalyzed by PW₉V₃ under 1 atm of air without additives, with addition of 0.6 mmol HCOOH and with addition of 1.0 μmol 4- <i>t</i> -butylcatechol; all reactions at ambient temperature	44
Figure 2-10. X-ray diffraction patterns of (a) TiO ₂ , (b) reduced Pt/TiO ₂ , (c) Au/TiO ₂	47
Figure 2-11. Oxidative removal of formaldehyde catalyzed by PW₉V₃ , PW₈V₄ , PW₆V₆ , reduced Pt/TiO ₂ and Au/TiO ₂ in the presence of water. Concentration of formaldehyde, [CH₂O] = 0.52 M, [catalyst] = 3.8 mM, 1 atm of air, 2 mL of solvent, 40 °C, 144 h.	48
Figure 2-12. FT-IR spectra of (a) PW₉V₃ , (b) PW₈V₄ and (c) PW₆V₆ before and after catalytic reactions	50

- Figure 3-1.** Combined polyhedral and ball-and-stick representations of **MnV₁₃** and the synthesis scheme for **1**. Red: VO₆; yellow: MnO₆; violet: potassium. .65
- Figure 3-2.** (a) Polyhedral and ball-and-stick representation of **MnV₁₄**. (b) Simplified representation of **MnV₁₄** showing a **jba1** topology with a total point symbol of {3¹⁰2{3¹⁴.4⁷}4{3¹⁸.4¹⁰}8{3⁴⁴.4⁴⁶.5}.....66
- Figure 3-3.** (a) Polyhedral and ball-and-stick representation of a portion of K₂[MnV₁₄O₄₀]⁴⁻ framework in the *ab*-plane. Each potassium ion bridges two **MnV₁₄** clusters. (b) Stacking of the two-dimensional layers of K₂[MnV₁₄O₄₀]⁴⁻ networks in the *ab*-plane. The figures on the right show the polyhedral representations.67
- Figure 3-4.** (a) FT-IR spectra of **1** and **K₇MnV₁₃**. (b) Diffuse reflectance spectrum of **1**.....68
- Figure 3-5.** Thermogravimetric analysis of **1**.....68
- Figure 3-6.** ⁵¹V NMR spectrum of **1** in D₂O. The integration of the peaks from left to right are: 219.33, 20.36, 10.53, 1.91, 1.00, 0.19, respectively, which gives the ratio as 1154:107:55:10:5:1.69
- Figure 3-7.** Magnetic susceptibility data of **1** (corrected for diamagnetic contributions only, with no TIP correction) depicted as the temperature dependence of $\chi_m T$ at 0.1 Tesla; inset: molar magnetization M_m vs. applied field B at 2 K.71
- Figure 3-8.** Magnetic susceptibility data of **1** (corrected for diamagnetic and TIP contributions and assuming 1.07 Mn(IV) or down to 1.00 Mn(IV) + 0.03 Mn(II) per formula unit) depicted as the temperature dependence of $\chi_m T$ at 0.1 Tesla; inset: molar magnetization M_m vs. applied field B at 2 K; open circles: data, black line: best fit.....72

Figure 3-9. Oxidative removal of CEES catalyzed by 1 and by K₇MnV₁₃	73
Figure 3-10. FT-IR spectra of 1 before and after catalytic CEES oxidation.	74
Figure 3-11. PXRD pattern of 1 before and after catalytic CEES oxidation.	74
Figure 4-1. (a) Polyhedral representation of the one-dimensional polyanion chain of KGeNb . (b) Precise structural environments of two potassium counter cations interacting with the polymeric polyanion unit (bond lengths in Å)	87
Figure 4-2. (a) Hydrolytic decomposition pathway of DMMP to MP. (b) DMMP decomposition using KGeNb and KSiNb ; conditions: [DMMP] = 15.5 mM, 18 μmol KGeNb or KSiNb , 0.5 mL D ₂ O and 1.0 mL H ₂ O at room temperature. (c) DECP decomposition using KGeNb and KSiNb ; conditions: [DECP] = 100 mM, 11 μmol KGeNb or KSiNb , 600 μL of DMF and 50μL of H ₂ O at room temperature. (d) Hydrolytic decomposition pathway of DECP to DEHP.	88
Figure 4-3. ³¹ P NMR spectra of (a) DMMP, (b) methyl phosphonic acid (MP) and (c) DMMP decomposition by KGeNb after 24 h in 0.5 mL D ₂ O and 1.0 mL H ₂ O.	89
Figure 4-4. Red circles: hydrolysis of DMMP using KGeNb . Conditions: [DMMP] = 15.5 mM, 18 μmol KGeNb , 0.5 mL D ₂ O and 1.0 mL H ₂ O at room temperature. Black squares: inhibition of DMMP hydrolysis by MP, 15.5 mM MP was added.	90
Figure 4-5. Optical microscope images of KSiNb and KGeNb crystals.	91
Figure 4-6. DMMP hydrolysis by the supernatant after suspensions of KGeNb or KSiNb are used for DMMP hydrolysis then the suspensions filtered and the filtrate assessed for activity. Conditions: [DMMP] = 15.5 mM, 18	

<p>$\mu\text{mol KSiNb}$ or KGeNb, 0.5 mL D_2O and 1.0 mL H_2O at room temperature.</p>	92
<p>Figure 4-7. ^{31}P NMP spectra showing the reuse of KGeNb for second run, reaction time = 12 h.</p>	92
<p>Figure 4-8. FT-IR spectra of KGeNb before and after DMMP hydrolysis.</p>	93
<p>Figure 4-9. FT-IR spectra of KSiNb before and after DMMP hydrolysis.</p>	93
<p>Figure 4-10. Plot of the initial rate versus DMMP concentration in the decontamination of DMMP using KGeNb. Conditions: $[\text{DMMP}] = 15.5 \sim 121.4 \text{ mM}$, $[\text{KGeNb}] = 18 \mu\text{mol}$, 0.5 mL D_2O and 1.0 mL H_2O at room temperature</p>	94
<p>Figure 4-11. Plot of the initial rate versus the amount of KGeNb in the decontamination of DMMP using KGeNb. Conditions: $[\text{DMMP}] = 15.5 \text{ mM}$, amount of KGeNb added: 4.0 ~ 27.0 μmol, 1.5 mL of <i>N</i>-ethylmorpholine aqueous solution (0.45 M) as a buffer at pH 10.</p>	95
<p>Figure 4-12. Hydrolysis of GD using KSiNb (red squares). 2.5 μmol of KSiNb and 14 μmol of GD was added to 0.75 mL of H_2O in an NMR tube. The mixture was vigorously shaken at room temperature. Every several minutes, the contents were assessed by ^{31}P NMR spectroscopy to monitor the reaction. Due to the lack of continuous stirring, it shows a relatively lower activity (16 % of GD is removed) compared with the continuous stirred system (43 % of GD is consumed).</p>	98
<p>Figure 4-13. Adsorption and hydrolysis of GB on KSiNb as studied by DRIFTS (0 to 202 minutes at ambient temperature).....</p>	99
<p>Figure 4-14. Adsorption and hydrolysis of GB on KGeNb as studied by DRIFTS (0 to 320 minutes at ambient temperature).....</p>	100

Figure 4-15. Difference DRIFTS spectra of HD sorption onto KGeNb	102
Figure 4-16. Difference DRIFTS spectra of HD sorption onto KSiNb	102
Figure 4-17. The calculated model complexes 1 and 2 for KSiNb and KGeNb with DMMP simulant. Also shown in the figure are some important bond distances (in Å), and the DMMP coordination energies. Numbers given before and after “/” are for X = Si and Ge, respectively. Energies given after the reaction without and with parenthesis are ΔE and ΔG values.	103
Figure 5-1. FT-IR spectra of the tetrabutylammonium (TBA) salts of Ni₂ and Ni₃	114
Figure 5-2. Thermogravimetric analysis of TBA Ni₂ . The calculated weight percent of water loss corresponds to 27 water molecules.	115
Figure 5-3. Thermogravimetric analysis of TBA Ni₃ . The calculated weight percent of water loss corresponds to 28 water molecules.	115
Figure 5-4. (a) Polyhedral and ball-and-stick representation of X-ray crystal structure of Ni₂ . (b) Illustration for the definition of αααα isomer of Ni₂	121
Figure 5-5. (a) Polyhedral and ball-and-stick representation of X-ray crystal structure of Ni₃ . (b) Connectivity and bond angles diagram for Ni₃	122
Figure 5-6. FT-IR spectra of Ni₂ and Ni₃ compared to the component trivalent polyanion ligand, [α-P ₂ W ₁₅ O ₅₆] ¹²⁻	123
Figure 5-7. Normalized UV-vis absorption spectra of Na ₈ Li ₁₂ Ni₂ and Na ₄ Li ₅ Ni₃ . Conditions: 0.5 mM in 1 M NaCl aqueous solution.	124
Figure 5-8. (a) Cyclic voltammograms of 4.0 mM Na ₈ Li ₁₂ Ni₂ at different scan rates (pH=8.0). (b) The plot of maximum anodic peak currents for part “a” versus the square root of scan rates. (c) Cyclic voltammograms of 4.0 mM Na ₄ Li ₅ Ni₃ at different scan rates (pH=7.5). (d) The plot of maximum anodic peak currents for part “c” versus the square root of scan rates.	

Conditions: 200 mM sodium phosphate buffer deaerated with Ar; 1 M NaCl as a supporting electrolyte. 124

Figure 5-9. (A) Photocatalytic hydrogen evolution using 20 μM Ni_2 (green) and Ni_3 (black). Conditions: LED light (20 mW, 455 nm), $[\text{Ir}(\text{ppy})_2(\text{dtbbpy})]^+$ (0.2 mM), TEOA (0.25 M), 2 mL $\text{CH}_3\text{CN}/\text{DMF}$ (1/3) deairated with Ar. (B) Emission spectra of $[\text{Ir}(\text{ppy})_2(\text{dtbbpy})]^+$ (0.1 mM) as a function of added Ni_3 . (C) Emission spectra of $[\text{Ir}(\text{ppy})_2(\text{dtbbpy})]^+$ (0.1 mM) as a function of added TEOA. 125

Figure 5-10. FT-IR spectra of TBANi_3 before and after catalytic reactions..... 127

Figure 5-11. Time profile of UV-vis spectra of TBANi_3 in $\text{CH}_3\text{CN}/\text{DMF}$ containing 0.25 M TEOA. 127

Figure 5-12. Stern-Volmer plot assessing interaction involving TEOA. The calculated quenching rate constant is $3.1 \times 10^7 \text{ M}^{-1} \text{ s}^{-1}$ 128

Figure 6-1. A) PXRD patterns of a) simulated MIL-53, b) MIL-53, c) NH_2 -MIL-53 and d) **PNPMOF**. B) FT-IR spectra of a) MIL-53, b) NH_2 -MIL-53 and c) **PNPMOF**. C) Diffuse reflectance spectra of a) MIL-53, b) POM-Pt NPs@MIL-53 (the MOF without the anilinium side chain), c) **PNPMOF** and d) NH_2 -MIL-53. Inset: photograph of these samples in small vials. D) Photo-luminescence spectra of a) NH_2 -MIL-53, b) NH_2 -MIL-53 combined with $\text{H}_3\text{PW}_{12}\text{O}_{40}$ and c) **PNPMOF**. The weighed quantities of the MOF samples are the same in all spectra (Figs C and D). 141

Figure 6-2 A): TEM images of POM-Pt NPs@ NH_2 -MIL-53 (**PNPMOF**). The large dark approximately spherical particles are the POM-capped Pt NPs. The scale bar in the graph corresponds to 200 nm. B): TEM image of POM-

stabilized Pt NPs. C) Z-contrast TEM image of PNPMOF . D) Z-contrast TEM image of NH ₂ -MIL-53 mixed with the commercial Pt black.	142
Figure 6-3. EDX analysis of PNPMOF	144
Figure 6-4. TGA of a) MIL-53, b) NH ₂ -MIL-53 and c) PNPMOF . PNPMOF shows a similar thermal behavior to that of NH ₂ -MIL-53. Both are stable up to 500 °C.....	145
Figure 6-5. BET fitting curve for MIL-53. (MIL-53 surface area = 1174 m ² /g).....	145
Figure 6-6. BET fitting curve for NH ₂ -MIL-53. (NH ₂ -MIL-53 surface area = 912 m ² /g). This is lower than that of MIL-53 (1174 m ² /g) because NH ₂ groups partially block the pores of NH ₂ -MIL-53.	146
Figure 6-7. BET fitting curve for PNPMOF . (surface area = 684 m ² /g).	146
Figure 6-8. A) Time-dependent hydrogen evolution by PNPMOF under different pH conditions. B) Time-dependent H ₂ evolution of a) PNPMOF , b) 2-aminoterephthalic acid mixed with POM-stabilized Pt NPs, c) NH ₂ -MIL-53 mixed with commercial Pt black and d) POM-Pt NPs@NH ₂ -silica. C) Normalized fluorescence decay of a) 2-aminoterephthalic acid in the solid state, b) NH ₂ -MIL-53, c) PNPMOF . The solid lines are best fits according to single exponential decay for a) and bi-exponential decays for b) and c). D) The hydrogen peak in GC traces in successive experiments using the same catalyst. (Fresh solutions were used for each run; reaction time = 6 h all cases).....	148
Figure 6-9. pH dependence of hydrogen evolution by PNPMOF using ascorbic (AA) as sacrificial electron donor..	149
Figure 6-10. Time-dependent hydrogen evolution curves for PNPMOF using different concentrations of AA	149

Figure 6-11. Oxidation of 2-aminoterephthalic acid by $\text{H}_3\text{PW}_{12}\text{O}_{40}$. When 50 μM 2-aminoterephthalic acid was mixed with 0.1 M $\text{H}_3\text{PW}_{12}\text{O}_{40}$ in distilled water in the dark purged with Ar, the color of the solution changes from light yellow (left) to dark blue (right) (a characteristic color for reduced $\text{H}_3\text{PW}_{12}\text{O}_{40}$) after 1 hour indicating that the 2-aminoterephthalic acid is oxidized by $\text{H}_3\text{PW}_{12}\text{O}_{40}$	150
Figure 6-12. ATR-IR spectra of PNPMOF at different pH values. The “sample” is for PNPMOF with no additional added acid.	154
Figure 6-13. UV-vis spectra of a) 2-aminoterephthalic acid in distilled water (60 μM) and b) the filtrate solution after the first run. The UV-vis spectra of the filtrate solution indicate a negligible amount of organic linker is present arguing strongly that the MOF structure is maintained during the catalytic reactions.	154
Figure 6-14. PXRD patterns of PNPMOF before and after catalysis.	155
Figure 6-15. FT-IR spectra of PNPMOF before and after catalysis.	155

List of Tables

Table 2-1. Aerobic Oxidation of Formaldehyde Catalyzed by PW₈V₄ in Different Solutions.	40
Table 2-2. Aerobic Oxidation of Formaldehyde Catalyzed by PW₈V₄ , as a Function of Substrate and Catalyst Concentration	40
Table 2-3. Aerobic Oxidation of Formaldehyde Catalyzed by Different POMs.	46
Table 3-1. Crystal data and structure refinement for 3.1	62
Table 4-1. The crystallographic data for KGeNb	82
Table 4-2. Comparison of DMMP and DECP decomposition by different materials at room temperature under the same conditions.	95
Table 5-1. Crystal data and structure refinement for Ni₂ and Ni₃	119
Table 5-2. Control experiments for photocatalytic hydrogen evolution after 3.5 hours by different water reduction catalysts (WRCs) under otherwise identical conditions: DMF/CH ₃ CN/H ₂ O (2 mL) mixed solvent solution containing 20 μM catalyst, 0.25 M TEOA and 0.2 mM [Ir(ppy) ₂ (dtbbpy)] ⁺	126
Table 6-1. Control experiments for photocatalytic hydrogen evolution under standard conditions after 6 hours.....	151
Table 6-2. Average lifetimes for different samples from time-resolved fluorescence decay measurements.	152

List of Schemes

Scheme 5-1. Synthetic Routes to Ni₂ , Ni₃ and Ni₁₄	118
Scheme 6-1. Route to PNPMOF (symbols not to scale)	140
Scheme 6-2. Illustration of the Pt NPs and the windows on the NH ₂ -MIL-53 surface	143
Scheme 6-3. Scheme showing the proposed mechanism for photocatalytic H ₂ evolution in the PNPMOF system (symbols are <i>not</i> to scale)	153

List of Abbreviations

Å	Angstrom
<i>a, b, c</i>	unit cell axial lengths
<i>Z</i>	number of molecules per unit cell
α, β, γ	interaxial angles between unit cell vectors
θ	the glancing angle of the X-ray beam to the “reflecting plane”
λ	wavelength
μ	the total linear absorption coefficient (with unit of cm^{-1})
anal.	analysis
°C	degrees Celsius
calcd.	calculated
cif	crystallographic information file
cm^{-1}	reciprocal centimeter (wavenumber)
DLS	dynamic light scattering
<i>F</i> (000)	structure factor for the unit cell
FT-IR	Fourier transform infrared spectroscopy
TGA	thermogravimetric analysis
UV	ultraviolet
UV-Vis	ultraviolet-visible
δ	chemical shift (expressed in ppm for NMR)
ϵ	molar extinction (or absorption) coefficient
GC	gas chromatography
g	gram(s)
h	hour(s)
<i>I</i>	emission intensities of $[\text{Ir}(\text{ppy})_2(\text{dtbbpy})]^{+*}$ with quencher
I_0	emission intensities of $[\text{Ir}(\text{ppy})_2(\text{dtbbpy})]^{+*}$ without quencher
$[\text{Ir}(\text{ppy})_2(\text{dtbbpy})][\text{PF}_6]$	(4,4'-di- <i>tert</i> -butyl-2,2'-dipyridyl)-bis-(2-phenylpyridine(-1H)-iridium(III) hexafluorophosphate
<i>J</i>	coupling constant in Hertz
K	Kevin
m	medium (IR)
s	strong (IR)
sh	shoulder (IR)
w	weak (IR)
M	molarity
mg	milligram(s)
MHz	megahertz
min	minute(s)
mL	milliliter(s)
mmol	millimole
nm	nanometer
NMR	nuclear magnetic resonance spectroscopy
pH	potential of hydrogen, a measure of the acidity or alkalinity
POM	polyoxometalate
TIC	toxic industry compound
CWA	chemical warfare agent
ppm	part per million
<i>R</i>	discrepancy index for crystal structure refinement
$[\text{Ru}(\text{bpy})_3]^{3+}$	Tris(2,2'-bipyridyl)triperchlororuthenium(III)
TBA	tetrabutylammonium
TMSP	transition-metal-substituted polyoxometalate
TOF	turnover frequency
TON	turnover number
WOC	water oxidation catalyst
WRC	water reduction catalyst

Chapter 1.

Introduction:

Overview of the Structures, Properties and Applications of Polyoxometalates in Toxic Compound Decontamination and Solar Energy Conversion

“In Complexity in Chemistry and Beyond: Interplay Theory and Experiment: New and Old Aspects of Complexity in Modern Research, Multi-electron Transfer Catalysts for Air-Based Organic Oxidations and Water Oxidation; 2012, p 229-242; Hill, C., Musaev, G. D., Eds.; Springer Netherlands: Dordrecht” Reproduced partially with permission from Springer

As one of the contributors; with Zhen Luo, Jie Song, Guibo Zhu, Chongchao Zhao, Hongjin Lv, James W. Vickers, Yurii V. Geletii, Djamaladdin G. Musaev, and Craig L. Hill*, W. Guo contributed sections 1.1, 1.4 and the majority of 1.2 to this work; all the authors contributed extensively to sections 1.2 and 1.3.

1.1 General Structures of POMs

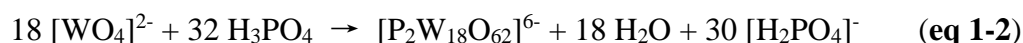
The history of POM chemistry can be traced back to 1826 when Berzelius first reported the light yellow crystalline solid (12-molybdophosphate) formed from the reaction of ammonium molybdate with phosphoric acid.¹⁻³ Later the research on POM chemistry progressed rapidly with the development of advanced analytical research techniques such as Nuclear Magnetic Resonance (NMR), Fourier Transform Infrared Spectroscopy (FTIR) and X-ray crystallography.⁴⁻⁹ POMs are a family of early transition metal-oxygen-anion clusters which have the general formulas of $[M_mO_n]^{p-}$ (isopolyanions) and $[X_xM_mO_n]^{p-}$ (heteropolyanions, X = Si^{IV}, Ge^{IV}, P^V, As^V, etc.).^{4,10-16} Based on the component early transition metals (M as denoted in the above formulas) POMs can be classified into several groups: polytungstates (M = W^{VI}),¹⁷⁻²⁵ polymolybdates (M = Mo^{VI}),²⁶⁻³⁶ polyvanadates (M = V^V),³⁷⁻⁴⁰ polyniobates (M = Nb^V),⁴¹ polytantalates (M = Ta^V),⁴²⁻⁴⁴ etc.

Polytungstates/polymolybdates are generally composed of multiple WO₆/MoO₆ octahedra sharing edges, corners and/or faces. Corner- and edge-sharing types are more stable than the face-sharing ones because the transition metal ions are more far from each other, thus decreasing their mutual repulsion.^{45,46} Two of the most commonly used plenary polytungstates/polymolybdates are the Keggin $[XM_{12}O_{40}]^{n-}$ (X = Si^{IV}, Ge^{IV}, P^V, As^V, etc. M = W^{VI} or Mo^{VI})^{3,47,48} and the Wells-Dawson $[X_2M_{18}O_{62}]^{n-}$ (X = P^V, As^V, M = W^{VI} or Mo^{VI}) types.⁴⁹ The Keggin polytungstate is constructed by a central XO₄ (X = P or Si) tetrahedron surrounded by four W₃O₁₃ triads at each of its vertices. The name, Keggin, is derived from the person who solved the structure of the isopolyanion, $[PW_{12}O_{40}]^{3-}$ in the early 1930s.^{3,47,48} It can be synthesized via the aggregation and condensation of $[WO_4]^{2-}$ at certain pH (**eq 1-1**). Further isolation can be achieved via crystallization or precipitation by adding extra counter cations.^{50,51} More recently, the

Keggin POMs which are solely composed of first-row transition metal-oxygen clusters (M = Fe/Ni) have been reported, although their properties and synthetic conditions are quite different from that of Keggin-type polytungstates/polymolybdates.^{52,53} The α -Keggin structure that has an idealized T_d symmetry in which all of the metal centers are equivalent is shown in **Figure 1-1**. Additional isomers: β (C_{3v} symmetry), γ (C_{2v} symmetry), δ (C_{3v} symmetry) and ε (T_d symmetry) isomers, can be derived from successive 60 °rotation of the four W_3O_{13} triads as proposed by Baker and Figgis.⁵⁴



Another type of well-studied plenary POMs is the Wells-Dawson type. **Figure 1-1** also shows the structure of the Wells-Dawson POM, $[\alpha-P_2W_{18}O_{62}]^{6-}$ that is built up by two central PO_4 tetrahedra, two W_3O_{13} triad and two W_6O_{14} belts. Baker and Figgis also proposed the existence of several isomers of Wells-Dawson POMs while only α and β isomers are the most commonly studied.^{54,55} They can be synthesized by refluxing a mixture of sodium tungstate and an excess of H_3PO_4 (**eq 1-2**).⁵⁶



The plenary polytungstates/polymolybdates can transform to lacunary POMs by losing one or more WO_6/MoO_6 octahedra through base hydrolysis. The extensively studied lacunary POMs include but not limited to the mono-vacant $[SiW_{11}O_{39}]^{8-}$,⁴⁶ the di-vacant $[SiW_{10}O_{36}]^{8-}$,⁴⁶ and the tri-vacant $[P_2W_{15}O_{56}]^{12-}$.^{57,58} Lacunary POMs that have vacant sites can further react with other transition metals forming transition-metal-substituted POMs (TMSPs) where the transition metals occupy the vacant sites.⁵⁹ Thus, lacunary POMs can be considered as inorganic polydentate ligands. For example, the mono-vacant $[PW_{11}O_{39}]^{7-}$ can form $[M(H_2O)PW_{11}O_{39}]^{n-}$ by reacting with different

transition metal ions.⁵⁹ In addition, the di-vacant $[\text{SiW}_{10}\text{O}_{36}]^{8-}$, and the tri-vacant $[\text{P}_2\text{W}_{15}\text{O}_{56}]^{12-}/[\text{PW}_9\text{O}_{34}]^{9-}$ have been used for the design of various POM architectures such as the sandwich type POMs (**Figure 1-1**).⁶⁰⁻⁶⁷ **Figure 1-1** shows the X-ray crystal structures of representative plenary and lacunary polytungstates as well as the assembly of some TMSPs. The structures of two sandwich type POMs, $[\{\text{Ru}_4\text{O}_4(\text{OH})_2(\text{H}_2\text{O})_4\}(\gamma\text{-SiW}_{10}\text{O}_{36})_2]^{10-}$ and $[\text{Co}_4(\text{H}_2\text{O})_2(\text{PW}_9\text{O}_{34})_2]^{10-}$ that are extensively studied as water oxidation catalysts are also shown in **Figure 1-1**.

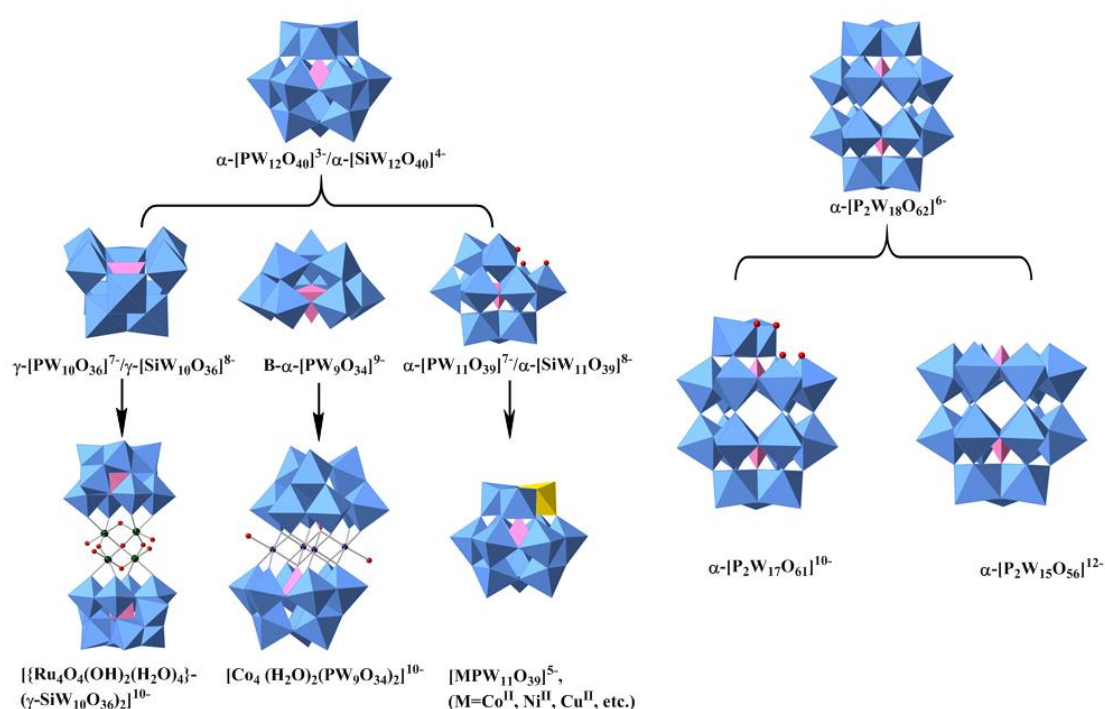


Figure 1-1. X-ray crystal structures of representative plenary and lacunary polytungstates as well as the assembly of some TMSPs. Color code: blue, WO_6 ; pink, PO_4/SiO_4 ; red balls, O; purple balls, Co; green balls, Ru; yellow, MO_6 (M = Co^{II} , Ni^{II} , Cu^{II} , etc.)

Even though there are thousands of polytungstate or polymolybdate structures reported, the studies on polyvanadates, polyniobates and polyantalates are not as

prevalent in the literature. Like polytungstates or polymolybdates, polyvanadates can be synthesized through the aggregation and condensation of octahedral hydroxide/oxo vanadium complexes under acidic aqueous conditions. Decavanadate ($[\text{V}_{10}\text{O}_{28}\text{H}_3]^{3-}$) is one of the well studied polyvanadates.⁶⁸⁻⁷² Other reported polyvanadates include polyvanadophosphate ($[\text{PV}_{14}\text{O}_{42}]^{9-}$),⁷³ vanadomanganate(IV) anions $[\text{MnV}_{13}\text{O}_{38}]^{7-}$ (**MnV₁₃**), $[\text{Mn}_2\text{V}_{22}\text{O}_{64}]^{10-}$ (**Mn₂V₂₂**) and $[\text{Mn}_3\text{V}_{12}\text{O}_{40}\text{H}_3]^{5-}$ (**Mn₃V₁₂**), etc.^{74,75} In addition, polyvanadates can also be used as building blocks to form linked frameworks. For example, Lindqvist hexavanadate has been functionalized by multidentate alkoxy $(\text{HOCH}_2)_3\text{CR}$ ($\text{R}=\text{CH}_3$, CH_2OH , CH_2COOH , etc) groups which can be further modified forming 1-, 2- and 3-dimensional frameworks.⁷⁶⁻⁸¹ The alkoxy groups substitute the bridging oxo groups between the vanadium ions in the triangular arrangement. **Figure 1-2** shows the polyhedral representation of $[\text{V}_{10}\text{O}_{28}\text{H}_3]^{3-}$ and two of the possible correlations of the alkoxy groups with hexavanadate.

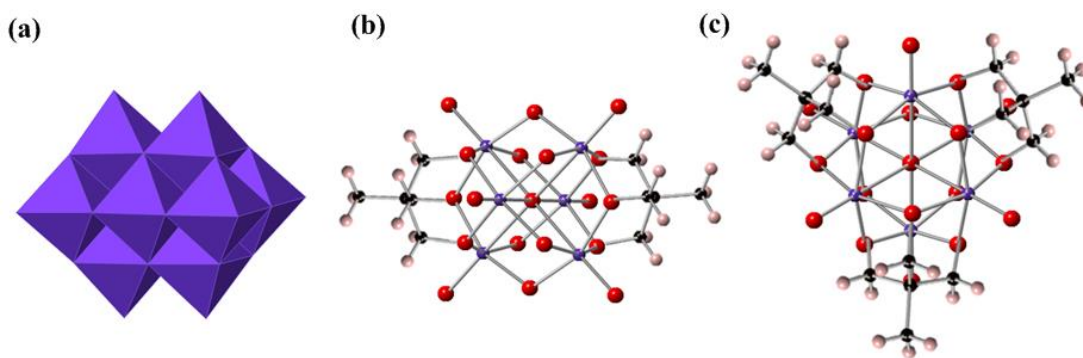


Figure 1-2 (a) Polyhedral representation of the X-ray crystal structure of $[\text{V}_{10}\text{O}_{28}\text{H}_3]^{3-}$, (b) coordination of alkoxy group with hexavanadate in $[\text{V}_6^{\text{V}}\text{O}_{13}[(\text{OCH}_2)_3\text{CH}_3]_2]^{2-}$ and (c) coordination of alkoxy groups with hexavanadate in $[\text{V}_6^{\text{V}}\text{V}_5^{\text{IV}}\text{O}_7(\text{OH})_3[(\text{OCH}_2)_3\text{CH}_3]_3]^{-}$.⁷⁶⁻⁸¹ Color code: purple octahedra, VO_6 ; purple balls, vanadium atoms; red balls, oxygen atoms; black balls, carbon atoms; pink balls, hydrogen atoms.

Vanadium, as one of Group V transition metals, shows similar structural and synthetic properties to that of Group VI metals (Mo and W) when forming POMs. However, two other Group V metals, niobium and tantalum, exhibit quite different behavior than vanadium, molybdenum and tungsten.⁴⁴ The formation of polyniobates or polytantalates usually requires quite basic conditions ($\text{pH} > 10$).⁴¹ Their structures were mainly limited to the Lindqvist hexaniobate ($[\text{Nb}_6\text{O}_{19}]^{8-}$) and hexatantalate ($[\text{Ta}_6\text{O}_{19}]^{8-}$) at the end of 20th century.⁸² It has only been in recent years that several different types of polyniobates have been reported, such as the lacunary Keggin ion derivative, $[\text{H}_2\text{Si}_4\text{Nb}_{16}\text{O}_{56}]^{14-}$, the Keggin type, $[\text{PNb}_{12}\text{O}_{40}(\text{VO})_6]^{3-}$ that is composed of a Keggin $\{\text{PNb}_{12}\}$ capped by six vanadyl groups, the $[\text{Nb}_{24}\text{O}_{72}\text{H}_9]^{15-}$, etc (**Figure 1-3**).⁸³⁻⁸⁶ The use of organic counter ions under high pressure or reflux conditions would likely lead to the formation of larger and/or new cluster geometries.⁸² One counter argument against such syntheses is the difficulty in predicting and controlling the structures. As discussed above, POMs can be constituted by multiple transition metals. The different constituting elements of POMs and their various structures endow them with diverse properties and applications in medicine,⁸⁷⁻⁹⁴ magnetism,⁹⁵⁻⁹⁹ photochemistry¹⁰⁰⁻¹⁰² and in particular catalysis.^{7,67,103-110}

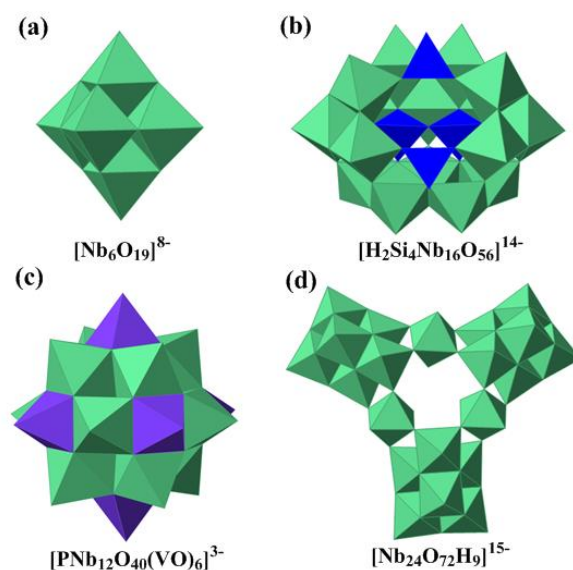
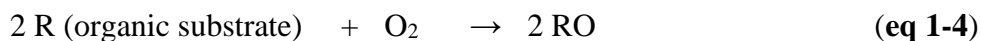
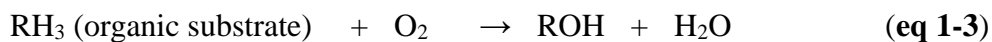


Figure 1-3. X-ray crystal structures of (a) $[\text{Nb}_6\text{O}_{19}]^{8-}$, (b) $[\text{H}_2\text{Si}_4\text{Nb}_{16}\text{O}_{56}]^{14-}$, (c) $[\text{PNb}_{12}\text{O}_{40}(\text{VO})_6]^{3-}$ and (d) $[\text{Nb}_{24}\text{O}_{72}\text{H}_9]^{15-}$. Color code: purple octahedra, VO_6 ; green octahedral, NbO_6 ; blue tetrahedral, SiO_4 ; hydrogen atoms are omitted for clarity.

1.2 Catalytic Properties of POMs in Toxic Compound Decontamination

1.2.1 Air-based oxidation of organic compounds by POMs.

The air-based oxidations of organic compounds are of significant importance in green synthetic organic chemistry. They can proceed through monooxygenase (**eq 1-3**) or dioxygenase (**eq 1-4**) processes with the exception of radical chain processes which are common in the oxidation of organic compounds. In both of the two processes, air or oxygen is used and there are no deleterious by-products.¹¹¹⁻¹¹⁴ The environmental arguments for such processes alone are considerable and growing. These reactions result in the multi-electron reduction of O_2 and oxidation of the organic substrate (reactant).



However, the above air-based reactions under ambient conditions are always hard to realize partly because autoxidation (radical chain) processes usually have relatively high activation energies.^{111,115,116} Catalysts have been developed to increase the reaction rates and selectivity of air-based oxidation of organic compounds.^{76,117-120} Examples include but are not limited to nanomaterials such as nanosized Au, Pt, Pd and metal oxides.¹²¹⁻¹²⁶ Another class of catalysts developed for air-based oxidations that are fast under ambient conditions (use air at room temperature) are POMs.^{76,117-120,127-131} The surface of the molecular metal-oxo clusters in POMs is similar to that of solid metal oxide crystals. Therefore, POMs not only have the properties of molecular species (such as solubility) but also exhibit similar features to that solid metal oxides.

POMs can function as an acid, base or oxidant depending on their constituting transition metal elements, counter cations and structures. The redox properties of POMs are of particular importance because they directly impact most applications of POMs in air-based oxidation of many classes of organic compounds as well as in artificial photosynthesis.^{67,132} The transition metals in $[\text{M}_m\text{O}_n]^{p-}$ (isopolyanions) and $[\text{X}_x\text{M}_m\text{O}_n]^{p-}$ (heteropolyanions) are typically in d^0 or d^1 electronic configurations. Therefore, they are very likely to accept multiple external electrons accompanied by protonation without major structural changes.¹³³⁻¹³⁷ The redox properties of POMs are mainly determined by the particular transition metal centers that constitute the polyanion units. Specifically, $\text{V}^{\text{V/IV}}$ has the highest potential, $\text{Mo}^{\text{V/IV}}$ is next, and $\text{W}^{\text{V/IV}}$ has the lowest potential, while the Nb^{V} and Ta^{V} centers show little or no redox reactivity.¹³² Therefore, polyvanadates and/or polymolybdates are constantly used as catalysts for the

oxidation of organic compounds. For example, the Keggin-type heteropolyanions $\text{PMo}_{12-n}\text{V}_n\text{O}_{40}^{(3+n)-}$ can catalyze the air-based oxidation of many organic compounds including the alkanes, alcohols and aldehydes.¹³⁸ A catalytic cycle that summarizes the general mechanism for these oxidations as well as the structure of $\text{PMo}_{10}\text{V}_2\text{O}_{40}^{5-}$ is shown in **Figure 1-4**. The first step in the mechanism is the oxidation of the substrate by the oxidized-POM (**eq 1-5**), and the second step is the air-based oxidation of reduced-POMs (**eq1-6**).^{127,128}

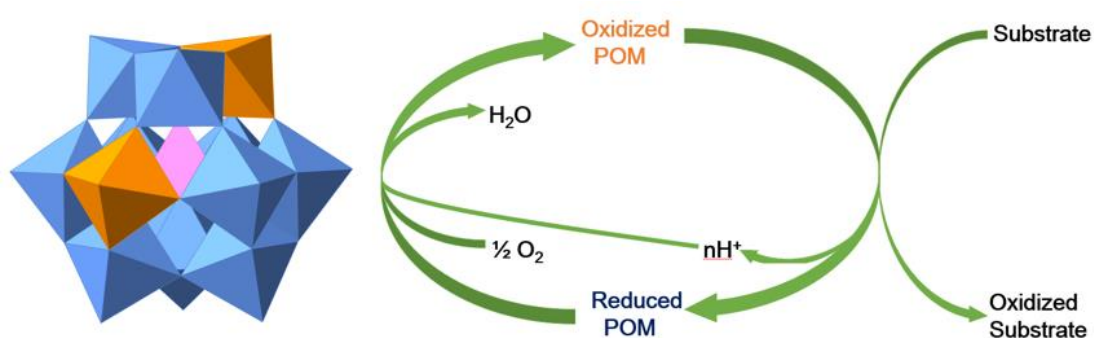


Figure 1-4. Left: Polyhedral representation of $\text{PMo}_{10}\text{V}_2\text{O}_{40}^{5-}$, color code: blue, MoO_6 ; orange, VO_6 ; pink, PO_4 . Two VO_6 octahedra are statistically distributed among the 12 positions. Right: The general two-step mechanism for POM-catalyzed O_2 -based oxidations of organic compounds.

1.2.2 The use of POMs in the decontamination of toxic compounds

The removal of TICs and/or CWAs by POMs can proceed via different pathways of which air-based catalytic oxidative reactions are of particular value. They can be conducted under mild conditions inexpensively.^{117,118,139-142} Moreover, the logistic

(and associated economic) burden for such decontamination technology is minimal. Most decontamination technology in military or civilian venues involves the use of highly reactive solutions, foams or powders that themselves have handling, transportation and safety challenges. This isn't the case if air and air only is the reactive decontaminating agent. In addition, no energy sources are needed for air-based decontamination because all air-based oxidations of organic substrates, including the TICs and CWAs, are thermodynamically favorable. The released energy sustains the reaction provided the catalytic process is sufficiently rapid. Also, the safety concerns associated with the use of air-based oxidation processes are minimal: there is no toxic solution, gel or powder to deal with and no associated liquid or solid waste to remediate. Another pathway to the decontamination of TICs and in particular CWAs by POMs that draws the attention from researchers is to utilize the acid/base property of POMs.^{143,144} Nerve agents and vesicants are two of the most commonly used CWAs, and they can all be decontaminated via hydrolytic reactions with POM-based materials as catalysts.

Various POM-based materials have been applied as catalysts to remove toxic compounds (major TICs and CWAs). For example, a combination of POMs with metal-organic frameworks generates a series of POM-MOF materials.¹⁴⁵⁻¹⁵¹ One POM-MOF, $[\text{Cu}_3(\text{C}_9\text{H}_3\text{O}_6)_2]_4[\{(\text{CH}_3)_4\text{N}\}_4\text{CuPW}_{11}\text{O}_{39}\text{H}]$ was shown to be able to catalytically oxidize thiols to disulfides and to efficiently convert toxic H_2S to S_8 .¹⁵² In addition, a sodalite-type porous POM-MOF, $\text{H}_3[(\text{Cu}_4\text{Cl})_3(\text{C}_9\text{H}_3\text{O}_6)_8]_2[\text{PW}_{12}\text{O}_{40}]_3(\text{C}_4\text{H}_{12}\text{N})_6 \cdot 3\text{H}_2\text{O}$, was reported and shown to be able to hydrolytically remove dimethyl methylphosphonate (DMMP, a CWA simulant).¹⁴⁷ The structures of the above two POM-MOF materials are shown in **Figure 1-5**. In the above POM-MOF materials, the POMs are located in some of the large MOF pores. They not only exhibit the properties

of both MOFs and POMs, but also would likely to stimulate synergistic catalytic activities. However, they are heterogeneous materials thus making it difficult to study the reaction mechanism. Co-catalysts, including iron bromide and nitrate complexes together with POMs, were found to be efficient catalysts for air-based oxidation of 2-chloroethyl ethyl sulfide (CEES, a mustard simulant).¹⁵³⁻¹⁵⁶ They are multi-component systems that constitute some of the most complex synthetic catalysts known. This hinders the study of their reaction mechanisms.

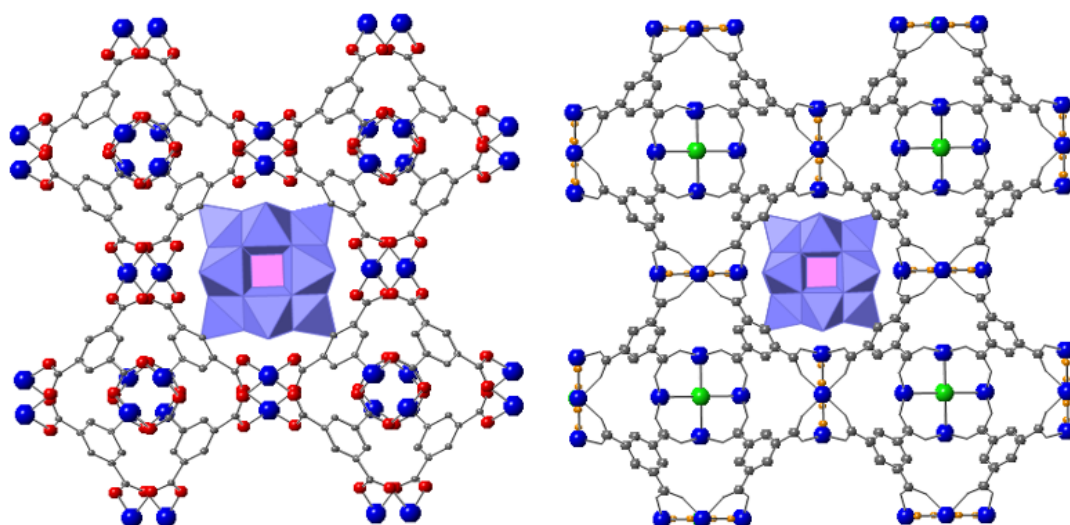


Figure 1-5. X-ray crystal structures of left: $[\text{Cu}_3(\text{C}_9\text{H}_3\text{O}_6)_2]_4 [\{ (\text{CH}_3)_4\text{N} \}_4\text{CuPW}_{11}\text{O}_{39}\text{H}]$ and right: $\text{H}_3[(\text{Cu}_4\text{Cl})_3(\text{C}_9\text{H}_3\text{O}_6)_8]_2[\text{PW}_{12}\text{O}_{40}]_3(\text{C}_4\text{H}_{12}\text{N})_6 \cdot 3\text{H}_2\text{O}$. One of the large pores in MOFs containing the pink and purple Keggin-type POM is shown. Color code: red, oxygen atoms; gray, carbon atoms; green, chlorine atoms; blue, copper atoms; pink, PO_4 tetrahedra; purple, WO_6 octahedra. In the left figure, the Cu atom in the POM is statistically positioned over the 12 metal positions. Counter cations and hydrogen atoms are omitted for clarity.

Synthetic organic dyes are another type of TIC. Many dyes have been synthesized but then reported to be hazardous. A series of Keggin/Wells-Dawson POM-based materials have been prepared that show effective photocatalytic activity for the degradation of organic dyes.¹⁵⁷⁻¹⁶² They utilize the photo-responsive property of POMs: that POMs can be excited under ultraviolet light irradiation. Irradiated POMs can also generate hydroxyl radicals from water which can further destroy organic dyes. Methylene blue (MB) and methyl orange (MO) are commonly used as models of organic dye contaminants to access the photocatalytic activity of POM-based materials for degradation of organic dyes. However, the use of ultraviolet light limits the wide practical applications of POMs to the removal of environmentally undesirable organic compounds. To this end, developing efficient, simple and practical catalytic systems to remove TICs and CWAs remains a noteworthy challenge.

1.3 The use of POMs in solar energy conversion

The production of alternative and renewable energy to power the planet is a pressing international concern.¹⁶³⁻¹⁶⁶ The various forms of renewable energy (principally hydroelectric, geothermal, biofuels, wind, tides, and solar) constitute only about 10% of total energy consumption in most developed countries. Typically 5-10% of societally usable energy comes from nuclear and the remaining 80% comes from the burning of fossil fuels, which unavoidably produces CO₂ and H₂O. Critically, only solar has the capacity to power the planet given projected increases in the global population and standard of living.¹⁶⁴ (Developed societies consume far more energy than underdeveloped ones and the development of highly populated nations including China, India, Malaysia and Indonesia is rapid and substantial at present.) A consequence of technical realities (declining accessible fossil fuel availability and environmental changes), is that there are few governments not investing in renewable energy. As a

consequence of this and the rapidly increasing technical information available, the world-wide research effort in this area has become commensurately substantial.

Energy must not only be generated but also stored in safe, viable and economical ways.¹⁶⁷ Of the ways to store energy, most prominently heat, electricity and fuel, it is latter (fuel) which is critically needed.^{164,166,168} Energy stored in the form or heat or electricity will never have the weight and volume density to power ships and aircraft. A very high percentage of the global economy depends on the commodities transported by ships. Thus the need for making not only electricity from ambient sunlight (photovoltaics, etc.) more efficiently and cheaply but more importantly, the need for making “solar fuel” is clear.

Four unit operations are needed to convert sunlight into solar fuel: (1) an efficient absorber of solar light; (2) a charge separation structure enabling the absorbed photon energy to be converted with high quantum yield into a charge-separated state (exciton); (3) harvesting the electron in this excited state and using it to reduce low-energy molecules, particularly CO₂ and H₂O, thus converting them into high energy molecules (reduced molecules or “fuels”); and (4) harvesting the hole (positive charge) in the excited state four times sequentially to oxidize water to oxygen.¹⁶⁵ Advances are needed in all four of the above unit operations. Developing catalysts for the multi-electron reduction CO₂ to fuels, the hydrogen production and the oxidation of H₂O to O₂ exhibit potential challenges.

There have been many reports on POM-based catalysts for catalytic water oxidation and hydrogen production.^{67,169-171} The POMs utilized are mostly TMSPs that are composed of polytungstates as ligands binding with redox-active transition metals. In 2010 a sandwich POM, [Co₄(H₂O)₂(PW₉O₃₄)₂]¹⁰⁻ (**Co₄P₂**; X-ray structure in **Figure 1-**

1) was demonstrated to catalyze efficient H₂O oxidation by persulfate using visible light and the standard photosensitizer [Ru(bpy)₃]²⁺.^{172,173} Later in 2014, a similar sandwich POM, [Co₄(H₂O)₂(VW₉O₃₄)₂]¹⁰⁻ (**Co₄V₂**), was prepared and shown to have a turnover rate of >1000 O₂ molecules per second at pH 9, making it the fastest water oxidation catalyst (WOC), at least at that time.¹⁷⁴

Some sandwich type POMs have also been prepared as catalysts for hydrogen evolution in the presence of photosensitizers and sacrificial electron donors. The tetra-transition-metal POMs, [Mn₄(H₂O)₂(VW₉O₃₄)₂]¹⁰⁻ (**Mn₄V₂**) and [Ni₄(H₂O)₂(PW₉O₃₄)₂]¹⁰⁻ (**Ni₄P₂**) are prominent examples.^{170,171} They display a sandwich type structure as that of **Co₄P₂** in **Figure 1-1** by changing the transition metals in the belt positions and the heteroatoms. In addition, they all have free coordination sites on two of the transition metals that bind water and that are presumably active sites for water oxidation or for hydrogen production. However, another nickel-containing POM, [{Ni₄(OH)₃AsO₄}₄(B-α-PW₉O₃₄)₄]²⁸⁻ (**Ni₁₆As₄P₄**) is also reported to be an efficient catalyst for photocatalytic hydrogen generation.¹⁶⁹ This hexadecyl-nickel-containing POM does not exhibit free coordination sites yet shows HEC activity. The activity might derive from the unique structure, the arsenic centers or other reasons that will require further study. Investigating the different structures of POMs and probing their potential catalytic hydrogen evolution activity continues to attract interest.

1.4 Goal of this work and outline

The first objective of this thesis is to develop efficient POM-based materials for decontamination of toxic compounds including TICs and CWAs, and to investigate the reaction mechanisms via kinetic studies and DFT calculations. **Chapter 2-4** reports the synthesis, structures, and reactivity of different types of POMs in the destruction of

TICs and CWAs. Specifically, **Chapter 2** describes the structures and activities of three tetra-*n*-butylammonium (TBA) salts of polyvanadotungstates, $[n\text{-Bu}_4\text{N}]_6[\text{PW}_9\text{V}_3\text{O}_{40}]$ (**PW₉V₃**), $[n\text{-Bu}_4\text{N}]_5\text{H}_2\text{PW}_8\text{V}_4\text{O}_{40}$ (**PW₈V₄**), $[n\text{-Bu}_4\text{N}]_4\text{H}_5\text{PW}_6\text{V}_6\text{O}_{40}\cdot 20\text{H}_2\text{O}$ (**PW₆V₆**). They are shown to be effective catalysts for the aerobic oxidation of formaldehyde to formic acid under ambient conditions. A layered manganese(IV)-containing heteropolyvanadate with a 1:14 Stoichiometry, $\text{K}_4\text{Li}_2[\text{MnV}_{14}\text{O}_{40}] \cdot 21\text{H}_2\text{O}$ is reported in **Chapter 3**. The synthesis, characterization and magnetic studies are described in detail. Its catalytic activity for oxidative removal of 2-chloroethyl ethyl sulfide is also discussed. **Chapter 4** reports the decontamination of a wide range of chemical warfare agents and their simulants by a new one-dimensional polymeric polyniobate (P-PONb), $\text{K}_{12}[\text{Ti}_2\text{O}_2][\text{GeNb}_{12}\text{O}_{40}] \cdot 19\text{H}_2\text{O}$, under mild conditions and in the dark.

The second goal of this dissertation is to develop effective POM-based materials for photocatalytic hydrogen evolution, to modify these reaction systems, and to study their reaction mechanisms. Specifically, **Chapter 5** addresses the structures, characterizations and catalytic hydrogen generation activity of a new tri-nickel-containing Wells-Dawson POM, $[\text{Ni}_3(\text{OH})_3(\text{H}_2\text{O})_3\text{P}_2\text{W}_{16}\text{O}_{59}]^{9-}$. **Chapter 6** describes a method that combines POMs, Pt nanoparticles (NPs) and MOFs into a hybrid material which shows synergistic hydrogen production activity. The POM ($\text{H}_3\text{PW}_{12}\text{O}_{40}$) in the hybrid reduces H_2PtCl_6 to Pt NPs and stabilizes the Pt NPs. Moreover, these structural and active components show synergistic effects with respect to the catalysis of water reduction-hydrogen evolution.

References

- (1) Berzelius, J. J. *Poggendorfs Ann. Phys. Chem.* **1826**, 6, 369, 380.
- (2) Pauling, L. *J. Am. Chem. Soc.* **1929**, 51, 2868.
- (3) Keggin, J. F. *Nature* **1933**, 131, 908.
- (4) Pope, M. T. In *Comprehensive Coordination Chemistry*; Wilkinson, G., Gillard, R. D., Eds.; Pergamon: New York, 1987, p 1023-1058.
- (5) Pope, M. T.; Müller, A. *Angew. Chem.* **1991**, 103, 56-70.
- (6) Pope, M. T. In *Prog. Inorg. Chem.*; Lippard, S. J., Ed.; John Wiley & Sons, Inc.: New York, 1991; Vol. 39, p 181-257.
- (7) *Special Thematic Issue on Polyoxometalates*; Hill, C. L., Ed., 1998; Vol. 98, No. 1.
- (8) Miras, H. N.; Yan, J.; Long, D.-L.; Cronin, L. *Chem. Soc. Rev.* **2012**, 41, 7403-7430.
- (9) Cronin, L.; Müller, A. *Chem. Soc. Rev.* **2012**, 41, 7333-7334.
- (10) Pope, M. T. In *Comprehensive Coordination Chemistry II: From Biology to Nanotechnology*; Wedd, A. G., Ed.; Elsevier Ltd.: Oxford, UK, 2004; Vol. 4, p 635-678.
- (11) Long, D.-L.; Tsunashima, R.; Cronin, L. *Angew. Chem. Int. Ed.* **2010**, 49, 1736-1758.
- (12) Borrás-Almenar, J. J.; Coronado, E.; Müller, A.; Pope, M. T. *Polyoxometalate Molecular Science. Proceedings of the NATO Advanced Study Institute, Tenerife, Spain from 25 August to 4 September 2001*; Kluwer Academic Publishers: Dordrecht, 2003; Vol. 98.
- (13) Pope, M. T. *Heteropoly and Isopoly Oxometalates*; Nauka. Sib. Otd., Novosibirsk, USSR, 1990.
- (14) Day, V. W.; Klemperer, W. G. *Science* **1985**, 228, 533-541.
- (15) *Polyoxometalates: From Platonic Solids to Anti-retroviral Activity*; Pope, M. T.; Müller, A., Eds.; Kluwer Academic Publishers: Dordrecht, Netherlands, 1993.
- (16) Hill, C. L. *Chem. Rev.* **1998**, 98, 1-2.
- (17) Zheng, S.-T.; Yang, G.-Y. *Chem. Soc. Rev.* **2012**, 41, 7623-7646.
- (18) Song, Y.-F.; Tsunashima, R. *Chem. Soc. Rev.* **2012**, 41, 7384-7402.
- (19) Lopez, X.; Carbo, J. J.; Bo, C.; Poblet, J. M. *Chem. Soc. Rev.* **2012**, 41, 7537-7571.

- (20) Clemente-Juan, J. M.; Coronado, E.; Gaita-Arino, A. *Chem. Soc. Rev.* **2012**, *41*, 7464-7478.
- (21) Nyman, M.; Burns, P. C. *Chem. Soc. Rev.* **2012**, *41*, 7354-7367.
- (22) Oms, O.; Dolbecq, A.; Mialane, P. *Chem. Soc. Rev.* **2012**, *41*, 7497-7536.
- (23) Contant, R.; Herve, G. *Rev. Inorg. Chem.* **2002**, *22*, 63-111.
- (24) Couto, F. A. R. S.; Cavaleiro, A. M. V.; Pedrosa de Jesus, J. D.; Sim õ, J. E. J. *Inorg. Chim. Acta* **1998**, *281*, 225-228.
- (25) Leyrie, M.; Thouvenot, R.; T é z é A.; Herv é G. *New J. Chem.* **1992**, *16*, 475-481.
- (26) Müller, A.; Das, S. K.; Krickemeyer, E.; Kuhlmann, C.; Sadakane, M.; Dickman, M. H.; Pope, M. T. *Inorg. Synth.* **2004**, *34*, 191-200.
- (27) Botto, I. L.; Garcia, A. C.; Thomas, H. J. *J. Phys. Chem. Solids* **1992**, *53*, 1075-1080.
- (28) Li, F.; Xu, L. *Dalton Trans.* **2011**, *40*, 4024-4034.
- (29) Hori, T.; Himeno, S. *Bunseki Kagaku* **1991**, *40*, 507-524.
- (30) Ohashi, Y.; Yanagi, K.; Sasada, Y.; Yamase, T. *Bull. Chem. Soc. Jpn.* **1982**, *55*, 1254-1260.
- (31) Tytko, K. H.; Glemser, O. *Adv. Inorg. Chem. Radiochem* **1976**, *19*, 239-315.
- (32) Misono, M.; Mizuno, N.; Mori, H.; Lee, K. Y.; Jiao, J.; Okuhara, T. *Prepr. Am. Chem. Soc. Div. Pet. Chem.* **1990**, *35*, 49-52.
- (33) Bharadwaj, P. K.; Ohashi, Y.; Sasada, Y.; Sasaki, Y.; Yamase, T. *Acta Crystallogr., Sect. C: Cryst. Struct. Commun.* **1984**, *C40*, 48-50.
- (34) Buckley, R. I.; Clark, R. J. H. *Coord. Chem. Rev.* **1985**, *65*, 167-218.
- (35) Tytko, K. H.; Baethe, G. Z. *Anorg. Allg. Chem.* **1987**, *555*, 85-97.
- (36) Weakley, T. J. R. *Struct. Bond.* **1974**, *18*, 131-176.
- (37) Bouhedja, L.; Steunou, N.; Maquet, J.; Livage, J. *J. Solid State Chem.* **2001**, *162*, 315-321.
- (38) Müller, A.; Sessoli, R.; Krickemeyer, E.; B ö gge, H.; Meyer, J.; Gatteschi, D.; Pardi, L.; Westphal, J.; Hovemeier, K.; Rohlfing, R.; D ö rring, J.; Hellweg, F.; Beugholt, C.; Schmidtman, M. *Inorg. Chem.* **1997**, *36*, 5239-5250.

- (39) Gatteschi, D.; Pardi, L.; Barra, A. L.; Müller, A. *Mol. Eng.* **1993**, *3*, 157-169.
- (40) Yamase, T.; Ohtaka, K.; Suzuki, M. *J. Chem. Soc., Dalton Trans.* **1996**, 282-289.
- (41) Nyman, M. *Dalton Trans.* **2011**, *40*, 8049-8058.
- (42) Djordjevic, C.; Vuletic, N. *Inorg. Chem.* **1968**, *7*, 1864-1868.
- (43) Fairbrother, F. *The Chemistry of Niobium and Tantalum*; Elsevier: Amsterdam, 1967.
- (44) Sloan, H. *Annu. Rep. Prog. Chem. Sect. A: Inorg. Chem.* **1994**, *90*, 131-140.
- (45) Kepert, D. L. *Prog. Inorg. Chem. (F. Albert Cotton, Editor. Interscience)* **1962**, *4*, 199-274.
- (46) Teze, A.; Herve, G. *J. Inorg. Nucl. Chem.* **1977**, *39*, 2151-2154.
- (47) Baker, L. C. W.; Figgis, J. S. *J. Am. Chem. Soc.* **1970**, *92*, 3794-3797.
- (48) Brown, G. M.; Noe-Spirlet, M. R.; Busing, W. R.; Levy, H. A. *Acta Crystallogr., Sect. B: Struct. Sci.* **1977**, *B33*, 1038-1046.
- (49) Wells, A. F. *Structural Inorganic Chemistry*; Clarendon Press: Oxford, 1945.
- (50) Tarasova, N. S.; Kazanskii, L. P.; Dorokhova, E. N. *Zh. Neorg. Khim.* **1981**, *26*, 625-629.
- (51) Chorghade, G. S.; Pope, M. T. *J. Am. Chem. Soc.* **1987**, *109*, 5134-5138.
- (52) Dong, L.; Huang, R.; Wei, Y.; Chu, W. *Inorg. Chem.* **2009**, *48*, 7528-7530.
- (53) Sadeghi, O.; Zakharov, L. N.; Nyman, M. *Science (Washington, DC, U. S.)* **2015**, *347*, 1359-1362.
- (54) Baker, L. C. W.; Figgis, J. S. *J. Amer. Chem. Soc.* **1970**, *92*, 3794-3797.
- (55) Contant, R.; Thouvenot, R. *Inorg. Chim. Acta* **1993**, *212*, 41-50.
- (56) Wu, H. *J. Biol. Chem.* **1920**, *43*, 189-220.
- (57) Contant, R.; Ciabrini, J. P. *J. Chem. Res., Synop.* **1977**, 222.
- (58) Finke, R. G.; Droege, M. W. *Inorg. Chem.* **1983**, *22*, 1006-1008.
- (59) Cao, R.; O'Halloran, K. P.; Hillesheim, D. A.; Hardcastle, K. I.; Hill, C. L. *CrystEngComm* **2010**, *12*, 1518-1525.
- (60) Anderson, T. M.; Zhang, X.; Hardcastle, K. I.; Hill, C. L. *Inorg. Chem.* **2002**, *41*, 2477-2488.

- (61) Ruhlmann, L.; Nadjo, L.; Canny, J.; Contant, R.; Thouvenot, R. *Eur. J. Inorg. Chem.* **2002**, 975-986.
- (62) Car, P.-E.; Guttentag, M.; Baldrige, K. K.; Albertoa, R.; Patzke, G. R. *Green Chem.* **2012**, *14*, 1680-1688.
- (63) Anderson, T. M.; Fang, X.; Mbomekalle, I. M.; Keita, B.; Nadjo, L.; Hardcastle, K. I.; Farsidjani, A.; Hill, C. L. *J. Cluster Sci.* **2006**, *17*, 183-195.
- (64) Anderson, T. M.; Hardcastle, K. I.; Okun, N.; Hill, C. L. *Inorg. Chem.* **2001**, *40*, 6418-6425.
- (65) Bi, L.-H.; Hou, G.-F.; Li, B.; Wu, L.-X.; Kortz, U. *Dalton Trans.* **2009**, 6345-6353.
- (66) Kortz, U.; Isber, S.; Dickman, M. H.; Ravot, D. *Inorg. Chem.* **2000**, *39*, 2915-2922.
- (67) Lv, H.; Geletii, Y. V.; Zhao, C.; Vickers, J. W.; Zhu, G.; Luo, Z.; Song, J.; Lian, T.; Musaev, D. G.; Hill, C. L. *Chem. Soc. Rev.* **2012**, *41*, 7572-7589.
- (68) Hou, D.; Hagen, K. S.; Hill, C. L. *J. Am. Chem. Soc.* **1992**, *114*, 5864-5866.
- (69) Pettersson, L.; Andersson, I.; Howarth, O. W. *Inorg. Chem.* **1992**, *31*, 4032-4033.
- (70) Howarth, O. W.; Jarrold, M. J. *Chem. Soc., Dalton Trans.* **1978**, 503-506.
- (71) Druskovich, D. M.; Kepert, D. L. *J. Chem. Soc., Dalton Trans.* **1975**, 947-951.
- (72) Roman, P.; Aranzabe, A.; Luque, A.; Gutierrezorrilla, J. M.; Martinezripoll, M. J. *Chem. Soc., Dalton Trans.* **1995**, 2225-2231.
- (73) Kato, R.; Kobayashi, A.; Sasaki, Y. *Inorg. Chem.* **1982**, *21*, 240-246.
- (74) Flynn, C. M., Jr.; Pope, M. T. *Inorg. Chem.* **1970**, *9*, 2009-2014.
- (75) Ichida, H.; Nagai, K.; Sasaki, Y.; Pope, M. T. *J. Am. Chem. Soc.* **1989**, *111*, 586-591.
- (76) Hill, C. L.; Anderson, T. M.; Han, J.; Hillesheim, D. A.; Geletii, Y. V.; Okun, N. M.; Cao, R.; Botar, B.; Musaev, D. G.; Morokuma, K. *J. Mol. Catal. A: Chem.* **2006**, *251*, 234-238.
- (77) Chen, Q.; Zubieta, J. J. *J. Chem. Soc., Chem. Commun.* **1993**, 1180-1182.
- (78) Müller, A.; Meyer, J.; Bogge, H.; Stammler, A.; Botar, A. *Z. Anorg. Allg. Chem.* **1995**, *621*, 1818-1831.
- (79) Hou, D.; Kim, G.-S.; Hagen, K. S.; Hill, C. L. *Inorg. Chim. Acta* **1993**, *211*, 127-130.
- (80) Gao, Y.; Chi, Y.; Hu, C. *Polyhedron* **2014**, *83*, 242-258.

- (81) Han, J. W.; Hill, C. L. *J. Am. Chem. Soc.* **2007**, *129*, 15094-15095.
- (82) Nyman, M.; Alam, T. M.; Bonhomme, F.; Rodriguez, M. A.; Frazer, C. S.; Welk, M. *E. J. Cluster Sci.* **2006**, *17*, 197-219.
- (83) Bonhomme, F.; Larentzos, J. P.; Alam, T. M.; Maginn, E. J.; Nyman, M. *Inorg. Chem.* **2005**, *44*, 1774-1785.
- (84) Nyman, M.; Bonhomme, F.; Alam, T. M.; Rodriguez, M. A.; Cherry, B. R.; Krumhansl, J. L.; Nenoff, T. M.; Sattler, A. M. *Science* **2002**, *297*, 996-998.
- (85) Shen, J.-Q.; Zhang, Y.; Zhang, Z.-M.; Li, Y.-G.; Gao, Y.-Q.; Wang, E.-B. *Chem. Commun.* **2014**, *50*, 6017-6019.
- (86) Niu, J.; Ma, P.; Niu, H.; Li, J.; Zhao, J.; Song, Y.; Wang, J. *Chem. - Eur. J.* **2007**, *13*, 8739-8748.
- (87) Barnard, D. L.; Hill, C. L.; Gage, T.; Matheson, J. E.; Huffman, J. H.; Sidwell, R. W.; Otto, M. I.; Schinazi, R. F. *Antiviral Res.* **1997**, *34*, 27-37.
- (88) Hill, C. L.; Weeks, M. S.; Schinazi, R. F. *J. Med. Chem.* **1990**, *33*, 2767-2772.
- (89) Schinazi, R. F.; Sijbesma, R.; Srdanov, G.; Hill, C. L.; Wudl, F. *Antimicrob. Agents Chemother.* **1993**, *37*, 1707-1710.
- (90) Shigeta, S.; Mori, S.; Watanabe, J.; Baba, M.; Khenkin, A. M.; Hill, C. L.; Schinazi, R. F. *Antiviral Chem. Chemother.* **1995**, *6*, 114-122.
- (91) Fukuda, N.; Yamase, T. *Biol. Pharm. Bull.* **1997**, *20*, 927-930.
- (92) Hasenknopf, B. *Front. Biosci.* **2005**, *10*, 275-287.
- (93) Rhule, J. T.; Hill, C. L.; Judd, D. A.; Schinazi, R. F. *Chem. Rev.* **1998**, *98*, 327-357.
- (94) Lee, I. S.; Long, J. R.; Prusiner, S. B.; Safar, J. G. *J. Am. Chem. Soc.* **2005**, *127*, 13802-13803.
- (95) Clemente-Juan, J. M.; Coronado, E. *Chem. Rev.* **1999**, *193-195*, 361-394.
- (96) Coronado, E.; Galan-Mascaros, J. R.; Gimenez-Saiz, C.; Gomez-Garcia, C. J.; Triki, S. *J. Am. Chem. Soc.* **1998**, *120*, 4671-4681.
- (97) Speldrich, M.; Schilder, H.; Lueken, H.; Kögerler, P. *Isr. J. Chem.* **2011**, *51*, 215-227.

- (98) Müller, A.; Das, S. K.; Talismanova, M. O.; Bogge, H.; Kogerler, P.; Schmidtman, M.; Talismanov, S. S.; Luban, M.; Krickemeyer, E. *Angew. Chem. Int. Ed.* **2002**, *41*, 579-582.
- (99) Kögerler, P.; Tsukerblat, B.; Müller, A. *Dalton Trans.* **2010**, *39*, 21-36.
- (100) Zhao, C.; Huang, Z.; Rodríguez-Córdoba, W.; Kambara, C. S.; O'Halloran, K. P.; Hardcastle, K. I.; Musaev, D. G.; Lian, T.; Hill, C. L. *J. Am. Chem. Soc.* **2011**, *133*, 20134-20137.
- (101) Zhao, C.; Kambara, C. S.; Glass, E. N.; Hill, C. L. In *244th ACS National Meeting & Exposition, August 19-23, 2012, INOR-749*. Philadelphia, PA, 2012.
- (102) Glass, E. N.; Fielden, J.; Kaledin, A. L.; Musaev, D. G.; Lian, T.; Hill, C. L. *Chem.-Eur. J.* **2014**, *20*, 4297-4307.
- (103) Katsoulis, D. E. *Chem. Rev.* **1998**, *98*, 359-388.
- (104) Misono, M. *Kagaku No Ryoiki* **1981**, *35*, 519-526.
- (105) Izumi, Y.; Hasebe, R.; Urabe, K. *J. Catal.* **1983**, *84*, 402-409.
- (106) Hill, C. L.; Bouchard, D. A. *J. Am. Chem. Soc.* **1985**, *107*, 5148-5157.
- (107) Hill, C. L.; Brown, R. B., Jr.; Renneke, R. F. *Prepr. Am. Chem. Soc. Div. Pet. Chem.* **1987**, *32*, 205-209.
- (108) Domen, K. *Kikan Kagaku Sosetsu* **1993**, *20*, 170-176.
- (109) Misono, M. In *Polyoxometalates: From Platonic Solids to Anti-retroviral Activity*; Pope, M. T., Müller, A., Eds.; Kluwer Academic Publishers: Dordrecht, Netherlands, 1993, p 255-265.
- (110) Wang, S.-S.; Yang, G.-Y. *Chem. Rev.* **2015**, *115*, 4893-4962.
- (111) Sheldon, R. A.; Kochi, J. K.; Academic Press: New York, 1981.
- (112) Hill, C. L. *Nature* **1999**, *401*, 436-437.
- (113) Neumann, R. In *Transition Metals for Organic Synthesis (2nd Edition)*; Beller, M., Bolm, C., Eds.; Wiley-VCH: Weinheim, 2004; Vol. 2, p 415-426.
- (114) Neumann, R. *Mod. Oxidation Methods* **2004**, 223-251.
- (115) Black, J. F. *J. Am. Chem. Soc.* **1978**, *100*, 527-535.
- (116) Partenheimer, W. *Catal. Today* **1995**, *23*, 69-157.

- (117) Rhule, J. T.; Neiwert, W. A.; Hardcastle, K. I.; Do, B. T.; Hill, C. L. *J. Am. Chem. Soc.* **2001**, *123*, 12101-12102.
- (118) Okun, N. M.; Anderson, T. M.; Hill, C. L. *J. Mol. Catal. A: Chem.* **2003**, *197*, 283-290.
- (119) Hill, C. L.; Delannoy, L.; Duncan, D. C.; Weinstock, I. A.; Renneke, R. F.; Reiner, R. S.; Atalla, R. H.; Han, J. W.; Hillesheim, D. A.; Cao, R.; Anderson, T. M.; Okun, N. M.; Musaev, D. G.; Geletii, Y. V. *C. R. Chimie.* **2007**, *10*, 305-312.
- (120) Guo, W.; Luo, Z.; Song, J.; Zhu, G.; Zhao, C.; Lv, H.; Vickers, J. W.; Geletii, Y. V.; Musaev, D. G.; Hill, C. L. In *Complexity in Chemistry and Beyond: Interplay Theory and Experiment*; Hill, C. L., Musaev, D. G., Eds.; Springer: 2012, p 229-242.
- (121) Chen, M. S.; Goodman, D. W. *Science* **2004**, *306*, 252-255.
- (122) Chen, M.; Cai, Y.; Yan, Z.; Goodman, D. W. *J. Am. Chem. Soc.* **2006**, *128*, 6341-6346.
- (123) Guzman, J.; Gates, B. C. *J. Am. Chem. Soc.* **2004**, *126*, 2672-2673.
- (124) Kulkarni, A.; Lobo-Lapidus, R. J.; Gates, B. C. *Chem. Commun.* **2010**, *46*, 5997-6015.
- (125) Kim, W. B.; Voitl, T.; Rodriguez-Rivera, G. J.; Dumesic, J. A. *Science* **2004**, *305*, 1280-1283.
- (126) Soares, J. M. C.; Bowker, M. *Appl. Catal., A* **2005**, *291*, 136-144.
- (127) Hill, C. L.; Prosser-McCartha, C. M. *Coord. Chem. Rev.* **1995**, *143*, 407-455.
- (128) Neumann, R. *Prog. Inorg. Chem.* **1998**, *47*, 317-370.
- (129) Mizuno, N.; Misono, M. *Chem. Rev.* **1998**, *98*, 199-218.
- (130) Okuhara, T.; Mizuno, N.; Misono, M. *Appl. Catal., A* **2001**, *222*, 63-77.
- (131) Nakagawa, Y.; Kamata, K.; Kotani, M.; Yamaguchi, K.; Mizuno, N. *Angew. Chem. Int. Ed.* **2005**, *44*, 5136-5141.
- (132) Hill, C. L. In *Comprehensive Coordination Chemistry-II: From Biology to Nanotechnology*; Wedd, A. G., Ed.; Elsevier Ltd.: Oxford, UK, 2004; Vol. 4, p 679-759.

- (133) Misono, M. In *Chem. Uses Molybdenum, Proc. Int. Conf.*; Barry, H. F., Mitchell, P. C. H., Eds.; Climax Molybdenum Co. Mich., Ann Arbor, Mich.: 1982; Vol. 4th, p 289-295.
- (134) Chuvaev, V. F.; Sagalovich, V. P. *Fiz. khim. Osnovy Prakt. Ispol'z. Izo i Geteropolisoedin., Dnepropetrovsk* **1983**, 136-145.
- (135) Yamase, T. *Yuki Gosei Kagaku Kyokaiishi (In Japanese)* **1985**, 43, 249-261.
- (136) Ono, Y. In *Perspective in Catalysis*; Thomas, J. M., Zamaraev, K. I., Eds.; Blackwell: Oxford, UK, 1992, p 431-464.
- (137) Streb, C. *Dalton Trans.* **2012**, 41, 1651-1659.
- (138) Kozhevnikov, I. V. *J. Mol. Catal. A: Chem.* **1997**, 117, 151-158.
- (139) Boring, E.; Geletii, Y. V.; Hill, C. L. *J. Am. Chem. Soc.* **2001**, 123, 1625-1635.
- (140) Boring, E.; Geletii, Y. V.; Hill, C. L. In *Advances in Catalytic Activation of Dioxygen by Metal Complexes*; Simandi, L. I., Ed.; Kluwer Academic Publishers: Dordrecht, 2003; Vol. 26, p 227-264.
- (141) Kholdeeva, O. A.; Timofeeva, M. N.; Maksimov, G. M.; Maksimovskaya, R. I.; Neiwert, W. A.; Hill, C. L. *Inorg. Chem.* **2005**, 44, 666-672.
- (142) Yang, Y. C.; Baker, J. A.; Ward, J. R. *Chem. Rev.* **1992**, 92, 1729-1743.
- (143) Kinnan, M. K.; Creasy, W. R.; Fullmer, L. B.; Schreuder-Gibson, H. L.; Nyman, M. *Eur. J. Inorg. Chem.* **2014**, 2361-2367.
- (144) Mizrahi, D. M.; Saphier, S.; Columbus, I. *J. Haz. Mater.* **2010**, 179, 495-499.
- (145) Shi, Z.; Kong, Z.-G.; Wang, Q.-W.; Li, C.-B. *Inorg. Chem. Commun.* **2012**, 20, 131-134.
- (146) Maksimchuk, N. V.; Kholdeeva, O. A.; Kovalenko, K. A.; Fedin, V. P. *Isr. J. Chem.* **2011**, 51, 281-289.
- (147) Ma, F.-J.; Liu, S.-X.; Sun, C.-Y.; Liang, D.-D.; Ren, G.-J.; Wei, F.; Chen, Y.-G.; Su, Z.-M. *J. Am. Chem. Soc.* **2011**, 133, 4178-4181.
- (148) Fu, H.; Li, Y.; Lu, Y.; Chen, W.; Wu, Q.; Meng, J.; Wang, X.; Zhang, Z.; Wang, E. *Cryst. Growth Des.* **2011**, 11, 458-465.

- (149) Yu, F.; Zheng, P.-Q.; Long, Y.-X.; Ren, Y.-P.; Kong, X.-J.; Long, L.-S.; Yuan, Y.-Z.; Huang, R.-B.; Zheng, L.-S. *Eur. J. Inorg. Chem.* **2010**, 4526-4531.
- (150) Pang, H.-j.; Peng, J.; Zhang, C.-j.; Li, Y.-g.; Zhang, P.-p.; Ma, H.-y.; Su, Z.-m. *Chem. Commun.* **2010**, 46, 5097-5099.
- (151) Rodriguez-Albelo, L. M.; Ruiz-Salvador, A. R.; Sampieri, A.; Lewis, D. W.; Gómez, A.; Nohra, B.; Mialane, P.; Marrot, J.; S écheresse, F.; Mellot-Draznieks, C.; Biboum, R. N.; Keita, B.; Nadjjo, L.; Dolbecq, A. *J. Am. Chem. Soc.* **2009**, *131*, 16078–16087.
- (152) Song, J.; Luo, Z.; Britt, D.; Furukawa, H.; Yaghi, O. M.; Hardcastle, K. I.; Hill, C. L. *J. Am. Chem. Soc.* **2011**, *133*, 16839-16846.
- (153) Okun, N. M.; Tarr, J. C.; Hilleshiem, D. A.; Zhang, L.; Hardcastle, K. I.; Hill, C. L. *J. Mol. Catal. A. Chem.* **2006**, *246*, 11-17.
- (154) Mart ín, S. E.; Rossi, L. I. *Tetrahedron Lett.* **2001**, *42*, 7147-7151.
- (155) Firouzabadi, H.; Iranpour, N.; Zolfigol, M. A. *Synth. Commun.* **1998**, *28*, 1179-1187.
- (156) Luo, Z.; Geletii, Y. V.; Hillesheim, D. A.; Wang, Y.; Hill, C. L. *ACS Catal.* **2011**, *1*, 1364-1370.
- (157) Yang, Y.; Wu, Q.; Guo, Y.; Hu, C.; Wanga, E. *J. Mol. Catal. A: Chem.* **2005**, *225*, 203-212.
- (158) Qua, X.; Guo, Y.; Hu, C. *J. Mol. Catal. A: Chem.* **2007**, *262*, 128-135.
- (159) Ji, K. H.; Jang, D. M.; Cho, Y. J.; Myung, Y.; Kim, H. S.; Kim, Y.; Park, J. J. *Phys. Chem. C* **2009**, *113*, 19966-19972.
- (160) Xu, L.-J.; Zhou, W.-Z.; Zhang, L.-Y.; Li, B.; Zang, H.-Y.; Wang, Y.-H.; Li, Y.-G. *CrystEngComm* **2015**, *17*, 3708-3714.
- (161) Lei, P.; Chen, C.; Yang, J.; Ma, W.; Zhao, J.; Zang, L. *Environ. Sci. Technol.* **2005**, *39*, 8466-8474.
- (162) Hao, H.-F.; Zhou, W.-Z.; Zang, H.-Y.; Tan, H.-Q.; Qi, Y.-F.; Wang, Y.-H.; Li, Y.-G. *Chemistry – An Asian Journal* **2015**, *10*, 1676-1683.
- (163) Chow, J.; Kopp, R. J.; Portney, P. R. *Science* **2003**, *302*, 1528-1531.

- (164) Lewis, N. S.; Nocera, D. G. *Proc. Natl. Acad. Sci.* **2006**, *103*(43), 15729-15735.
- (165) Balzani, V.; Credi, A.; Venturi, M. *ChemSusChem* **2008**, *1*, 26-58.
- (166) Gray, H. B. *Nat. Chem.* **2009**, *1*, 7-7.
- (167) Cook, T. R.; Dogutan, D. K.; Reece, S. Y.; Surendranath, Y.; Teets, T. S.; Nocera, D. G. *Chem. Rev.* **2010**, *110*, 6474-6502.
- (168) Hammarstrom, L.; Hammes-Schiffer, S. *Acc. Chem. Res.* **2009**, *42*, 1859-1860.
- (169) Lv, H.; Chi, Y.; Leusen, J. v.; Kögerler, P.; Chen, Z.; Bacsa, J.; Guo, W.; Lian, T.; Hill, C. L. *Chem. Eur. J.* **2015**, *21*, Published online 8 Oct 2015.
- (170) Lv, H.; Guo, W.; Wu, K.; Chen, Z.; Bacsa, J.; Musaev, D. G.; Geletii, Y. V.; Lauinger, S. M.; Lian, T.; Hill, C. L. *J. Am. Chem. Soc.* **2014**, *136*, 14015-14018.
- (171) Lv, H.; Song, J.; Zhu, H.; Geletii, Y. V.; Bacsa, J.; Zhao, C.; Lian, T.; Musaev, D. G.; Hill, C. L. *J. Catal.* **2013**, *307*, 48-54.
- (172) Yin, Q.; Tan, J. M.; Besson, C.; Geletii, Y. V.; Musaev, D. G.; Kuznetsov, A. E.; Luo, Z.; Hardcastle, K. I.; Hill, C. L. *Science* **2010**, *328*, 342-345.
- (173) Vickers, J. W.; Lv, H.; Sumliner, J. M.; Zhu, G.; Luo, Z.; Musaev, D. G.; Geletii, Y. V.; Hill, C. L. *J. Am. Chem. Soc.* **2013**, *135*, 14110-14118.
- (174) Lv, H.; Song, J.; Geletii, Y. V.; Vickers, J. W.; Sumliner, J. M.; Musaev, D. G.; Kögerler, P.; Zhuk, P. F.; Bacsa, J.; Zhu, G.; Hill, C. L. *J. Am. Chem. Soc.* **2014**, *136*, 9268-9271.

Chapter 2.

Introduction:

Polyvanadotungstates for Aerobic Oxidation of Formaldehyde under ambient conditions

Reproduced with permission from *ACS Catal.*, **2014**, 4(4), 1154-1161. Copyright 2014 American Chemical Society

As a main contributor of this work; with Zhen Luo, Hongjin Lv, and Craig L. Hill*, W. Guo contributed the syntheses, characterizations, investigating and analyzing the catalysts' activities to this work. Z. Luo designed the formaldehyde detection method. H. Lv conducted the NMR measurements. W. Guo and C. L. Hill designed the experiments and prepared the manuscript.

2.1 Introduction

Formaldehyde (CH₂O) is a toxic compound that is ubiquitous in human environments. As a consequence, it is of central concern in context with human health and also high on the list of toxic industrial chemicals (TICs).¹ The long-term exposure to formaldehyde may cause irritation of the mucous membranes of the eyes and is associated with diseases of the nasal and respiratory tract.² It was classified as a known carcinogen by the State of California and the World Health Organization in 2004.³⁻¹¹ Thus, the removal of formaldehyde is a crucial goal for researchers.

Air-based catalytic organic oxidations have gained much attention recently, because they utilize only ambient O₂ which is less expensive and more abundant than other oxidants while generating few if any deleterious by-products if appropriate catalysts can be developed.¹²⁻²⁴ Moreover, aerobic organic oxidation reactions are highly attractive for decontamination of a wide variety of toxic compounds in human environments, including TICs^{20,25-29} and chemical warfare agents (CWAs)^{23,30} under mild conditions. Therefore, the aerobic catalytic oxidation of formaldehyde to formic acid, CO and/or CO₂ under ambient conditions is highly attractive from multiple vantages.²⁸

Generally, mixtures of metal oxides,³¹ precious metals³² and supported precious metals³³⁻³⁶ have been evaluated as catalysts for the oxidation of formaldehyde. Among the metal oxides, MnO₂ has been shown to have a high reactivity for formaldehyde oxidation at moderate conversions.^{31,32,37,38} Precious metals such as Au, Ru, Rh and Pt have been found to be effective catalysts for formaldehyde conversion at moderate temperature.³⁹⁻⁴² For example, Zhang *et al.* and Huang *et al.* reported that the Pt nanoparticles supported on TiO₂ are an effective catalyst for formaldehyde oxidation at room temperature,^{43,44} while catalysts such as Au and Ag supported on

TiO₂, CeO₂, Al₂O₃, MnO_x-CeO₂ and SBA-15 effect formaldehyde oxidation with almost 100% conversion at temperatures of 373 K or higher.^{45,46} Unfortunately, most of the systems reported so far are either based on precious metals which are prohibitively expensive for practical applications and not readily available, or involve catalytic oxidations that must be performed at temperatures of 400 K to 500 K or higher. However, logistics considerations dictate that many TIC and CWA decontamination and deodorization technologies are far more useful if applicable under ambient conditions.

The second class of catalysts developed for the aerobic oxidation of formaldehyde under ambient conditions (using air at room temperature) are polyoxometalates (POMs), and in particular POMs with 3d metals substituted in surface positions.^{28,29,47,48} As elaborated in Chapter 1, POMs are a very large and growing family of metal oxide clusters with versatile applications in many areas including catalysis.⁴⁹⁻⁵⁴ In particular, organic oxidations catalyzed by POMs have received much attention because the acid-base and redox properties of POMs are highly tunable.^{51,55} In addition, POMs are thermally, oxidatively and hydrolytically stable under oxidative conditions.^{51,56} In 2004, Kholdeeva, Hill and their coworkers reported that supported Keggin-type Co-containing POMs, [n-Bu₄N]₄HPW₁₁CoO₃₉ and [n-Bu₄N]₅PW₁₁CoO₃₉ were effective catalysts for the aerobic oxidation of aldehydes (including formaldehyde) under ambient conditions.⁴⁷ In 2005, they reported the catalytic activity of the Keggin-type Ce-containing POM (NaH₃[SiW₁₁Ce^{IV}O₃₉]) for the aerobic oxidation of formaldehyde.²⁸ The Ce-containing POM was shown to be a selective and effective catalyst for production of formic acid with a CH₂O conversion of *ca.* 20% under mild conditions. Vanadium-substituted heteropolyanions, PMO_{12-n}V_nO₄₀⁽³⁺ⁿ⁾⁻ (**PMO_{12-n}V_n**) and PW_{12-n}V_nO₄₀⁽³⁺ⁿ⁾⁻ (**PW_{12-n}V_n**) (with n = 1-6).⁵⁷⁻⁶¹ have been reported to catalyze the

aerobic oxidation of many organic compounds including ketones and aldehydes (some of which are TICs) under ambient conditions.^{53,58,60,62-72} However, formaldehyde oxidation under ambient conditions catalyzed by polyvanadotungstates is unknown.

We report here that the TBA salts of polyvanadotungstates, $[n\text{-Bu}_4\text{N}]_6[\text{PW}_9\text{V}_3\text{O}_{40}]$ (**PW₉V₃**), $[n\text{-Bu}_4\text{N}]_5\text{H}_2\text{PW}_8\text{V}_4\text{O}_{40}$ (**PW₈V₄**), $[n\text{-Bu}_4\text{N}]_4\text{H}_5\text{PW}_6\text{V}_6\text{O}_{40}\cdot 20\text{H}_2\text{O}$ (**PW₆V₆**) POMs are efficient catalysts for the aerobic oxidation of formaldehyde to formic acid under ambient conditions (using only air at room temperature). Comparison of four POMs ($[n\text{-Bu}_4\text{N}]_5[\text{W}_3\text{V}_3\text{O}_{19}]$, $[n\text{-Bu}_4\text{N}]_3\text{H}_3\text{V}_{10}\text{O}_{28}$, $[n\text{-Bu}_4\text{N}]_7\text{SiW}_9\text{V}_3\text{O}_{40}$, $[n\text{-Bu}_4\text{N}]_9\text{P}_2\text{W}_{15}\text{V}_3\text{O}_{62}$), each with extensive and reversible redox chemistry, confirms that the catalytic activity is derived from the polyanion properties (structure, V(V/VI) potential, etc.). Importantly, these formaldehyde removal reactions are less inhibited by water than these same oxidations catalyzed by supported noble metals. Under optimized conditions, a turnover number (TON) of *ca.* 57 is obtained with **PW₆V₆**.

2.2 Experimental

2.2.1 General Methods and Materials

All chemical reagents used were from commercially available sources and were used without further purification unless otherwise noted. The formaldehyde solutions were prepared by diluting 35% of aqueous formalin with acetonitrile (Fluka), *N,N*-dimethylacetamide, *N,N*-dimethylformamide or tetrahydrofuran as needed for each catalytic entry. Infrared spectra (2% sample in KBr pellet) were taken on a Nicolet TM 6700 FT-IR spectrometer. UV-vis spectra were acquired by an Agilent 8453 spectrophotometer equipped with a diode-array detector using a 1.0-cm-optical-path quartz cuvette with acetonitrile as the solvent. The thermogravimetric data were collected on a STA 6000 thermal analyzer. Elemental analyses (V and W) were done

by Galbraith Laboratories (Knoxville, Tennessee). ^1H and ^{31}P NMR spectra were acquired on a Varian INOVA 400 spectrometer using deuterated chloroform (δ 7.24 ppm) and H_3PO_4 (δ 0 ppm) as external standards. Gas chromatography (GC) analyses of liquid phase was performed on a Hewlett-Packard 6890 with a 5% phenyl methyl silicone capillary column (while the formic acid was independently detected with a Agilent J&W DB-FFAP column), a flame ionization detector, a Hewlett-Packard 3390A series integrator and N_2 as the carrier gas. The gas phase was analyzed using a Agilent 7890 gas chromatograph with a 5 Å molecular sieve column and argon carrier gas.

2.2.2 Preparation of Catalysts

Synthesis of $[n\text{-Bu}_4\text{N}]_6[\alpha\text{-}1,2,3\text{-PW}_9\text{V}_3\text{O}_{40}]$, (PW_9V_3). The TBA salt of the vanadium-substituted Keggin-type POM, was prepared by a modified literature method.⁷³ In a typical preparation, 8.2 g sodium acetate (100 mmol) in 6 mL of acetic acid was added to 100 mL of distilled water until a pH of approximately 5.0 was reached. To this solution, sodium metavanadate (3.05 g, 25 mmol) and $\text{Na}_9[\text{A-PW}_9\text{O}_{34}]$ (20 g, 8.2 mmol) were added. The solution was stirred for 24 h and filtered. Subsequently, TBABr (15 g, 48 mmol) in 20 mL distilled water was added to the solution to produce a light orange product (17.7 g, 54% yield based on vanadium) whose purity was confirmed by FT-IR spectroscopy. FT-IR (2000-500 cm^{-1} , KBr, cm^{-1}): 1482 (m), 1462 (sh), 1380 (w), 1152 (w), 1087 (s), 1053 (w), 1029 (sh), 994 (w), 949 (s), 879 (s), 792 (s), 732 (sh), 598 (w), 510 (w). The number of TBA cations was determined by TGA analysis. Elemental analysis (calcd/found): W 42.3/44.1, V 3.9/4.2.

Synthesis of $[n\text{-Bu}_4\text{N}]_5\text{H}_2\text{PW}_8\text{V}_4\text{O}_{40}$ (PW_8V_4). The TBA salt of the vanadium-substituted Keggin-type POM, was prepared by metathesis of $(\text{NH}_4)_6\text{HPW}_8\text{V}_4\text{O}_{40}\cdot 9\text{H}_2\text{O}$ ⁷⁴ with TBABr in distilled water. Typically, 0.483 g TBABr

(15 mmol) was added to an aqueous solution of $(\text{NH}_4)_6\text{HPW}_8\text{V}_4\text{O}_{40}\cdot 9\text{H}_2\text{O}$ (0.197 g, 0.1 mmol). The precipitate was centrifuged and washed with distilled water to remove excess TBABr. The product was recrystallized three times from acetonitrile (yield = 0.214 g, 60% yield based on vanadium in $(\text{NH}_4)_6\text{HPW}_8\text{V}_4\text{O}_{40}\cdot 9\text{H}_2\text{O}$). Its purity was confirmed by FT-IR spectroscopy. IR (2000-500 cm^{-1} , KBr, cm^{-1}): 1482 (m), 1380 (w), 1154 (w), 1100 (sh), 1078 (m), 1052 (sh), 950 (s), 882 (s), 789 (s), 595 (w), 509 (w). The number of TBA cations was determined by TGA analysis. Elemental analysis (calcd/found): W 41.5/40.2, V 5.7/5.9.

Synthesis of $[n\text{-Bu}_4\text{N}]_4\text{H}_5\text{PW}_6\text{V}_6\text{O}_{40}\cdot 20\text{H}_2\text{O}$ (PW_6V_6). The TBA salt of the vanadium-substituted Keggin-type POM, was prepared by a similar method as that of PW_8V_4 except that 0.228 g $(\text{NH}_4)_5\text{H}_4\text{PW}_6\text{V}_6\text{O}_{40}\cdot 6\text{H}_2\text{O}^{74}$ was used; yield = 0.167 g (49% yield based on vanadium in $(\text{NH}_4)_5\text{H}_4\text{PW}_6\text{V}_6\text{O}_{40}\cdot 6\text{H}_2\text{O}$). Its purity was confirmed by FT-IR spectroscopy. IR (2000-500 cm^{-1} , KBr, cm^{-1}): 1481(s), 1379 (m), 1152 (w), 1074 (m), 1030 (sh), 949(s), 886 (s), 798 (s), 594 (s), 509 (s). The number of TBA cations was determined by TGA analysis. Elemental analysis (calcd/found): W 32.0/31.4, V 8.9/8.6.

2.2.3 Preparation of $[n\text{-Bu}_4\text{N}]_5[\text{W}_3\text{V}_3\text{O}_{19}]$, $[n\text{-Bu}_4\text{N}]_3\text{H}_3\text{V}_{10}\text{O}_{28}$, $[n\text{-Bu}_4\text{N}]_7\text{SiW}_9\text{V}_3\text{O}_{40}$, $[n\text{-Bu}_4\text{N}]_9\text{P}_2\text{W}_{15}\text{V}_3\text{O}_{62}$, $[n\text{-Bu}_4\text{N}]_5\text{PW}_{11}\text{CoO}_{39}$ and $[n\text{-Bu}_4\text{N}]_4[\text{SiW}_{11}\text{Ce}^{\text{IV}}\text{O}_{39}]$

$[n\text{-Bu}_4\text{N}]_5[\text{W}_3\text{V}_3\text{O}_{19}]$ and $[n\text{-Bu}_4\text{N}]_4[\text{SiW}_{11}\text{Ce}^{\text{IV}}\text{O}_{39}]$ were prepared by metathesis of $(\text{NH}_4)_2\text{Na}_3[\text{W}_3\text{V}_3\text{O}_{19}]\cdot 20\text{H}_2\text{O}$ and $\text{NaH}_3[\text{SiW}_{11}\text{Ce}^{\text{IV}}\text{O}_{39}]$ with TBABr in distilled water.^{28,75} $[n\text{-Bu}_4\text{N}]_3\text{H}_3\text{V}_{10}\text{O}_{28}$, $[n\text{-Bu}_4\text{N}]_7\text{SiW}_9\text{V}_3\text{O}_{40}$, $[n\text{-Bu}_4\text{N}]_9\text{P}_2\text{W}_{15}\text{V}_3\text{O}_{62}$ and $[n\text{-Bu}_4\text{N}]_5\text{PW}_{11}\text{CoO}_{39}$ were prepared following literature methods.^{47,76,77}

2.2.4 Preparation of Internal Standard Acetone-2,4-DNP-Hydrazone Solution

To a solution of 150 mg of 2,4-dinitrophenylhydrazine (97%, 0.74 mmol) in 95 mL of anhydrous acetonitrile was added 5 mL of acetic acid, followed by addition of 50 μ L of aqueous solution of acetone (0.01M). The formed acetone-2,4-DNPH solution was stirred vigorously for at least three days before being used as internal standard solution.

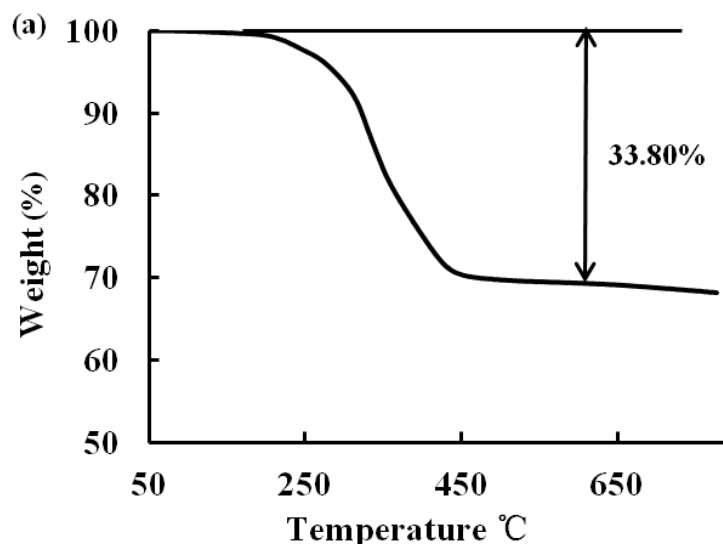
2.2.5 Catalytic Aerobic Oxidative Removal of Formaldehyde

Typical reactions were run in 15-mL glass vessels under ambient conditions (room temperature, 1 atm). The catalytic formaldehyde oxidations were carried out separately in solutions of acetonitrile (CH_3CN)/ H_2O (v/v = 20/1), *N,N*-dimethylacetamide (DMA)/ H_2O (v/v = 20/1), *N,N*-dimethylformamide (DMF)/ H_2O (v/v = 20/1), tetrahydrofuran (THF)/ H_2O (v/v = 20/1). The water in the reaction solutions was supplied by the aqueous formaldehyde (Formalin[®]) solution. Typically, 0.004 mmol of catalyst and 2 mL of solvent containing 0.52 mol/L of formaldehyde were mixed and stirred vigorously. The unreacted formaldehyde was quantified by stoichiometric conversion to the corresponding 2,4-dinitrophenylhydrazone (DNP-hydrazone) derivative using acetone-2,4-hydrazone as the internal standard by gas chromatography (GC). Typically, 10 μ L of the reaction solution was added to 1 mL of the internal standard solution (which contains excess DNPH) and stirred vigorously for 30 minutes. Aliquots were withdrawn from the Schlenk tube, and the unreacted formaldehyde was quantified by gas chromatography. The formic acid was independently analyzed by gas chromatography (GC) using decane as an internal standard. The post-reaction solutions were dried under vacuum, the residue weighed and the catalyst recycled. The products in the reaction using **PW₉V₃** as catalyst in DMA/ H_2O (v/v = 20/1), were also analyzed via ¹H NMR spectroscopy by diluting a 400 μ L aliquot of the reaction solution after 144 h with 400 μ L of deuterated chloroform.

2.3 Results and Discussion

2.3.1 Syntheses and characterization of catalysts

The vanadium-substituted Keggin-type heteropolyanions $\text{PMo}_{12-n}\text{V}_n$ and $\text{PW}_{12-n}\text{V}_n$, with $n = 1-6$, have been synthesized previously by our group⁷⁸⁻⁸¹ and other groups.^{57,59} They are composed of a central PO_4 tetrahedra surrounded by 12 randomly distributed WO_6 and VO_6 metal-oxygen octahedra.⁸² In this work, we prepared the TBA salt of PW_9V_3 by precipitation of the heteropolyanion using an excess of TBABr. The TBA salts of PW_8V_4 and PW_6V_6 were prepared by metathesis of $(\text{NH}_4)_6\text{HPW}_8\text{V}_4\text{O}_{40}\cdot 9\text{H}_2\text{O}$ and $(\text{NH}_4)_5\text{H}_4\text{PW}_6\text{V}_6\text{O}_{40}\cdot 6\text{H}_2\text{O}$ with TBABr in distilled water. TGA analyses confirms the number of TBA counterions in PW_9V_3 , PW_8V_4 and PW_6V_6 (6, 5 and 4 respectively) and that the first two POMs are anhydrous (no feature for loss of hydration water molecules) and the last POM is hydrophilic (feature showing 12% weight loss of hydration water molecules; **Figure 2-1**).



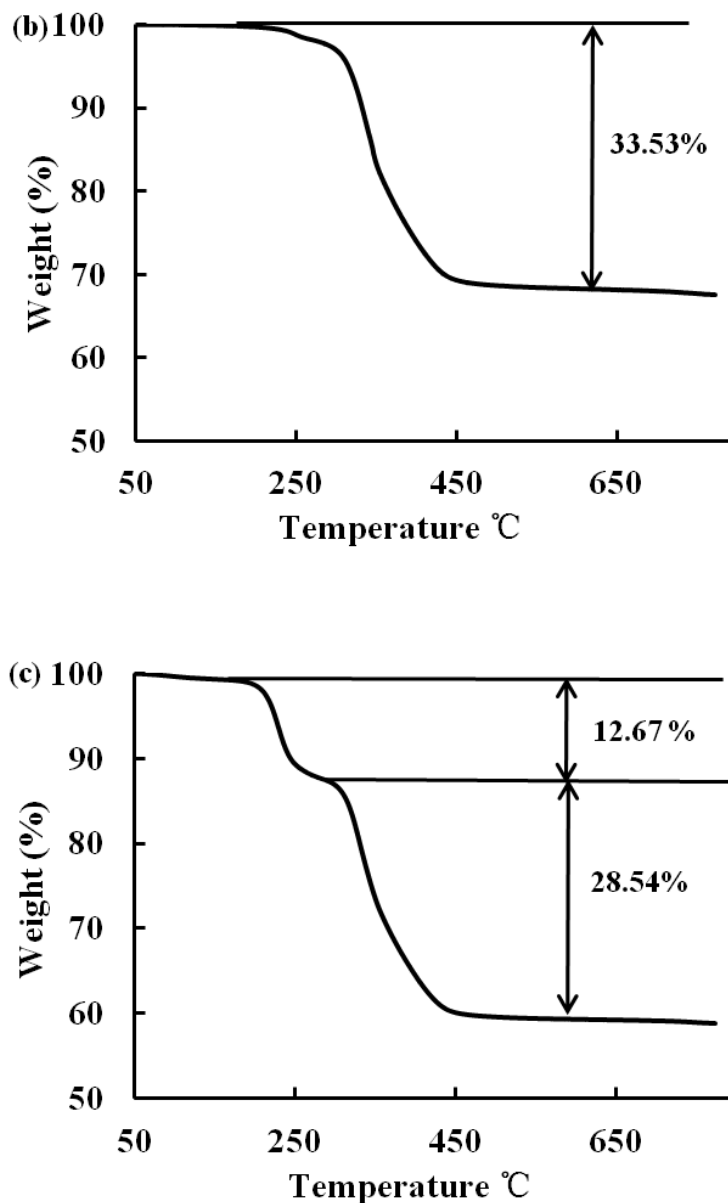


Figure 2-1. Thermogravimetric analysis of (a) PW_9V_3 , (b) PW_8V_4 and (c) PW_6V_6

Figure 2-2 shows the polyhedral structures of the three polyvanadotungstates studied in this work with 3, 4, and 6 vanadium centers, respectively. The compositions of vanadium and tungsten in each compound were determined by elemental analysis. The VO_6 octahedra in each compound are statistically distributed between many positions, especially for compounds synthesized using a one-pot method (e.g. PW_8V_4 and PW_6V_6 in this work). In other words, there are many heteropolyanion positional

isomers, which were identified some time ago for the analogous polyvanadomolybdates.^{58,83} These positional isomers co-crystallize leading to disorder in the solid state and general structural complexity.

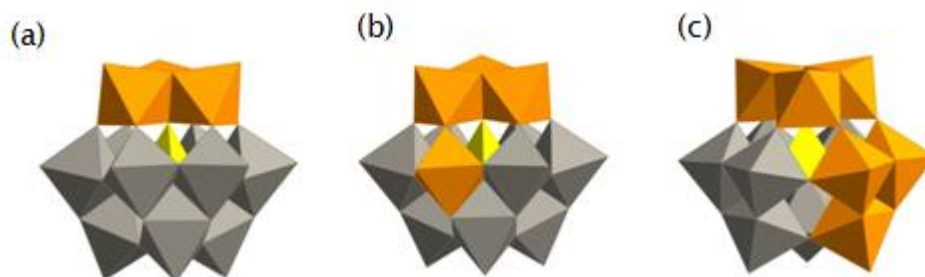


Figure 2-2. Representative polyhedral representations of the vanadium-substituted Keggin-type polyvanadotungstates of (a) PW_9V_3 , (b) PW_8V_4 and (c) PW_6V_6 based on X-ray crystal structures of the parent Keggin POMs. Code: orange octahedra, VO_6 ; yellow tetrahedral, PO_4 ; gray octahedra: WO_6 .

The ^{31}P NMR spectra of PW_9V_3 and PW_8V_4 show one major peak at -44.5 and -41.9 ppm, respectively, confirming the purity of these two compounds (**Figure 2-3**). However, the ^{31}P NMR spectrum of PW_6V_6 shows numerous signals indicating that there exist multiple positional isomers and also different polyvanadotungstates with varying V-to-W ratios (**Figure 2-3**). The formula of $[\textit{n}\text{-Bu}_4\text{N}]_4\text{H}_5\text{PW}_6\text{V}_6\text{O}_{40}\cdot 20\text{H}_2\text{O}$ was based on elemental analysis as well as thermogravimetric analysis. It is common to have multiple positional and compositional isomers in multi-vanadium-containing POMs.^{58,83}

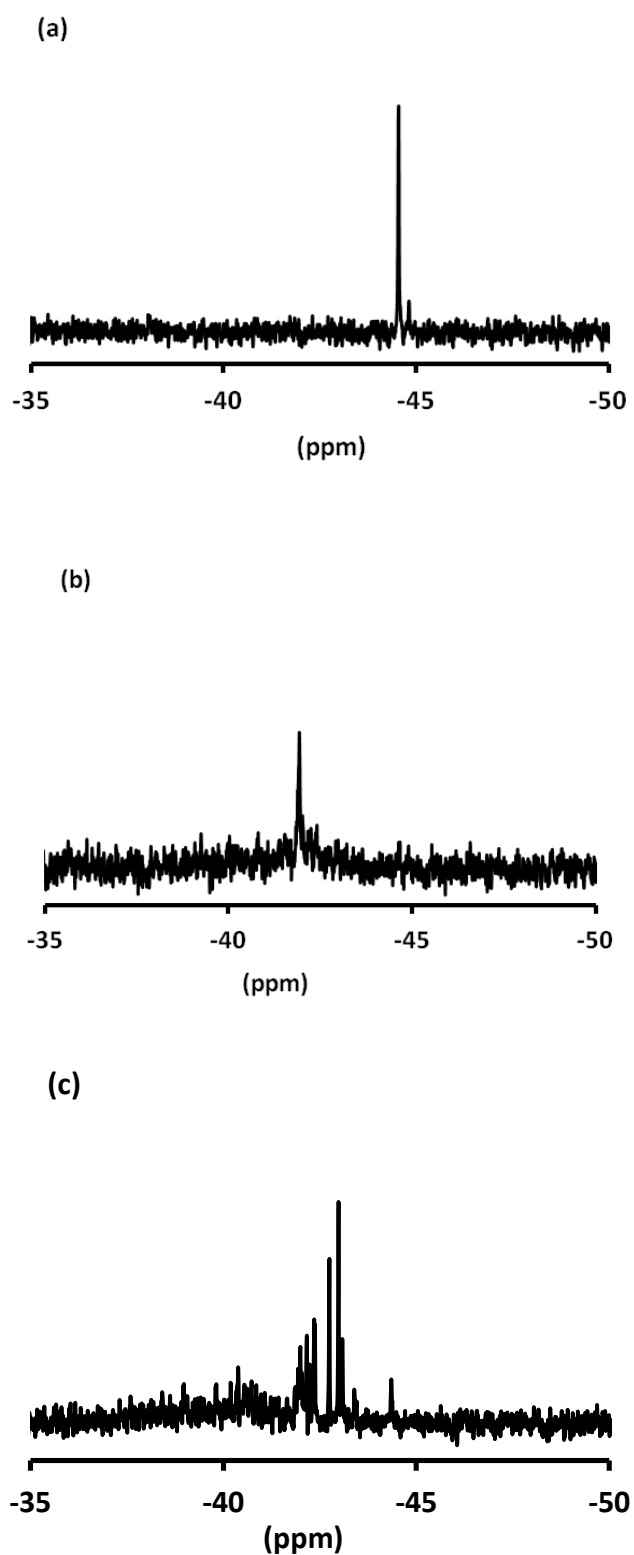


Figure 2-3. ^{31}P NMR of (a) PW_9V_3 , (b) PW_8V_4 and (c) PW_6V_6 with respect to 85% H_3PO_4 (0 ppm)

The FT-IR spectra of **PW₉V₃**, **PW₈V₄** and **PW₆V₆** are very similar and display a fingerprint region that is characteristic of substituted-Keggin-type POMs (**Figure 2-4**). The bands around 1080, 980, 890, 800 and 590 cm^{-1} are related to asymmetric vibrations of P-O_a, W=O_t, W-O_b-W, and W-O_c-W and the bending mode of O_a-P-O_a, respectively. When the tungsten is substituted by vanadium, the band for the P-O_a asymmetric stretch (around 1080 cm^{-1}) splits because of the decrease in structural symmetry. The shift and the split of the P-O_a band, as shown in the spectra, reflect the substitution of tungsten to vanadium.^{82,84} Moreover, the peak around 1100 cm^{-1} in the spectra of **PW₉V₃** exhibits a greater splitting than the corresponding peaks of **PW₈V₄** and **PW₆V₆**, indicating a lower local symmetry and greater deviation from idealized *T_d* symmetry for the former than the latter.

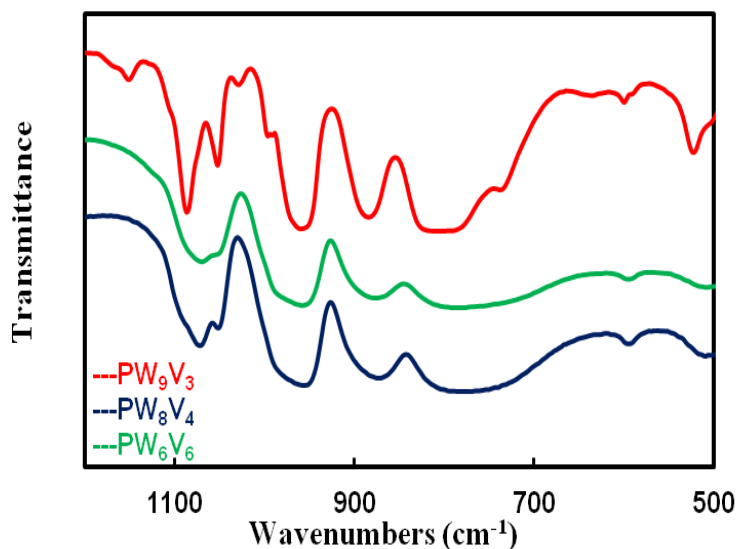


Figure 2-4. FT-IR spectra of **PW₉V₃** (red), **PW₈V₄** (blue) and **PW₆V₆** (green).

The normalized UV-vis absorption spectra of **PW₉V₃**, **PW₈V₄**, and **PW₆V₆** in anhydrous acetonitrile are presented in **Figure 2-5**. The ligand-to-metal charge-transfer (LMCT) band around 350-to-450 nm is attributed to the V(V) center. The corresponding oxo-to-W(VI) band should appear between 250 and 300 nm (not shown).

The new 350-to-450 nm band indicates substitution of W(VI) with V(V). The intensity of this band increases with increasing numbers of vanadium centers in each polyvanadotungstate. Thus color intensity follows the order: **PW₆V₆** (most intense) > **PW₈V₄** > **PW₉V₃** (least intense).

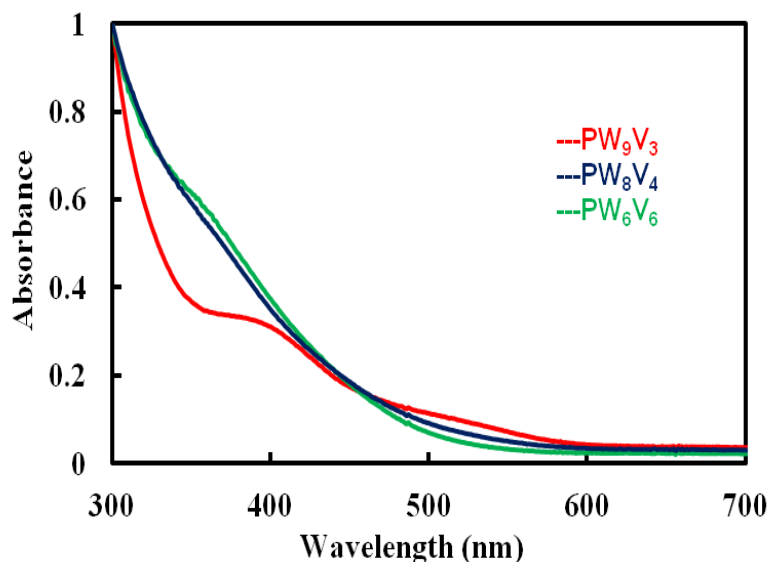


Figure 2-5. Normalized UV-vis absorption spectra of **PW₉V₃** (red), **PW₈V₄** (blue), and **PW₆V₆** (green). Conditions: 0.5 mM in 100% acetonitrile.

2.3.2 Catalytic Aerobic Oxidative Removal of Formaldehyde.

The TBA salts of **PW₉V₃**, **PW₈V₄** and **PW₆V₆** were assessed for their catalytic activity in the aerobic oxidation of formaldehyde to formic acid (**eq 2-1**) under ambient conditions (the O₂ in air at room temperature). Initial studies show that a catalytic amount of (NH₄)₆HPW₈V₄O₄₀·9H₂O added to an aqueous solution of formaldehyde results in oxidation to formic acid; no formaldehyde oxidation products are found in independent control experiments without catalyst. No CO or CO₂ is detected by the gas chromatography.



However, the hydration equilibrium constant (K_{eq} ; **eq 2-2**) for formaldehyde is quite large ($\sim 10^4$ at 20 °C),⁸⁵ indicating that formaldehyde exists primarily in hydrated forms (dihydroxymethane and polymers thereof). This in turn makes it far harder to oxidize. We therefore decided to investigate the effect of different solvents on the reaction conversion by carrying out the reaction at room temperature in the presence of 0.52 M formaldehyde and 4.0 mM catalyst.



The experimental results (**Table 2-1**) show that the reaction conversion for the aerobic oxidation of formaldehyde using **PW₈V₄** increases with solvent system in the following order: THF/H₂O < CH₃CN/H₂O < DMF/H₂O < DMA/H₂O, and this parallels solvent polarity: THF < CH₃CN < DMF < DMA.⁸⁶ In the polar solvent systems of CH₃CN, DMF and DMA, the activity of **PW₈V₄** is higher than that of (NH₄)₆HPW₈V₄O₄₀·9H₂O in aqueous solution. This likely derives in part from the fact that the extent of formaldehyde hydration in the polar solvent systems of CH₃CN, DMF and DMA is lower than that in 100% aqueous solution.⁸⁷ The THF/H₂O mixed solvent system exhibits similar aerobic formaldehyde oxidation activity to pure water with a TON of *ca.* 19. The DMA/H₂O solvent system was used for subsequent experiments because it was the most effective, and DMA, unlike DMF, is not prone to decomposition. The effect of solvent on the reaction (conversion, rates and selectivity) is not easily interpreted for these complex oxidations and was not further addressed in this initial study.

Table 2-1. Aerobic Oxidation of Formaldehyde Catalyzed by **PW₈V₄** in Different Solutions. ^a

Solvent	CH ₂ O Conversion (%) ^b	HCOOH Yield (%) ^c	TON ^d
H ₂ O	15	14	21
DMA/H ₂ O (v/v = 20/1)	35	32	47
CH ₃ CN/H ₂ O (v/v = 20/1)	30	28	43
THF/H ₂ O (v/v = 20/1)	14	14	19
DMF/H ₂ O (v/v = 20/1)	32	31	46

^a Reaction conditions: concentration of formaldehyde = [CH₂O] = 0.52 M, concentration of catalyst = [catalyst] = 4.0 mM, 1 atm of air, 2 mL of solvent, room temperature, 144 h reaction time. ^b CH₂O conversion (%) = moles of CH₂O consumed/moles of initial CH₂O. ^c GC yield based on initial CH₂O. ^d TON = moles of CH₂O consumed/moles of catalyst.

These **PW₈V₄**-catalyzed air-based formaldehyde oxidations were studied as a function of formaldehyde and catalyst concentration (**Table 2-2**) in DMA/H₂O (v/v = 20/1). The optimal solvent system and concentrations (substrate and **PW₈V₄** catalyst) affords a TON of *ca.* 47 (Entry 4 in **Table 2-2**).

Table 2-2. Aerobic Oxidation of Formaldehyde Catalyzed by **PW₈V₄**, as a Function of Substrate and Catalyst Concentration^a

Entry	[PW ₈ V ₄]	Initial [CH ₂ O]	CH ₂ O conversion (%) ^b	TON ^c
1	3.8 mM	0.065 M	12	2

2	3.8 mM	0.130 M	21	7
3	3.8 mM	0.260 M	31	21
4	3.8 mM	0.520 M	35	47
5	7.6 mM	0.520 M	45	31
6	11.4 mM	0.520 M	48	22
7	15.3 mM	0.520 M	47	16
8	19.1 mM	0.520 M	45	12

^a Reaction Conditions: concentration of formaldehyde, [CH₂O] = 65 mM – 520 mM, concentration of catalyst [PW₈V₄] = 3.8 mM – 19.1 mM, 1 atm of air, 2 mL of solvent, ambient temperature, 144 h. ^b CH₂O conversion (%) = moles of CH₂O consumed/moles of initial CH₂O. ^c TON = moles of formaldehyde consumed/moles of catalyst.

Two different aspects of the kinetics of aerobic formaldehyde oxidation by **PW₈V₄**, **PW₆V₆** and **PW₉V₃** in DMA/H₂O (v:v = 20:1) are shown in **Figure 2-6**. All of the catalysts are quite active relative to the control (no activity). Of particular interest, are the aerobic formaldehyde oxidations catalyzed by **PW₈V₄** and **PW₆V₆**; these are faster than those catalyzed by **PW₉V₃** indicating that the number of redox sites V(V/VI) and the number of counterions are significant factors in catalytic activity.²⁹ Some POM-catalyzed oxidation reactions are known to be co-catalyzed by acid. Some more highly protonated POMs are more reactive than less protonated ones despite the fact that higher levels of POM protonation parallel the number of V(V)-for-W(VI) substitutions. The number of these metal substitutions increases the polyanion charge which lowers the POM vanadium(VI/V) potential. This, in turn, lowers the overall organic substrate oxidation rate if POM oxidation of substrate is the rate limiting step in the mechanism.⁵²

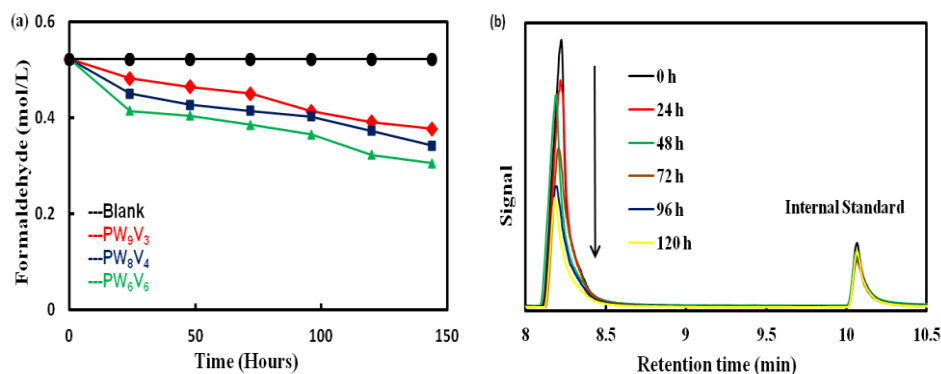
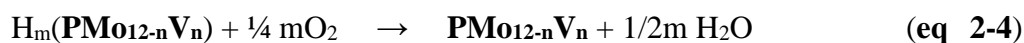
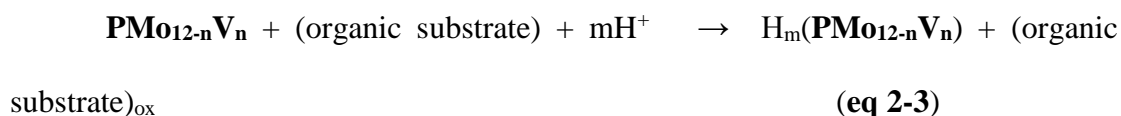


Figure 2-6. (a) Time profile of formaldehyde consumption catalyzed by **PW₉V₃** (red diamonds), **PW₈V₄** (blue squares), **PW₆V₆** (green triangles) and blank (black circles) in DMA/H₂O (v/v = 20/1). (b) The formaldehyde DNP-hydrazone peaks as detected by GC at various time points over 120 h using **PW₉V₃** as the catalyst in DMA/H₂O (v/v = 20/1). A TON of 28 was achieved.

It has been fairly well established that some of the organic oxidations catalyzed by the analogous polyvanadomolybdate systems, **PMo_{12-n}V_n**, proceed via the general two-step mechanism (eq 2-3 and 2-4).^{51,55,58,88} It was found that **PMo₁₂** (with n = 0) is not a highly reactive catalyst for the aerobic oxidation of aldehydes under ambient conditions. The reversible V(V/IV) redox couple is involved in the efficient oxidation of organic compounds catalyzed by vanadium-substituted Keggin-type heteropolyanions.^{51,55,89}



However, several lines of evidence are consistent with radical chain mechanism⁹⁰⁻⁹² for aerobic formaldehyde oxidation catalyzed by PW_9V_3 . First, the initial rate of the reaction is pseudo-first order in formaldehyde and parabolic order in catalyst, i.e. the rate increases, maximizes and then decreases with increasing catalyst concentration (**Figure 2-7**). Similar parabolic catalyst concentration dependences are a well-documented and studied feature of metal-catalyzed autoxidation reactions.⁹³ Second, the rate is essentially independent of oxygen pressure (**Figure 2-8**). Third, the reaction is retarded by addition of small quantities of the radical scavenger, 4-*t*-butylcatechol (1.0 μmol), or formic acid (0.6 mmol) (**Figure 2-9**).^{94,95} Similar phenomena were also identified for aerobic formaldehyde oxidation catalyzed by $\text{NaH}_3[\text{SiW}_{11}\text{Ce}^{\text{IV}}\text{O}_{39}]$.²⁸

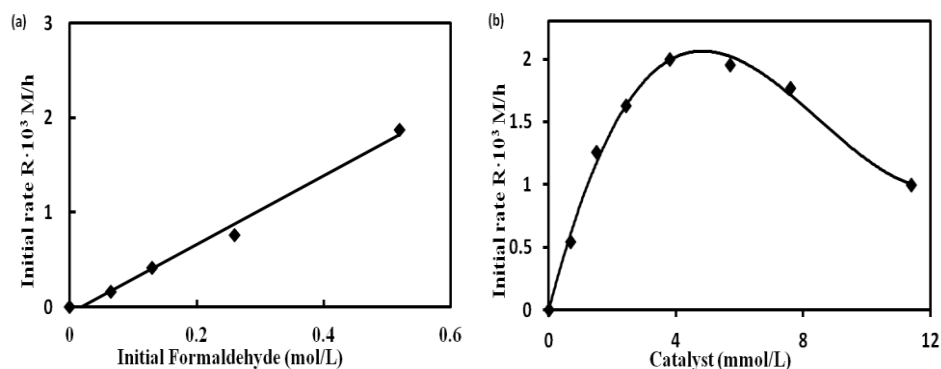


Figure 2-7. (a) Initial rate of formaldehyde oxidation as a function of the initial reactant concentration ($[\text{PW}_9\text{V}_3] = 3.8 \text{ mM}$); (b) initial rate of formaldehyde oxidation as a function of the initial catalyst (PW_9V_3) concentration ($[\text{CH}_2\text{O}] = 0.52 \text{ M}$)

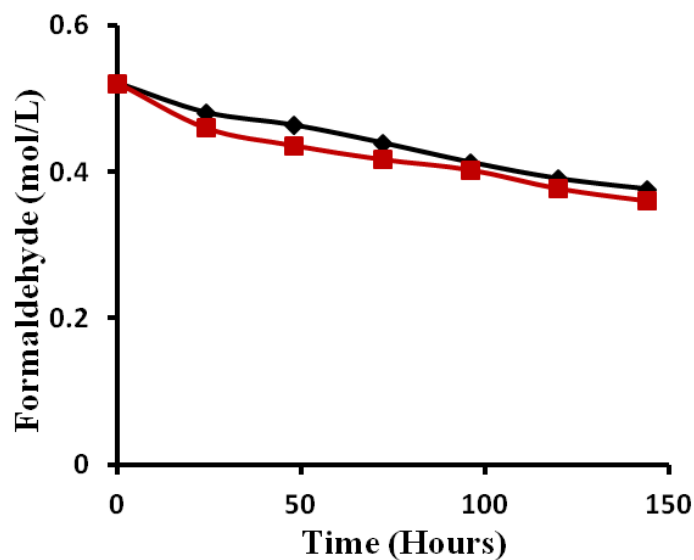


Figure 2-8. Time profile of formaldehyde consumption catalyzed by PW_9V_3 under 1 atm oxygen (red squares) and under 1 atm of air (black diamonds) in DMA/ H_2O (v/v = 20/1) at ambient temperature

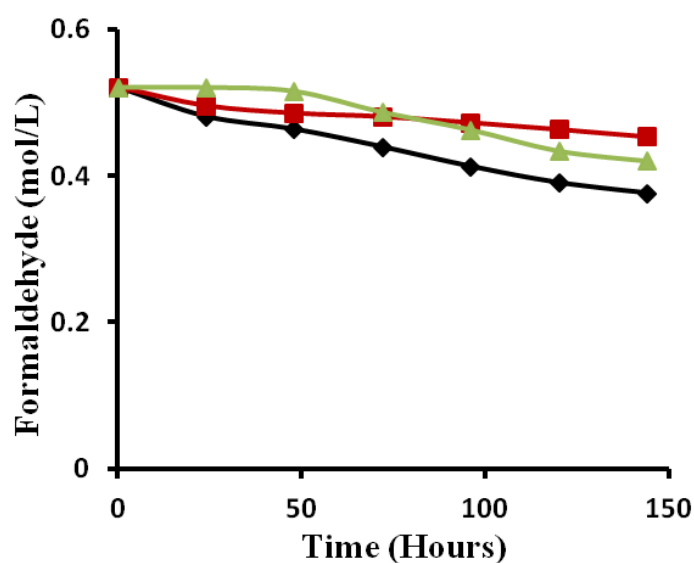
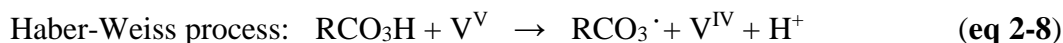
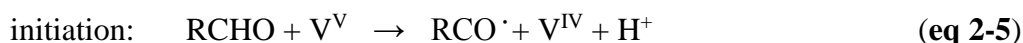


Figure 2-9. Time profile of formaldehyde consumption catalyzed by PW_9V_3 under 1 atm of air without additives (black diamonds), with addition of 0.6 mmol HCOOH (red squares) and with addition of 1.0 μmol 4-*t*-butylcatechol (green triangles); all reactions at ambient temperature

These observations not only indicate that oxygen is not involved in the rate-limiting step but also argue against the well-established two-step mechanism; they are more consistent with radical chain autoxidation. The processes in **eqs 2-5 to 2-10** are likely based on the above experimental results and literature studies.^{28,93} These processes include the aldehyde autoxidation steps (**eqs 2-5 to 2-7**) and the Haber-Weiss aqueous-phase hydroperoxide decomposition processes (**eqs 2-8 and 2-9**) together with the Baeyer-Villiger oxidation of formaldehyde by treatment with peroxy acid (**eq 2-10**). These processes taking place simultaneously give rise to complex dependences on catalyst/initiator concentration.



2.3.3 Comparison of supported noble metal and POM catalysts for aerobic formaldehyde oxidation.

Six POMs, each with extensive and reversible redox chemistry, were also prepared and evaluated as catalysts for the aerobic oxidation of formaldehyde under ambient conditions (**Table 2-3**). These POMs include: $[\textit{n}\text{-Bu}_4\text{N}]_5[\text{W}_3\text{V}_3\text{O}_{19}]$, $[\textit{n}\text{-Bu}_4\text{N}]_3\text{H}_3\text{V}_{10}\text{O}_{28}$, a POM with little documented ability to catalyze aerobic organic oxidations,⁹⁶⁻⁹⁸ $[\textit{n}\text{-Bu}_4\text{N}]_7\text{SiW}_9\text{V}_3\text{O}_{40}$, a Keggin-type tri-vanadium-containing POM with silicon as the heteroatom, $[\textit{n}\text{-Bu}_4\text{N}]_9\text{P}_2\text{W}_{15}\text{V}_3\text{O}_{62}$, a Wells-Dawson POM with three incorporated vanadium centers, $[\textit{n}\text{-Bu}_4\text{N}]_5\text{PW}_{11}\text{CoO}_{39}$, a Keggin-type Co-

containing POM with phosphorus as the heteroatom, and $[n\text{-Bu}_4\text{N}]_4[\text{SiW}_{11}\text{Ce}^{\text{IV}}\text{O}_{39}]$, a Keggin-type Ce-containing POM. Four of the V-containing complexes are effectively inactive. This finding also indicates that the polyanion properties (structure, V(V/VI) potential, etc.) largely dictate reactivity in the radical-chain aerobic oxidation of formaldehyde. The polyvanadotungstates exhibit a comparable activity to the well-documented Keggin-type Co-containing and Ce-containing POMs in DMA/H₂O.

Table 2-3. Aerobic Oxidation of Formaldehyde Catalyzed by Different POMs. ^a

Entry	Catalyst	CH ₂ O	HCOOH	TON ^d
		conversion (%) ^b	Yield (%) ^c	
1	PW₉V₃	28	26	38
2	PW₈V₄	35	32	47
3	PW₆V₆	42	41	57
4	$[n\text{-Bu}_4\text{N}]_5[\text{W}_3\text{V}_3\text{O}_{19}]$	0	--	--
5	$[n\text{-Bu}_4\text{N}]_3\text{H}_3\text{V}_{10}\text{O}_{28}$	0	--	--
6	$[n\text{-Bu}_4\text{N}]_7\text{SiW}_9\text{V}_3\text{O}_{40}$	0	--	--
7	$[n\text{-Bu}_4\text{N}]_9\text{P}_2\text{W}_{15}\text{V}_3\text{O}_{62}$	0	--	--
8	$[n\text{-Bu}_4\text{N}]_5\text{PW}_{11}\text{CoO}_{39}$	24	23	32
9	$[n\text{-Bu}_4\text{N}]_4[\text{SiW}_{11}\text{Ce}^{\text{IV}}\text{O}_{39}]$	39	39	53

^a Reaction Conditions: concentration of formaldehyde $[\text{CH}_2\text{O}] = 0.52$ M, concentration of catalyst = $[\text{catalyst}] = 3.8$ mM, 1 atm of air, 2 mL of solvent, ambient temperature, 144 h. ^b CH₂O conversion (%) = moles of CH₂O consumed/moles of initial CH₂O. ^c GC yield based on initial CH₂O. ^d TON = moles of formaldehyde consumed/moles of catalyst.

Some precious metals, e.g. Au, Ru, Pd and Pt, in high surface area formulations are known to be very effective catalysts for the gas phase aerobic oxidation of formaldehyde at moderate temperature.^{39,40} As noted above, Pt nanoparticles supported on TiO₂ have been shown to be an effective catalyst for formaldehyde oxidation at room temperature.^{33,43} Importantly, most of these noble-metal-catalyzed formaldehyde oxidations to date are gas phase reactions. However, water is ubiquitous in human environments and thus formaldehyde exists nearly exclusively in the hydrated form, (CH₂(OH)₂). Therefore, in this work, metal-oxide-supported Au and Pt nanoparticles (Au/TiO₂, reduced Pt/TiO₂) with 1 weight % loading (**Figure 2-10**) were prepared by the literature methods^{33,44} and assessed for their ability to catalyze aerobic oxidation of formaldehyde in the presence of water.

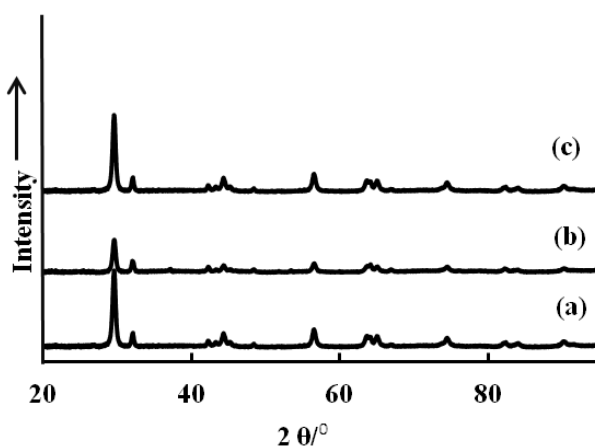


Figure 2-10. X-ray diffraction patterns of (a) TiO₂, (b) reduced Pt/TiO₂, (c) Au/TiO₂

The catalytic activity of PW₉V₃, PW₈V₄, PW₆V₆ and the supported noble metal catalysts in the presence of water at 40 °C are shown in **Figure 2-11**. In DMA/H₂O (v/v = 20/1) solvent system with *ca.* 4 vol % water, the reduced Pt/TiO₂ shows the highest activity with a formaldehyde conversion of 61%, a finding consistent with the results of Huang *et al.* and other groups.⁹⁹ The Au/TiO₂ also catalyzes formaldehyde oxidation with a conversion of 34%. Critically however, with an increase in water

concentration (vol %), the activity of the supported noble metal catalysts drops precipitously. In aqueous solutions (100 vol % water), the activity of the supported noble metal catalysts are markedly lower for aerobic formaldehyde oxidation than that of PW_9V_3 , PW_8V_4 and PW_6V_6 . The results above indicate that the polyvanadotungstates are water compatible active catalysts for oxidative removal of formaldehyde.

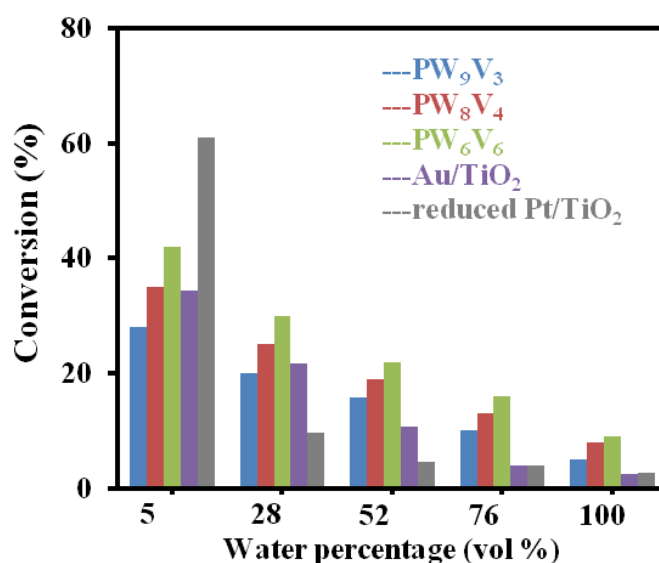
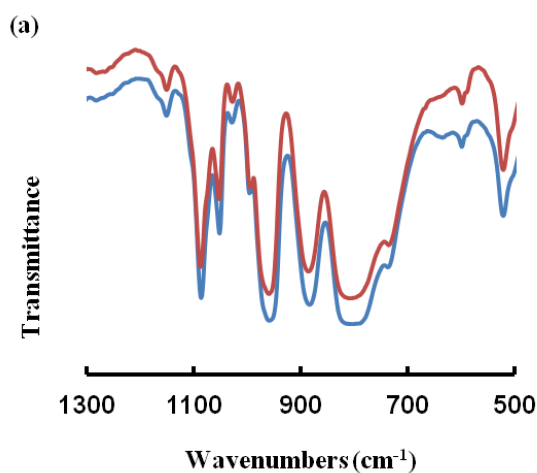


Figure 2-11. Oxidative removal of formaldehyde catalyzed by PW_9V_3 , PW_8V_4 , PW_6V_6 , reduced Pt/TiO_2 and Au/TiO_2 in the presence of water. Concentration of formaldehyde, $[\text{CH}_2\text{O}] = 0.52 \text{ M}$, $[\text{catalyst}] = 3.8 \text{ mM}$, 1 atm of air, 2 mL of solvent, 40 °C, 144 h.

2.3.4 Catalyst stability and reusability.

From a practical point of view, stability and reusability issues should be taken into account when using catalysts for organic reactions. A quite stable catalyst that can be recovered and reused several times and that does not become easily deactivated is highly attractive. The stability and reusability of the TBA salts of the

polyvanadotungstates were investigated for aerobic formaldehyde oxidation in three successive runs. The post-reaction solutions in each run were completely dried under vacuum, weighed and the catalyst recycled. The recovered catalysts were reused in subsequent reactions under conditions identical to those in the first run. Two lines of evidence indicate that the vanadium-substituted POMs are quite stable under turnover conditions: (1) the recycled POMs catalyze aerobic oxidation of formaldehyde for at least three cycles without significant activity loss; (2) the FT-IR spectra of **PW₉V₃**, **PW₈V₄** and **PW₆V₆** after the catalytic reactions retain all the characteristic peaks of the substituted Keggin type POMs (**Figure 2-12**). These results indicate that TBA salts of the polyvanadotungstates exhibit excellent stability and reusability for the aerobic oxidation of formaldehyde.



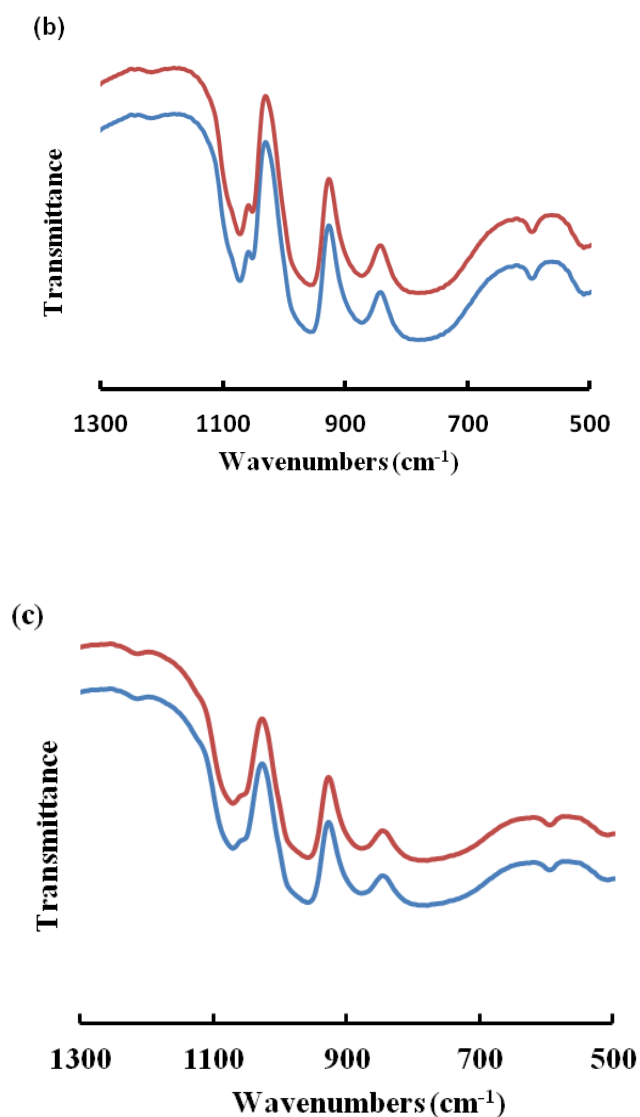


Figure 2-12. FT-IR spectra of (a) **PW₉V₃**, (b) **PW₈V₄** and (c) **PW₆V₆** before (red) and after (blue) catalytic reactions

2.4 Conclusions

The present study reveals that the tetra-*n*-butylammonium (TBA) salts of polyvanadotungstates, [*n*-Bu₄N]₆[PW₉V₃O₄₀] (**PW₉V₃**), [*n*-Bu₄N]₆HPW₈V₄O₄₀ · 9H₂O (**PW₈V₄**), [*n*-Bu₄N]₅H₄PW₆V₆O₄₀ · 6H₂O (**PW₆V₆**), can work as robust catalysts for the aerobic oxidation of formaldehyde under ambient conditions. This is of note because

formaldehyde is both a major toxic industrial chemical (TIC) and a general health concern in human environments, The catalysts work best in the mixed solvent system of (DMA)/water (v:v = 20:1). Optimization of the reaction conditions led to a system that affords 57 turnovers. A kinetics study of a representative reaction (**PW₉V₃** catalyst; 0.52 M aqueous formaldehyde reagent, and 1.0 atmosphere of air) establishes that the reaction is first order in formaldehyde substrate, parabolic order in catalyst and zero order in O₂, findings that are all consistent with a radical chain mechanism. Comparison with other related POMs and metal oxide supported Pt/Au catalysts indicates that the TBA salts of polyvanadotungstates show promise as water-compatible catalysts (can be made and used in water) for oxidative removal of formaldehyde under ambient, high-humidity conditions.

References

- (1) Dietert, R. R.; Hedge, A. *Crit. Rev. Toxicol.* **1996**, *26*, 633-707.
- (2) Kelly, T. J.; Smith, D. L.; Satola, J. *Environ. Sci. Technol.* **1999**, *33*, 81-88.
- (3) Zhong, W.; Que Hee, S. S. *Mutat. Res-Gen. Tox. En.* **2004**, *563*, 13-24.
- (4) Marsh, G. M.; Youk, A. O. *Regul. Toxicol. Pharm.* **2004**, *40*, 113-124.
- (5) Heck, H. d. A.; Casanova, M. *Regul. Toxicol. Pharm.* **2004**, *40*, 92-106.
- (6) Hauptmann, M.; Lubin, J. H.; Stewart, P. A.; Hayes, R. B.; Blair, A. *Am. J. Epidemiol.* **2004**, *159*, 1117-1130.
- (7) Conolly, R. B.; Kimbell, J. S.; Janszen, D.; Schlosser, P. M.; Kalisak, D.; Preston, J.; Miller, F. J. *Toxicol. Sci.* **2004**, *82*, 279-296.
- (8) Collins, J. J.; Lineker, G. A. *Regul. Toxicol. Pharm.* **2004**, *40*, 81-91.
- (9) Cole, P.; Axten, C. *Regul. Toxicol. Pharm.* **2004**, *40*, 107-112.
- (10) Cogan, P. S.; Koch, T. H. *J. Med. Chem.* **2004**, *47*, 5690-5699.

- (11) Burke, P. J.; Kalet, B. T.; Koch, T. H. *J. Med. Chem.* **2004**, *47*, 6509-6518.
- (12) Sheldon, R. A.; Kochi, J. K.; *Metal-catalyzed oxidations of organic compounds*; Academic Press: New York, 1981.
- (13) Renneke, R. F.; Pasquali, M.; Hill, C. L. *J. Am. Chem. Soc.* **1990**, *112*, 6585-6594.
- (14) Harrup, M. K.; Hill, C. L. *J. Mol. Catal. A: Chem.* **1996**, *106*, 57-66.
- (15) Hill, C. L.; Gall, R. D. *J. Mol. Catal. A: Chem.* **1996**, *114*, 103-111.
- (16) Kholdeeva, O. A.; Tkachev, A. V.; Romannikov, V. N.; Khavrutskii, I. V.; Zamaraev, K. I. *Stud. Surf. Sci. Catal.* **1997**, *108*, 337-344.
- (17) Hill, C. L.; Renneke, R. F.; Combs, L. *Tetrahedron* **1988**, *44*, 7499-7507.
- (18) Hill, C. L. *Nature* **1999**, *401*, 436-437.
- (19) Boring, E.; Geletii, Y.; Hill, C. L. *J. Mol. Catal. A: Chem.* **2001**, *176*, 49-63.
- (20) Boring, E.; Geletii, Y. V.; Hill, C. L. In *Advances in Catalytic Activation of Dioxygen by Metal Complexes*; Simandi, L. I., Ed.; Kluwer Academic Publishers: Dordrecht, 2003; Vol. 26, p 227-264.
- (21) Okun, N. M.; Anderson, T. M.; Hill, C. L. *J. Am. Chem. Soc.* **2003**, *125*, 3194-3195.
- (22) Botar, B.; Geletii, Y. V.; Kögerler, P.; Musaev, D. G.; Morokuma, K.; Weinstock, I. A.; Hill, C. L. *J. Am. Chem. Soc.* **2006**, *128*, 11268-11277.
- (23) Hill, C. L.; Okun, N. M.; Hillesheim, D. A.; Geletii, Y. V. In *Anti-Terrorism and Homeland Defense: Polymers and Materials, ACS Symposium Series 980, Chapter 12*; Reynolds, J. G., Lawson, G. E., Koester, C. J., Eds.; American Chemical Society: Washington, D.C., 2007, p 198-209.
- (24) Cao, R.; Han, J. W.; Anderson, T. M.; Hillesheim, D. A.; Hardcastle, K. I.; Slonkina, E.; Hedman, B.; Hodgson, K. O.; Kirk, M. L.; Musaev, D. G.; Morokuma, K.; Geletii, Y. V.; Hill, C. L. *Adv. Inorg. Chem.* **2008**, *60* (Chapter 6), 245-272.
- (25) Song, J.; Luo, Z.; Britt, D.; Furukawa, H.; Yaghi, O. M.; Hardcastle, K. I.; Hill, C. L. *J. Am. Chem. Soc.* **2011**, *133*, 16839-16846.
- (26) Rhule, J. T.; Neiwert, W. A.; Hardcastle, K. I.; Do, B. T.; Hill, C. L. *J. Am. Chem. Soc.* **2001**, *123*, 12101-12102.

- (27) Okun, N. M.; Anderson, T. M.; Hill, C. L. *J. Mol. Catal. A: Chem.* **2003**, *197*, 283-290.
- (28) Kholdeeva, O. A.; Timofeeva, M. N.; Maksimov, G. M.; Maksimovskaya, R. I.; Neiwert, W. A.; Hill, C. L. *Inorg. Chem.* **2005**, *44*, 666-672.
- (29) Kholdeeva, O. A.; Timofeeva, M. N.; Maksimov, G. M.; Maksimovskaya, R. I.; Rodionova, A. A.; Hill, C. L. In *Catalysis of Organic Reactions*; Sowa, J. R., Jr., Ed.; Marcel Dekker, Inc.: New York, 2005, p 429-433.
- (30) Yang, Y. C.; Baker, J. A.; Ward, J. R. *Chem. Rev.* **1992**, *92*, 1729-1743.
- (31) Sekine, Y. *Atmos. Environ.* **2002**, *36*, 5543-5547.
- (32) Tang, X.; Li, Y.; Huang, X.; Xu, Y.; Zhu, H.; Wang, J.; Shen, W. *Appl. Catal., B* **2006**, *62*, 265-273.
- (33) Zhang, C.; He, H.; Tanaka, K.-i. *Catal. Commun.* **2005**, *6*, 211-214.
- (34) Li, H.-F.; Zhang, N.; Chen, P.; Luo, M.-F.; Lu, J.-Q. *Appl. Catal., B* **2011**, *110*, 279-285.
- (35) Qu, Z.; Shen, S.; Chen, D.; Wang, Y. *J. Mol. Catal. A: Chem.* **2012**, *356*, 171-177.
- (36) Li, S.; Lu, X.; Guo, W.; Zhu, H.; Li, M.; Zhao, L.; Li, Y.; Shan, H. *J. Organomet. Chem.* **2012**, *704*, 38-48.
- (37) Miyawaki, J.; Lee, G.-H.; Yeh, J.; Shiratori, N.; Shimohara, T.; Mochida, I.; Yoon, S.-H. *Catal. Today* **2012**, *185*, 278-283.
- (38) Xing, Y.; Chen, B.; Guo, T.; Ying, G. *Environ. Prog. Sustainable Energy* **2013**, *32*, 115-119.
- (39) Imamura, S.; Uematsu, Y.; Utani, K.; Ito, T. *Ind. Eng. Chem. Res.* **1991**, *30*, 18-21.
- (40) Álvarez-Galván, M. C.; Pawelec, B.; de la Peña O'Shea, V. A.; Fierro, J. L. G.; Arias, P. L. *Appl. Catal., B* **2004**, *51*, 83-91.
- (41) Chen, M. S.; Goodman, D. W. *Science* **2004**, *306*, 252-255.
- (42) Chen, M.; Cai, Y.; Yan, Z.; Goodman, D. W. *J. Am. Chem. Soc.* **2006**, *128*, 6341-6346.
- (43) Zhang, C.; He, H.; Tanaka, K.-i. *Appl. Catal., B* **2006**, *65*, 37-43.

- (44) Huang, H.; Leung, D. Y. C.; Ye, D. *J. Mater. Chem.* **2011**, *21*, 9647-9652.
- (45) Zhang, Y.; Shen, Y.; Yang, X.; Sheng, S.; Wang, T.; Adebajo, M. F.; Zhu, H. *J. Mol. Catal. A: Chem.* **2010**, *316*, 100-105.
- (46) Ma, C.; Wang, D.; Xue, W.; Dou, B.; Wang, H.; Hao, Z. *Environ. Sci. Technol.* **2011**, *45*, 3628-3634.
- (47) Kholdeeva, O. A.; Vanina, M. P.; Timofeeva, M. N.; Maksimovskaya, R. I.; Trubitsina, T. A.; Melgunov, M. S.; Burgina, E. B.; Mrowiec-Bialon, J.; Jarzebski, A. B.; Hill, C. L. *J. Catal.* **2004**, *226*, 363-371.
- (48) Kholdeeva, O. A.; Maksimchuk, N. V.; Maksimov, G. M. *Catal. Today* **2010**, *157*, 107-113.
- (49) Pope, M. T. In *Prog. Inorg. Chem.*; Lippard, S. J., Ed.; John Wiley & Sons, Inc.: New York, 1991; Vol. 39, p 181-257.
- (50) Pope, M. T.; Müller, A. *Angew. Chem.* **1991**, *103*, 56-70.
- (51) Hill, C. L.; Prosser-McCartha, C. M. *Coord. Chem. Rev.* **1995**, *143*, 407-455.
- (52) Hill, C. L. In *Comprehensive Coordination Chemistry-II: From Biology to Nanotechnology*; Wedd, A. G., Ed.; Elsevier Ltd.: Oxford, UK, 2004; Vol. 4, p 679-759.
- (53) Neumann, R.; Levin, M. *J. Org. Chem.* **1991**, *56*, 5707-5710.
- (54) Lv, H.; Geletii, Y. V.; Zhao, C.; Vickers, J. W.; Zhu, G.; Luo, Z.; Song, J.; Lian, T.; Musaev, D. G.; Hill, C. L. *Chem. Soc. Rev.* **2012**, *41*, 7572-7589.
- (55) Neumann, R. *Prog. Inorg. Chem.* **1998**, *47*, 317-370.
- (56) Vickers, J. W.; Lv, H.; Sumliner, J. M.; Zhu, G.; Luo, Z.; Musaev, D. G.; Geletii, Y. V.; Hill, C. L. *J. Am. Chem. Soc.* **2013**, *135*, 14110-14118.
- (57) Fujibayashi, S.-y.; Nakayama, K.; Hamamoto, M.; Sakaguchi, S.; Nishiyama, Y.; Ishii, Y. *J. Mol. Catal. A: Chem.* **1996**, *110*, 105-117.
- (58) Kozhevnikov, I. V. *J. Mol. Catal. A: Chem.* **1997**, *117*, 151-158.
- (59) Kozhevnikov, I. V. *Chem. Rev.* **1998**, *98*, 171-198.
- (60) Shinachi, S.; Matsushita, M.; Yamaguchi, K.; Mizuno, N. *J. Catal.* **2005**, *233*, 81-89.

- (61) Kholdeeva, O. A.; Grigoriev, V. A.; Maksimov, G. M.; Fedotov, M. A.; Golovin, A. V.; Zamaraev, K. I. *J. Mol. Catal. A: Chem.* **1996**, *114*, 123-130.
- (62) Mizuno, N.; Watanabe, T.; Misono, M. *J. Phys. Chem.* **1985**, *89*, 80-85.
- (63) Black, J. B.; Clayden, N. J.; Gai, P. L.; Scott, J. D.; Serwicka, E. M.; Goodenough, J. B. *J. Catal.* **1987**, *106*, 1-15.
- (64) Mizuno, N.; Watanabe, T.; Misono, M. *J. Phys. Chem.* **1990**, *94*, 890-894.
- (65) Mizuno, N.; Watanabe, T.; Misono, M. *Bull. Chem. Soc. Jpn.* **1991**, *64*, 243-247.
- (66) Combs-Walker, L. A.; Hill, C. L. *Inorg. Chem.* **1991**, *30*, 4016-4026.
- (67) Lissel, M.; Jansen in de Wal, H.; Neumann, R. *Tetrahedron Lett.* **1992**, *33*, 1795-1798.
- (68) Khenkin, A. M.; Rosenberger, A.; Neumann, R. *J. Catal.* **1999**, *182*, 82-91.
- (69) Ali, B. E.; El-Ghanam, A. M.; Fettouhi, M. *J. Mol. Catal. A: Chem.* **2001**, *165*, 283-290.
- (70) Khenkin, A. M.; Weiner, L.; Wang, Y.; Neumann, R. *J. Am. Chem. Soc.* **2001**, *123*, 8531-8542.
- (71) Khenkin, A. M.; Neumann, R. *J. Org. Chem.* **2002**, *67*, 7075-7079.
- (72) Khenkin, A. M.; Neumann, R. *J. Am. Chem. Soc.* **2002**, *124*, 4198-4199.
- (73) Domaille, P. J. In *Inorg. Synth.*; Ginsberg, A. P., Ed.; John Wiley and Sons: New York, 1990; Vol. 27, p 96-104.
- (74) Smith, D. P.; Pope, M. T. *Inorg. Chem.* **1973**, *12*, 331-336.
- (75) Xu, Y.; Xu, J.-Q.; Yang, G.-Y.; Wang, T.-G.; Xing, Y.; LIN, Y.-H.; Jia, H.-Q. *Acta Cryst. Sect. C* **1998**, *C54*, 563-565.
- (76) Finke, R. G.; Rapko, B.; Saxton, R. J.; Domaille, P. J. *J. Am. Chem. Soc.* **1986**, *108*, 2947-2960.
- (77) Day, V. W.; Klemperer, W. G.; Maltbie, D. J. *J. Am. Chem. Soc.* **1987**, *109*, 2991-3002.
- (78) Prosser-McCartha, C. M.; Kadkhodayan, M.; Williamson, M. M.; Bouchard, D. A.; Hill, C. L. *J. Chem. Soc., Chem. Commun.* **1986**, *24*, 1747-1748.
- (79) Williamson, M. M.; Bouchard, D. A.; Hill, C. L. *Inorg. Chem.* **1987**, *26*, 1436-1441.

- (80) Gall, R. D.; Faraj, M.; Hill, C. L. *Inorg. Chem.* **1994**, *33*, 5015-5021.
- (81) Chen, Q.; Hill, C. L. *Inorg. Chem.* **1996**, *35*, 2403-2405.
- (82) Nakka, L.; Molinari, J. E.; Wachs, I. E. *J. Am. Chem. Soc.* **2009**, *131*, 15544-15554.
- (83) Hamamoto, M.; Nakayama, K.; Nishiyama, Y.; Ishii, Y. *J. Org. Chem.* **1993**, *58*, 6421-6425.
- (84) Rocchiccioli-Deltcheff, C.; Fournier, M. *J. Chem. Soc., Faraday Trans.* **1991**, *87*, 3913-3920.
- (85) Bieber, R.; Trümpler, G. *Helv. Chim. Acta* **1947**, *30*, 1860-1865.
- (86) Maroncelli, M.; Fleming, G. R. *J. Chem. Phys.* **1987**, *86*, 6221.
- (87) Winkelman, J. G. M.; Voorwinde, O. K.; Ottens, M.; Beenackers, A. A. C. M.; Janssen, L. P. B. M. *Chem. Eng. Sci.* **2002**, *57*, 4067-4076.
- (88) Kozhevnikov, I. V.; Matveev, K. I. *Russ. Chem. Rev.* **1982**, *51*, 1075-1088.
- (89) Kozhevnikov, I. V. *Catalysis by Polyoxometalates*; Wiley: Chichester, England, 2002; Vol. 2.
- (90) Loury, M. *Comptes Rendus* **1964**, *258*, 238-239.
- (91) Hendriks, C. F.; Beek, H. C. A. v.; Heertjes, P. M. *Ind. Eng. Chem. Prod. Res. Dev.* **1977**, *16*, 270-275.
- (92) Hendriks, C. F.; Beek, H. C. A. v.; Heertjes, P. M. *Ind. Eng. Chem. Prod. Res. Dev.* **1978**, *17*, 260-264.
- (93) Black, J. F. *J. Am. Chem. Soc.* **1978**, *100*, 527-535.
- (94) Taube, H. *J. Am. Chem. Soc.* **1941**, *63*, 2453-2458.
- (95) Yapsaklı, K.; Can, Z. S. *Water Qual. Res. J. Canada* **2004**, *39*, 140-148.
- (96) Villa, A. L.; Vos, D. E. D.; Verpoort, F.; Sels, B. F.; Jacobs, P. A. *J. Catal.* **2001**, *198*, 223-231.
- (97) Csányi, L. J.; Jáky, K.; Dombi, G.; Evanics, F.; Dezs, G.; Kóta, Z. *J. Mol. Catal. A: Chem.* **2003**, *195*, 101-111.
- (98) Maciejewska, G.; Nosek, M.; Glowiak, T.; Starosta, J.; Cieslak-Golonka, M. *Polyhedron* **2003**, *22*, 1415-1423.

(99) Huang, H.; Leung, D. Y. C. *J. Catal.* **2011**, 280, 60-67.

Chapter 3.

A Manganese(IV)-containing Heteropolyvanadate for Oxidative Removal of 2-Chloroethyl Ethyl Sulfide

Reproduced with permission from *Inorg. Chem.*, **2015**, *54*(22), 10604-10609.
Copyright 2015 American Chemical Society

As a main contributor of this work; with John Bacsá, Jan van Leusen, Kevin P. Sullivan, Hongjin Lv, Paul Kögerler and Craig L. Hill*, W. Guo contributed the syntheses, characterizations, investigating and analyzing the catalyst' activities to this work. J. Bacsá conducted and analyzed the X-ray crystallographic and topology studies. J. Leusen and P. Kögerler performed and analyzed the magnetochemical experiments. K. P. Sullivan and H. Lv conducted the NMR measurements. W. Guo and C. L. Hill designed the experiments and prepared the manuscript.

3.1 Introduction

Polyoxometalates (POMs) are a family of metal oxide clusters with versatile properties in electrochemistry, magnetism, medicine and catalysis.¹⁻⁴ They not only exhibit similar structures to metal oxide surfaces but also possess multiple structural topologies and range in size from a few metal centers to giant clusters.⁵⁻¹⁰ Generally, POMs can be divided into several groups based on their component transition metals including but not limited to polytungstates, polymolybdates, polyvanadates, and polyniobates. In addition, a multitude of mixed metal oxometalates are known.¹¹ While the literature on polyvanadates is not as extensive as that on polytungstates or polymolybdates, it is nonetheless substantial and rapidly growing.¹²⁻¹⁶ Prominent polyvanadates include decavanadate ($[\text{V}_{10}\text{O}_{28}]^{6-}$),¹⁷⁻¹⁹ the polyvanadophosphate ($[\text{PV}_{14}\text{O}_{42}]^{9-}$)²⁰ and some vanadium-substituted polytungstates and polymolybdates.²¹⁻²⁵ In addition, heteropolyvanadates such as vanadomanganate(IV) anions $[\text{MnV}_{13}\text{O}_{38}]^{7-}$ (**MnV₁₃**), $[\text{Mn}_2\text{V}_{22}\text{O}_{64}]^{10-}$ (**Mn₂V₂₂**) and $[\text{Mn}_3\text{V}_{12}\text{O}_{40}\text{H}_3]^{5-}$ (**Mn₃V₁₂**) have received attention since they were first reported by Pope and co-workers.^{26,27} The catalytic properties, tumor-inhibition activities, and antibiotic properties of **MnV₁₃** have also been reported.^{28,29} Moreover, some families of polyvanadates are effective catalysts for the oxidation of various organic compounds including toxic industrial chemicals and chemical warfare agents (particularly mustard gas).^{4,21,30-37}

More recently, **MnV₁₃** and its analogue $[\text{NiV}_{13}\text{O}_{38}]^{7-}$ (**NiV₁₃**) together with low-valent transition metals (Co, Ni and Mn) or rare-earth metals were used to construct two-dimensional or three-dimensional extended frameworks.³⁸⁻⁴³ For example, **MnV₁₃** and **NiV₁₃** react with lanthanide cations to form two-dimensional heteropolyvanadates.³⁹ Recently, Wang and co-workers synthesized a series of inorganic porous frameworks using **MnV₁₃** and rare-earth metals as building units. The

POM-based porous frameworks show selective adsorption behavior and catalytic activity towards oxidation of sulfides.³⁸ However, despite great efforts made in synthesizing heteropolyvanadates, only a few have been reported. To date only **MnV₁₃** and **NiV₁₃** have been used as polyvanadate building blocks to construct two-dimensional or three-dimensional extended frameworks. Here, we report the synthesis, structure, magnetism and catalytic properties of a two-dimensional (2D) layered manganese(IV)-containing symmetrical heteropolyvanadate with a 1:14 stoichiometry: **K₄Li₂[MnV₁₄O₄₀] · 21H₂O (1)**. The unique 1:14 geometry is stabilized by capping potassium ions as indicated from ⁵¹V NMR spectroscopy in combination with single crystal X-ray diffraction studies. The magnetic and catalytic properties of **1** towards the mustard simulant, CEES are explored.

3.2 Experimental

3.2.1 General Methods and Materials

All chemicals were commercially purchased and used as supplied. The potassium salt of **MnV₁₃**, **K₇[MnV₁₃O₃₈] · 18H₂O (K₇**MnV₁₃)** was prepared by a reported literature method.²⁶ FT-IR spectroscopy was used to determine its purity. These spectra were measured on a Nicolet TM 600 FT-IR spectrometer (2% sample in KBr pellet). Visible diffuse reflectance spectra were obtained on Miniscan XE Plus from Hunter Associates Lab. Thermogravimetric analyses were conducted on a STA 6000 thermal analyzer. Elemental analyses (K, Li, Mn and V) were performed by Galbraith Laboratories (Knoxville, Tennessee). ⁵¹V NMR (151.6 MHz) spectra were run on a Unity Plus 600 spectrometer equipped with a Varian 600 SW/PF6 probe head at 298 K. The compounds were placed in 5 mm O.D. NMR tubes. All the chemical shifts were referenced to neat VOCl₃ (taken as 0 ppm at 25 °C). Gas chromatography (GC) analyses were used to detect the reagents and products from the catalytic reactions. The GC**

analyses of the liquid phase from catalytic reaction systems were conducted on a Hewlett-Packard 6890 instrument equipped with a 5% phenyl methyl silicone capillary column, a Hewlett-Packard 3390A series integrator, a flame ionization detector with N₂ as the carrier gas.

3.2.2 Synthesis of 1

A 15 mL aqueous lithium acetate solution (1.98 g, 2.0 M) was adjusted to pH 4 using 100% acetic acid (8.5 mL). To this solution was then added 0.25 g K₇[MnV₁₃O₃₈]•18H₂O (0.13 mmol) and 0.02 g V₂O₅ (0.13 mmol). The mixture was heated at 90 °C for 3 h and then cooled to room temperature and filtered. Orange prism-shaped crystals were obtained after slow evaporation over a period of one week. Yield: 120 mg (44% based on Mn). Anal. Calcd for K₄MnO₆₁V₁₄Li₂H₄₂: K, 7.8; Mn, 2.7; V, 35.7; Li, 0.7%. Found: K, 8.2; Mn, 2.4; V, 35.3; Li, 1.1%. FTIR (1100-400 cm⁻¹, 2% KBr pellets): 990 (w), 963 (s), 907 (w), 849 (w), 806 (m), 750 (w), 662 (m), 597 (m), 525 (w), 435 (w).

3.2.3 X-ray Crystallography

A suitable crystal (0.43 × 0.39 × 0.33 mm³) was selected and mounted on a loop with Paratone oil. Data were collected using an APEX-II CCD diffractometer with a cryostream operating at $T = 110(2)$ K. Data were measured using ω scans of 1° and for 30s per frame with Mo K α radiation (fine-focus sealed tube, 45kV, 35mA). Using **Olex2**⁴⁴ the structure was solved with the **Superflip** structure solution program⁴⁵ by the Charge Flipping solution method and refined by least squares using **ShelXL**⁴⁶. The total number of runs and images was based on the strategy calculation from the program **APEXII**.⁴⁷ The maximum resolution was $\Theta = 29.57^\circ$. Data reduction was performed using the **SAINT** software.⁴⁸ The final completeness is 99.9% out to 29.57° in Θ . **SADABS-2012/1** was used for absorption correction.⁴⁷ The absorption coefficient (μ)

of this material is 3.322 mm^{-1} and the minimum and maximum transmissions are 0.356 and 0.485. The unit cell parameters were refined using **SAINT**⁴⁸ on 9873 reflections, 37% of the observed reflections. The structure was solved in the space group *I4/mmm*. All atoms were refined anisotropically. The counter ions and water molecules are completely disordered. Formal charges for all the Mn(IV) and V(V) centers were assigned by summing valences of the chemical bonds to the metal centers. The amorphous regions were treated using the Squeeze routine in Platon.⁴⁹ The number of water molecules and remaining cations was also determined by elemental analyses and thermogravimetric analysis. Platon recovers 231 electrons from each formula unit which matches a formula containing 21 water molecules, two potassium and two lithium ions. The crystallographic data are summarized in **Table 3-1**.

Table 3-1. Crystal data and structure refinement for **1**

Formula	$\text{K}_4\text{MnO}_6\text{V}_{14}\text{Li}_2\text{H}_{42}$
Dcalc./ g cm^{-3}	2.653
μ/mm^{-1}	3.223
Formula Weight/ gmol^{-1}	1956.67
Max Size/mm	0.43
Mid Size/mm	0.39
Min Size/mm	0.33
T/K	110(2)
Crystal System	tetragonal
Space Group	<i>I4/mmm</i>
a/Å	11.2933(2)
b/Å	11.2933(2)

$c/\text{\AA}$	19.4985(4)
$\alpha/^\circ$	90
$\beta/^\circ$	90
$\gamma/^\circ$	90
$V/\text{\AA}^3$	2486.81(10)
Z	2
Z'	0.0625
Qmin/ $^\circ$	2.084
Qmax/ $^\circ$	29.570
Measured Refl.	26957
Independent Refl.	1052
Reflections Used	964
Rint	0.0314
Parameters	53
Restraints	0
Largest Peak	1.653
Deepest Hole	-2.578
GooF	1.272
wR ₂ (all data)	0.2129
wR ₂	0.2042
R ₁ (all data)	0.0608
R ₁	0.0560

$$R_1 = \frac{\sum ||F_0| - |F_c||}{\sum |F_0|}; \quad wR_2 = \frac{\sum [w(F_0^2 - F_c^2)^2]}{\sum [w(F_0^2)^2]}^{1/2}$$

3.2.4 Magnetochemical Characterization

Magnetic data of **1** were recorded using a Quantum Design MPMS-5XL SQUID magnetometer. The polycrystalline samples were compacted and immobilized into cylindrical PTFE capsules. Data were acquired as a function of the field (0.1–5.0 T at 2 K) as well as temperature (2.0–290 K at 0.1 T), and were corrected for the diamagnetic contributions of the sample holder and the title compound ($\chi_{\text{dia}}(\mathbf{1}) = -9.78 \times 10^{-4} \text{ cm}^3 \text{ mol}^{-1}$).

3.2.5 Catalytic Oxidation of 2-Chloroethyl Ethyl Sulfide (CEES)

In a typical reaction, 10 mg of **1** (3.5 μmol) was added into 2 mL of toluene containing 0.2 mmol 1,3-dichlorobenzene (internal standard), 0.2 mmol of CEES and 0.5 mmol of *tert*-butyl hydroperoxide. The mixture was placed in a vessel, mixed and stirred vigorously. Aliquots were withdrawn from the vessel every 60 min. The reagents and products were detected by GC. Complex **1** was recycled by centrifugation, washed with toluene and air dried.

3.3 Results and Discussion

3.3.1 Synthesis and Structure

The precursor structure, the lacunary **MnV₁₃** polyanion, exhibits a vacant coordination site which formally can add another VO₆ octahedron to form **MnV₁₄**. The synthetic scheme for **1** is shown in **Figure 3-1**. In pH 4.0 buffered aqueous solution, **MnV₁₃** in the presence of V₂O₅ transforms to **MnV₁₄** in 44% isolated yield. Introducing low valent transition metal cations such as Co²⁺, Mn²⁺ and Cu²⁺ to the synthetic solution does not influence the crystallization process indicating the unique stabilizing effect of K⁺ ions as compared to the Co²⁺, Mn²⁺ and Cu²⁺ ions.

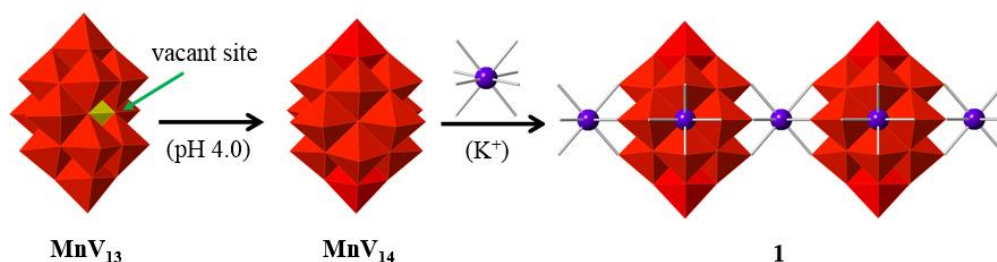


Figure 3-1. Combined polyhedral and ball-and-stick representations of **MnV₁₃** and the synthesis scheme for **1**. Red: VO₆; yellow: MnO₆; violet: potassium.

Unlike the previously reported **MnV₁₃** clusters with C_{2v} symmetry, **MnV₁₄** has 1:14 stoichiometry with D_{4h} symmetry that is composed of a central MnO₆ octahedron completely enclosed by 14 distorted VO₆ octahedra (**Figure 3-2**). The Mn-O and V-O bond lengths range from 1.85(7) to 1.90(2) Å and from 1.59(4) to 2.38(6) Å, respectively. The O-Mn-O angles are the octahedral values, while the O-V-O angles show considerable distortion and are in the range of 68.6(3)° to 170.2(4)°. These values are consistent with those reported for heteropolyvanadates.⁴¹ The simplified representation of **MnV₁₄** exhibits a new topology with a total point symbol of $\{3^{10}\}2\{3^{14}.4^7\}4\{3^{18}.4^{10}\}8\{3^{44}.4^{46}.5\}$ and is denoted in TOPOS as **jba1**.⁵⁰ The underlying symmetry is clearly visible in the simplified polyhedron that was obtained by removing all the oxygen atoms (**Figure 3-2**). Although it is a very simple polyhedron, we cannot find it among the lists of known polyhedra. It is not a Johnson polyhedron and it is not an Archimedean solid, prism or antiprism.

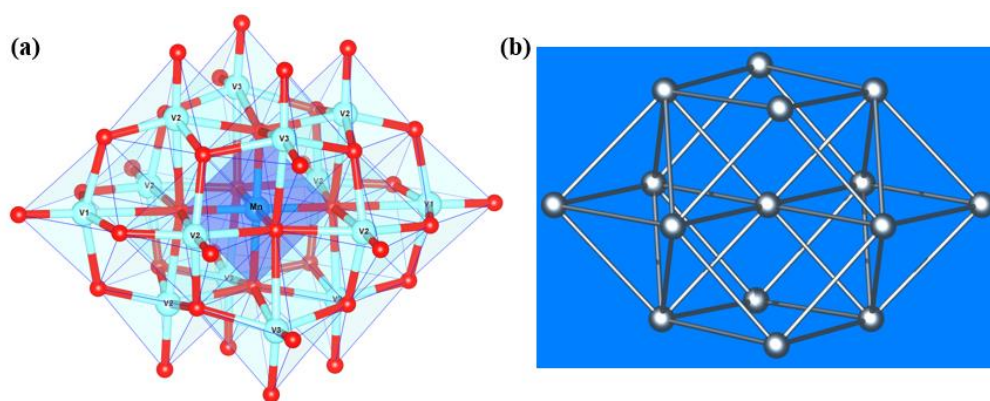


Figure 3-2. a) Polyhedral and ball-and-stick representation of MnV_{14} ; Color code: V, light blue; O, red; Mn, dark blue. b) Simplified representation of MnV_{14} showing a **jba1** topology with a total point symbol of $\{3^{10}2\{3^{14}.4^7\}4\{3^{18}.4^{10}\}8\{3^{44}.4^{46}.5\}$.

Single crystal X-ray crystallographic analyses reveal that **1** crystallizes in the tetrahedral holohedral $4/mmm$, space group $I4/mmm$. The structure is a notable example of a crystal making full use of chemical symmetry. The solid state crystal structure of **1** shows an infinite 2D framework with large voids and channels (**Figure 3-3**). The four square faces in each polyhedron are in the crystallographic ab plane and are capped by potassium ions. Each potassium ion bridges two MnV_{14} clusters forming an extended square network in the ab plane formulated as $\text{K}_2[\text{MnV}_{14}\text{O}_{40}]^{4-}$. The eight-coordinate potassium ions which exhibit square prismatic coordination geometry are located at the intersection of the fourfold axis with the two two-fold axes. The K-O bond lengths are in the range of 2.71(4) to 2.72(1) Å. The resulting 2D network is layered by the same repeating unit while the MnV_{14} clusters are located in the octagonal window of the first layer forming a (ABABAB...) layered structure (**Figure 3-3**). Bond-valence sum calculations reveal that the Mn atoms are in the +4 oxidation state and all V atoms are in the +5 oxidation state.⁵¹ Therefore, the overall charge of $\text{K}_2[\text{MnV}_{14}\text{O}_{40}]^{4-}$ is determined as -4. The remaining compensating K^+ ions and Li^+ ions as well as lattice

water molecules determined by elemental analyses reside in the void space between the layers and the octagonal windows.

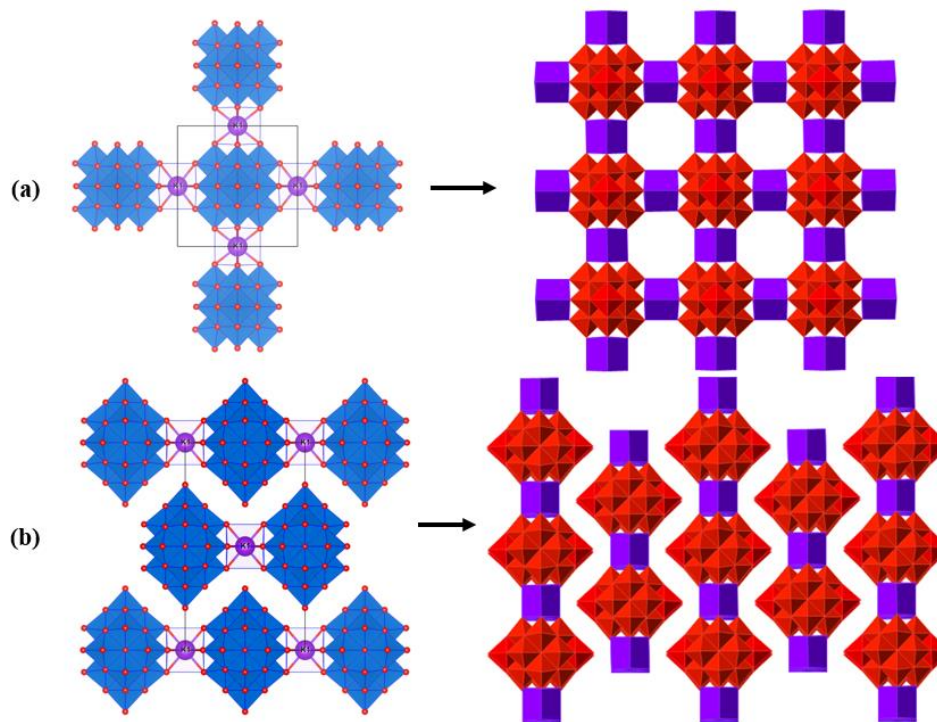


Figure 3-3. (a) Polyhedral and ball-and-stick representation of a portion of $\text{K}_2[\text{MnV}_{14}\text{O}_{40}]^{4-}$ framework in the ab -plane. Each potassium ion bridges two MnV_{14} clusters. (b) Stacking of the two-dimensional layers of $\text{K}_2[\text{MnV}_{14}\text{O}_{40}]^{4-}$ networks in the ab -plane. Color code: VO_6 , dark blue octahedra with oxygen red balls; K, violet balls. The figures on the right show the polyhedral representations. Color code: VO_6 , red octahedra; KO_8 , violet polyhedra.

3.3.2 Characterization.

The FT-IR spectrum of **1** is shown in **Figure 3-4**. It shows a very similar FT-IR spectrum to that of $\text{K}_7\text{MnV}_{13}$. The characteristic peaks at *ca.* 990, 963, 907, 849, 806, 750, 662, 597, 525 and 435 cm^{-1} are attributed to V=O and V-O-V vibrations.^{52,53} The diffuse reflectance spectrum of **1** is displayed in **Figure 3-4**. The broad band at *ca.* 400

nm to 510 nm is attributed to the ligand-to-vanadium(V) charge transfer. The TG analysis of **3.1** is shown in **Figure 3-5**. A weight loss of 19.5% is observed corresponding to the loss of 21 lattice water molecules per **1**.

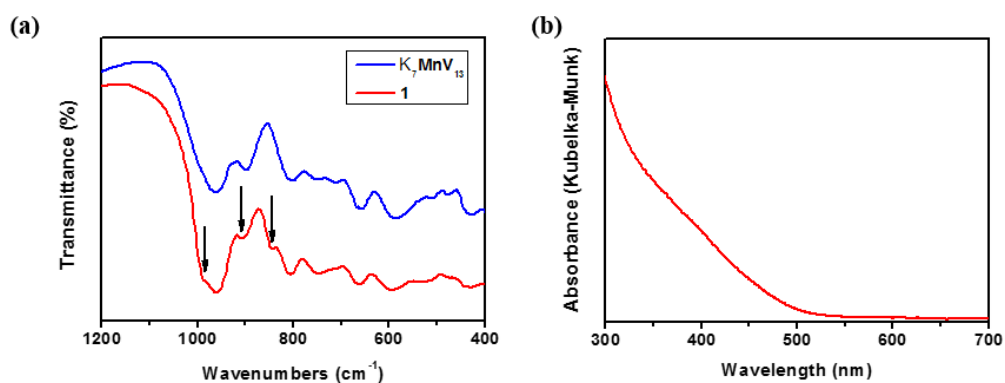


Figure 3-4. (a) FT-IR spectra of **3.1** and K_7MnV_{13} . (b) Diffuse reflectance spectrum of **1**.

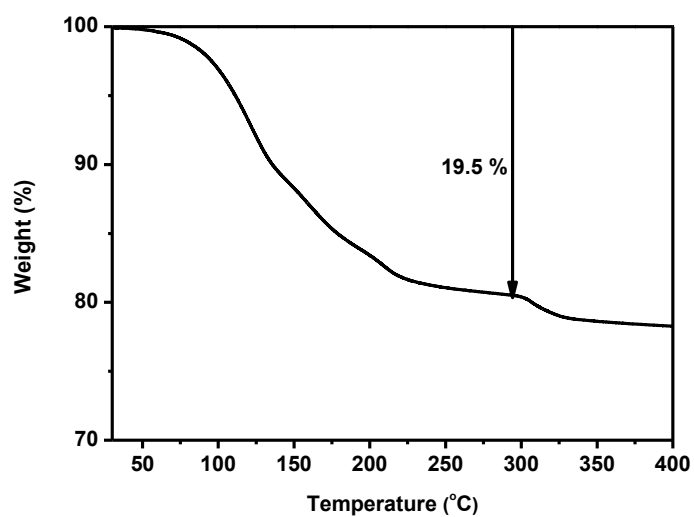


Figure 3-5. Thermogravimetric analysis of **1**.

In addition, the ^{51}V NMR spectrum of **1** in D_2O is shown in **Figure 3-6**. It should display three distinct peaks with a ratio of 1:2:4 according to the symmetry of **1**. However, six peaks were observed; the three small peaks in the region from -520 to -400 ppm are the well-documented peaks of $[\text{V}_{10}\text{O}_{28}]^{6-}$.⁵⁴ This indicates that when **1** is dissolved in D_2O , the potassium ions dissociate from **1** and the MnV_{14} polyanion slowly decomposes. The decomposition of **1** in D_2O further confirms that the potassium ions connecting the MnV_{14} polyanions help to stabilize the overall structure when they crystallize in the solid state. A similar stabilization effect was reported previously when MnV_{13} was connected by lanthanide ions to form a 2D structure.³⁹

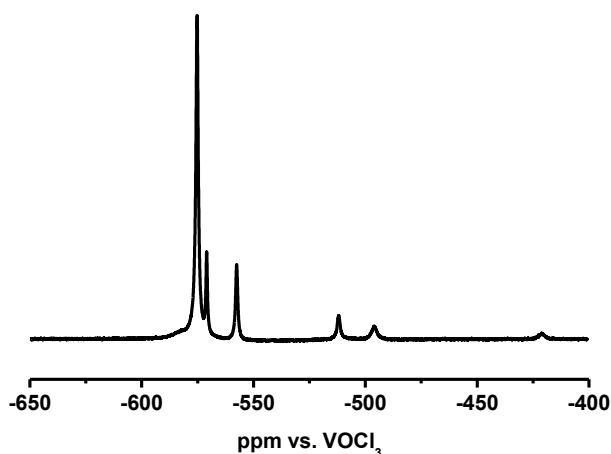


Figure 3-6. ^{51}V NMR spectrum of **1** in D_2O . The integration of the peaks from left to right are: 219.33, 20.36, 10.53, 1.91, 1.00, 0.19, respectively, which gives the ratio as 1154:107:55:10:5:1.

3.3.3 Magnetic Properties.

The paramagnetic characteristics of an octahedrally coordinated high-spin Mn(IV) center ($3d^3$ electron configuration) may be described as an isotropic effective $S_{\text{eff}} = 3/2$

system, since the octahedral ligand field splits the 4F ground term into ${}^4T_{1g}$, ${}^4T_{2g}$ terms, and a ${}^4A_{2g}$ ground term, i.e. an orbital momentum singlet, that is energetically moderately separated from the excited states for first period transition metals. Due to spin-orbit coupling (d^3 : less than half-filled d subshell), g_{eff} here is thus expected to be slightly below the Landé factor of the free electron g_e . Therefore, down to low temperatures where saturation effects become significant, the low-field $\chi_m T$ values are expected to be temperature-independent with $\chi_m T = g_{\text{eff}}^2 S_{\text{eff}}(S_{\text{eff}} + 1)/8$ slightly smaller than the spin-only value of $1.875 \text{ cm}^3 \text{ K mol}^{-1}$. Additionally, the low-temperature M_m vs. B curve should exhibit a saturation value of $g_{\text{eff}} S_{\text{eff}} N_A \mu_B \lesssim 3 N_A \mu_B$. In contrast, the magnetic susceptibility and magnetization data of **1** (**Figure 3-7**) reveal a different behavior: First, although the $\chi_m T$ vs. T curve is linear for $T \geq 20 \text{ K}$, it is characterized by a distinct slope indicating temperature independent paramagnetic (TIP) contributions. Although the V(V) centers of **1** are formally fully oxidized and thus technically diamagnetic, fully oxidized polyoxometalates are however empirically known to exhibit significant TIP behavior.⁵⁵⁻⁵⁸ Second, the molar magnetization at 2 K reveals a saturation value above $3 N_A \mu_B$, just as the TIP-corrected $\chi_m T$ vs. T curve reveals a $\chi_m T$ value at 290 K which is above the spin-only value. We thus assume that a very small percentage of the K^+ and Li^+ counter ions, likely located between the network layers, are randomly substituted by paramagnetic manganese cations, either Mn(IV) (spin-3/2) or lower valencies like Mn(II) (spin-5/2) in the hypothetical case that Mn(IV) is reduced during synthesis. Third, a small deviation from the linear behavior of $\chi_m T$ is observed for $T < 20 \text{ K}$ that is not satisfactorily explained by saturation effects only, indicating minor antiferromagnetic exchange interactions within the compound.

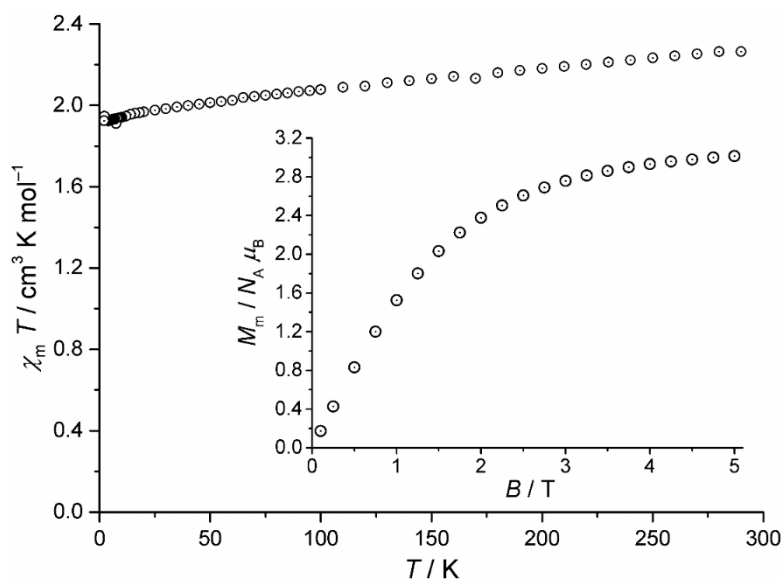


Figure 3-7. Magnetic susceptibility data of **1** (corrected for diamagnetic contributions only, with no TIP correction) depicted as the temperature dependence of $\chi_m T$ at 0.1 Tesla; inset: molar magnetization M_m vs. applied field B at 2 K.

To meet all three observations, we include an additive parameter χ_{TIP} in the magnetic susceptibility (TIP contribution), a factor representing the additional fraction of Mn(IV) per formula unit and assume the molecular-field model by a parameter zJ (minor intermolecular coupling interactions) in our fitting routines. The data and the best fit ($SQ = 0.9\%$, using CONDON 2.0)⁵⁹ to the combined magnetic susceptibility and molar magnetization data of **1** are shown in **Figure 3-8**. The best fit yields $\chi_{\text{TIP}} = +1.02 \times 10^{-3} \text{ cm}^3 \text{ mol}^{-1}$, equivalent to 1.07 Mn(IV) per formula unit (or down to 1.00 Mn(IV) + 0.03 Mn(II) per formula unit), $zJ = -0.01 \text{ cm}^{-1}$, and $g_{\text{eff}} = 1.98$ ($S_{\text{eff}} = 3/2$). This set of parameters complies with all theoretical expectations and assumptions for this scenario ($\chi_{\text{TIP}} > 0$, $zJ < 0$, $g_{\text{eff}} \lesssim g_e$), and reproduces the data very well. In particular, the corrected data shown in **Figure 3-8** are in agreement with an octahedrally coordinated, high-spin Mn(IV) center with very small antiferromagnetic exchange

interactions. In addition, the M_m vs. B curve indicates a saturation magnetization that is below $3 N_A \mu_B$, as expected.

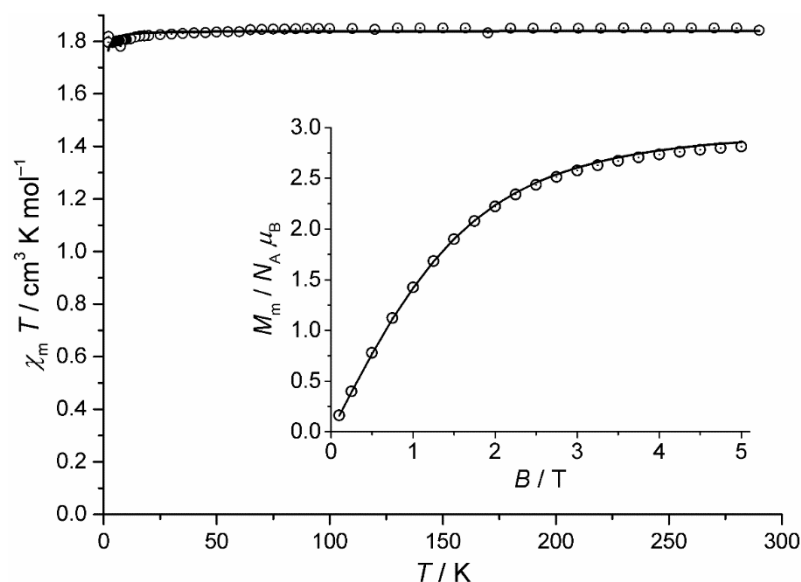


Figure 3-8. Magnetic susceptibility data of **1** (corrected for diamagnetic and TIP contributions and assuming 1.07 Mn(IV) or down to 1.00 Mn(IV) + 0.03 Mn(II) per formula unit) depicted as the temperature dependence of $\chi_m T$ at 0.1 Tesla; inset: molar magnetization M_m vs. applied field B at 2 K; open circles: data, black line: best fit.

3.3.4 Catalytic Properties.

Compound **1** in the solid state was investigated for its catalytic ability to oxidize the mustard gas simulant 2-chloroethyl ethyl sulfide (CEES, a simulant for mustard) using *t*-butyl hydroperoxide as the oxidant. As shown in **Figure 3-9**, after eight hours, almost all of the CEES is removed with a turnover number of 40. Without the addition of *t*-butyl hydroperoxide, a green color is observed after 10 min, which is due to the reduction of V(V) to V(IV) by CEES. When *t*-butyl hydroperoxide is added to this green suspension, the color immediately changes back to orange. Interestingly, the

activity of **1** is higher than that of $\text{K}_7\text{MnV}_{13}$. This likely reflects the lower negative charge of MnV_{14} (-6 vs. -7) making it a better oxidant for CEES. The FT-IR spectra and the PXRD pattern of **1** before and after catalytic reactions are almost identical indicating that the catalyst remains structurally intact under turnover conditions (**Figure 3-10 and 3-11**).

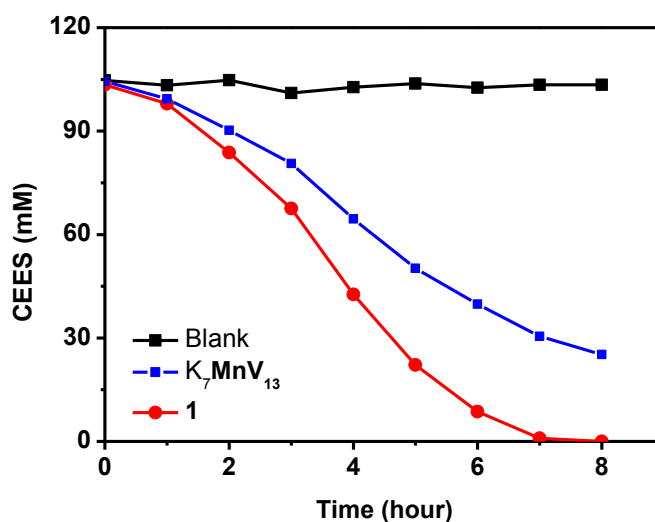


Figure 3-9. Oxidative removal of CEES catalyzed by **1** and by $\text{K}_7\text{MnV}_{13}$.

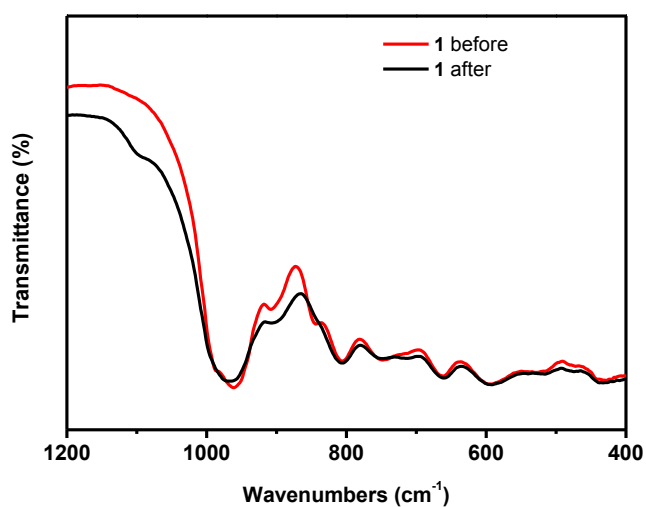


Figure 3-10. FT-IR spectra of **1** before and after catalytic CEES oxidation.

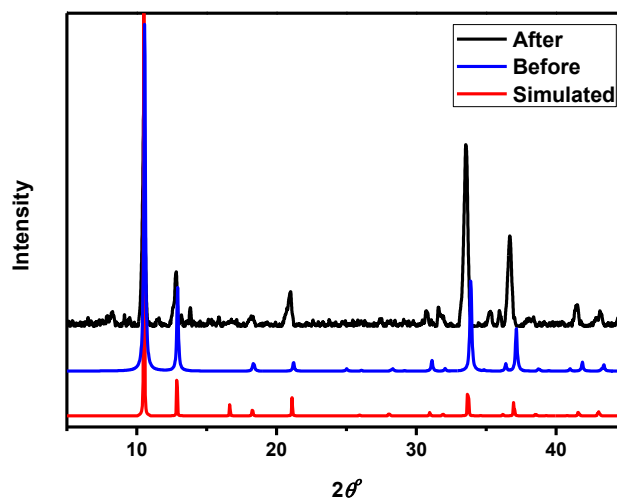


Figure 3-11. PXRD pattern of **1** before and after catalytic CEES oxidation.

3.4 Conclusions

The novel manganese(IV)-containing symmetrical heteropolyvanadate with a 1:14 stoichiometry, $\text{K}_4\text{Li}_2[\text{MnV}_{14}\text{O}_{40}] \cdot 21\text{H}_2\text{O}$ has been prepared and characterized. In the crystalline solid state, the heteropoly anion, MnV_{14} , which is composed of 14 edge-sharing VO_6 octahedra surrounding a central MnO_6 octahedron, is connected by multiple potassium ions into a 2D layered network (ABABAB...). The simplified representation of MnV_{14} shows a new topology termed **jba1**. The 1:14-stoichiometry heteropoly anion is stabilized by capping potassium ions as shown by ^{51}V NMR spectroscopy. Magnetic studies show very small antiferromagnetic intermolecular exchange interactions corresponding to an octahedrally coordinated, high-spin Mn(IV) center. Compound **1** is an effective catalyst for CEES oxidation by *t*-butyl

hydroperoxide; a TON of 40 is achieved after eight hours, which shows potential interest towards air decontamination technology. The **MnV₁₄** unit may provide a new model to the design of nanoclusters with targeted catalytic and magnetic properties.

References

- (1) *Polyoxometalate Chemistry From Topology via Self-Assembly to Applications*; Pope, M. T.; Müller, A., Eds.; Kluwer Academic Publishers: Dordrecht, 2001.
- (2) *Polyoxometalate Chemistry for Nano-Composite Design*; Yamase, T.; Pope, M. T., Eds.; Kluwer Academic/Plenum Publishers: New York, 2002; Vol. 2.
- (3) Pope, M. T. In *Comprehensive Coordination Chemistry II: From Biology to Nanotechnology*; Wedd, A. G., Ed.; Elsevier Ltd.: Oxford, UK, 2004; Vol. 4, p 635-678.
- (4) Miras, H. N.; Yan, J.; Long, D.-L.; Cronin, L. *Chem. Soc. Rev.* **2012**, *41*, 7403-7430.
- (5) Finke, R. G.; Rapko, B.; Saxton, R. J.; Domaille, P. J. *J. Am. Chem. Soc.* **1986**, *108*, 2947-2960.
- (6) Mal, S. S.; Kortz, U. *Angew. Chem. Int. Ed.* **2005**, *44*, 3777-3780.
- (7) Müller, A.; Serain, C. *Acc. Chem. Res.* **2000**, *33*, 2-10.
- (8) Schäffer, C.; Merca, A.; Bögge, H.; Todea, A. M.; Kistler, M. L.; Liu, T.; Thouvenot, R.; Gouzerh, P.; Müller, A. *Angew. Chem. Int. Ed.* **2009**, *48*, 149-153.
- (9) Cronin, L.; Müller, A. *Chem. Soc. Rev.* **2012**, *41*, 7333-7334.
- (10) Mitchell, S. G.; Boyd, T.; Miras, H. N.; Long, D.-L.; Cronin, L. *Inorg. Chem.* **2011**, *50*, 136-143.
- (11) Pope, M. T. *Heteropoly and Isopoly Oxometalates*; Springer-Verlag: Berlin, 1983.
- (12) Monakhov, K. Yu.; Bensch, W.; Kögerler, P. *Chem. Soc. Rev.* **2015**, *accepted*, DOI: 10.1039/c5cs00531k.
- (13) Kortz, U.; Hussain, F.; Reicke, M. *Angew. Chem. Int. Ed.* **2005**, *44*, 3773-3777.
- (14) Contant, R.; Herve, G. *Rev. Inorg. Chem.* **2002**, *22*, 63-111.

- (15) Li, F.; Xu, L. *Dalton Trans.* **2011**, *40*, 4024-4034.
- (16) Artero, V.; Proust, A.; Herson, P.; Villain, F.; Moulin, C. C. d.; Gouzerh, P. *J. Am. Chem. Soc.* **2003**, *125*, 11156-11157.
- (17) Rakovsky, E.; Zurkova, L. *Monogr. Ser. Int. Conf. Coord. Chem.* **1999**, *4*, 465-470.
- (18) Chen, L.; Jiang, F.; Lin, Z.; Zhou, Y.; Yue, C.; Hong, M. *J. Am. Chem. Soc.* **2005**, *127*, 8588-8589.
- (19) Kumagai, H.; Arishima, M.; Kitagawa, S.; Ymada, K.; Kawata, S.; Kaizaki, S. *Inorg. Chem.* **2002**, *41*, 1989-1992.
- (20) Kato, R.; Kobayashi, A.; Sasaki, Y. *Inorg. Chem.* **1982**, *21*, 240-246.
- (21) Yonehara, K.; Kamata, K.; Yamaguchi, K.; Mizuno, N. *Chem. Commun.* **2011**, *47*, 1692-1694.
- (22) Kuznetsov, A. E.; Geletii, Y. V.; Hill, C. L.; Morokuma, K.; Musaev, D. G. *Inorg. Chem.* **2009**, *48*, 1871-1878.
- (23) Nomiya, K.; Sakai, Y.; Yamada, Y.; Hasegawa, T. *J. Chem. Soc., Dalton Trans.* **2001**, 52-56.
- (24) Nomiya, K.; Nemoto, Y.; Hasegawa, T.; Matsuoka, S. *J. Mol. Catal. A: Chem.* **2000**, *152*, 55-68.
- (25) Nomiya, K.; Hasegawa, T. *Chem. Lett.* **2000**, 410-411.
- (26) Flynn, C. M.; Pope, M. T. *J. Am. Chem. Soc.* **1970**, *92*, 85-90.
- (27) Ichida, H.; Nagai, K.; Sasaki, Y.; Pope, M. T. *J. Am. Chem. Soc.* **1989**, *111*, 586-591.
- (28) Tatsuno, Y.; Nakamura, C.; Saito, T. *J. Mol. Catal.* **1987**, *42*, 57-66.
- (29) Fukuda, N.; Yamase, T. *Biol. Pharm. Bull.* **1997**, *20*, 927-930.
- (30) Guo, W.; Luo, Z.; Lv, H.; Hill, C. L. *ACS Catal.* **2014**, *4*, 1151-1161.
- (31) Haimov, A.; Cohen, H.; Neumann, R. *J. Am. Chem. Soc.* **2004**, *126*, 11762-11763.
- (32) Bar-Nahum, I.; Khenkin, A. M.; Neumann, R. *J. Am. Chem. Soc.* **2004**, *126*, 10236-10237.
- (33) Neumann, R.; Dahan, M. *J. Am. Chem. Soc.* **1998**, *120*, 11969-11976.

- (34) Suzuki, K.; Tang, F.; Kikukawa, Y.; Yamaguchi, K.; Mizuno, N. *Angew. Chem. Int. Ed.* **2014**, *53*, 5356-5360.
- (35) Kamata, K.; Yamaguchi, S.; Kotani, M.; Yamaguchi, K.; Mizuno, N. *Angew. Chem. Int. Ed.* **2008**, *47*, 2407-2410.
- (36) Nishiyama, Y.; Nakagawa, Y.; Mizuno, N. *Angew. Chem. Int. Ed.* **2007**, *46*, 4006.
- (37) Nakagawa, Y.; Mizuno, N. *Inorg. Chem.* **2007**, *46*, 1727-1736.
- (38) Liu, D.; Lu, Y.; Tan, H.-Q.; Chen, W.-L.; Zhang, Z.-M.; Li, Y.-G.; Wang, E. *Chem. Commun.* **2013**, *49*, 3673-3675.
- (39) Liu, S.; Li, D.; Xie, L.; Cheng, H.; Zhao, X.; Su, Z. *Inorg. Chem.* **2006**, *45*, 8036-8040.
- (40) Liu, D.; Lu, Y.; Li, Y.-G.; Tan, H.-Q.; Chen, W.-L.; Zhang, Z.-M.; Wang, E. *Dalton Trans.* **2013**, *42*, 14445-14453.
- (41) Lan, Q.; Tan, H.; Liu, D.; Wang, E. *J. Solid State Chem.* **2013**, *199*, 129-133.
- (42) Liu, D.; Lu, Y.; Tan, H.-Q.; Wang, T.-T.; Wang, E.-B. *Cryst. Growth Des.* **2015**, *15*, 103-114.
- (43) Li, D.; Liu, S.; Sun, C.; Xie, L.; Wang, E.; Hu, N.; Jia, H. *Inorg. Chem. Commun.* **2005**, *8*, 433-436.
- (44) Dolomanov, O. V.; Bourhis, L. J.; Gildea, R. J.; Howard, J. A. K.; Puschmann, H. *J. Appl. Crystallogr.* **2009**, *42*, 339-341.
- (45) Palatinus, L.; Chapuis, G. *J. Appl. Crystallogr.* **2007**, *40*, 786-790.
- (46) Sheldrick, G. *Acta Cryst. A* **2008**, *64*, 112-122.
- (47) Bruker, *APEXII v2014.1-1*, Bruker AXS, Inc., Madison, WI, **2014**.
- (48) Bruker, *SAINT v8.34A*, Bruker AXS, Inc., Madison, WI, **2013**.
- (49) Spek, A. L. *J. Appl. Crystallogr.* **2003**, *36*, 7-13.
- (50) Blatov, V. A.; Shevchenko, A. P.; Proserpio, D. M. *Cryst. Growth Des.* **2014**, *14*, 3576-3586.
- (51) O'Keeffe, M.; Brese, N. E. *Acta Crystallographica Section B* **1992**, *48*, 152-154.

- (52) Cavaco, I.; Pessoa, J. C.; Duarte, M. T.; Matias, P. M.; Henriques, R. T. *Polyhedron* **1993**, *12*, 1231-1237.
- (53) Flynn, C. M., Jr.; Pope, M. T. *Inorg. Chem.* **1973**, *12*, 1626-1634.
- (54) Ramos, S.; Duarte, R. O.; Moura, J. J. G.; Aureliano, M. *Dalton Trans.* **2009**, 7985-7994.
- (55) Ouahab, L.; Bencharif, M.; Mhanni, A.; Pelloquin, D.; Halet, J. F.; Pena, O.; Padiou, J.; Grandjean, D.; Garrigoulagrange, C.; Amiell, J.; Delhaus, P. *Chem. Mater.* **1992**, *4*, 666-674.
- (56) Lemagueres, P.; Ouahab, L.; Golhen, S.; Grandjean, D.; Pena, O.; Jegaden, J. C.; Gomezgarcia, C. J.; Delhaes, P. *Inorg. Chem.* **1994**, *33*, 5180-5187.
- (57) Juraja, S.; Vu, T.; Richardt, P. J. S.; Bond, A. M.; Cardwell, T. J.; Cashion, J. D.; Fallon, G. D.; Lazarev, G.; Moubaraki, B.; Murray, K. S.; Wedd, A. G. *Inorg. Chem.* **2002**, *41*, 1072-1078.
- (58) Shi, Z.; Peng, J.; Gomez-Garcia, C. J.; Benmansour, S.; Gu, X. *J. Solid State Chem.* **2006**, *179*, 253-265.
- (59) van Leusen, J.; Speldrich, M.; Schilder, H.; Kögerler, P. *Coord. Chem. Rev.* **2015**, *289-290*, 137-148.

Chapter 4.

Heteropolyniobates for Liquid- and Gas-Phase Decontamination of Chemical Warfare Agents

Reproduced with permission from *Angew. Chem. Int. Ed.* **2016**, *55*, 7403-7407.

Copyright 2016 WILEY-VCH Verlag GmbH & Co. KGaA, Weinheim

As a main contributor of this work; with Hongjin Lv, Kevin P. Sullivan, Wesley O. Gordon, Alex Balboa, George W. Wagner, Djamaladdin G. Musaev, Dr. John Bacsa and Craig L. Hill*, W. Guo contributed the majority of characterizations, investigating and analyzing the catalysts' activities to this work. H. Lv prepared the catalysts and conceived the research. K. P. Sullivan performed the decontamination of diethyl cyanophosphonate experiments. W. O. Gordon, A. Balboa and G. W. Wager conducted the live agent experiments. D. G. Musaev performed and analyzed the DFT calculations. J. Bacsa conducted and analyzed the X-ray crystallographic studies. W. Guo and C. L. Hill designed the experiments and prepared the manuscript.

4.1 Introduction

Chemical warfare agents (CWAs), used in past wars and recent terrorist attacks, represent a significant threat to humankind.¹⁻³ Among all of the classes of chemical weapons, vesicants (such as sulfur mustard) and nerve agents are the most common.⁴ Sulfur mustard is one of the most effective CWAs used in modern warfare.⁵ Nerve agents are organophosphorus compounds containing P-X bonds (X=F, CN, SR etc.),^{6,7} that rapidly inactivate acetylcholinesterase, the enzyme which facilitates hydrolysis of the neurotransmitter acetylcholine in the nervous system, leading to a range of incapacitating states and in higher concentrations, death.⁸ There remains a need to develop materials and methods to rapidly, fully and catalytically decontaminate all the main CWAs under mild conditions.

Both organic and inorganic materials have been developed to catalyze hydrolysis of nerve agents and their simulants.^{4,9-20} A series of Zr-based metal-organic frameworks (MOFs, especially UiO-66, NU-1000 and MOF-808) that contain strongly acidic Zr(IV) sites, have shown significant catalytic activities for hydrolyzing nerve agents and the simulant dimethyl 4-nitrophenyl phosphate (DMNP).²¹⁻²⁴ However, the catalytic hydrolysis of DMNP by the Zr-based MOFs often requires the addition of *N*-ethylmorpholine as a buffer and a proximal base. These MOFs are of low activity decontaminating the relatively inert nerve agent simulant, DMNP.²⁵ Recently, a porphyrinic MOF that catalyzes selective photooxidation of a sulfur mustard simulant was also reported.²⁶

Polyoxometalates (POMs), one polyoxoniobate (PONb), [Nb₆O₁₉]⁸⁻ and other Nb-based solid materials have also been investigated for the degradation of CWAs and/or their simulants.²⁷⁻³¹ POMs are a class of metal oxide clusters with versatile applications in magnetism, medicine, electrochemistry and catalysis.³²⁻³⁶ PONbs are a subclass of

POMs with high negative charges per polyanion oxygen and commensurately basic surface oxygens.³⁷⁻⁴¹ We report here that a heterogeneous one-dimensional polymeric heteropolyaniobate: $K_{12}[Ti_2O_2][GeNb_{12}O_{40}] \cdot 19H_2O$ (**KGeNb**) is as effective as any basic heterogeneous CWA hydrolysis catalyst to date and the mechanism is probed by kinetics and other methods. The activity of its structural analogue, $K_{12}[Ti_2O_2][SiNb_{12}O_{40}] \cdot 22H_2O$ (**KSiNb**), towards the decontamination of CWAs is also discussed.

4.2 Experimental

4.2.1 General Methods and Materials

All reagents used were commercially available. $K_{12}[Ti_2O_2][SiNb_{12}O_{40}] \cdot 22H_2O$ (**KSiNb**) was prepared by a reported literature method.⁴² Powder X-ray diffraction (PXRD) and FT-IR spectroscopy were used to determine its purity. The PXRD data were acquired on a D8 Discover Powder Instrument using monochromatic Co K α ($\gamma = 1.78901 \text{ \AA}$) radiation. The FT-IR spectra (2% sample in KBr pellets) were collected on a Nicolet TM 600 FT-IR spectrometer. Thermogravimetric analyses were conducted on a STA 6000 thermal analyzer. Elemental analyses (K, Ti, Si, Ge and Nb) were performed by Galbraith Laboratories (Knoxville, Tennessee). ³¹P NMR (202.46 MHz) spectroscopy conducted on a Mercury 300 spectrometer, was used to detect the reagents and products from the catalytic reactions. Samples were placed in 5 mm O.D. NMR tubes and chemical shifts were referenced to H₃PO₄ (taken as 0 ppm at 25 °C).

4.2.2 Synthesis of a new polymeric polyanionate, KGeNb

Typically, amorphous Nb₂O₅ \cdot xH₂O (0.35 g, 2.6 mmol) was added to an aqueous KOH solution (8 mL, 0.8 M) followed by tetraethoxygermane (0.23 g, 0.9 mmol) and tetraisopropyltitanium (0.13 g, 0.45 mmol). The mixture was stirred at room

temperature for 30 min, then transferred to a 20 mL autoclave and heated at 220 °C for 20 h. Colorless needle-like crystals were collected by filtration and washed with deionized water. Yield: 0.61 g (51 % based on Nb). Anal. Calcd for $\text{K}_{12}[\text{Ti}_2\text{O}_2][\text{GeNb}_{12}\text{O}_{40}] \cdot 19\text{H}_2\text{O}$ (**KGeNb**): K, 17.0; Ti, 3.5; Ge, 2.6; Nb, 40.3. Found: K, 17.6; Ti, 2.9; Ge, 3.0; Nb, 40.8. FTIR (1100-400 cm^{-1} , 2% KBr pellets): 873 (s), 784 (w), 743 (w), 682 (s), 545 (w).

4.2.3 X-ray Crystallography

A suitable colorless needle-like crystal was selected and mounted on a loop using Paratone oil on a Bruker D8 diffractometer with APEX2 detector. The crystal was cooled to $T = 173(2)$ K during data collection. The ω scans of 1° and for 30s per frame with Mo $\text{K}\alpha$ radiation (45kV, 35mA, fine-focus sealed tube) was applied when collecting data. The total number of runs and images was determined based on strategy calculation from **APEXII**.⁴³ The **SAINT** software was used for data reduction.⁴⁴ **SADABS-2014/5** was used for absorption correction.⁴⁵ The unit cell parameters were refined using **SAINT** on 8908 reflections. The structure was solved with the **Superflip** structure solution program⁴⁶ by the Charge Flipping solution method using **Olex2**⁴⁷ and refined by least squares using **ShelXL**.⁴⁸ The structure was solved in the space group P-4c2. All atoms were refined anisotropically. The amorphous regions were treated using the Squeeze routine in Platon.⁴⁹ The number of water molecules was determined by thermogravimetric analysis.

Table 4-1. The crystallographic data for **KGeNb**.

Formula	$\text{Ge K}_{12} \text{Nb}_{12} \text{O}_{58} \text{Ti}_2 \text{H}_{32}$
Dcalc./ Mg cm^{-3}	3.078
Absorption Coefficient μ/mm^{-1}	3.988

Formula Weight/gmol ⁻¹	2712.76
Crystal Size /mm ³	0.65 x 0.11 x 0.09
T/K	173(2)
Crystal System	tetragonal
Space Group	P-4c2
a/Å	15.9789(6)
b/Å	15.9789(6)
c/Å	22.927
α/°	90
β/°	90
γ/°	90
V/Å ³	5853.8(4)
Z	4
Theta range for data collection/ °	2.531 to 33.139
Reflections collected	76956
Independent reflections	11160 [R(int) = 0.0563]
Absorption correction	Semi-empirical from equivalents
Restraints / parameters	45/ 385
Largest Peak	4.692
Deepest Hole	-1.431
GooF	1.051
wR2 (all data)	0.1374
wR2	0.1249
R1 (all data)	0.0722
R1	0.0518

$$R1 = \frac{\sum||F_0| - |F_c||}{\sum|F_0|}; wR2 = \frac{\sum[w(F_0^2 - F_c^2)^2]}{\sum[w(F_0^2)^2]}^{1/2}$$

4.2.4 Degradation of DMMP by KSiNb and KGeNb

In a typical reaction, 18 μmol of **KSiNb** or **KGeNb**, DMMP (2.5 μL) and D_2O (0.5 mL) were mixed with 1.0 mL of deionized water in a 2-mL scintillation vial. This mixture was vigorously stirred at room temperature. Every several hours, a 400 μL aliquot of the solvent was transferred into the NMR tube for ^{31}P NMR measurement; the aliquot was then transferred back to the vial for further reaction. After 264 hours, the solid was collected by centrifugation, washed extensively with deionized water and dried. The resulting solid was then characterized by FT-IR, and used for successive runs.

4.2.5 Degradation of DECP by KSiNb and KGeNb

In a typical reaction, 11 μmol of **KSiNb** or **KGeNb** was suspended in 600 μL of DMF placed in an 5-mL O.D. NMR tube. Subsequently, 10 μL of DECP and 50 μL of H_2O were added. The mixture was vigorously shaken at room temperature. Every several minutes, the contents were assessed by ^{31}P NMR spectroscopy to monitor the reaction. After 100 min, the solid was collected by centrifugation, washed extensively with deionized water and dried.

4.2.6 Degradation of live agent (GD) by KSiNb

In a typical reaction, 5 μmol of **KSiNb** and 28 μmol of GD was stirred continually in 1.5 mL water for 1 h, after which 0.75 mL aliquot of the solvent was transferred to an NMR tube for acquisition of the ^{31}P NMR spectra (Varian 400 INOVA NMR spectrometer). About 43% of the GD is consumed with continuous stirring. A control was conducted under the same conditions but without the addition of **KSiNb**. For kinetics study in Figure S12, 2.5 μmol of **KSiNb** and 14 μmol of GD was added to 0.75 mL of H_2O in an NMR tube. The mixture was vigorously shaken at room temperature.

Every several minutes, the contents were assessed by ^{31}P NMR spectroscopy to monitor the reaction.

4.2.7 Gas Phase Adsorptive Degradation of Live Agents (GB and HD) on KSiNb and KGeNb

Adsorption and reaction of the live agents GB and HD were followed *in situ* on the **KSiNb** and **KGeNb** with Diffuse Reflectance Infrared Spectroscopy (DRIFTS). In a typical experiment, 10-15 mg of the P-PONb was packed into a 6-mm diameter porous ceramic cup, and the sample was purged in a small stainless steel vessel under dry nitrogen for 24 hours to remove excess water and to provide a stable background for DRIFTS experiments. After the purge, the sample was rapidly transferred to a Pike Technologies Diffuse IR environmental cell with a KBr window, where the sample was maintained at 25 °C under a 10 mL/min ultra-high purity He flow. FTIR spectra were collected using a Thermo Nicolet 6700 spectrometer set with a resolution of 2 cm^{-1} using a liquid nitrogen cooled MCT/A detector. Spectra were collected periodically until it was confirmed that gas phase water and CO_2 were no longer present in the cell and that the sample had equilibrated in the He stream (typically 2 hr). After equilibration, a background spectrum (1024 scans) was collected to be used as a reference for the remainder of the experiment. He saturated with chemical agent vapor was introduced via a temperature controlled saturator cell that contained ~ 2 mL of agent and that was held at 20 °C. Spectra were collected in the form of difference spectra, where positive peaks represent newly formed species while negative peaks indicate depletion of species near the surface.

4.2.8 Computational Studies.

Polyanions, $\{[(\text{OH})_2\text{Ti}[\text{XNb}_{12}\text{O}_{40}-(\text{Ti}_2\text{O}_2)-\text{O}_{40}\text{Nb}_{12}\text{XTi}(\text{OH})_2], \text{ where } \text{X} = \text{Si (1) and Ge (2), were chosen as a model for KSiNb and KGeNb polymers. In these models we$

eliminated K counter cations and associated water molecules in order to make the calculations technically feasible. Furthermore, the end oxo-groups of the terminal TiO_2 -fragment were capped by protons. The geometry of these model systems was optimized in implicit dichloromethane solution, with no geometric (or symmetry) constraints, at their ground singlet electronic state (Table S2). In these calculations, we used the DFT method (M06L functional)⁵⁰ in conjunction with the split-valence 6-31G(d,p) basis sets for O, C, H and P, and lanl2dz basis sets and associated ECPs for the Nb, Ti, Ge and Si atoms,⁵¹⁻⁵³ which below are referred to as M06L/BS1. The solvent effects were approximated by the polarizable continuum model (CPCM).⁵⁴⁻⁵⁶ All calculations were carried out with the Gaussian 09 software package.⁵⁷

4.3 Results and Discussion

4.3.1 Synthesis and structure of **KGeNb**

In 2002, Nyman and co-workers reported the single crystal structure of $\text{K}_{12}[\text{Ti}_2\text{O}_2][\text{SiNb}_{12}\text{O}_{40}] \cdot 22\text{H}_2\text{O}$ (**KSiNb**).⁴² In 2005, the structures of the sodium salts of $[\text{Ti}_2\text{O}_2][\text{SiNb}_{12}\text{O}_{40}]^{12-}$ and $[\text{Ti}_2\text{O}_2][\text{GeNb}_{12}\text{O}_{40}]^{12-}$ were inferred from PXRD data.⁵⁸ However, given the remarkable basic reactivity of these one-dimensional polyniobates, we sought a high-resolution single-crystal structural determination of these nanothread-like materials in order to facilitate more detailed experimental and computational study of their surface-related reactions.

Although significant efforts failed to produce single crystals of the sodium salt of the germanium-based heteropolyanion, $[\text{Ti}_2\text{O}_2][\text{GeNb}_{12}\text{O}_{40}]^{12-}$, the corresponding potassium salt, **KGeNb**,⁵⁹ was readily synthesized under hydrothermal conditions from $\text{Nb}_2\text{O}_5 \cdot x\text{H}_2\text{O}$, tetraethoxygermane and tetraisopropyltitanium in an aqueous solution of KOH. Not surprisingly considering the similar size and properties of the Ge(IV) and

Si(IV) heteroatoms, **KGeNb** and **KSiNb** are isostructural. These nano-scale threads are composed of silico/germano-dodecaniobate Keggin ions connected by two edge-sharing TiO_6 octahedra ($[\text{Ti}_2\text{O}_2]^{4+}$) forming one-dimensional infinite chains (**Figure 4-1**).⁵⁸ The K^+ counter cations are situated between the 1D polyanions, and **Figure 4-1** shows that two of the K^+ ions reside in pockets defined by adjacent Keggin units in each polyanion polymer. The rate of nerve agent decomposition by $[\text{Nb}_6\text{O}_{19}]^{8-}$ is affected by counter cations.²⁷ Although the specific counter cation effect in **KGeNb** is complicated, the short bond lengths (2.621~3.329 Å) including one to the Ti-O-Ti oxygen (O4 from the X-ray structure) implicates a non-innocent role for these counter cations in the organophosphate compound degradation mechanism.

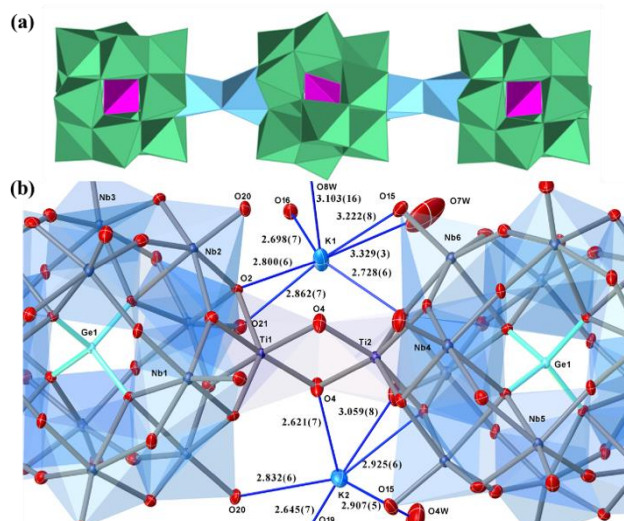


Figure 4-1. (a) Polyhedral representation of the one-dimensional polyanion chain of **KGeNb**. Color code: green: NbO_6 ; blue: TiO_6 ; pink: GeO_4 . (b) Precise structural environments of two potassium counter cations interacting with the polymeric polyanion unit (bond lengths in Å)

4.3.2 Decontamination of chemical warfare agents and simulants by KGeNb

The U.S. Army nominated DMMP as an ideal model chemical for toxicology and carcinogenesis studies.²⁵ In this study, **KSiNb** and the new more reactive P-PONb, **KGeNb**, hydrolyze DMMP to methyl phosphonic acid (MP) under mild conditions (with only water at room temperature (**Figure 4-2**). Hydrolysis of the phosphate ester bonds was observed and monitored by ³¹P NMR spectroscopy (**Figure 4-3**). The extent of conversion was calculated as the ratio of the integrated ³¹P NMR peak for MP (the only hydrolysis product) to that of DMMP. **KGeNb** converts 54 % of this quite inert simulant over the time course of 264 h. The rates of DMMP hydrolysis by **KGeNb** or **KSiNb** slow down after ca. 100 h due to the production of MP which inhibits the reaction (**Figure 4-4**).

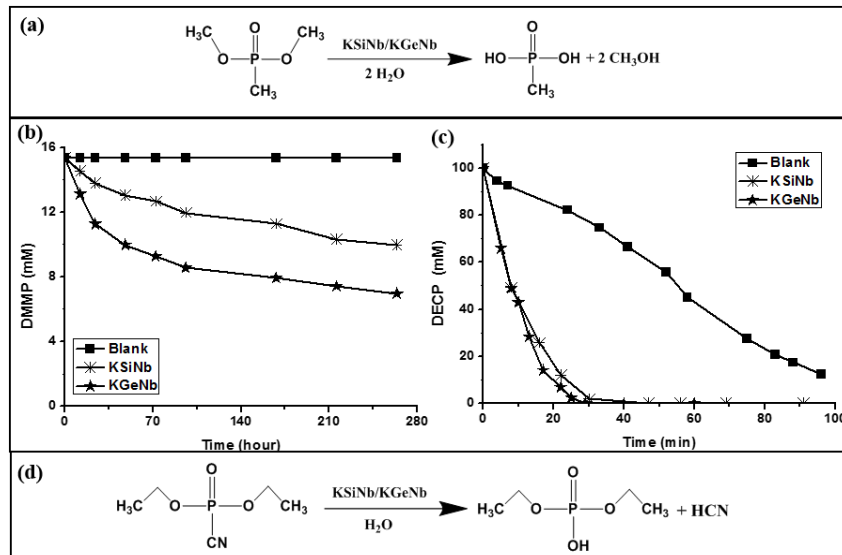


Figure 4-2. (a) Hydrolytic decomposition pathway of DMMP to MP. (b) DMMP decomposition using **KGeNb** and **KSiNb**; conditions: [DMMP] = 15.5 mM, 18 μmol **KGeNb** or **KSiNb**, 0.5 mL D₂O and 1.0 mL H₂O at room temperature. (c) DECP decomposition using **KGeNb** and **KSiNb**; conditions: [DECP] = 100 mM, 11 μmol

KGeNb or **KSiNb**, 600 μL of DMF and 50 μL of H₂O at room temperature. (d)
Hydrolytic decomposition pathway of DECP to DEHP.

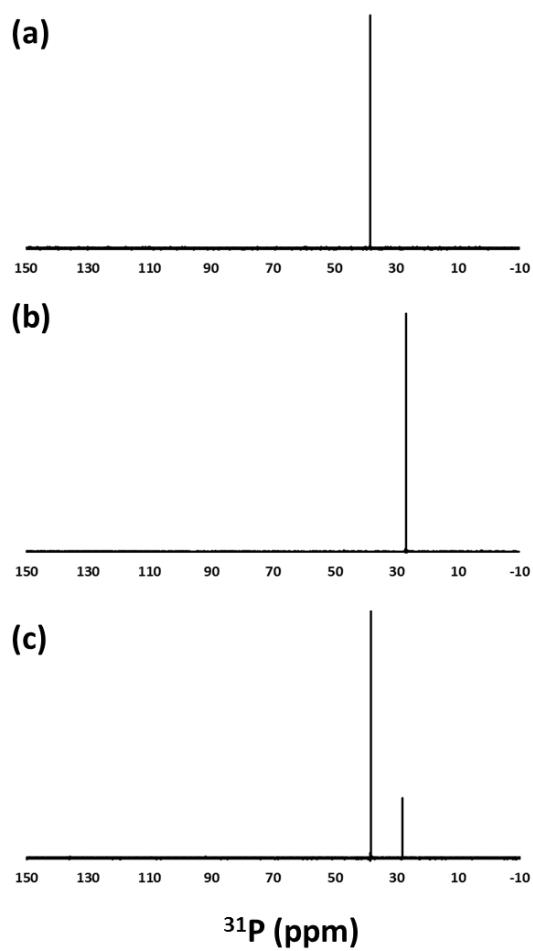


Figure 4-3. ³¹P NMR spectra of (a) DMMP, (b) methyl phosphonic acid (MP) and (c) DMMP decomposition by **KGeNb** after 24 h in 0.5 mL D₂O and 1.0 mL H₂O.

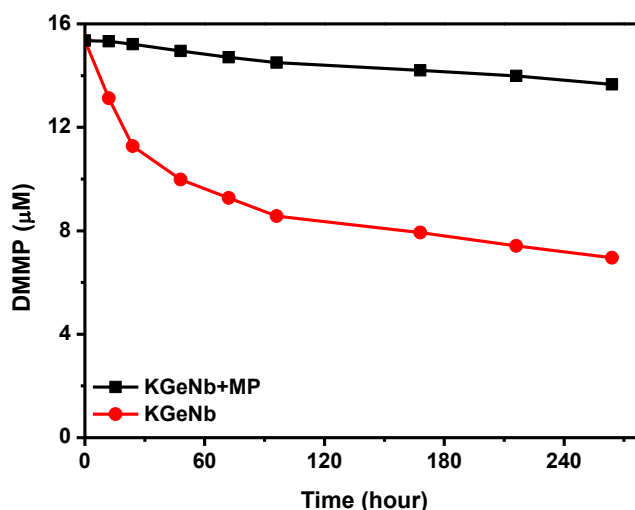


Figure 4-4. Red circles: hydrolysis of DMMP using **KGeNb**. Conditions: [DMMP] = 15.5 mM, 18 μmol **KGeNb**, 0.5 mL D_2O and 1.0 mL H_2O at room temperature. Black squares: inhibition of DMMP hydrolysis by MP, 15.5 mM MP was added.

The higher hydrolytic activity of **KGeNb** relative to **KSiNb** could be explained by (a) smaller crystallites of the former than the latter, (b) slight dissolution of these P-PONbs to form hydrolytically active soluble monomeric polyniobate species, with **KGeNb** being slightly more soluble than **KSiNb**, or (c) an intrinsically more reactive polymeric polyanion for **KGeNb** than for **KSiNb**. Scenario (a) is not likely because examination of **KGeNb** and **KSiNb** by optical microscope shows similar crystallite sizes for both (**Figure 4-5**). Furthermore, both of these P-PONbs were ground to make particles that were smaller and quite uniform prior to use in the decontamination reactions.

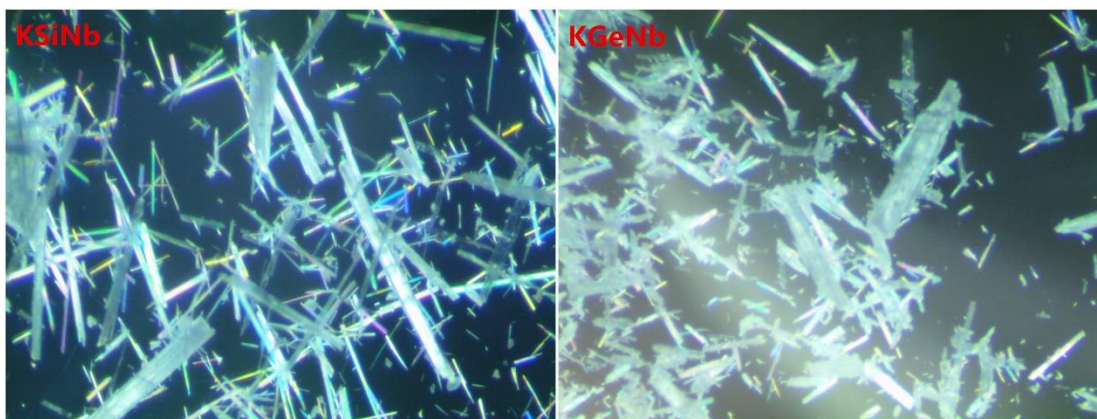


Figure 4-5. Optical microscope images of **KSiNb** and **KGeNb** crystals.

Scenario (b) is very unlikely from five lines of evidence: (1) there is no detectable activity in the supernatant after suspensions of **KGeNb** or **KSiNb** are used for DMMP hydrolysis (the suspensions were filtered and the filtrate assessed for activity after use; **Figure 4-6**); (2) elemental analysis of the filtrate indicates negligible amounts of Si, Nb or Ge are present; (3) the weighable amount of **KGeNb** and **KSiNb** is the same before and after reaction; (4) the **KGeNb** collected after reaction, washed extensively with deionized water, dried under vacuum and re-used in successive DMMP hydrolysis runs shows comparable activity to the first run (**Figure 4-7**); and (5) the FT-IR of **KGeNb** and **KSiNb** before and after the reaction with DMMP remain identical (**Figures 4-8 and 4-9**). All these argue for the heterogeneous nature of the catalytic hydrolysis. Thus, scenario (c) is possible and might derive from the subtle effects on the negative charge density of the polyanion oxygens by larger size of the central GeO_4 tetrahedron versus the central SiO_4 tetrahedron.

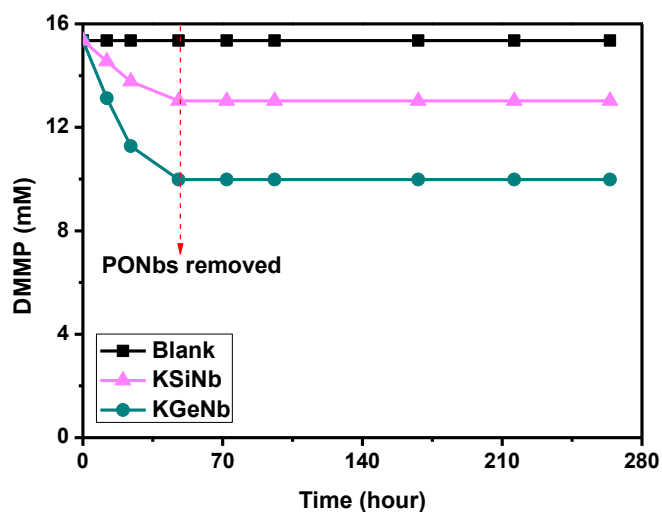


Figure 4-6. DMMP hydrolysis by the supernatant after suspensions of **KGeNb** or **KSiNb** are used for DMMP hydrolysis then the suspensions filtered and the filtrate assessed for activity. Conditions: [DMMP] = 15.5 mM, 18 μ mol **KSiNb** or **KGeNb**, 0.5 mL D₂O and 1.0 mL H₂O at room temperature.

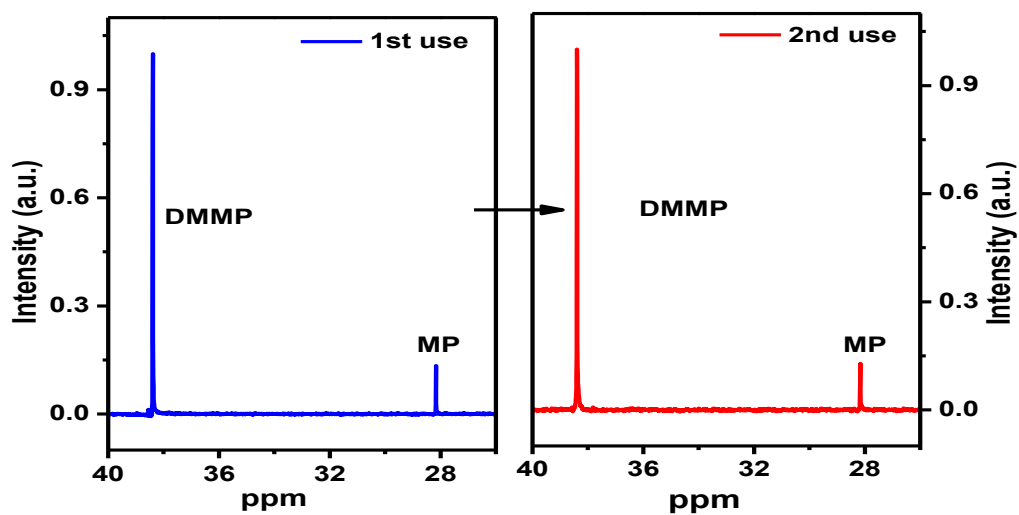


Figure 4-7. ³¹P NMR spectra showing the reuse of **KGeNb** for second run, reaction time = 12 h.

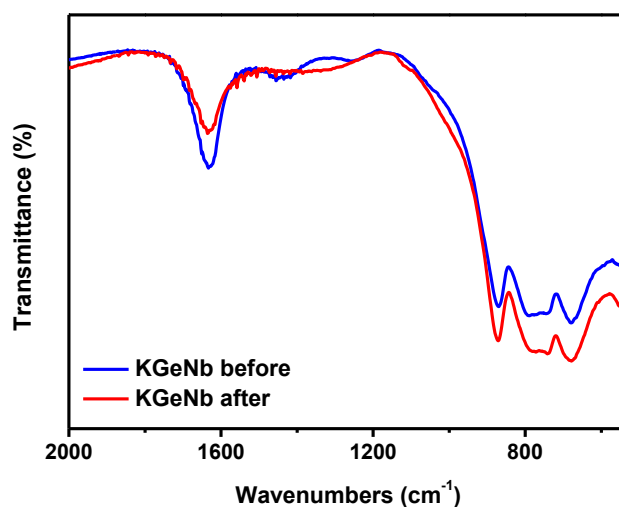


Figure 4-8. FT-IR spectra of KGeNb before and after DMMP hydrolysis.

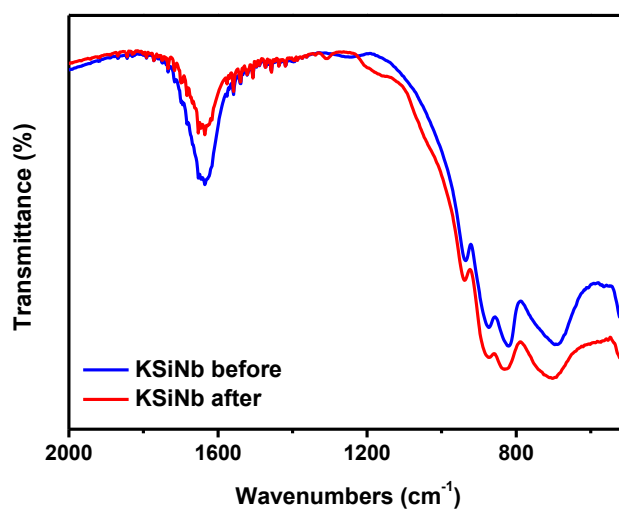


Figure 4-9. FT-IR spectra of KSiNb before and after DMMP hydrolysis.

The initial rate for reaction of DMMP with **KGeNb** is approximately first order with respect to DMMP (**Figure 4-10**) and the quantity of insoluble **KGeNb** present (at constant pH=10, **Figure 4-11**), which is strong evidence for a general base-catalyzed mechanism. We note the well-established qualification that getting the order in a heterogeneous catalyst is subject to more error than for homogeneous reactants where

the concentration is precisely defined. We also measured the kinetic solvent isotope effect for DMMP hydrolysis.⁶⁰ The ratio of reaction rate constants, $k(\text{H}_2\text{O})/k(\text{D}_2\text{O})$, was determined to be 1.4, which is also consistent with a general base-catalyzed reaction.⁶¹ A third argument for general base catalysis is that the rate of DMMP hydrolysis by hydroxide alone is far lower than by P-PONbs at that same pH (pH=10) (**Table 4-2**). The collective data indicate that generation of hydroxide by reaction of the P-PONb with water in an initial pre-equilibrium (specific base catalysis) does not account for the great majority of the nerve agent simulant hydrolysis by these basic polymeric nano-scale thread-like materials. A general-base hydrolysis mechanism dictates that the slow step of the overall hydrolysis mechanism involves deprotonation of a water molecule by the P-PONb while the incipient forming hydroxide simultaneously attacks its electrophilic partner, the nerve agent simulant phosphorus atom. This is also consistent with the mechanism proposed for the decomposition of diisopropyl fluorophosphates by $[\text{Nb}_6\text{O}_{19}]^{8-}$.²⁷ The subsequent charge neutralization of product species by proton transfer is fast and does not contribute to the observed rate.

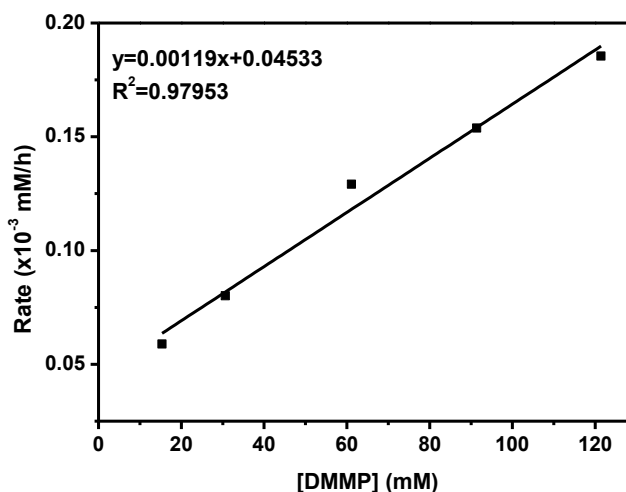


Figure 4-10. Plot of the initial rate versus DMMP concentration in the decontamination

of DMMP using **KGeNb**. Conditions: [DMMP] = 15.5 ~ 121.4 mM, [**KGeNb**] = 18 μmol , 0.5 mL D₂O and 1.0 mL H₂O at room temperature

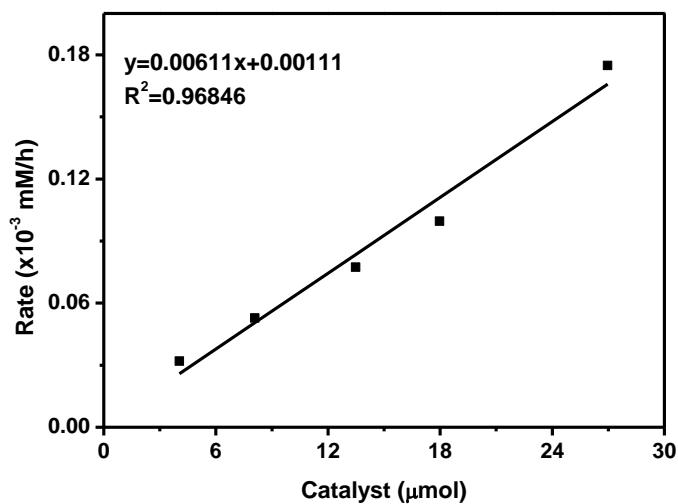


Figure 4-11. Plot of the initial rate versus the amount of **KGeNb** in the decontamination of DMMP using **KGeNb**. Conditions: [DMMP] = 15.5 mM, amount of **KGeNb** added: 4.0 ~ 27.0 μmol , 1.5 mL of *N*-ethylmorpholine aqueous solution (0.45 M) as a buffer at pH 10.

Table 4-2. Comparison of DMMP and DECP decomposition by different materials at room temperature under the same conditions.^[a]

Materials	Substrate	Time	Conversion	$t_{1/2}$ (h)
KGeNb	DMMP	24 h	25%	54
UiO-66	DMMP	24 h	<1%	>1343
MOF-808	DMMP	24 h	<1%	>1343

NaOH ^[b]	DMMP	24 h	4%	336
K₈Nb₆O₁₉	DMMP	24 h	5%	269
KGeNb	DECP	30 min	100%	0.1
UiO-66	DECP	30 min	32%	1.3
MOF-808	DECP	30 min	50%	0.4
K₈Nb₆O₁₉	DECP	30 min	90%	0.2
MgO	DECP	30 min	90%	0.2
TiO₂	DECP	30 min	87%	0.2
KSiNb	GD	1 h	43%	1.2
Cs₈Nb₆O₁₉	GD	1 h	37%	1.4
N/A ^[c]	GD	1 h	<1%	31

[a] Conditions for DMMP hydrolysis: [DMMP] = 15.5 mM, 50 mg of materials for each entry, 0.5 mL D₂O and 1.0 mL H₂O. Conditions for DECP hydrolysis: [DECP] = 100 mM, 30 mg of material for each entry, 600 μL of DMF and 50 μL of H₂O. [b] NaOH was prepared as a homogeneous phase with a pH of 10. [c] No MOF, POM or other active material added.

Figure 4-2 also shows the time profile and the reaction pathway for the hydrolytic degradation of another CWA simulant, diethyl cyanophosphate (DECP) to diethyl hydrogen phosphate (DEHP) by **KGeNb** and **KSiNb**. Hydrolysis of the P-CN bond was observed and monitored by ³¹P NMR spectroscopy. Within 30 min, all DECP is

removed. The addition of **KGeNb** or **KSiNb** to the mixture greatly accelerates the reaction. A TON of ca. 6 is achieved in 30 min. Without addition of extra base to remove the acidic and thus self-inhibiting hydrolysis product, nor with strong mixing or other means to increase the TON, this level of reactivity under ambient conditions is of interest for human protection in some real-world environments. Keep in mind that the deployed decontaminating technologies in use by the U.S. Army are essentially stoichiometric. Any catalytic method that could use ambient water (humid air) for hydrolysis or ambient O₂ (air) for oxidative decontamination remains of considerable interest. **KGeNb** and **KSiNb** both contain many water of hydration (hydrogen-bonded to the basic polyniobate oxygens) and thus should be able to catalytically remove many equivalents of nerve agent per repeating unit in their as-synthesized forms.

Table 4-2 summarizes the activities of **KGeNb**, the reported Zr-based MOFs as well as the monomeric polyniobate, [Nb₆O₁₉]⁸⁻, against DMMP and DECP under the same mild conditions. The half-life, t_{1/2} (50% conversion) is also listed.¹² UiO-66 or MOF-808 show no detectable hydrolysis of DMMP under the same conditions, although under other conditions some of these MOFs do hydrolyze DMMP.²³ Control experiments using Nb₂O₅, NbO₂, TiO₂ or MgO show no degradation of DMMP whatsoever,⁹ and a lower activity towards DECP by MgO or TiO₂ compared with **KGeNb** is observed (**Table 4-2**). **KGeNb** is also more active than [Nb₆O₁₉]⁸⁻ towards DMMP or DECP under the same conditions. Since the P-PONbs under the reaction conditions in this study are effectively insoluble, the local negative charges of the polymeric polyanions consequently appear to be vital for efficient basic nerve agent simulant hydrolysis.

KSiNb was investigated for its activity towards the degradation of live agent, GD (**Table 4-2** and **Figure 4-12**). After 1 h, 43% of the GD is consumed with continuous

stirring, which is more active than that of $[\text{Nb}_6\text{O}_{19}]^{8-}$. The control reaction (same conditions but no P-PONb added) shows negligible reaction of GD within 1h. Degradation of GB by **KGeNb** and **KSiNb** was also studied in the gas phase (GB vapor passed over the P-PONb) using Diffuse Reflectance Infrared Fourier Transform Spectroscopy (DRIFTS). **Figure 4-13** and **Figure 4-14** indicate that GB is partially hydrolyzed on **KGeNb** and **KSiNb** at room temperature (see SI for details and spectral characterization).

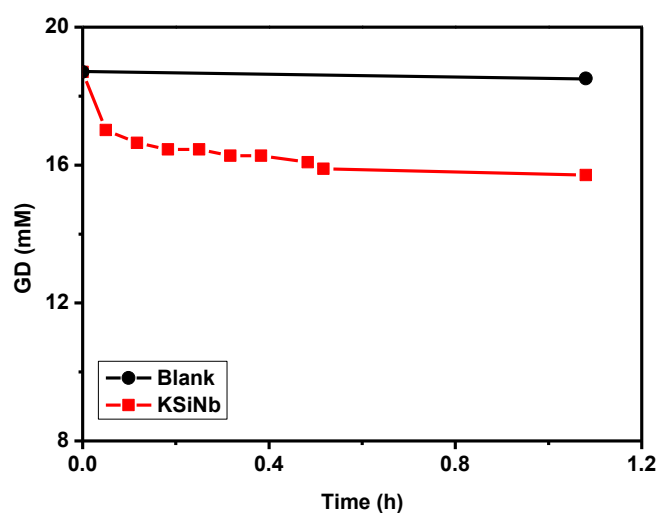


Figure 4-12. Hydrolysis of GD using **KSiNb** (red squares). 2.5 μmol of **KSiNb** and 14 μmol of GD was added to 0.75 mL of H_2O in an NMR tube. The mixture was vigorously shaken at room temperature. Every several minutes, the contents were assessed by ^{31}P NMR spectroscopy to monitor the reaction. Due to the lack of continuous stirring, it shows a relatively lower activity (16 % of GD is removed) compared with the continuous stirred system (43 % of GD is consumed).

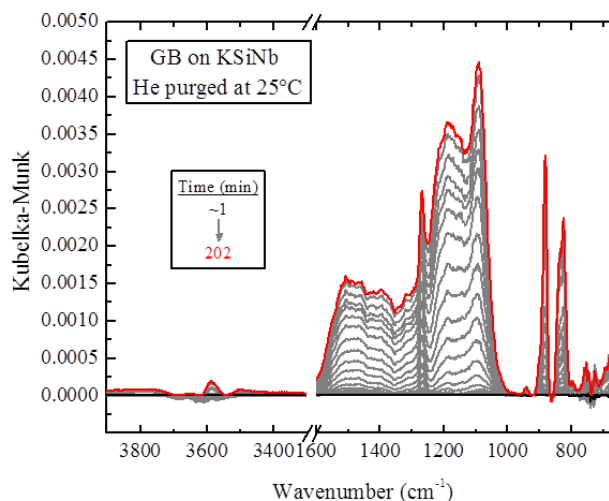


Figure 4-13. Adsorption and hydrolysis of GB on **KSiNb** as studied by DRIFTS (0 to 202 minutes at ambient temperature).

Analysis of results indicate there is a mixture of intact GB and GB hydrolysis products on the surface. On the **KSiNb** sample, perturbation of the hydroxyls is indicated by the slight negative features from 3715 – 3622 cm^{-1} coupled with the positive ν (O-H) stretch at 3585 cm^{-1} . There were no peaks observed in the ν (C-H) stretching region, however, a peak is observed at 1268 cm^{-1} which is assigned to the ν (P=O) stretch of hydrogen bound GB on the **KSiNb** sample. This peak is redshifted from the gas phase value for this mode from 1303 cm^{-1} . Two large and broad peaks are observed at 1188 and 1092 $^{-1}$. These peaks are in the expected region of the ν (C-C) and ν (C-O) stretches, however their broadness and position are consistent with a second hydrolyzed species which would result in ν_a (O-P-O) and ν_s (O-P-O) stretches in this region. The small feature at 940 cm^{-1} is attributed to a ρ_a (CH_3). A peak is observed at 881 cm^{-1} , which is tentatively assigned as ν_a ((HO)-P) stretch (as determined via a harmonic frequency calculation on the methyl phosphonic acid

species). Finally, an apparent doublet is observed centered around 829 cm^{-1} . This peak is assigned to the ν (P-F) stretch, but it is also redshifted from the gas phase value at 844 cm^{-1} , suggesting a species either from a reacted GB or one in which the fluorine is interacting with the **KSiNb** in some manner. Finally, there is a slight negative feature at 860 cm^{-1} , this feature is due to the perturbation of a **KSiNb** mode upon GB adsorption. In summary, while there is significant evidence of some hydrolysis of GB, but there also is unreacted, hydrogen bound GB on the POM.

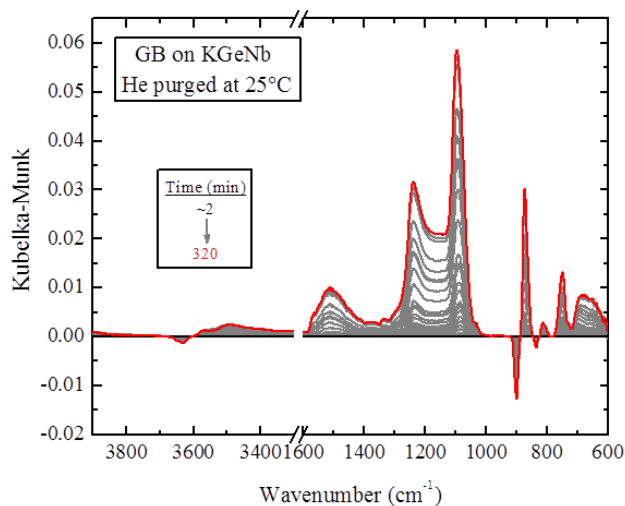


Figure 4-14. Adsorption and hydrolysis of GB on **KGeNb** as studied by DRIFTS (0 to 320 minutes at ambient temperature).

Analysis of results indicate that mostly GB hydrolysis products are observed (no intact GB). Upon adsorption of GB onto the **KGeNb** sample, a negative peak at 3633 cm^{-1} coupled with positive peaks in the $3555 - 3200\text{ cm}^{-1}$ region indicate perturbation of hydroxyls on the POM. Unlike the **KSiNb** sample, no clear ν (P=O) modes was observed which would signal the presence of unreacted, hydrogen bound GB. The large and broad modes at 1239 and 1097 cm^{-1} are consistent with a mixture of the ν (C-

C) and ν (C-O) stretches in addition to ν_a (O-P-O) and ν_s (O-P-O) of hydrolyzed GB. The intense peak at 872 cm^{-1} is tentatively assigned as ν_a ((HO)-P) stretch on the surface, and the relatively weak and red-shifted ν (P-F) stretch also is consistent with some GB reaction. As seen with **KSiNb**, negative features at 900 and 836 cm^{-1} are assigned as POM vibrations perturbed by GB adsorption or reaction.

KGeNb and **KSiNb** were also investigated for the degradation of HD using DRIFTS (**Figure 4-15** and **Figure 4-16**). Difference IR spectra collected *in situ* of the **KGeNb** during HD exposure did not show peaks associated with intact HD adsorbed to the surface of the material. Instead, perturbation of water molecules and/or hydroxo groups of **KGeNb** and **KSiNb** was noted by a negative feature at 3630 cm^{-1} . A multiplet of peaks was observed from 1230 to 1050 cm^{-1} which likely derives from the formation of the hydrolysis products: half mustard (HM) and thiodiglycol (TDG). Negative peaks in the $930 - 820\text{ cm}^{-1}$ range are due to depletion of modes of **KGeNb** and **KSiNb**. The DRIFTS results suggest that HD largely hydrolyzes to HM and TDG upon exposure to these P-PONbs, even under a dry He flow. Reactivity of these 1D materials under humid conditions would likely increase.

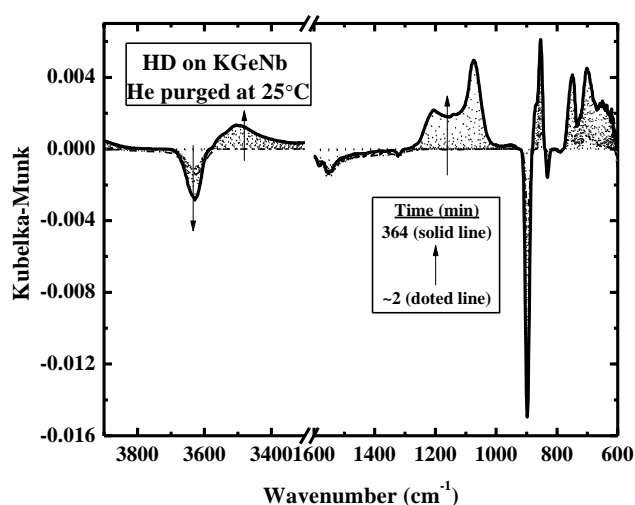


Figure 4-15. Difference DRIFTS spectra of HD sorption onto **KGeNb**.

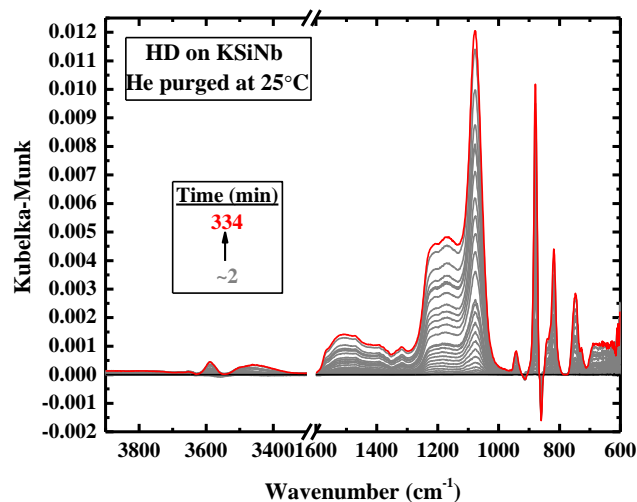


Figure 4-16. Difference DRIFTS spectra of HD sorption onto **KSiNb**.

4.3.3 Computational studies

Polyanions, $\{[(\text{OH})_2\text{Ti}[\text{XNb}_{12}\text{O}_{40}-(\text{Ti}_2\text{O}_2)-\text{O}_{40}\text{Nb}_{12}\text{XTi}(\text{OH})_2],$ where $\text{X} = \text{Si}$ (1) and Ge (2), were chosen as a model of the **KSiNb** and **KGeNb** polymers. Calculations show that DMMP coordinates to model complexes **1** and **2** via hydrogen bonding. The calculated bonding energies of 23-24 (10-11) kcal/mol are consistent with this bonding pattern. Furthermore, as a result of this weak interaction, coordination of DMMP only slightly changes the geometry of **1** or **2** (**Figure 4-17**). As noted above, this reaction very likely proceeds via a general-base hydrolysis mechanism, the rate-limiting transition state of which involves a water molecule being deprotonated by the P-PONb oxygen atoms forming hydroxide which attacks the electrophilic phosphorus of DMMP. The potassium counter cation and one of the oxo-centers of P-PONb (terminal or bridging) are likely also involved. The subsequent proton transfer to $-\text{OCH}_3$ fragment

is expected to be fast. Elucidation of the latter mechanistic details requires dynamic studies and more complex model systems, which are beyond the scope of this paper.

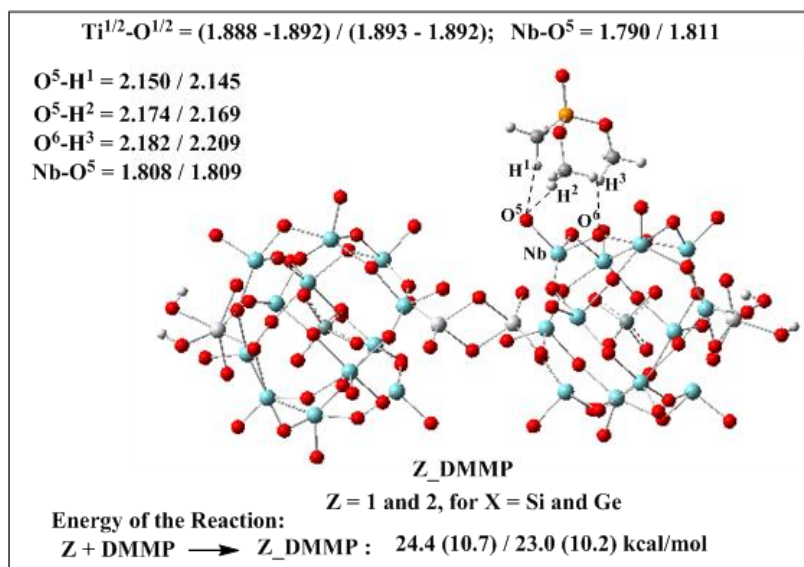


Figure 4-17. The calculated model complexes 1 and 2 for **KSiNb** and **KGeNb** with DMMP simulant. Also shown in the figure are some important bond distances (in Å), and the DMMP coordination energies. Numbers given before and after “/” are for X = Si and Ge, respectively. Energies given after the reaction without and with parenthesis are ΔE and ΔG values.

4.4 Conclusions

In summary, the newly prepared one-dimensional P-PONb, **KGeNb**, is as active as any known base for hydrolysis of nerve agents and their simulants. Importantly, **KGeNb** is far more reactive than hydroxide alone toward the simulants at the same pH in water. Experimental and calculated data implicate a general-base catalysis mechanism for hydrolysis of DMMP, and by extension, likely the live nerve agents themselves. The P-PONbs remove the CWAs, GD (Soman), GB (Sarin) and HD

(mustard) effectively. Hydrolytic breakdown of the CWA proceeds in either solution or the gas phase.

References

- (1) Raushel, F. M. *Nature (London, U. K.)* **2011**, *469*, 310-311.
- (2) Enserink, M. *Science* **2013**, *341*, 1050-1051.
- (3) Nikitin, M. B. D; Feickert, P. K. K., A. *Syria's Chemical Weapons: Issues for Congress* **2013**, report # R42848.
- (4) Sharma, N.; Kakkar, R. *Adv. Mat. Lett.* **2013**, *4*, 508
- (5) "Introduction to and Mitigation of Psychological Effects of Weapons of Mass Destruction (WMD)": R. H. Pastel, E. C. Ritchie in *Psychological Responses to the New Terrorism: A NATO-Russia Dialogue*, IOS Press, Amsterdam, **2005**, pp. 9-24.
- (6) Kim, K.; Tsay, O. G.; Atwood, D. A.; Churchill, D. G. *Chem. Rev.* **2011**, *111*, 5345-5403.
- (7) Yang, Y. C.; Baker, J. A.; Ward, J. R. *Chem. Rev.* **1992**, *92*, 1729-1743.
- (8) Bigley, A. N.; Raushel, F. M. *Biochim. Biophys. Acta, Proteins Proteomics* **2013**, *1834*, 443-453.
- (9) Wagner, G. W.; Bartram, P. W. *J. Mol. Catal. A: Chem.* **1999**, *144*, 419-424.
- (10) Lunn, G.; Sansone, E. B. *Appl. Biochem. Biotechnol.* **1994**, *49*, 165-172.
- (11) Bromberg, L.; Hatton, T. A. *Polymer* **2007**, *48*, 7490-7498.
- (12) Chen, L.; Bromberg, L.; Lee, J. A.; Zhang, H.; Schreuder-Gibson, H.; Gibson, P.; Walker, J.; Hammond, P. T.; Hatton, T. A.; Rutledge, G. C. *Chem. Mater.* **2010**, *22*, 1429-1436.
- (13) Morales-Rojas, H.; Moss, R. A. *Chem. Rev.* **2002**, *102*, 2497-2522.

- (14) Bromberg, L.; Hatton, T. A. *Ind. & Eng. Chem. Res.* **2007**, *46*, 3296-3303.
- (15) Bromberg, L.; Zhang, H.; Hatton, T. A. *Chem. Mater.* **2008**, *20*, 2001-2008.
- (16) Xie, Y.; Popov, B. N. *Anal. Chem.* **2000**, *72*, 2075-2079.
- (17) Bandosz, T. J.; Laskoski, M.; Mahle, J.; Mogilevsky, G.; Peterson, G. W.; Rossin, J. A.; Wagner, G. W. *J. Phys. Chem. C* **2012**, *116*, 11606-11614.
- (18) Wagner, G. W.; Peterson, G. W.; Mahle, J. J. *Ind. Eng. Chem. Res.* **2012**, *51*, 3598-3603.
- (19) Peterson, G. W.; Rossin, J. A. *Ind. Eng. Chem. Res.* **2012**, *51*, 2675-2681.
- (20) Kiselev, A.; Mattson, A.; Andersson, M.; Palmqvist, A. E. C.; Österlund, L. J. *Photochem. Photobiol. A: Chem.* **2006**, *184*, 125-134.
- (21) Moon, S. Y.; Liu, Y.; Hupp, J. T.; Farha, O. K. *Angew. Chemie. Int. Ed.* **2015**, *54*, 6795-6799.
- (22) Katz, M. J.; Mondloch, J. E.; Totten, R. K.; Park, J. K.; Nguyen, S. T.; Farha, O. K.; Hupp, J. T. *Angew. Chem. Int. Ed.* **2014**, *53*, 497-501.
- (23) López-Maya, E.; Montoro, C.; Rodríguez-Albelo, L. M.; Cervantes, S. D. A.; Lozano-Pérez, A. A.; Cenís, J. L.; Barea, E.; Navarro, J. A. R. *Angew. Chemie. Int. Ed.* **2015**, *54*, 6790-6794.
- (24) Mondloch, J. E.; Katz, M. J.; III, W. C. I.; Ghosh, P.; Liao, P.; Bury, W.; Wagner, G. W.; Hall, M. G.; DeCoste, J. B.; Peterson, G. W.; Snurr, R. Q.; Cramer, C. J.; Hupp, J. T.; Farha, O. K. *Nat. Mater.* **2015**, *14*, 512-516.
- (25) *Toxicology and Carcinogenesis Studies of Dimethyl Methylphosphonate (CAS No. 756-79-6) in F344/N Rats and B6C3F₁ Mice (Gavage Studies)*, National toxicology program, U.S. Department of Health and Human Services, **1987**, Technical Report Series # 323.

- (26)Liu, Y.; Howarth, A. J.; Hupp, J. T.; Farha, O. K. *Angew. Chem., Int. Ed.* **2015**, *54*, 9001-9005.
- (27)Kinnan, M. K.; Creasy, W. R.; Fullmer, L. B.; Schreuder-Gibson, H. L.; Nyman, M. *Eur. J. Inorg. Chem.* **2014**, 2361-2367.
- (28)Ma, F.-J.; Liu, S.-X.; Sun, C.-Y.; Liang, D.-D.; Ren, G.-J.; Wei, F.; Chen, Y.-G.; Su, Z.-M. *J. Am. Chem. Soc.* **2011**, *133*, 4178-4181.
- (29)Mizrahi, D. M.; Saphier, S.; Columbus, I. *J. Haz. Mater.* **2010**, *179*, 495-499.
- (30)Okun, N. M.; Tarr, J. C.; Hilleshiem, D. A.; Zhang, L.; Hardcastle, K. I.; Hill, C. L. *J. Mol. Catal. A. Chem.* **2006**, *246*, 11-17.
- (31)Okun, N. M.; Anderson, T. M.; Hill, C. L. *J. Mol. Catal. A: Chem.* **2003**, *197*, 283-290.
- (32)*Polyoxometalate Chemistry for Nano-Composite Design*; Yamase, T.; Pope, M. T., Eds.; Kluwer Academic/Plenum Publishers: New York, 2002; Vol. 2.
- (33)Pope, M. T. In *Comprehensive Coordination Chemistry II: From Biology to Nanotechnology*; Wedd, A. G., Ed.; Elsevier Ltd.: Oxford, UK, 2004; Vol. 4, p 635-678.
- (34)Miras, H. N.; Yan, J.; Long, D.-L.; Cronin, L. *Chem. Soc. Rev.* **2012**, *41*, 7403-7430.
- (35)Lv, H.; Geletii, Y. V.; Zhao, C.; Vickers, J. W.; Zhu, G.; Luo, Z.; Song, J.; Lian, T.; Musaev, D. G.; Hill, C. L. *Chem. Soc. Rev.* **2012**, *41*, 7572-7589.
- (36)*Special Thematic Issue on Polyoxometalates*; Hill, C. L., Ed., 1998; Vol. 98, No. 1.
- (37)Antonio, M. R.; Nyman, M.; Anderson, T. M. *Angew. Chemie* **2009**, *121*, 6252-6256.

- (38) Nyman, M.; Alam, T. M.; Bonhomme, F.; Rodriguez, M. A.; Frazer, C. S.; Welk, M. E. *J. Cluster Sci.* **2006**, *17*, 197-219.
- (39) Nyman, M. *Dalton Trans.* **2011**, *40*, 8049-8058.
- (40) Villa, E. M.; C. André Ohlin, D.; Edina Balogh, D.; Travis M. Anderson, D.; May D. Nyman, D.; William H. Casey, P. *Angew. Chem. Int. Ed.* **2008**, *47*, 4844-4846.
- (41) Balogh, E.; Anderson, T. M.; Rustad, J. R.; Nyman, M.; Casey, W. H. *Inorg. Chem.* **2007**, *46*, 7032-7039.
- (42) Nyman, M.; Bonhomme, F.; Alam, T. M.; Rodriguez, M. A.; Cherry, B. R.; Krumhansl, J. L.; Nenoff, T. M.; Sattler, A. M. *Science* **2002**, *297*, 996-998.
- (43) Bruker, *APEXII v2014.1-1*, Bruker AXS, Inc., Madison, WI, **2014**.
- (44) Bruker, *SAINT v7.68A*, Bruker AXS, Inc., Madison, WI, **2009**.
- (45) Bruker, *SADABS-2012/4/5*, Bruker AXS, Inc., Madison, WI, **2014**.
- (46) Palatinus, L.; Chapuis, G.; *J. Appl. Crystallogr.* **2007**, *40*, 786-790.
- (47) Dolomanov, O. V.; Bourhis, L. J.; Gildea, R. J.; Howard, J. A. K.; Puschmann, H. *J. Appl. Crystallogr.* **2009**, *42*, 339-341.
- (48) Sheldrick, G. *Acta Cryst. A* **2008**, *64*, 112-122.
- (49) Spek, A. L. *J. Appl. Crystallogr.* **2003**, *36*, 7-13.
- (50) Zhao, Y.; Truhlar, D. G. *J. Chem. Phys.* **2006**, *125*, 194101/194101-194101/194118.
- (51) Hay, P. J.; Wadt, W. R. *J. Chem. Phys.* **1985**, *82*, 270-283.
- (52) Hay, P. J.; Wadt, W. R. *J. Chem. Phys.* **1985**, *82*, 299-310.
- (53) Wadt, W. R.; Hay, P. J. *J. Chem. Phys.* **1985**, *82*, 284-298.
- (54) Cancès, E.; Mennucci, B.; Tomasi, J. *J. Chem. Phys.* **1997**, *107*, 3032-3041.
- (55) Mennucci, B.; Tomasi, J. *J. Chem. Phys.* **1997**, *106*, 5151-5158.

(56) Scalmani, G.; Frisch, M. J. *J. Chem. Phys.* **2010**, *132*, 114110/114111-114110/114115.

(57) Frisch, M. J.; Trucks, G.W.; Schlegel, H.B.; et al. *Gaussian 09, Rev. D. 01*, Gaussian, Inc., Wallingford, CT, **2009**.

(58) Bonhomme, F.; Larentzos, J. P.; Alam, T. M.; Maginn, E. J.; Nyman, M. *Inorg. Chem.* **2005**, *44*, 1774-1785.

(59) CCDC 1453051 contain the supplementary crystallographic data for this paper. These data are provided free of charge by The Cambridge Crystallographic Data Centre.

(60) Jencks, W. P. *Catalysis in Chemistry and Enzymology*; McGraw-Hill, 1969.

(61) Bunton, C. A.; Diaz, S. *J. Org. Chem.* **1976**, *41*, 33-36.

Chapter 5.

Di- and Trinickel Polyoxometalates for Photocatalytic Hydrogen Evolution

Reproduced with permission from *Inorg. Chem.*, **2016**, 55(2), 461-466. Copyright 2016 American Chemical Society

As a main contributor of this work; with Hongjin Lv, John Bacsa, Yuanzhe Gao, Je Seong Lee and Craig L. Hill*, W. Guo contributed the syntheses, characterizations, investigating and analyzing the catalysts' activities to this work. H. Lv designed the catalytic experiments. J. Bacsa conducted and analyzed the X-ray crystallographic studies. Y. Gao conducted the FTIR measurements. J. S. Lee prepared the precursors for catalysts syntheses. W. Guo and C. L. Hill designed the experiments and prepared the manuscript.

5.1 Introduction

Polyoxometalates (POMs), a very large family of early transition metal oxide clusters, have attracted much attention because of their dramatic structure variability and consequent widely-ranging applications.¹⁻⁶ Most d-block elements have been incorporated into POMs resulting in transition-metal-substituted POMs (TMSPs) which exhibit noteworthy catalytic,⁷⁻¹¹ magnetic¹²⁻²⁰ and electrochemical properties.²¹⁻

28

Transition metals such as Co^{II} , Ni^{II} , Cu^{II} , Mn^{II} , Zn^{II} and Fe^{III} react with di-vacant $[\text{SiW}_{10}\text{O}_{36}]^{8-}$ and tri-vacant lacunary POMs, $[\text{P}_2\text{W}_{15}\text{O}_{56}]^{12-}$, $[\text{PW}_9\text{O}_{34}]^{9-}$ or $[\text{SiW}_9\text{O}_{34}]^{10-}$ to form sandwich-type POMs. In these cases, the two lacunary POMs are usually connected by three or four transition metal centers.²⁹⁻³³ Fewer sandwich-type POMs contain two transition metal centers, and most of these still exhibit defect sites in which alkali cation(s) can bind.³⁴⁻³⁶ For example, Cronin and co-workers reported the lacunary POMs where two $[\text{P}_2\text{W}_{15}\text{O}_{56}]^{12-}$ are joined by two transition metal ions yielding $[\text{M}_2(\text{P}_2\text{W}_{15}\text{O}_{56})_2]^{20-}$ ($\text{M} = \text{Mn}^{\text{II}}$, Co^{II} and Ni^{II}) showing a $\alpha\beta\beta\alpha$ isomeric geometry.³⁷ In addition, the sandwich type lacunary POMs with two metal centers can further be used to construct heterobimetallic POMs in which the alkali cations are replaced by other transition metals. For example, a $[\{\text{M}(\text{OH}_2)_2(\mu_3\text{-OH})_2\{\text{Zn}(\text{OH}_2)\}_2\{\gamma\text{-SiW}_{10}\text{O}_{36}\}_2]^{8-}$ ($\text{M} = \text{Co}^{\text{II}}$ and Ni^{II}) heterobimetallic substituted POM was synthesized and used to construct a porous ionic cage-like framework.³⁸

TMSPs that are not of the sandwich structure motif are also well known and have well-developed chemistry. Exemplary common structural families include $[\text{MXW}_{11}\text{O}_m]^{n-}$, $[\text{M}_3\text{XW}_9\text{O}_{40}]^{n-}$ and $[\text{M}_3\text{P}_2\text{W}_{15}\text{O}_{62}]^{n-}$ ($\text{X} = \text{Si}^{\text{IV}}$, Ge^{IV} , P^{V} , As^{V} , etc.). In $[\text{MXW}_{11}\text{O}_m]^{n-}$, M can be a high-valent transition metal ion such as V^{V} or low-valent transition metal ions such as Co^{II} , Ni^{II} , Cu^{II} , Mn^{II} and Zn^{II} .^{1,39} However, in

$[M_3XW_9O_{40}]^{n-}$ and $[M_3P_2W_{15}O_{62}]^{n-}$, M are usually high-valent transition metal ions including V^V , Nb^V , Ta^V and Sn^{IV} , which presumably results from the size of the transition metals, the overall charge of the POMs and other thermodynamic factors.⁴⁰⁻

⁴³ The $[M_3XW_9O_{40}]^{n-}$ structure type, where M are the low-valent transition metal ions, is uncommon. Nevertheless, in 1999, Coronado and co-workers reported a POM, $[Ni_3(H_2O)_3PW_{10}O_{39}(H_2O)]^{7-}$, that contains a triangular Ni_3O_{13} unit, a lacunary $[PW_9O_{34}]^{9-}$ ligand and a WO_6 octahedron.⁴⁴ In 2002, our group reported a tri-substituted Wells-Dawson structure with three iron centers, $[(Fe^{III}OH_2)_3P_2W_{15}O_{59}]^{9-}$.⁴⁵ Significantly, monomeric tri-nickel-substituted POMs with the well-known $[P_2W_{15}O_{56}]^{12-}$ ligand prepared via conventional methods have not been reported.

Some TMSPs are efficient water oxidation catalysts (WOCs) under electrochemical, thermal and photochemical conditions.^{10,46} Recently, TMSPs are also emerging as effective visible-light-driven water reduction catalysts (WRCs). The tetra-manganese POM, $[Mn_4(H_2O)_2(VW_9O_{34})_2]^{10-}$ (**Mn₄V₂**), the tetra-nickel POM, $[Ni_4(H_2O)_2(PW_9O_{34})_2]^{10-}$ (**Ni₄P₂**) and the hexadecyl-nickel POM, $[\{Ni_4(OH)_3AsO_4\}_4(B-\alpha-PW_9O_{34})_4]^{28-}$ (**Ni₁₆As₄P₄**) are efficient and robust homogeneous catalysts for visible-light-driven H_2 evolution.⁴⁷⁻⁴⁹ Herein, we report the syntheses, structures and catalytic properties of the di-, and tri-nickel-containing POMs. The di-nickel-substituted $[Ni_2(P_2W_{15}O_{56})_2]^{20-}$ (**Ni₂**) is a sandwich-type POM showing an unusual $\alpha\alpha\alpha\alpha$ inter-unit coordination geometry, while the tri-nickel-containing Wells-Dawson POM, $[Ni_3(OH)_3(H_2O)_3P_2W_{16}O_{59}]^{9-}$ (**Ni₃**) exhibits a unique structure where the $[\alpha-P_2W_{15}O_{56}]^{12-}$ ligand is capped by a triangular Ni_3O_{13} unit and a WO_6 octahedron. Their ability to catalyze visible-light-driven hydrogen evolution is discussed.

5.2 Experimental

5.2.1 General Methods and Materials

All chemicals used were of reagent grade and used as commercially supplied. $\text{Na}_{12}[\alpha\text{-P}_2\text{W}_{15}\text{O}_{56}]\cdot 24\text{H}_2\text{O}$ was synthesized following the reported literature method,⁵⁰ and its purity assessed by FT-IR spectroscopy. These spectra were obtained by a Nicolet TM 600 FT-IR spectrometer (2% sample in KBr pellet). UV-vis absorption spectra were obtained on an Agilent 8453 spectrophotometer with a diode-array detector using a 1.0-cm-optical-path quartz cuvette. Thermogravimetric analyses were acquired on a STA 6000 thermal analyzer. Elemental analyses (Li, Na, Ni, W and P) were performed by Galbraith Laboratories (Knoxville, Tennessee). The steady-state luminescence quenching spectra were recorded on a FluoroMax 3 spectrofluorimeter. Gas chromatography (GC) (Hewlett-Packard 7890 instrument equipped with a 5 Å molecular sieve column and a TCD detector with Ar as the carrier gas) was used to detect the hydrogen evolved during catalytic water reduction reactions. Cyclic voltammograms (CV) were measured on a BASi CV-50W voltammetric analyzer using a Pt-wire auxiliary electrode, a Ag/AgCl (3 M NaCl) BASi reference electrode and a glassy carbon working electrode. CVs were conducted in 200 mM sodium phosphate buffer (pH=7.5 and 8.0) with 1 M NaCl as a supporting electrolyte.

5.2.2 Synthesis of $\text{Na}_8\text{Li}_{12}[\text{Ni}_2(\text{P}_2\text{W}_{15}\text{O}_{56})_2] \cdot 74\text{H}_2\text{O}$

$\text{Na}_8\text{Li}_{12}\text{Ni}_2$. The sodium and lithium salt of Ni_2 , $\text{Na}_8\text{Li}_{12}\text{Ni}_2$, was prepared as follows. Solid $\text{NiCl}_2\cdot 6\text{H}_2\text{O}$ (0.29 g, 1.2 mmol) was dissolved in 20 mL of 4.0 M aqueous LiCl followed by addition of 0.19 g (0.49 mmol) $\text{Na}_3\text{PO}_4\cdot 12\text{H}_2\text{O}$. The mixture was stirred for 5 min, then adjusted to pH=8.0 by adding 1.0 M LiOH. Then $\text{Na}_{12}[\alpha\text{-P}_2\text{W}_{15}\text{O}_{56}]\cdot 24\text{H}_2\text{O}$ (3.0 g, 0.6 mmol) was added. The mixture was heated at 60 °C for 1 h and then cooled to room temperature and filtered. After slow evaporation for several

days light green crystals were obtained. Yield: 2.5 g (40%). Anal. Calcd for $\text{Na}_8\text{Ni}_2\text{O}_{186}\text{W}_{30}\text{P}_4\text{Li}_{12}\text{H}_{148}$: Na, 2.01; Ni, 1.28; W, 60.3; P, 1.35; Li, 0.91. Found: Na, 1.84; Ni, 1.28; W, 58.3; P, 1.28; Li, 1.05. FTIR (1100-400 cm^{-1} , 2% KBr pellets): 1083 (s), 1041 (m), 1016 (w), 994 (w), 936 (s), 893 (w), 809 (w), 747 (m), 529 (w).

5.2.3 Synthesis of $\text{Na}_4\text{Li}_5[\text{Ni}_3(\text{OH})_3(\text{H}_2\text{O})_3\text{P}_2\text{W}_{16}\text{O}_{59}] \cdot 48\text{H}_2\text{O}$

$\text{Na}_4\text{Li}_5\text{Ni}_3$. The sodium and lithium salt of Ni_3 , $\text{Na}_4\text{Li}_5\text{Ni}_3$, was prepared following a method similar to that for $\text{Na}_8\text{Li}_{12}\text{Ni}_2$. Specifically, $\text{NiCl}_2 \cdot 6\text{H}_2\text{O}$ (0.58 g, 2.4 mmol) was dissolved in 20.0 mL of aqueous 4.0 M LiCl followed by the addition of 0.19 g of $\text{Na}_3\text{PO}_4 \cdot 12\text{H}_2\text{O}$ (0.49 mmol). The mixture was stirred for 5 min, and the solution was adjusted to pH=7.5 by adding 1 M LiOH. $\text{Na}_{12}[\alpha\text{-P}_2\text{W}_{15}\text{O}_{56}] \cdot 24\text{H}_2\text{O}$ (3.0 g, 0.6 mmol) was then added. The resulting mixture was heated at 60 °C for 1 h and then cooled to room temperature and filtered. After slow evaporation for several days dark green crystals were obtained. Yield: 1.1 g (30%). Anal. Calcd for $\text{Na}_4\text{Ni}_3\text{O}_{113}\text{W}_{16}\text{P}_2\text{Li}_5\text{H}_{105}$: Na, 1.76; Ni, 3.37; W, 56.3; P, 1.18; Li, 0.66. Found: Na, 1.74; Ni, 3.27; W, 56.1; P, 1.11; Li, 0.65. FTIR (1100-400 cm^{-1} , 2% KBr pellets): 1084 (s), 1049 (m), 999 (w), 936 (s), 891 (w), 823 (w), 735 (m), 525 (w).

5.2.4 Synthesis of TBANi_2 and TBANi_3

The tetrabutylammonium (TBA) salts of Ni_2 and Ni_3 ($\text{TBA}_8\text{Na}_8\text{Li}_4[\text{Ni}_2(\text{P}_2\text{W}_{15}\text{O}_{56})_2] \cdot 27\text{H}_2\text{O}$ and $\text{TBA}_8\text{Li}[\text{Ni}_3(\text{OH})_3(\text{H}_2\text{O})_3\text{P}_2\text{W}_{16}\text{O}_{59}] \cdot 28\text{H}_2\text{O}$) were readily prepared using an extraction metathesis process.⁵¹ Typically, an aqueous solution of $\text{Na}_8\text{Li}_{12}\text{Ni}_2$ or $\text{Na}_4\text{Li}_5\text{Ni}_3$ (0.1 mmol in 10 mL H_2O) was added to the solution of TBABr in dichloromethane (10 mmol). The mixture was vigorously shaken, and the polyanions were transferred to the organic layer which was then separated and washed extensively with deionized water. The TBA salt of Ni_2 or Ni_3 was dissolved in acetonitrile, and diethyl ether vapor was

slowly diffused into the solution resulting in production of green well-formed crystals. The FT-IR spectra of TBANi_2 and TBANi_3 are displayed in **Figure 5-1** showing that the polyanion structures have remained intact. The formula of TBANi_2 and TBANi_3 are determined based on thermogravimetric analysis as well as elemental analysis. The TGA of TBANi_2 and TBANi_3 are shown in **Figure 5-2** and **Figure 5-3**. The calculated weight loss percent corresponds to 8 TBA and 27 water molecules per TBANi_2 , and 8 TBA and 28 water molecules per TBANi_3 . Anal. Calcd for TBANi_2 : C, 15.2; H, 2.8; N, 1.1; Na, 1.8; Li, 0.27. Found: C, 15.5; H, 3.1; N, 1.2; Na, 1.4; Li, 0.16. Anal. Calcd for TBANi_3 : C, 22.9; H, 4.3; N, 1.6; Li, 0.1. Found: C, 23.3; H, 4.5; N, 1.9; Li, 0.2.

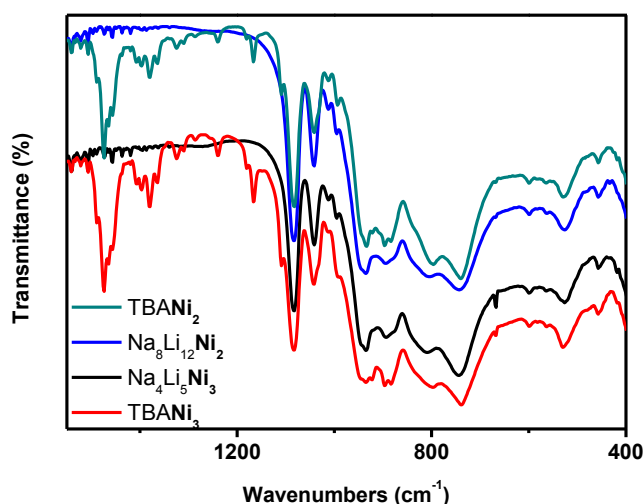


Figure 5-1. FT-IR spectra of the tetrabutylammonium (TBA) salts of Ni_2 and Ni_3 .

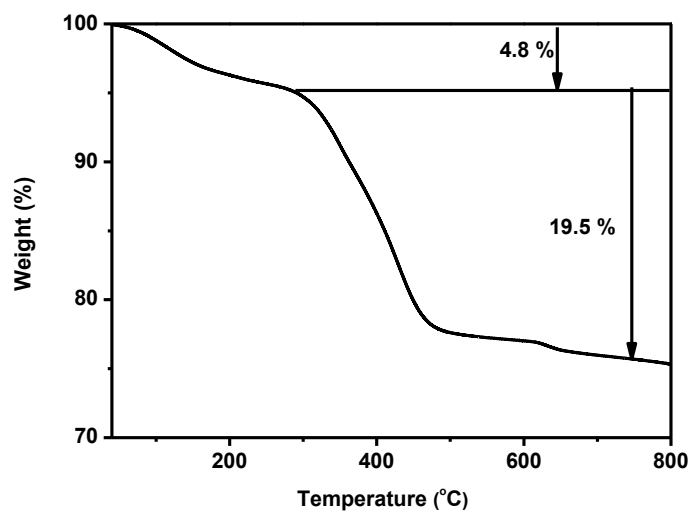


Figure 5-2. Thermogravimetric analysis of TBANi₂. The calculated weight percent of water loss corresponds to 27 water molecules.

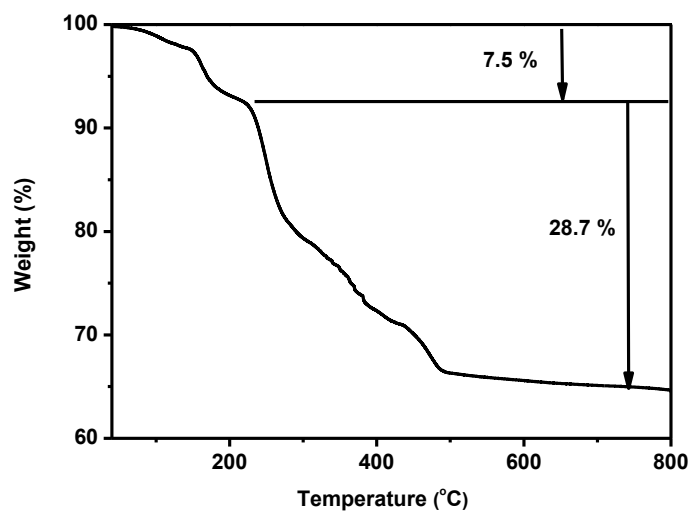


Figure 5-3. Thermogravimetric analysis of TBANi₃. The calculated weight percent of water loss corresponds to 28 water molecules.

5.2.5 X-ray Crystallography

Suitable crystals of $\text{Na}_8\text{Li}_{12}\text{Ni}_2/\text{Na}_4\text{Li}_5\text{Ni}_3$ were selected and mounted on a loop with Paratone oil. Data were collected using a Bruker APEX-II CCD diffractometer equipped with an Oxford Cryosystems low-temperature apparatus operating at $T = 110(2)$ K. Data were measured using ω scans by Mo $K\alpha$ radiation (fine-focus sealed tube, 45kV, 30mA). The total number of runs and images was based on the strategy calculation from the program **APEXII**.⁵² Data reduction was performed using the **SAINT** software⁵³ which corrects for Lorentz polarization. Cell parameters were retrieved using the **SAINT** software and refined using **SAINT**. The structure was solved by Charge Flipping using the **Superflip** structure solution program⁵⁴ and refined by Least Squares using version 2013-4 of **ShelXL**.⁵⁵ All non-hydrogen atoms were refined anisotropically. The crystallographic data are summarized in **Table 5-1**.

5.2.6 Photocatalytic experimental processes

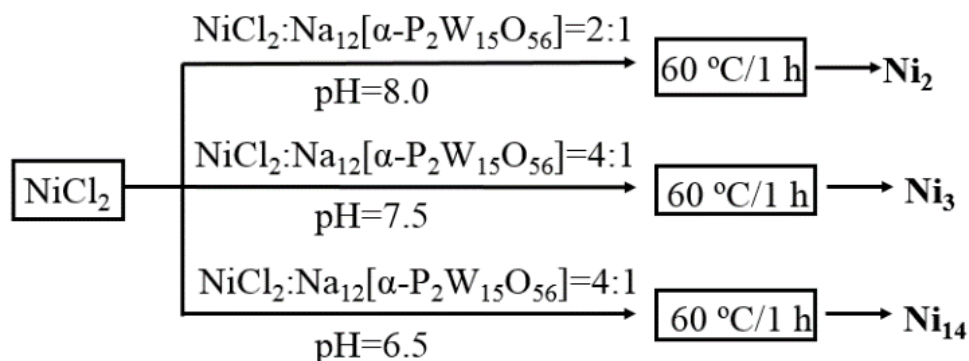
The general procedure for hydrogen evolution catalyzed by TBANi_2 or TBANi_3 is as follows. These experiments were performed in 2.5 mL septum-sealed glass vials. Typically, 2 mL of a DMF/ CH_3CN / H_2O (14:5:1) mixed solvent solution containing 20 μM catalyst, 0.25 M triethanolamine (TEOA) and 0.2 mM (4,4'-di-*tert*-butyl-2,2'-dipyridyl)-bis-(2-phenylpyridine(-1H))-iridium(III) hexafluorophosphate, $[\text{Ir}(\text{ppy})_2(\text{dtbbpy})][\text{PF}_6]$ ($[\text{Ir}(\text{ppy})_2(\text{dtbbpy})]^+$), as the photosensitizer, were added to the vial. The molar percentage of the catalyst used with respect to TEOA, photosensitizer and POM in total is calculated as 0.08 %. The vials were subsequently sealed with a rubber septum, deoxygenated by bubbling Ar for 30 min, and then irradiated by a 455 nm LED-light source (light intensity 20 mW; beam diameter ~ 0.4 cm) at room temperature with magnetic stirring for 4 h. The product hydrogen in the vial headspace was analyzed by GC. The post-reaction solution was collected, the polyanions

precipitated by adding a saturated solution of $[\text{Ru}(\text{bpy})_3]^{2+}$ in CH_3CN . The resulting mixture was centrifuged and the separated solid was dried.

5.3 Results and Discussion

5.3.1 Syntheses

The factors that affect the equilibria among different species during POM synthesis are mainly the pH of the solution, the concentration of the reagents, the counterions and their concentration(s), the temperature and the solvent.⁴⁴ **Scheme 5-1** illustrates the general synthetic procedure for **Ni₂** and **Ni₃**. At pH 8.0, a 2:1 ratio of Ni^{2+} to $[\alpha\text{-P}_2\text{W}_{15}\text{O}_{56}]^{12-}$ does not yield the sandwich-type POM which has four nickel centers, but a POM (**Ni₂**) that only has two nickel ions in the core linking two $[\alpha\text{-P}_2\text{W}_{15}\text{O}_{56}]^{12-}$ polyanions. The ratio of Ni^{2+} to $[\alpha\text{-P}_2\text{W}_{15}\text{O}_{56}]^{12-}$ was further increased to 4:1 and 8:1 with in an attempt to synthesize the sandwich-type POM which has four nickel centers. However, only **Ni₂** was obtained in these cases indicating that the amount of nickel ions does not have a big influence on the final products. Nevertheless, when the pH of the solution was lowered to 7.5, **Ni₃** was obtained with a 4:1 ratio of Ni^{2+} to $[\alpha\text{-P}_2\text{W}_{15}\text{O}_{56}]^{12-}$. This is contrary to the phenomenon reported previously in which higher pH favors higher nuclearities of transition metals.⁴⁴ At pH 6.5 with a 4:1 ratio of Ni^{2+} to $[\alpha\text{-P}_2\text{W}_{15}\text{O}_{56}]^{12-}$, the POM, $[\text{Ni}_{14}(\text{OH})_6(\text{H}_2\text{O})_{10}(\text{HPO}_4)_4(\text{P}_2\text{W}_{15}\text{O}_{56})_4]^{34-}$ (**Ni₁₄**) was obtained when extra phosphate was added. This structure was published previously in the form of Rb salt,⁵⁶ therefore its structure is not discussed here.

Scheme 5-1. Synthetic Routes to **Ni₂**, **Ni₃** and **Ni₁₄**.

5.3.2 Structures and Characterizations

The crystal data for **Ni₂** and **Ni₃** are summarized in **Table 5-1**. **Ni₂** crystallizes in the triclinic space group $P\bar{1}$. **Figure 5-4** shows the polyhedral and ball-and-stick representation of **Ni₂**. It is a sandwich-type polyanion containing two transition metal ions as well as two open lacunary sites in the central belt for further incorporation of other transition metals or alkali metals. Crystallographic measurements indicate that lithium ions reside in the lacunary sites. According to the convention for the nomenclature of these kinds of sandwich-type POMs, the two $\{\text{W}_3\}$ caps at each side of the cluster are defined as α and the two di-nickel, multi-oxygen interfaces defining the central belt can be in the same orientation to the caps (α) or the opposite orientation (β).³⁷ **Ni₂** exhibits a $\alpha\alpha\alpha\alpha$ geometry (**Figure 5-4**), and while the dinuclear sandwich polytungstates with a $\alpha\alpha\alpha\alpha$ geometry have been found for $\alpha\alpha\alpha\alpha$ - $[(\text{NaOH}_2)_2\text{Fe}^{\text{III}}_2(\text{P}_2\text{W}_{15}\text{O}_{56})_2]^{16-}$, $\alpha\alpha\alpha\alpha$ - $[(\text{NaOH}_2)_2\text{Cu}^{\text{II}}_2(\text{P}_2\text{W}_{15}\text{O}_{56})_2]^{18-}$, $\alpha\alpha\alpha\alpha$ - $[(\text{NaOH}_2)_2\text{Co}^{\text{II}}_2(\text{P}_2\text{W}_{15}\text{O}_{56})_2]^{18-}$ etc, this intra-unit POM connectivity is rare. The outside sites on the central belt of these $\alpha\alpha\alpha\alpha$ sandwich POMs are most frequently occupied by hydrated sodium ions.^{36,57,58} The relevant Ni^{II}-Ni^{II} distance is 3.118 Å, and the Ni^{II}-O-Ni^{II} angle is 57.20°. The TBA salt of the $\alpha\beta\beta\alpha$ isomer of **Ni₂** was reported by

Cronin and co-workers in 2012.³⁷ It was also noted that under the same synthetic conditions, the dinuclear sandwich POMs containing Mn^{II}, Co^{II} and Ni^{II} all exhibit the more common $\alpha\beta\beta\alpha$ geometry except the Fe^{III} isomer which has the $\alpha\alpha\alpha\alpha$ geometry. The crystallization of $\alpha\alpha\alpha\alpha$ -Ni₂ indicates that the formation of POM isomers is not only dependent on the relative charge and size of the transition metals (Fe^{III} vs. Mn^{II}, Co^{II} and Ni^{II}) but depends on the synthetic conditions as well as counterions.

Table 5-1. Crystal data and structure refinement for Ni₂ and Ni₃

	Na ₈ Li ₁₂ Ni ₂	Na ₄ Li ₅ Ni ₃
Empirical Formula	Na ₈ Ni ₂ O ₁₈₆ W ₃₀ P ₄ Li ₁₂ H ₁₄₈	Na ₄ Ni ₃ O ₁₁₃ W ₁₆ P ₂ Li ₆ H ₁₀₅
Formula Weight	9149.17	4235.67
Temperature	110(2) K	110(2) K
Wavelength	0.71073 Å	0.71073 Å
Crystal system	Triclinic	Orthorhombic
Space group	P-1	Pbca
Unit cell dimensions	a = 13.2155(15) Å b = 13.380(2) Å c = 25.206(4) Å α = 75.983(2)° β = 81.838(2)° γ = 61.8110(10)°	a = 24.364(5) Å b = 24.299(5) Å c = 28.863(6) Å α = 90° β = 90° γ = 90°
Volume	3809.4(9) Å ³	17087(6) Å ³
Z	1	8
Density calculated	3.988 Mg/m ³	3.293 Mg/m ³
Absorption coefficient	22.992 mm ⁻¹	22.205 mm ⁻¹

F(000)	4096	14608
Crystal size (mm ³)	0.335 x 0.282 x 0.228	0.317 x 0.311 x 0.124
Index ranges	-18<=h<=18, 18<=k<=18, -35<=l<=35	-33<=h<=34, 20<=k<=34, -40<=l<=40
Reflections collected	64611	229489
Independent reflections	21521 [R(int) = 0.0508]	25653 [R(int) = 0.0750]
Completeness to theta = 25.242 °	99.8 %	100.0 %
Max. and min. transmission	0.1281 and 0.0492	0.2267 and 0.0161
Refinement method	Full-matrix least-squares on F ²	Full-matrix least-squares on F ²
Goodness-of-fit on F ²	1.056	1.114
Final R indices [I>2σ(I)]	^[a] R1 = 0.0509, ^[b] wR2 = 0.1148	^[a] R1 = 0.0618, ^[b] wR2 = 0.1257
R indices (all data)	R1 = 0.0775, wR2 = 0.1273	R1 = 0.0862, wR2 = 0.1384

$$^{[a]}R_1 = \frac{\sum ||F_0| - |F_c||}{\sum |F_0|}; \quad ^{[b]}wR_2 = \frac{\sum [w(F_0^2 - F_c^2)^2]}{\sum [w(F_0^2)^2]}^{1/2}$$

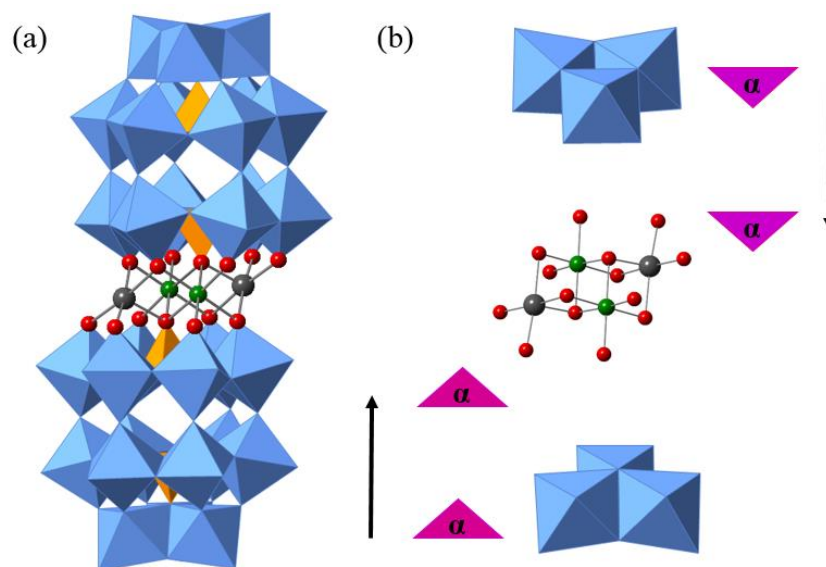


Figure 5-4. (a) Polyhedral and ball-and-stick representation of X-ray crystal structure of **Ni₂**. Red ball: oxygen; grey ball: lithium; blue octahedra: WO_6 ; green ball: nickel; orange tetrahedra: PO_4 . (b) Illustration for the definition of $\alpha\alpha\alpha\alpha$ isomer of **Ni₂**.

Ni₃ contains a triangular Ni_3O_{13} unit which is composed of three edge-sharing NiO_6 octahedra, a $[\alpha\text{-P}_2\text{W}_{15}\text{O}_{56}]^{12-}$ ligand and a capping WO_6 octahedron. **Ni₃** crystallizes in the orthorhombic space group *Pbca*. **Figure 5-5** shows the polyhedral and ball-and-stick representation of **Ni₃**. This new polyanion has a structure similar to that of the Keggin-type analogue,⁴⁴ $[\text{Ni}_3(\text{H}_2\text{O})_3\text{PW}_{10}\text{O}_{39}(\text{H}_2\text{O})]^{7-}$ except that the $[\text{PW}_9\text{O}_{34}]^{9-}$ ligand is replaced by $[\alpha\text{-P}_2\text{W}_{15}\text{O}_{56}]^{12-}$. The terminal oxygen on each of the NiO_6 octahedra is from a coordinated water molecule. In contrast, the three oxygen atoms connecting to the capping WO_6 and the Ni_3O_{13} unit are singly protonated as inferred from bond lengths and bond valence sum calculations. This gives the polyanion an overall charge of 9-. Unlike the tri-substituted Wells-Dawson structure with three iron centers, $[\alpha\text{-(Fe}^{\text{III}}\text{OH}_2)_3\text{P}_2\text{W}_{15}\text{O}_{59}]^{9-}$,⁴⁵ **Ni₃** needs an additional cap of tungsten to stabilize the Wells-Dawson-like $\{\text{P}_2\text{Ni}_3\text{W}_{15}\text{O}_{62}\}$ unit. This stabilization likely reflects the larger size and lower charge of Ni(II) versus Fe(III). The Ni(II)–Ni(II) distances are 3.129 Å, 3.118 Å

and 3.115 Å respectively. The connectivity and Ni^{II}-O-Ni^{II} angles are summarized in Figure 2b.

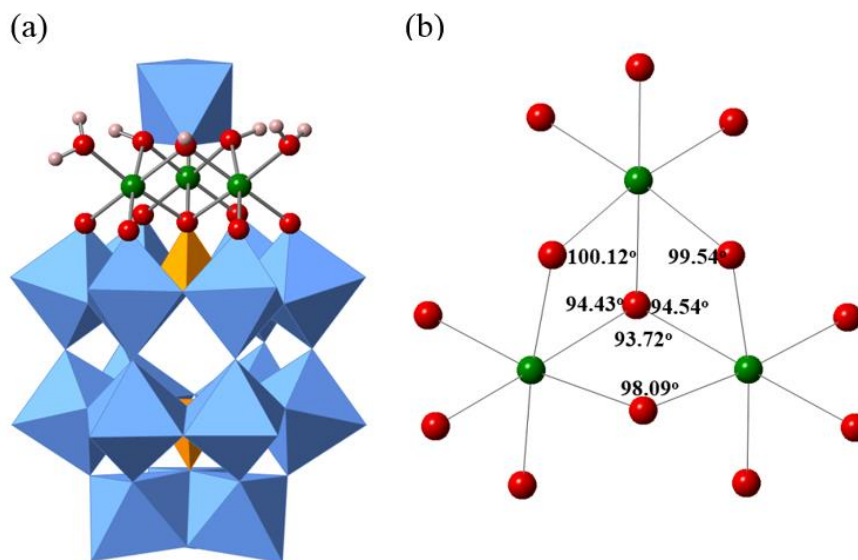


Figure 5-5. (a) Polyhedral and ball-and-stick representation of X-ray crystal structure of Ni₃. Red: oxygen; blue octahedra: WO₆; green: nickel; orange tetrahedra: PO₄. (b) Connectivity and bond angles diagram for Ni₃.

The FT-IR spectra of Ni₂ and Ni₃ are shown in **Figure 5-6**. Their spectra display similar characteristic peaks to those of [α-P₂W₁₅O₅₆]¹²⁻. Both complexes have characteristic vibrational bands of heteropolytungstates including terminal W-O and W-O-W structural units.⁵⁹ The shifts and changes of the P-O stretches at ca. 1130, 1075 and 1008 cm⁻¹ are introduced by insertion of the nickel centers. The splitting of the *v*₃ mode of the central PO₄ unit is not observed, which is commonly seen in this type of TMSPs, particularly in cases where Ni(II) has been incorporated into the lacuna and not the other divalent 3d transition metal cations.⁵⁹ The small peaks at ca. 456 cm⁻¹ are assigned to Ni-O stretches.⁶⁰ The UV-vis spectra of Ni₂ and Ni₃ are shown in **Figure**

5-7. Both spectra exhibit peaks from 400 to 500 nm and a weak absorption from 650 to 800 nm; all of these derive from the $\text{Ni}^{\text{II}}\text{O}_6$ centers. The redox behavior of Ni_2 and Ni_3 were studied in sodium phosphate buffer (pH 8.0 and 7.5 respectively). **Figure 5-8** shows the CVs of 4.0 mM Ni_2 and Ni_3 in deairedated buffer solution. Both CVs have similar poorly-resolved, quasi-reversible redox waves. In the negative-domain region, the clear W(VI)-to-W(V) reduction peaks may overlap with the Ni(II)-to-Ni(I) peaks. The maximum anodic peak current is proportional to the square root of the scan rates consistent with diffusion-controlled interfacial redox processes.

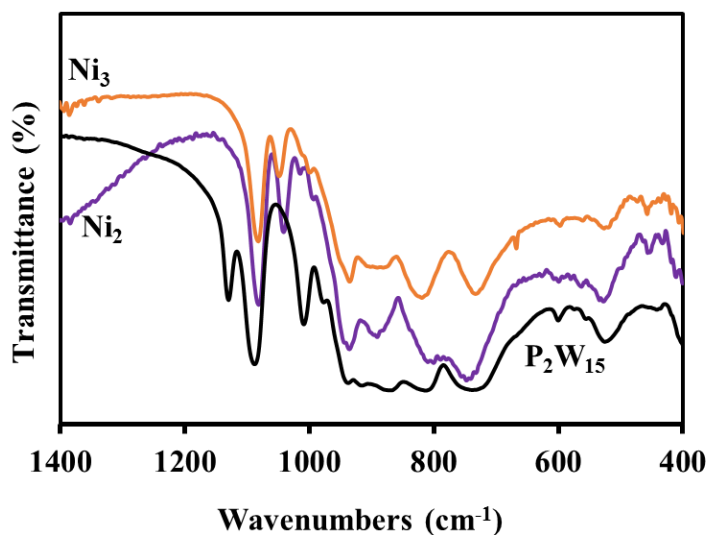


Figure 5-6. FT-IR spectra of Ni_2 and Ni_3 compared to the component trivalent polyanion ligand, $[\alpha\text{-P}_2\text{W}_{15}\text{O}_{56}]^{12-}$.

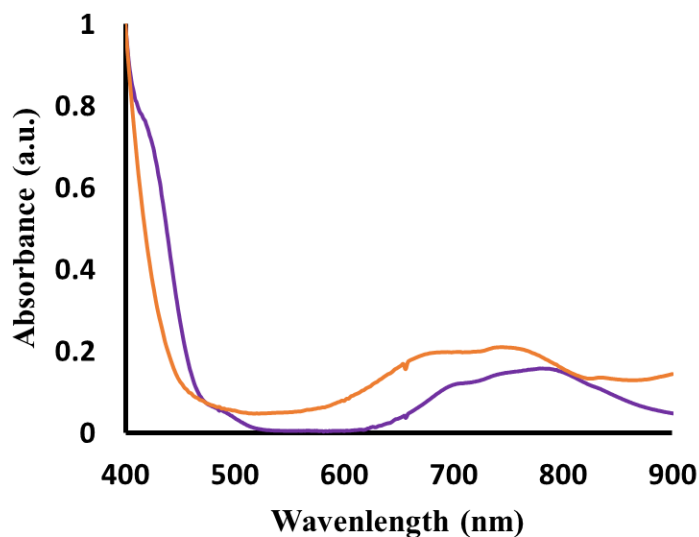


Figure 5-7. Normalized UV-vis absorption spectra of $\text{Na}_8\text{Li}_{12}\text{Ni}_2$ and $\text{Na}_4\text{Li}_5\text{Ni}_3$. Conditions: 0.5 mM in 1 M NaCl aqueous solution.

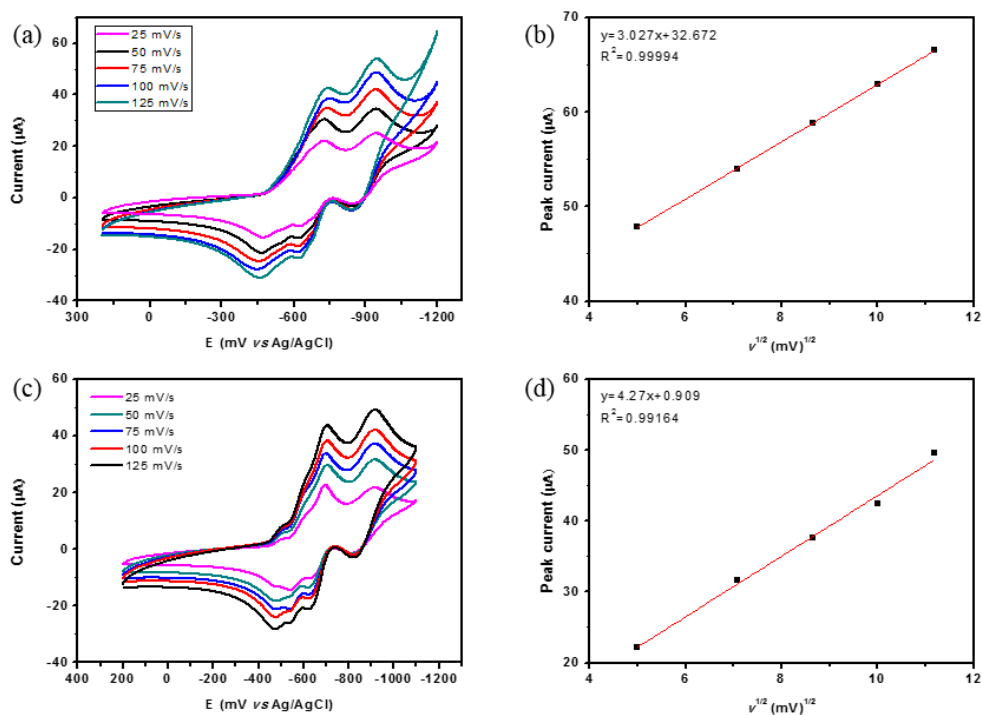


Figure 5-8. (a) Cyclic voltammograms of 4.0 mM $\text{Na}_8\text{Li}_{12}\text{Ni}_2$ at different scan rates (pH=8.0). (b) The plot of maximum anodic peak currents for part “a” versus the square

root of scan rates. (c) Cyclic voltammograms of 4.0 mM $\text{Na}_4\text{Li}_5\text{Ni}_3$ at different scan rates (pH=7.5). (d) The plot of maximum anodic peak currents for part “c” versus the square root of scan rates. Conditions: 200 mM sodium phosphate buffer deaerated with Ar; 1 M NaCl as a supporting electrolyte.

5.3.3 Photocatalytic hydrogen evolution

Sunlight-driven photocatalytic water splitting is of major current interest.⁶¹⁻⁶³ Ni_2 and Ni_3 were investigated for their ability to catalyze water reduction in conjunction visible-light photosensitization. As shown in **Figure 5-9**, Ni_3 shows a high activity for hydrogen evolution with a TON of 160 within *ca.* 3 hours, the conversion of water to hydrogen is estimated as 0.12 %. Ni_3 has three nickel centers whose terminal oxygen atoms are presumably free to serve as catalytic reaction sites.

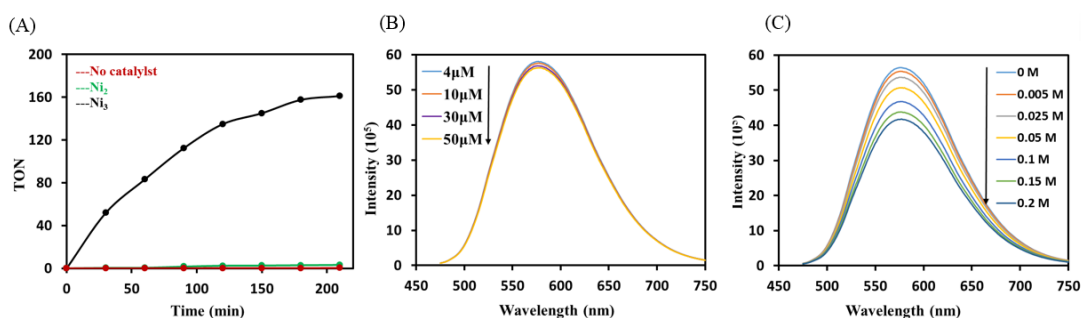


Figure 5-9. (A) Photocatalytic hydrogen evolution using 20 μM Ni_2 (green) and Ni_3 (black). Conditions: LED light (20 mW, 455 nm), $[\text{Ir}(\text{ppy})_2(\text{dtbbpy})]^+$ (0.2 mM), TEOA (0.25 M), 2 mL $\text{CH}_3\text{CN}/\text{DMF}$ (1/3) deaired with Ar. (B) Emission spectra of $[\text{Ir}(\text{ppy})_2(\text{dtbbpy})]^+$ (0.1 mM) as a function of added Ni_3 . (C) Emission spectra of $[\text{Ir}(\text{ppy})_2(\text{dtbbpy})]^+$ (0.1 mM) as a function of added TEOA.

Control experiments using NiCl_2 or $[\text{P}_2\text{W}_{15}\text{O}_{56}]^{12-}$ show much lower activities. Negligible activity was observed in the absence of $[\text{Ir}(\text{ppy})_2(\text{dtbbpy})]^+$ or in the dark confirming the photocatalytic nature of the system (**Table 5-2**). The stability of Ni_3 is

confirmed as follows: the FT-IR spectrum of **Ni₃** after catalytic reactions remains unchanged compared to the one before (**Figure 5-10**); no significant change is observed the UV-vis spectrum of **Ni₃** after 12 hours (**Figure 5-11**). Moreover, formation of nanoparticles is not observed by DLS (the counts are below the detectable limit).

Table 5-2. Control experiments for photocatalytic hydrogen evolution after 3.5 hours by different water reduction catalysts (WRCs) under otherwise identical conditions: DMF/CH₃CN/H₂O (2 mL) mixed solvent solution containing 20 μM catalyst, 0.25 M TEOA and 0.2 mM [Ir(ppy)₂(dtbbpy)]⁺.

Entry	Catalysts	TON
1	Ni₂	1
2	Ni₃	161
3	Na ₁₂ [α-P ₂ W ₁₅ O ₅₆]·24H ₂ O	1
4	NiCl ₂	60
5	No dye	N/A
6	No TEOA	N/A
7	No catalyst	1
8	Ni₁₄	260
9	Ni₄P₂	290
10	Ni₁₆As₄P₄	264

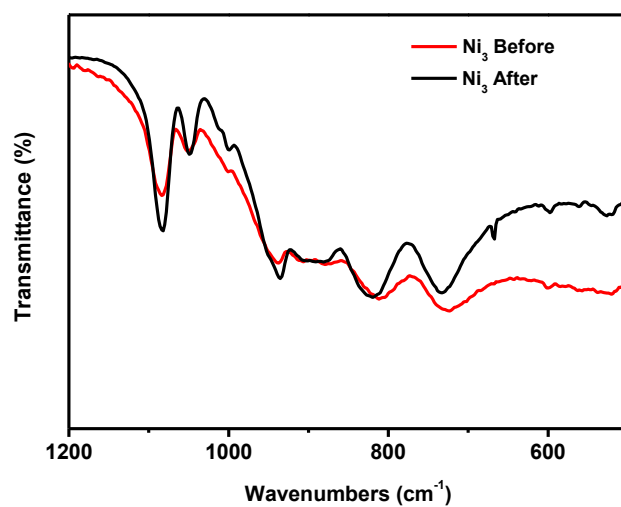


Figure 5-10. FT-IR spectra of TBANi₃ before and after catalytic reactions.

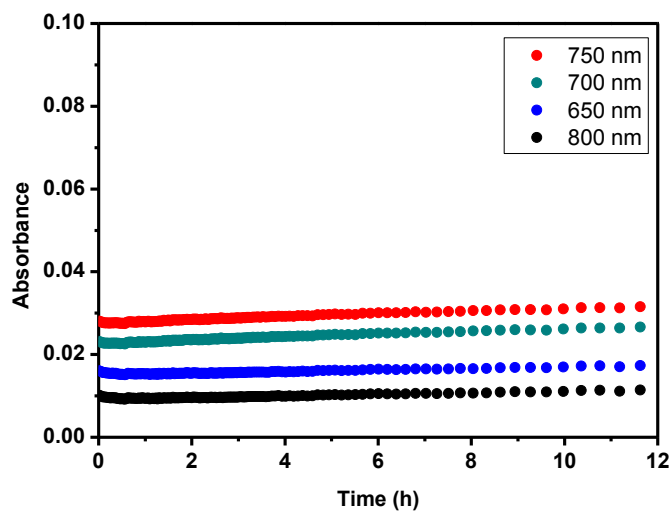


Figure 5-11. Time profile of UV-vis spectra of TBANi₃ in CH₃CN/DMF containing 0.25 M TEOA.

The excited photosensitizer can be quenched either by an electron donor or an acceptor in a photo-driven system.^{64,65} In the system catalyzed by Ni₄P₂,

$[\text{Ir}(\text{ppy})_2(\text{dtbbpy})]^{+*}$ can be both oxidatively and reductively quenched.⁴⁸ The quenching mechanism of the system in this study (oxidative vs. reductive) has been addressed (see the data in **Figure 5-9**). The decay of $[\text{Ir}(\text{ppy})_2(\text{dtbbpy})]^{+*}$ luminescence is only slightly accelerated by the presence of **Ni3** indicating that the oxidative quenching process is quite inefficient. This might be attributed to the relative lower negative charge of **Ni3** (9-) compared to that of **Ni4P2** (10-) thus the electrostatic attraction between **Ni3** polyanion and $[\text{Ir}(\text{ppy})_2(\text{dtbbpy})]^{+*}$ is weak. On the other hand, a Stern-Volmer analysis gives a reductive quenching rate constant of $3.1 \times 10^7 \text{ M}^{-1} \text{ s}^{-1}$ by TEOA confirming that the reductive quenching pathway is dominant (**Figure 5-12**).

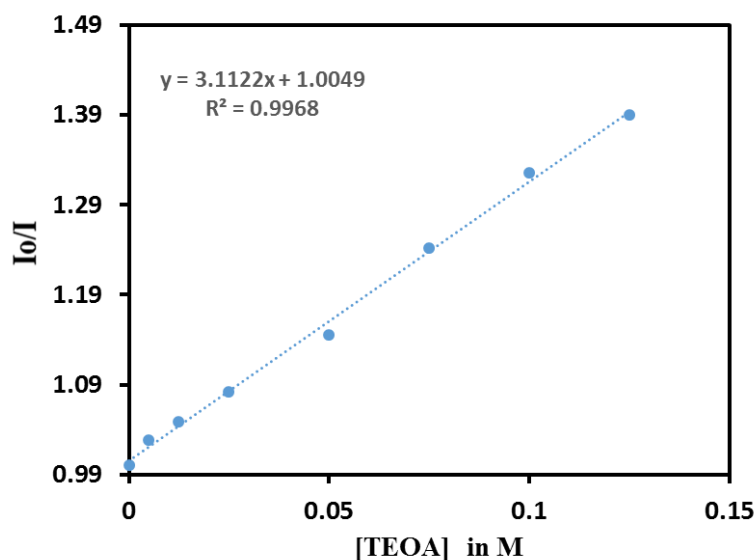


Figure 5-12. Stern-Volmer plot assessing interaction involving TEOA. The calculated quenching rate constant is $3.1 \times 10^7 \text{ M}^{-1} \text{ s}^{-1}$

5.3.4 Correlation between POM structure and hydrogen evolution activity

Ni₂ shows photoinduced hydrogen evolution activity approximately two orders of magnitude lower than **Ni₃**. This is likely a consequence of the fact that the two nickel centers in **Ni₂** are coordinatively saturated, and thus afford no open sites for water binding and reduction. However, **Ni₄P₂** (TON ~ 290), **Ni₁₄** (TON ~ 260) and **Ni₁₆As₄P₄** (TON ~ 264), which have more free active nickel centers or different heteroatoms, all display TON values higher by only a factor of ~ 2. This indicates that the catalytic activity for hydrogen evolution by POMs depends not only on the transition metals in the polyanion unit but also on other evident structure-dependent features: the number of active sites, nature of the heteroatom(s), and doubtless other factors which are under current systematic assessment.

5.4 Conclusions

New di- and tri-nickel-containing POMs have been synthesized and characterized. The di-substituted sandwich-type POM, $[\text{Ni}_2(\text{P}_2\text{W}_{15}\text{O}_{56})_2]^{20-}$ (**Ni₂**) with two nickel centers, exhibits an unusual $\alpha\alpha\alpha\alpha$ inter-unit orientation. The tri-substituted Wells-Dawson POM, $[\text{Ni}_3(\text{H}_2\text{O})_3\text{P}_2\text{W}_{16}\text{O}_{61}(\text{H}_2\text{O})]^{10-}$ (**Ni₃**), shows a similar but unique structure compared to that of the tri-nickel Keggin derivative, $[\text{Ni}_3(\text{H}_2\text{O})_3\text{PW}_{10}\text{O}_{39}(\text{H}_2\text{O})]^{7-}$: it is composed of three edge-sharing NiO_6 octahedra, a $[\alpha\text{-P}_2\text{W}_{15}\text{O}_{56}]^{12-}$ ligand and a WO_6 octahedron. **Ni₃** is an effective water reduction catalyst upon visible light photosensitization using the complex, $[\text{Ir}(\text{ppy})_2(\text{dtbbpy})]^+$. In contrast, **Ni₂** shows negligible activity which we attribute primarily to the lack of solvent-accessible positions on the nickel centers. The investigation of light-driven catalytic H_2 evolution activity as a function of the properties of the multi-Ni sites in different POMs is in progress.

References

- (1) Pope, M. T. *Heteropoly and Isopoly Oxometalates*; Springer-Verlag: Berlin, 1983.
- (2) *Polyoxometalates: From Platonic Solids to Anti-retroviral Activity*; Pope, M. T.; Müller, A., Eds.; Kluwer Academic Publishers: Dordrecht, Netherlands, 1993.
- (3) *Polyoxometalate Chemistry From Topology via Self-Assembly to Applications*; Pope, M. T.; Müller, A., Eds.; Kluwer Academic Publishers: Dordrecht, 2001.
- (4) Hill, C. L. *Chem. Rev.* **1998**, *98*, 1-2.
- (5) Long, D.-L.; Tsunashima, R.; Cronin, L. *Angew. Chem. Int. Ed.* **2010**, *49*, 1736-1758.
- (6) Long, D.-L.; Burkholder, E.; Cronin, L. *Chem. Soc. Rev.* **2007**, *36*, 105-121.
- (7) Mizuno, N.; Misono, M. *Chem. Rev.* **1998**, *98*, 199-218.
- (8) Neumann, R. *Prog. Inorg. Chem.* **1998**, *47*, 317-370.
- (9) Kozhevnikov, I. V. *Catalysis by Polyoxometalates*; Wiley: Chichester, England, 2002; Vol. 2.
- (10) Lv, H.; Geletii, Y. V.; Zhao, C.; Vickers, J. W.; Zhu, G.; Luo, Z.; Song, J.; Lian, T.; Musaev, D. G.; Hill, C. L. *Chem. Soc. Rev.* **2012**, *41*, 7572-7589.
- (11) Sartorel, A.; Bonchio, M.; Campagna, S.; Scandola, F. *Chem. Soc. Rev.* **2013**, *42*, 2262-2280.
- (12) Kögerler, P.; Cronin, L. *Angew. Chem. Int. Ed.* **2005**, *44*, 844-846.
- (13) Miras, H. N.; Yan, J.; Long, D.-L.; Cronin, L. *Chem. Soc. Rev.* **2012**, *41*, 7403-7430.
- (14) Casa ñ-Pastor, N.; Baker, L. C. W. *J. Am. Chem. Soc.* **1992**, *114*, 10384-10394.
- (15) Alonso, J. A. *Chem. Rev.* **2000**, *100*, 637-677.
- (16) Kortz, U.; Mbomekalle, I. M.; Keita, B.; Nadjo, L.; Berthet, P. *Inorg. Chem.* **2002**, *41*, 6412-6416.
- (17) Compain, J.-D.; Mialane, P.; Dolbecq, A.; Mbomekall é I. M.; Marrot, J.; S écheresse, F.; Rivi ère, E.; Rogez, G.; Wernsdorfer, W. *Angew. Chem. Int. Ed.* **2009**, *48*, 3077-3081.
- (18) Coronado, E.; G ómez-Garc á, C. J. *Chem. Rev.* **1998**, *98*, 273-296.
- (19) Coronado, E.; Day, P. *Chem. Rev.* **2004**, *104*, 5419-5448.

- (20) Clemente-Juan, J. M.; Coronado, E.; Gaita-Arino, A. *Chem. Soc. Rev.* **2012**, *41*, 7464-7478.
- (21) Keita, B.; Nadjó, L. *J. Electroanal. Chem. Interfacial Electrochem.* **1987**, *217*.
- (22) Czap, A.; Neuman, N. I.; Swaddle, T. W. *Inorg. Chem.* **2006**, *45*, 9518-9530.
- (23) Bi, L.-H.; Al-Kadamany, G.; Chubarova, E. V.; Dickman, M. H.; Chen, L.; Gopala, D. S.; Richards, R. M.; Keita, B.; Nadjó, L.; Jaensch, H.; Mathys, G.; Kortz, U. *Inorg. Chem.* **2009**, *48*, 10068-10077.
- (24) Bi, L.-H.; Kortz, U.; Nellutla, S.; Stowe, A. C.; Tol, J. v.; Dalal, N. S.; Keita, B.; Nadjó, L. *Inorg. Chem.* **2005**, *44*, 896-903.
- (25) Boulas, P. L.; Gomez-Kaifer, M.; Echegoyen, L. *Angew. Chem. Int. Ed.* **1998**, *37*, 216-247.
- (26) Guo, S.-X.; Lee, C.-Y.; Zhang, J.; Bond, A. M.; Geletii, Y. V.; Hill, C. L. *Inorg. Chem.* **2014**, *53*, 7561-7570.
- (27) Liu, Y.; Guo, S.-X.; Bond, A. M.; Zhang, J.; Geletii, Y. V.; Hill, C. L. *Inorg. Chem.* **2013**, *52*, 11986-11996.
- (28) Toma, F. M.; Sartorel, A.; Iurlo, M.; Carraro, M.; Parisse, P.; Maccato, C.; Rapino, S.; Gonzalez, B. R.; Amenitsch, H.; Ros, T. D.; Casalis, L.; Goldoni, A.; Marcaccio, M.; Scorrano, G.; Scoles, G.; Paolucci, F.; Prato, M.; Bonchio, M. *Nature Chem.* **2010**, *2*, 826-831.
- (29) Finke, R. G.; Droege, M. W. *Inorg. Chem.* **1983**, *22*, 1006-1008.
- (30) Gómez-García, C. J.; Borrás-Almenar, J. J.; Coronado, E.; Ouahab, L. *Inorg. Chem.* **1994**, *33*, 4016-4022.
- (31) Zhang, X.; Chen, Q.; Duncan, D. C.; Lachicotte, R. J.; Hill, C. L. *Inorg. Chem.* **1997**, *36*, 4381-4386.
- (32) Laronze, N.; Marrot, J.; Hervé G. *Inorg. Chem.* **2003**, *42*, 5857-5862.
- (33) Kortz, U.; Isber, S.; Dickman, M. H.; Ravot, D. *Inorg. Chem.* **2000**, *39*, 2915-2922.
- (34) Hou, Y.; Xu, L.; Cichon, M. J.; Lense, S.; Hardcastle, K. I.; Hill, C. L. *Inorg. Chem.* **2010**, *49*, 4125-4132.

- (35) Kortz, U.; Al-Kassem, N. K.; Savelieff, M. G.; Kadi, N. A. A.; Sadakane, M. *Inorg. Chem.* **2001**, *40*, 4742-4749.
- (36) Ruhlmann, L.; Canny, J.; Contant, R.; Thouvenot, R. *Inorg. Chem.* **2002**, *41*, 3811-3819.
- (37) Gabb, D.; Pradeep, C. P.; Miras, H. N.; Mitchell, S. G.; Long, D.-L.; Cronin, L. *Dalton Trans.* **2012**, *41*, 10000-10005.
- (38) Suzuki, K.; Kikukawa, Y.; Uchida, S.; Tokoro, H.; Imoto, K.; Ohkoshi, S.-i.; Mizuno, N. *Angew. Chem. Int. Ed.* **2012**, *51*, 1597-1601.
- (39) Tourné C. M.; Tourné G. F.; Malik, S. A.; Weakley, T. J. R. *J. Inorg. Nucl. Chem.* **1970**, *32*, 3875-3890.
- (40) Pohl, M.; Lin, Y.; Weakley, T. J. R.; Nomiya, K.; Kaneko, M.; Weiner, H.; Finke, R. *G. Inorg. Chem.* **1995**, *34*, 767-777.
- (41) Rapko, B. M.; Pohl, M.; Finke, R. *G. Inorg. Chem.* **1994**, *33*, 3625-3634.
- (42) Weiner, H.; Hayashi, Y.; Finke, R. *G. Inorg. Chem.* **1999**, *38*, 2579-2591.
- (43) Pohl, M.; Lyon, D. K.; Mizuno, N.; Nomiya, K.; Finke, R. *Inorg. Chem.* **1995**, *34*, 1413-1429.
- (44) Clemente-Juan, J. M.; Coronado, E.; Galán-Mascarós, J., J. R.; Gómez-García, C. J. *Inorg. Chem.* **1999**, *38*, 55-63.
- (45) Anderson, T. M.; Zhang, X.; Hardcastle, K. I.; Hill, C. L. *Inorg. Chem.* **2002**, *41*, 2477-2488.
- (46) Geletii, Y. V.; Yin, Q.; Hou, Y.; Huang, Z.; Ma, H.; Song, J.; Besson, C.; Luo, Z.; Cao, R.; O'Halloran, K. P.; Zhu, G.; Zhao, C.; Vickers, J. W.; Ding, Y.; Mohebbi, S.; Kuznetsov, A. E.; Musaev, D. G.; Lian, T.; Hill, C. L. *Isr. J. Chem.* **2011**, *51*, 238-246.
- (47) Lv, H.; Song, J.; Zhu, H.; Geletii, Y. V.; Bacsa, J.; Zhao, C.; Lian, T.; Musaev, D. G.; Hill, C. L. *J. Catal.* **2013**, *307*, 48-54.
- (48) Lv, H.; Guo, W.; Wu, K.; Chen, Z.; Bacsa, J.; Musaev, D. G.; Geletii, Y. V.; Lauinger, S. M.; Lian, T.; Hill, C. L. *J. Am. Chem. Soc.* **2014**, *136*, 14015-14018.

- (49) Lv, H.; Chi, Y.; van Leusen, J.; Kögerler, P.; Chen, Z.; Bacsa, J.; Guo, W.; Lian, T.; Hill, C. L. *Chem. Eur. J.* **2015**, accepted.
- (50) Randall, W. J.; Droege, M. W.; Mizuno, N.; Nomiya, K.; Weakley, T. J. R.; Finke, R. G. In *Inorg. Synth.*; Cowley, A. H., Ed.; John Wiley & Sons, Inc.: New York, 1997; Vol. 31, p 167-185.
- (51) Katsoulis, D. E.; Pope, M. T. *J. Am. Chem. Soc.* **1984**, *106*, 2737-2738.
- (52) Bruker, *APEXII v2014.1-1*, Bruker AXS, Inc., Madison, WI, **2014**.
- (53) Bruker, *SAINT v8.34A*, Bruker AXS, Inc., Madison, WI, **2013**.
- (54) Palatinus, L.; Chapuis, G. *J. Appl. Crystallogr.* **2007**, *40*, 786-790.
- (55) Sheldrick, G. M. *Acta Crystallogr., Sect. A: Found. Crystallogr.* **2008**, *64*, 112-122.
- (56) Ibrahim, M.; Xiang, Y.; Bassil, B. S.; Lan, Y.; Powell, A. K.; de Oliveira, P.; Keita, B.; Kortz, U. *Inorg. Chem.* **2013**, *52*, 8399-8408.
- (57) Zhang, X.; Anderson, T. M.; Chen, Q.; Hill, C. L. *Inorg. Chem.* **2001**, *40*, 418-419.
- (58) Anderson, T. M.; Fang, X.; Mbomekalle, I. M.; Keita, B.; Nadjo, L.; Hardcastle, K. I.; Farsidjani, A.; Hill, C. L. *J. Cluster Sci.* **2006**, *17*, 183-195.
- (59) Rocchiccioli-Deltcheff, C.; Thouvenot, R. *J. Chem. Res., Synop.* **1977**, *2*, 46-47.
- (60) Son, J.-H.; Ohlin, C. A.; Casey, W. H. *Dalton Trans.* **2013**, *42*, 7529-7533.
- (61) Liu, J.; Liu, Y.; Liu, N.; Han, Y.; Zhang, X.; Huang, H.; Lifshitz, Y.; Lee, S.-T.; Zhong, J.; Kang, Z. *Science* **2015**, *347*, 970-974.
- (62) Hisatomi, T.; Kubota, J.; Domen, K. *Chem. Soc. Rev.* **2014**, *43*, 7520-7535.
- (63) Young, K. J.; Martini, L. A.; Milot, R. L.; III, R. C. S.; Batista, V. S.; Schmuttenmaer, C. A.; Crabtree, R. H.; Brudvig, G. W. *Coord. Chem. Rev.* **2012**, *256*, 2503-2520.
- (64) Prier, C. K.; Rankic, D. A.; MacMillan, D. W. C. *Che. Rev.* **2013**, *113*, 5322-5363.
- (65) Sun, H.; Hoffman, M. Z. *J. Phys. Chem.* **1994**, *98*, 11719-11726.

Chapter 6.

A Hybrid Nanocomposite of Polyoxometalates, Pt Nanoparticles and Metal-Organic Frameworks for Synergistic Hydrogen Evolution

Reproduced from *J. Mater. Chem. A.*, **2016**, *4*, 5952-5957 with permission from The Royal Society of Chemistry

As a main contributor of this work; with Hongjin Lv, Zheyuan Chen, Kevin P. Sullivan, Sarah M. Lauinger, Yingnan Chi, Jordan M. Sumliner, Tianquan Lian and Craig L. Hill*, W. Guo contributed the syntheses, characterizations, investigating and analyzing the catalysts' activities to this work. H. Lv designed the catalytic experiments. Z. Chen and T. Lian performed and analyzed the fluorescence lifetime measurements. K. P. Sullivan and S. M. Lauinger conducted the TEM and EDX measurements. Y. Chi prepared the MOF materials. J. M. Jordan designed the visible diffuse reflectance set up. W. Guo and C. L. Hill designed the experiments and prepared the manuscript.

6.1 Introduction

Developing artificial photosynthetic systems that harvest sunlight, the most abundant source of renewable energy, has become a major goal of the research community.¹⁻⁸ Two essential components are needed for a light-driven photosynthetic system: the photosensitizer for light harvesting and the catalyst for water splitting and/or for carbon dioxide fixation.⁹ Recent progress has been made on various fronts lately including the use of semiconductors,¹⁰ metalloporphyrins,^{11, 12} polyoxometalates (POMs)¹³⁻²⁰ and metal-organic frameworks (MOFs)²¹⁻²⁶ as potential catalysts. POMs, a family of metal oxide cluster polyanions with highly variable functional properties, have applications in molecular magnetism, medicine and catalysis.²⁷⁻³⁶ Some POM catalysis is facilitated by their rich, and reversible redox chemistry.³⁷⁻³⁹ POMs stabilize noble-metal nanoparticles (NPs).⁴⁰⁻⁴³ The stabilized Pt NPs show enhanced activities in multiple reactions relative to commercial Pt black.^{44, 45} For example, CdS quantum dots with POM-encapsulated gold NPs are more efficient photocatalysts for H₂ evolution than gold NPs without POMs.⁴⁶

Simultaneously, noteworthy studies on photoactive MOF-based catalysis for energy-related reactions including water splitting and CO₂ reduction have gained much attention.^{21-23, 47-51} MOFs are a class of crystalline porous functional materials constructed from metal-oxide unites and organic linkers. The ultrahigh porosity and high thermal stability together with the potential active sites for redox reactions have led to some successful applications of MOFs in various fields: gas storage and separation, nonlinear optics and catalysis.⁵²⁻⁵⁶ For example, Lin and co-workers utilized a mix-and-match strategy to synthesize a series of photoactive MOFs for visible-light-driven CO₂ reduction and water splitting.^{47, 48, 57}

MOF composites have also been well-documented.⁵⁸ MOFs containing POMs and/or metal NPs have shown synergistic activity.⁵⁹⁻⁶⁷ Our group previously reported a Cu-containing POM-MOF that catalyzes aerobic sulfoxidation in which the MOF and the encapsulated POM exhibit synergistic hydrolytic stability and catalytic activity.⁶² MOFs are well documented to encapsulate NPs.⁶⁸ For example, MIL-101 with encapsulated gold NPs shows synergistic aerobic alcohol oxidation.⁶³

We report here an approach that combines POMs, Pt NPs and MOFs in a hybrid material, POM-Pt NPs@NH₂-MIL-53 (**PNPMOF**), with greatly enhanced photocatalytic H₂ evolution relative to each component alone. Pt NPs which are stabilized by Keggin POMs (H₃PW₁₂O₄₀) are loaded onto the surfaces of amine-functionalized MOF, NH₂-MIL-53 particles. This work also demonstrates that a POM can perform four separate functions simultaneously, a theme of potential value in construction of energy converting multicomponent assemblies. The stability of the **PNPMOF** composite under catalytic conditions was also investigated.

6.2 Experimental

6.2.1 General Methods and Materials

All chemicals used were from commercially available sources and were used without further purification unless otherwise noted. Infrared spectra (2% sample in KBr pellet) were recorded on a Nicolet TM 600 FT-IR spectrometer. Thermogravimetric analyses were performed on a STA 6000 thermal analyzer. Surface area measurement was carried out on a NOVA 200 BET surface analyzer from Quantachrome Corporation. Transmission electron microscopy (TEM) and Z-contrast TEM (Z-TEM) images were taken on a Hitachi H-7500 transmission electron microscope at an accelerating voltage of 75 kV. Scanning Electron Microscopy (SEM) images were obtained on a High Resolution S4800 Scanning

Electron Microscope operated at 30 kV. Energy-dispersive X-ray (EDX) analysis was performed on this SEM coupled with an EDX Si(Li) X-ray detector. The samples for TEM and SEM were prepared by dropping and coating the sonicated aqueous sample solution onto a carbon-coated copper grid and air dried. Steady-state luminescence quenching spectra were obtained using a FluoroMax 3 spectrofluorimeter. Time-resolved fluorescence decay measurements were conducted using a mode-locked Ti:sapphire laser (Tsunami oscillator pumped by 10 W Millennia EV, Spectra-Physics). Excitation pulses at 400 nm were generated by the second harmonic generation of the 800 nm pulses in a BBO crystal. The 540-620 nm emissions were detected using a microchannel plate photomultiplier tube (Hamamatsu R3809U-51). The repetition rate of output pulses centered at 800 nm was reduced from 80 MHz to 9MHz by a pulse picker (Conoptics, USA). The output was amplified and analyzed using a TCSPC board (Becker &Hickel SPC 600). UV-vis spectra were obtained on an Agilent 8453 spectrophotometer equipped with a diode-array detector using a 1.0-cm-optical-path quartz cuvette. Visible diffuse reflectance spectra were obtained using Miniscan XE Plus from Hunter Associates Lab. Elemental analyses (Al, P, W, Pt and N) were performed by Galbraith Laboratories (Knoxville, Tennessee). The Powder XRD data were collected on a D8 Discover Powder Instrument on monochromatic Cu K α ($\lambda = 1.54060 \text{ \AA}$) radiation. Amounts of hydrogen in the photocatalytic reduction experiments were measured by gas chromatography (GC) using a 5 \AA molecular sieve column and a TCD detector with Ar as the carrier gas.

6.2.2 Synthesis of NH₂-MIL-53.

The NH₂-MIL-53 was prepared by a modified literature method.⁶⁹ Typically, 0.153 g of aluminum chloride hexahydrate (0.63 mmol) was mixed with 0.168 g 2-aminoterephthalic acid (0.93 mmol) in 9 mL DMF. The solution was kept at 150 °C in a Teflon-lined autoclave bomb. After 72 h, the solids were separated by centrifugation and washed with DMF three times and with methanol three times. The solids were then dried under vacuum at 80 °C for 6 h. Yield: 0.05 g, 38%.

6.2.3 Synthesis of POM-Pt NPs@NH₂-MIL-53 (PNPMOF).

Isopropanol (14 μL) and H₂PtCl₆ (10 μL of 0.5 M) were added to an aqueous solution of 2 mL of H₃PW₁₂O₄₀ (0.1 M). The mixture was irradiated using a UV lamp for 2 h, and the color of the solution changed from light yellow to dark blue. The dark-blue solution was then mixed with 50 mg NH₂-MIL-53 and exposed to air forming **PNPMOF**. This product composite was separated by centrifugation and washed extensively with methanol and water.

6.2.4 Synthesis of POM-Pt NPs@NH₂-silica

This hybrid was prepared using a procedure similar to that used for **PNPMOF** except that commercial amino-functionalized silica gel was used instead of NH₂-MIL-53.

6.2.5 Photocatalytic experimental processes

The hydrogen evolution experiments were conducted in 2.5 mL septum-sealed glass vials containing 10 mg of **PNPMOF**. Typically, 2 mL of aqueous ascorbic acid (0.05-0.2 M) and 10 mg **PNPMOF** were added to the vials. The pH of the solution was adjusted by adding 0.1 M NaOH before use. The vials were then capped and deoxygenated by bubbling Ar for 30 min and irradiated by a Xe-lamp source (light intensity 150W, beam size 0.2 cm², 400 nm cutoff filter) at room temperature and

magnetically stirred for 6 h. The hydrogen in the headspace of the vials was analyzed by GC.

6.2.6 Recycle and Reuse

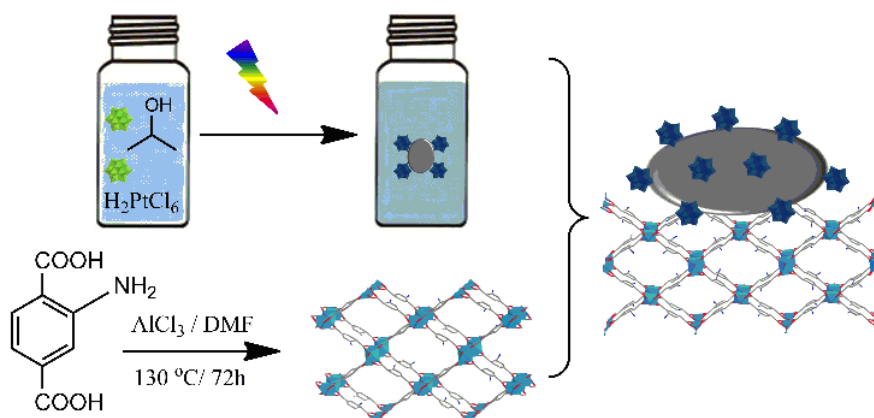
The solid in the reaction mixture after each photocatalytic experimental entry was collected by centrifugation and washed repeatedly with distilled water. The filtrate solution was investigated by UV-vis spectroscopy and analyzed by elemental analysis to detect any leaching of organic ligands or Pt NPs. The solid was then dried under vacuum before being used in successive catalytic runs. All reactions were conducted under the same conditions.

6.3 Results and Discussion

6.3.1 Synthesis and characterization of PNPMOF

Scheme 6-1 illustrates the preparation for **PNPMOF**. The POM-stabilized Pt NPs were prepared following a modified literature method.⁴⁴ $\text{H}_3\text{PW}_{12}\text{O}_{40}$ was first reduced by isopropanol upon UV light irradiation, and the dark blue reduced $[\text{PW}_{12}\text{O}_{40}]^{4-}$ product then was used to reduce H_2PtCl_6 forming Pt NPs. The negatively-charged POMs are well known to attach to the surface of Pt NPs and to stabilize these against aggregation.⁴⁰⁻⁴³ The resulting POM-stabilized Pt NPs were mixed with the amine-functionalized MOF, $\text{NH}_2\text{-MIL-53}$ which was prepared following a modified literature method,⁶⁹ forming **PNPMOF**. **PNPMOF** is partly cationic, i.e. bearing NH_3^+ groups below pH ~6 which electrostatically bind the negatively charged POM-stabilized Pt NPs. The final **PNPMOF** contains $\text{H}_3\text{PW}_{12}\text{O}_{40}$ and Pt NPs in 3.92 and 0.38 weight percents respectively by elemental analysis.

Scheme 6-1. Route to **PNPMOF** (symbols not to scale). Green polyhedra: $\text{H}_3\text{PW}_{12}\text{O}_{40}$; dark blue polyhedra: reduced POM units, $[\text{PW}_{12}\text{O}_{40}]^{4-}$; gray ellipses: Pt NPs; light blue octahedra: $\text{AlO}_4(\text{OH})_2$; gray sticks: carbon connector units; dark blue sticks: $-\text{NH}_2$ side chains; red sticks: oxygen.



The **PNPMOF** shows a PXRD pattern and an FT-IR spectrum that are very similar to those of $\text{NH}_2\text{-MIL-53}$ indicating that $\text{NH}_2\text{-MIL-53}$ structure is maintained (**Figure 6-1**). $\text{NH}_2\text{-MIL-53}$ is constructed by one-dimensional aluminum oxide chains joined together by 2-aminoterephthalate linkers.⁷⁰ The FT-IR spectrum (**Figure 6-1**) of **PNPMOF** shows typical bands of $\text{NH}_2\text{-MIL-53}$. The characteristic bands attributed to the symmetric and asymmetric stretches of free NH_2 groups (3390 and 3501 cm^{-1}) confirms that the NH_2 groups are successfully incorporated into the framework.²² Moreover, the splitting of the band at *ca.* 1430 cm^{-1} corresponding to the symmetric stretches of carboxylate groups is introduced by the amino groups which lower the overall symmetry.⁷¹ However, the vibrational peaks for $\text{H}_3\text{PW}_{12}\text{O}_{40}$ are not easily distinguished because they overlap with the strong stretching peaks of the organic linkers in $\text{NH}_2\text{-MIL-53}$ at the low POM loading in **PNPMOF**.

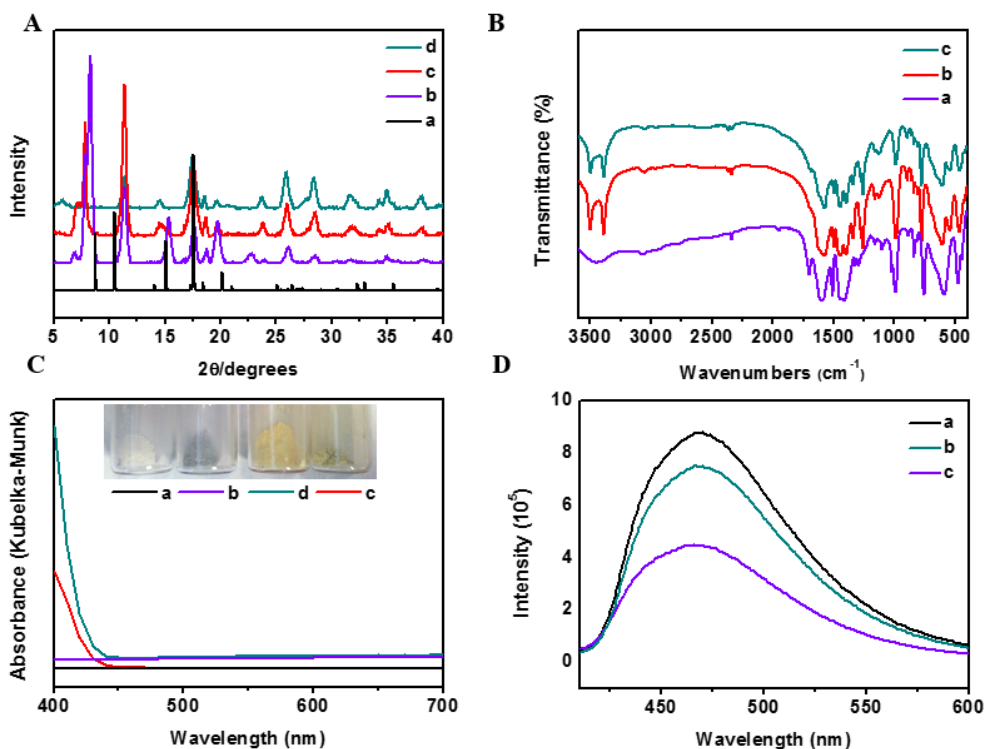


Figure 6-1. A) PXR D patterns of a) simulated MIL-53, b) MIL-53, c) NH₂-MIL-53 and d) **PNPMOF**. B) FT-IR spectra of a) MIL-53, b) NH₂-MIL-53 and c) **PNPMOF**. C) Diffuse reflectance spectra of a) MIL-53, b) POM-Pt NPs@MIL-53 (the MOF without the anilinium side chain), c) **PNPMOF** and d) NH₂-MIL-53. Inset: photograph of these samples in small vials. D) Photo-luminescence spectra of a) NH₂-MIL-53, b) NH₂-MIL-53 combined with H₃PW₁₂O₄₀ and c) **PNPMOF**. The weighed quantities of the MOF samples are the same in all spectra (Figures C and D).

Nevertheless, the TEM images (**Figure 6-2**) of **PNPMOF** show 50-80 nm Pt NPs are firmly adhering to the NH₂-MIL-53 particles. In contrast, The Z-TEM image of NH₂-MIL-53 mixed with the commercial Pt black (**Figure 6-2**) shows that the Pt particles are heavily aggregated, and the Pt particles are not firmly binding to NH₂-MIL-53 surfaces. This indicates that the POMs binding to the surface of the Pt(0) NPs greatly inhibit NP aggregation. We calculate that ca. 6% of the total NH₂ groups in the

entire MOF sample are connected to the Pt NPs on the particle surfaces (see **Scheme 6-2** in SI for detailed calculations). EDX spectroscopy further confirms the existence of the POM-stabilized Pt NPs as well as the NH₂-MIL-53 particles: distinct peaks for W and Pt are seen (**Figure 6-3**).

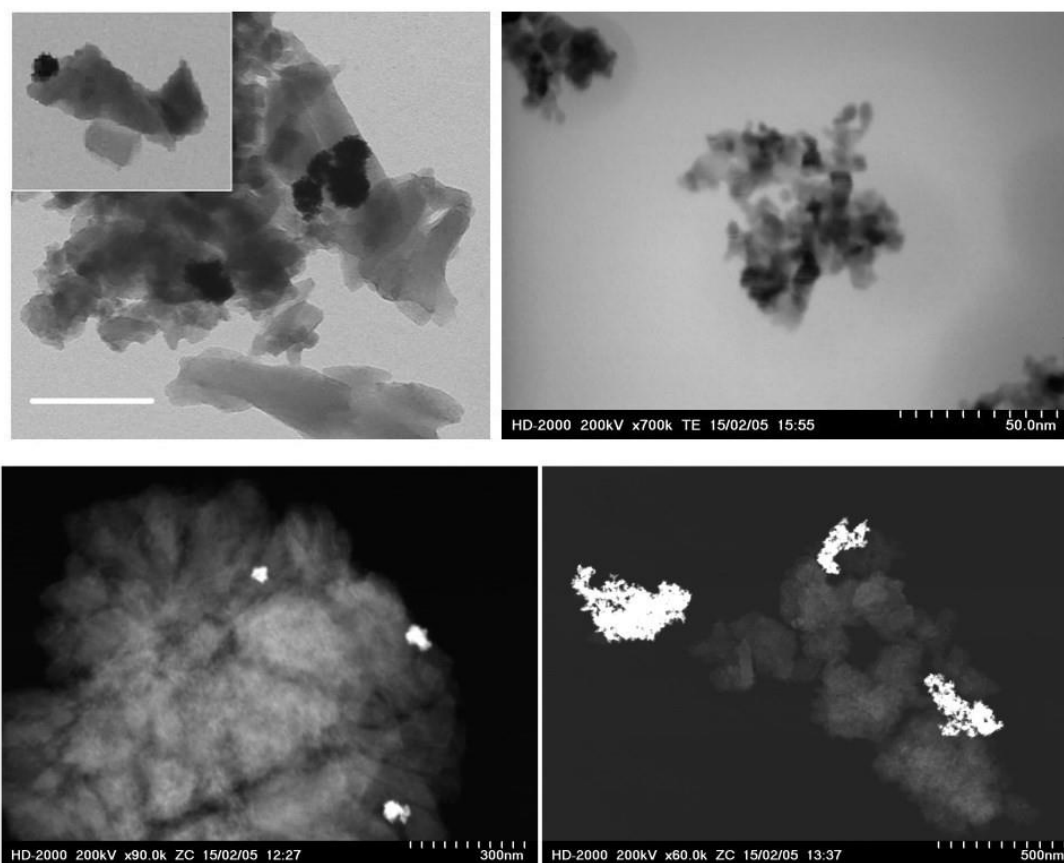
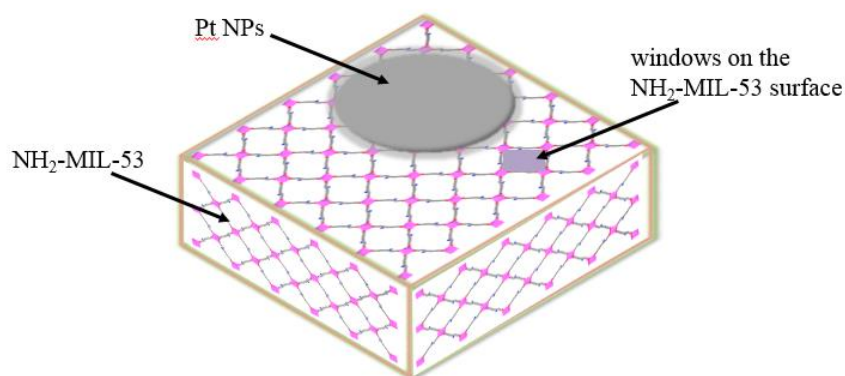


Figure 6-2 A): TEM images of POM-Pt NPs@NH₂-MIL-53 (**PNPMOF**). The large dark approximately spherical particles are the POM-capped Pt NPs. The scale bar in the graph corresponds to 200 nm. B): TEM image of POM-stabilized Pt NPs. C) Z-contrast TEM image of PNPMOF. D) Z-contrast TEM image of NH₂-MIL-53 mixed with the commercial Pt black.

Scheme 6-2. Illustration of the Pt NPs and the windows on the NH₂-MIL-53 surface. Based on the weight percent of Pt NPs (0.38 %) and the average size of Pt NPs (80 nm), the number of Pt NPs loaded onto the surface of NH₂-MIL-53 is calculated to be 2.0×10^{17} in a 100 g sample, and the number of NH₂ groups is calculated to be 1.4×10^{23} . Considering the pore window of NH₂-MIL-53 (0.7 nm \times 0.7 nm), the number of windows on the NH₂-MIL-53 surface that are covered by the Pt NPs is estimated to be: $3.14 \times (40\text{nm})^2 \times 2.0 \times 10^{17} / (0.7\text{nm} \times 0.7\text{nm}) = 2.05 \times 10^{21}$. Each window has four NH₂ groups, therefore, the number of NH₂ groups that are connected with each Pt NP is estimated to be: $4 \times 2.05 \times 10^{21} = 8.2 \times 10^{21}$. Therefore, about 6% ($= 8.2 \times 10^{21} / 1.4 \times 10^{23}$) of the total NH₂ groups are connected to Pt NPs.



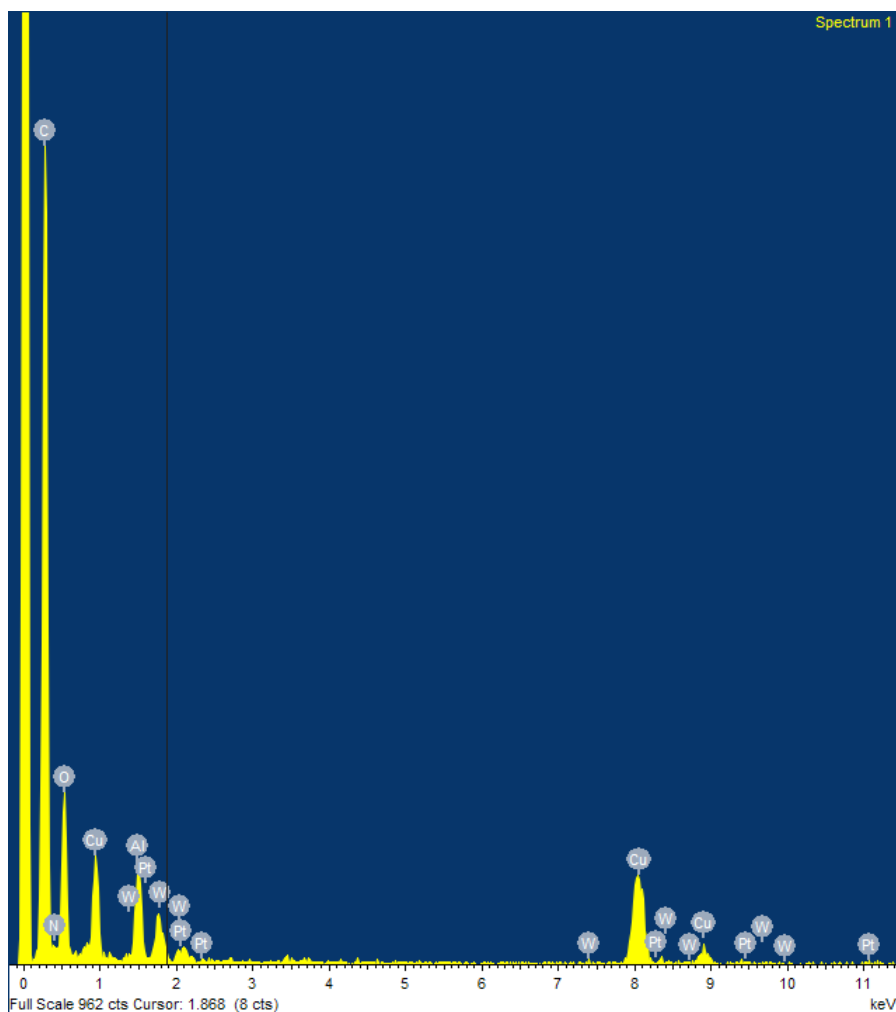


Figure 6-3. EDX analysis of **PNPMOF**

The **PNPMOF** has a similar thermal behavior to $\text{NH}_2\text{-MIL-53}$ (**Figure 6-4**). The BET surface area of **PNPMOF** ($684 \text{ m}^2/\text{g}$) is lower than that of $\text{NH}_2\text{-MIL-53}$ ($912 \text{ m}^2/\text{g}$) (**Figure 6-5**, **Figure 6-6** and **Figure 6-7**). These BET surface areas of 912 and $1174 \text{ m}^2/\text{g}$ are consistent with previously reported literature values.⁶⁹

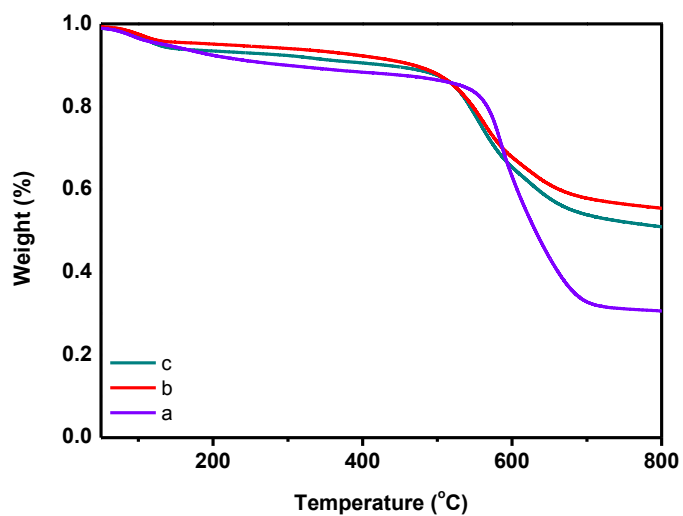


Figure 6-4. TGA of a) MIL-53 (purple), b) NH₂-MIL-53 (green) and c) PNPMOF (red). PNPMOF shows a similar thermal behavior to that of NH₂-MIL-53. Both are stable up to 500 °C.

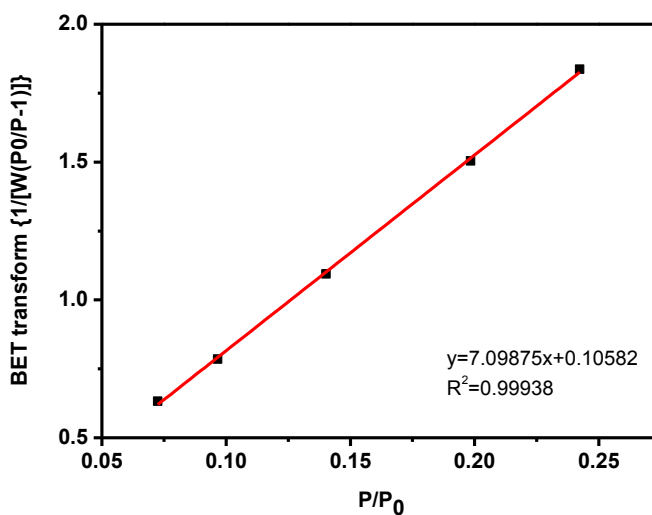


Figure 6-5. BET fitting curve for MIL-53. (MIL-53 surface area = 1174 m²/g).

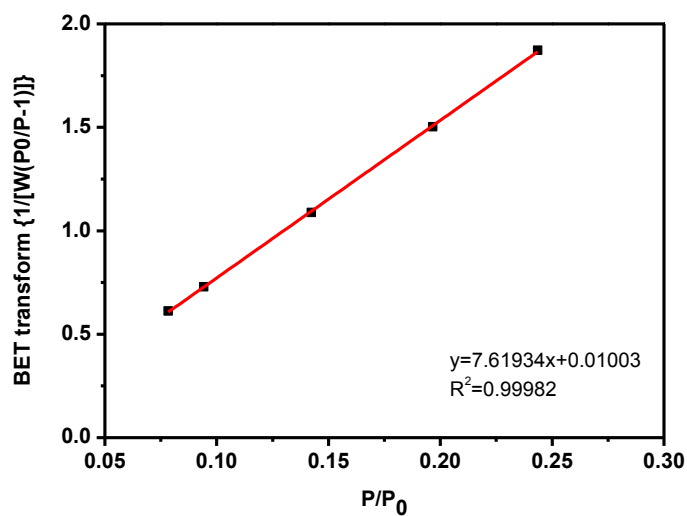


Figure 6-6. BET fitting curve for NH₂-MIL-53. (NH₂-MIL-53 surface area = 912 m²/g). This is lower than that of MIL-53 (1174 m²/g) because NH₂ groups partially block the pores of NH₂-MIL-53. These BET surface areas of 912 and 1174 m²/g are consistent with previously reported literature values.⁶⁹

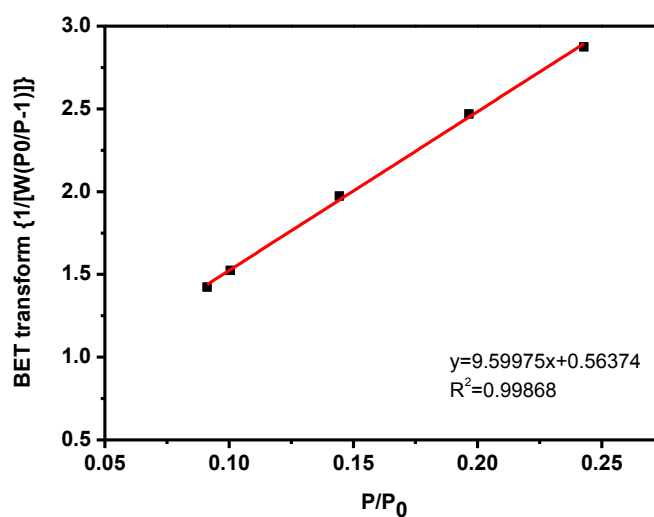


Figure 6-7. BET fitting curve for PNP MOF. (PNP MOF surface area = 684 m²/g).

Modification of the benzene-1,4-dicarboxylate organic linkers in MIL-125(Ti), with amino groups makes these units capable of absorbing visible light and transferring electrons to thermodynamically appropriate donors.²² Similarly, NH₂-MIL-53 exhibits a lone pair n- π^* transition of the amino groups with an absorption edge extending to 450 nm,^{72, 73} consistent with its light yellow color (**Figure 6-1**). As a result, NH₂-MIL-53 can function as robust light absorber in light-driven photocatalytic systems. The optical properties of **PNPMOF** are similar to those of NH₂-MIL-53. The presence of Pt NPs decreases the light harvesting ability of **PNPMOF**. The photo-luminescence spectra of **PNPMOF** are shown in Fig 1D. NH₂-MIL-53 displays a broad photo-luminescence with an emission maximum at 470 nm upon excitation at 400 nm, consistent with the known photo-luminescence of 2-aminoterephthalic acid.⁷⁴ When NH₂-MIL-53 is combined with H₃PW₁₂O₄₀, the emission intensity decreases, consistent with electron transfer between NH₂-MIL-53 and the POMs. In particular, a maximum decrease of intensity is observed in **PNPMOF**, which implies that electron transfer between NH₂-MIL-53 and the POM-stabilized Pt NPs is more efficient when NH₂-MIL-53, POMs and Pt NPs are all present but not bonded to one another. This is borne out by the synergistic catalytic activity of **PNPMOF**.

6.3.2 Photocatalytic hydrogen evolution

The **PNPMOF** was investigated for its photocatalytic H₂ evolution activity using ascorbic acid (AA) as sacrificial electron donor under visible light irradiation. The catalytic activity depends on solution pH (**Figure 6-8**). It maximizes at pH 4.5, at which point, the AA not only acts as a sacrificial reducing agent but also functions as a buffer with its reduced product, dehydroascorbic acid (dHAA).⁷⁵ At pH 4.5, *ca.* 1% of the NH₂ groups are protonated which can firmly bind the negatively charged Pt NPs; the remaining 99% that are unprotonated and can function as light absorbers (**Figure**

6-9).⁷⁶ Moreover, the activity increases slightly with AA concentration (**Figure 6-10**).

In the following photocatalytic reactions, 0.1 M AA at pH 4.5 was used and is denoted as the standard conditions.

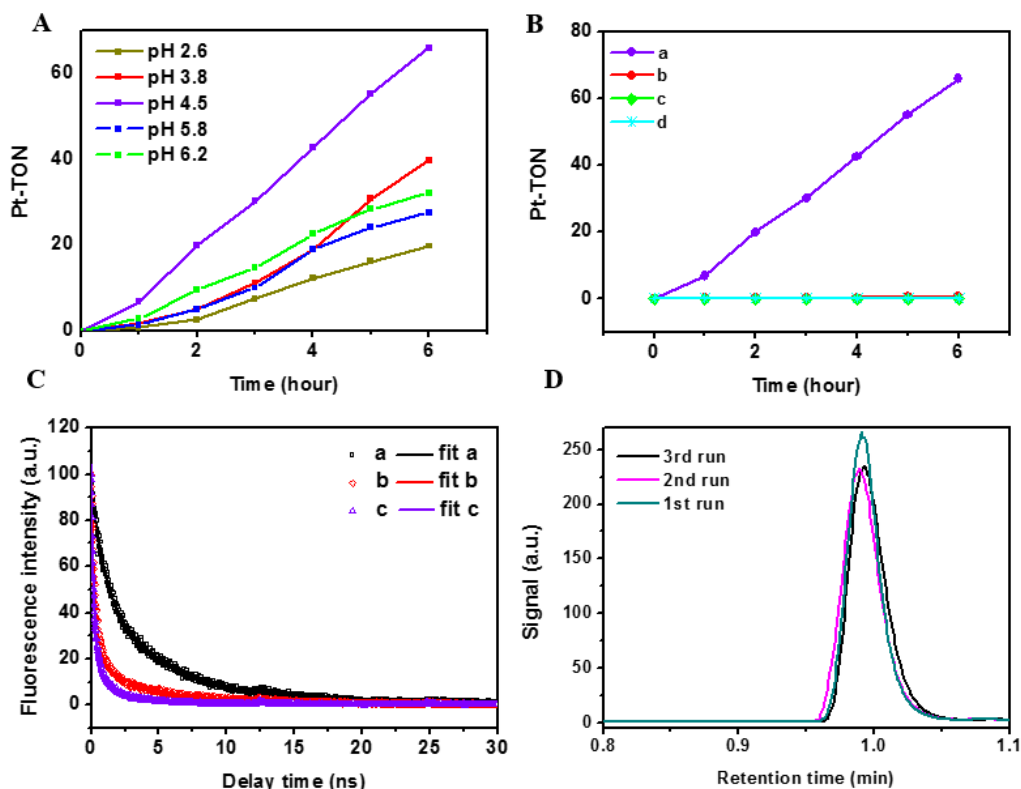


Figure 6-8. A) Time-dependent hydrogen evolution by PNPMOF under different pH conditions. B) Time-dependent H₂ evolution of a) PNPMOF, b) 2-aminoterephthalic acid mixed with POM-stabilized Pt NPs, c) NH₂-MIL-53 mixed with commercial Pt black and d) POM-Pt NPs@NH₂-silica. “Pt-TON” are turnovers with respect to total Pt atoms. C) Normalized fluorescence decay of a) 2-aminoterephthalic acid in the solid state, b) NH₂-MIL-53, c) PNPMOF. The solid lines are best fits according to single exponential decay for a) and bi-exponential decays for b) and c). D) The hydrogen peak in GC traces in successive experiments using the same catalyst. (Fresh solutions were used for each run; reaction time = 6 h all cases).

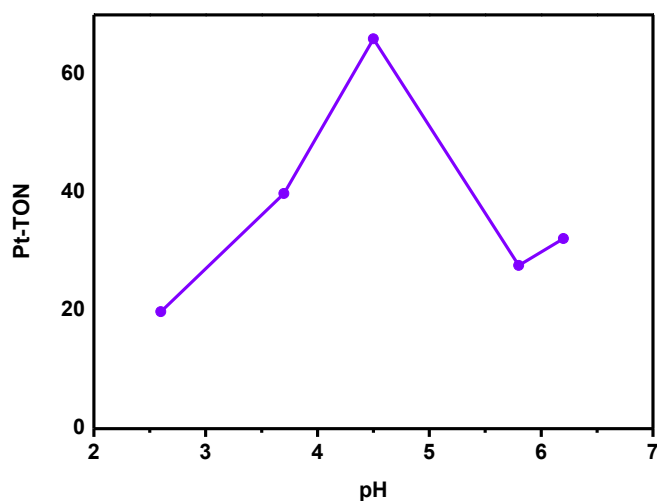


Figure 6-9. pH dependence of hydrogen evolution by **PNPMOF** using ascorbic (AA) as sacrificial electron donor. The amino group in $\text{NH}_2\text{-MIL-53}$ is assumed to have a similar pK_a to that of 3-nitroanilinium cation, which is 2.5.² Therefore, at pH 4.5, about 1% of NH_2 groups are protonated; the remaining unprotonated NH_2 groups function as light absorbers.

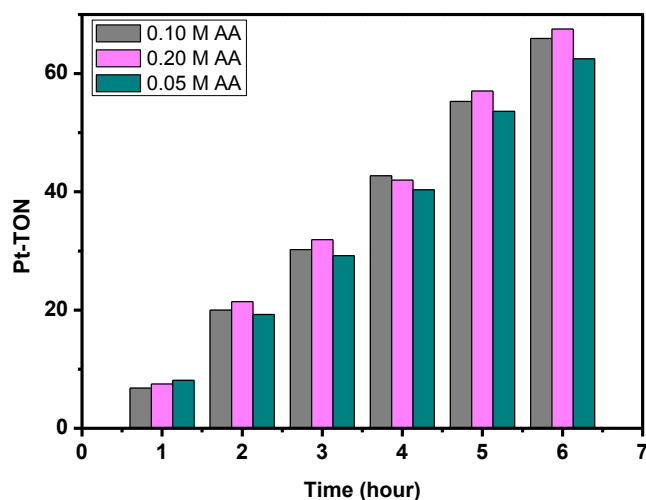


Figure 6-10. Time-dependent hydrogen evolution curves for **PNPMOF** using different concentrations of AA.

A TON of ca. 66 is achieved in 6 hours under standard conditions (**Figure 6-8**) with a quantum yield of 1.2×10^{-4} . In dramatic contrast, when POM-Pt NPs@NH₂-silica was used for photocatalytic H₂ production, no H₂ was detected because of the lack of a light absorbing unit. Significantly, the control experiment using commercial 2-aminoterephthalic acid instead of NH₂-MIL-53 only shows a TON of ca. 1 after 6 hours, which was presumably due to the fact that 2-aminoterephthalic acid was easily oxidized by POMs⁷⁷ thus losing its light absorbing ability (**Figure 6-11**). Moreover, this further indicates that the partially cationic NH₂-MIL-53 not only electrostatically binds to the negatively-charged Pt NPs but also helps to stabilize the 2-aminoterephthalic connectors. A similar stabilization effect of MOFs was observed previously.⁴⁷ In addition, it has been reported that the size of Pt NPs can affect the activity towards various reactions,⁷⁸⁻⁸² thus the efficiency of the photocatalytic system in this study might be further optimized via modifying the the size of Pt NPs.⁶⁸



Figure 6-11. Oxidation of 2-aminoterephthalic acid by H₃PW₁₂O₄₀. When 50 μ M 2-aminoterephthalic acid was mixed with 0.1 M H₃PW₁₂O₄₀ in distilled water in the dark purged with Ar, the color of the solution changes from light yellow (left) to dark blue (right) (a characteristic color for reduced H₃PW₁₂O₄₀) after 1 hour indicating that the 2-aminoterephthalic acid is oxidized by H₃PW₁₂O₄₀.

Importantly, a negligible amount of H₂ was identified when Pt black@NH₂-MIL-53 was used (**Figure 6-8**), implying the importance of the POMs in catalytic turnover, and specifically in charge separation and electron transfer processes.⁸³⁻⁸⁵ The control experiments based on each component were conducted (**Table 6-1**). No obvious activity is observed for each component alone: the MOF, the POM, the Pt NPs and the AA are all essential for H₂ evolution, as is visible light (no H₂ is detected in the dark). In addition, the photocatalytic system is not temperature dependent: reactions in 0 °C, 25 °C and 50 °C water bath show almost identical activity (**Table 6-1**).

Table 6-1. Control experiments for photocatalytic hydrogen evolution under standard conditions after 6 hours.

Entry	Catalyst	TON with respect to Pt
1	MIL-53	< 1% (limit of detection)
2	NH ₂ -MIL-53	< 1% (limit of detection)
3	PNPMOF	66
4	(<i>n</i> -BuN) ₃ PW ₁₂ O ₄₀	< 1% (limit of detection)
5	POM-stabilized Pt NPs	< 1% (limit of detection)
6	H ₂ PtCl ₆	< 1% (limit of detection)
7	NH ₂ -MIL-53 with H ₃ PW ₁₂ O ₄₀	< 1% (limit of detection)
8	Without the addition of AA	< 1% (limit of detection)
9	PNPMOF in 0 °C	58
10	PNPMOF in 25 °C	58
11	PNPMOF in 50 °C	59

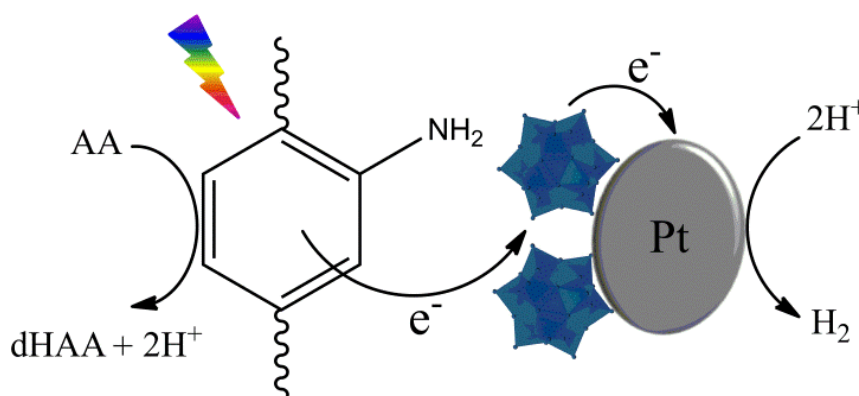
Fluorescence lifetime measurements were used to track the dynamics of photoexcited electrons in NH₂-MIL-53. As shown in **Figure 6-8**, the excited state of 2-aminoterephthalic acid in the solid state decays single-exponentially with a lifetime of 3.0 ns, while the excited state of NH₂-MIL-53, shows a bi-exponential decay with an average lifetime of $\tau = (A_1\tau_1^2 + A_2\tau_2^2) / (A_1\tau_1 + A_2\tau_2) = 2.1$ ns. However, when the NH₂-MIL-53 is combined with POM-stabilized Pt NPs, the average lifetime is only 0.7 ns (**Table 6-2**). The decreased lifetime from 2.1 ns to 0.7 ns suggests that additional decay channels exist in the presence of POM-stabilized Pt NPs, such as electron transfer and energy transfer from the photoexcited NH₂-MIL-53. The H₂ evolution in the photoexcited **PNPMOF** indicates the existence of photo-induced electron transfer. As a negligible amount of H₂ is evolved in the absence of NH₂-MIL-53 (**Table 6-1**), the photo-generated electrons have to be transferred from the photo-excited NH₂-MIL-53 to the POM-stabilized Pt NPs. Therefore, part of the decreased fluorescence lifetime is due to this electron transfer.

Table 6-2. Average lifetimes^a for different samples from time-resolved fluorescence decay measurements.

Sample	τ_1 (ns)	A ₁ (%)	τ_2 (ns)	A ₂ (%)	Average life time (ns)
2-Aminoterephthalic acid	0.71	49	3.5	51	3.0
NH ₂ -MIL-53	0.2	79	2.6	21	2.1
PNPMOF	0.14	79	1.0	21	0.7

^aAverage lifetime of $\tau = (A_1\tau_1^2 + A_2\tau_2^2) / (A_1\tau_1 + A_2\tau_2)$.

Scheme 6-3. Scheme showing the proposed mechanism for photocatalytic H₂ evolution in the **PNPMOF** system (symbols are *not* to scale)



Based on the above observations, a systematic mechanism for this light-induced H₂ evolution using **PNPMOF** as the catalyst and AA as the sacrificial electron donor is proposed in **Scheme 6-3**. Under visible light irradiation, the NH₂-MIL-53 forms electron-hole pairs. The electrons transfer to the POMs and then to the Pt NPs where H₂ is evolved.

The ATR-IR spectra indicate that this multi-component self-assembled photocatalyst system is quite stable from pH 2 to pH 8 (**Figure 6-12**). Moreover, the catalyst can be easily recycled and reused. After the first run, the catalyst was separated by centrifugation, washed with distilled water extensively and dried under vacuum. This recycled catalyst was reused for the second run. As shown in **Figure 6-8**, the catalyst showed an activity comparable to that in the first run. In addition, the filtrate solution after the first run was examined by elemental analysis, and only a trace amount of H₃PW₁₂O₄₀ was detected indicating that no apparent H₃PW₁₂O₄₀ or Pt was leached into the solution under turnover conditions. No photocatalytic activity was detected using the filtrate solution. The UV-vis spectra of the solution after the first run indicated a negligible amount of organic linker was present arguing strongly that the MOF

structure is maintained during the catalytic reactions (**Figure 6-13**). In addition, both the PXRD patterns and the FT-IR spectra of **PNPMOF** after catalysis retain all the characteristic peaks in the before-catalysis samples (**Figure 6-14** and **Figure 6-15**). The above observations confirm the robust nature of the **PNPMOF** composite.

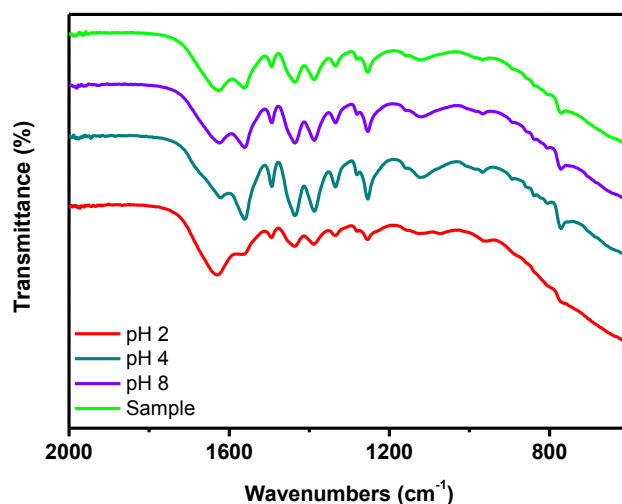


Figure 6-12. ATR-IR spectra of **PNPMOF** at different pH values. The “sample” is for **PNPMOF** with no additional added acid.

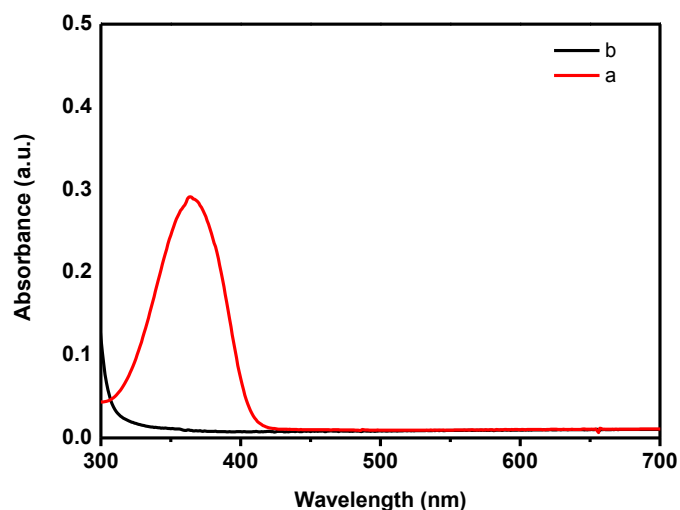


Figure 6-13. UV-vis spectra of a) 2-aminoterephthalic acid in distilled water (60 μ M) and b) the filtrate solution after the first run. The UV-vis spectra of the filtrate solution

indicate a negligible amount of organic linker is present arguing strongly that the MOF structure is maintained during the catalytic reactions.

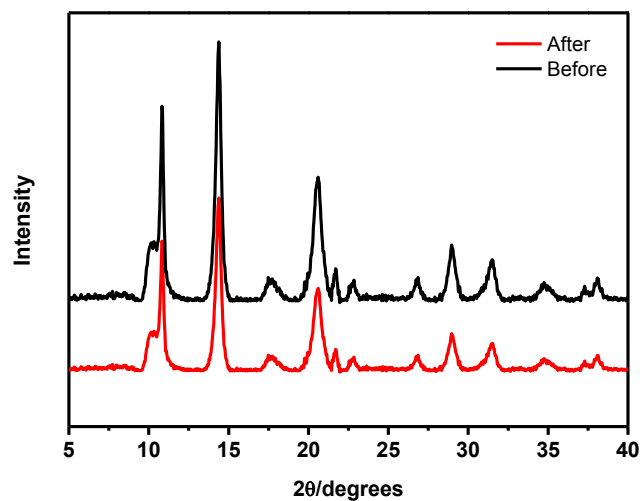


Figure 6-14. PXRD patterns of **PNPMOF** before and after catalysis.

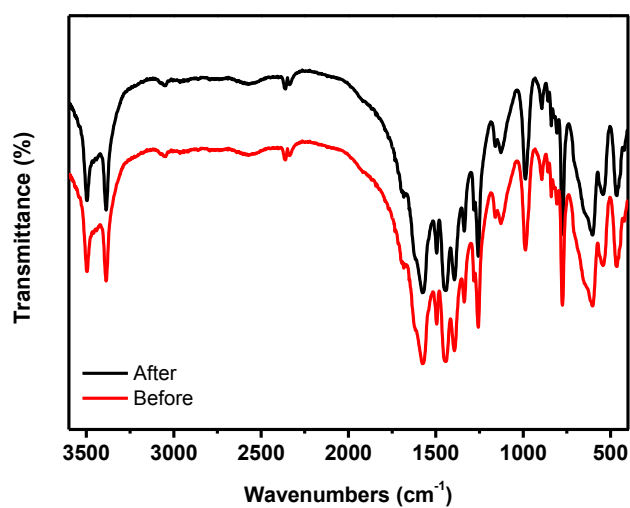


Figure 6-15. FT-IR spectra of **PNPMOF** before and after catalysis

6.4 Conclusions

In conclusion, POM-stabilized Pt NPs bind to NH₂-MIL-53 particles forming the **PNPMOF** which exhibits synergistic photocatalytic H₂ evolution activity (all 3 components alone are far less active). The surface protonated NH₂ units on the MOF particles bind the negatively-charged POM-stabilized Pt NPs, and the NH₂-MIL-53 in this work protects the light sensitive 2-aminoterephthalate groups from oxidation by the POMs as well. Significantly, the POMs exhibit four roles in the **PNPMOF**: they reduce H₂PtCl₆ to Pt NPs, stabilize Pt NPs, facilitate Pt NP association with the cationic support, and speed up catalytic H₂ evolution by promoting electron transfer between NH₂-MIL-53 and the catalytic Pt NPs. The **PNPMOF** composite is quite stable under turnover conditions. This work illustrates the prospect of other materials in which POMs exhibit more than one function including catalytic activity.

References

- (1) Wasielewski, M. R. *Acc. Chem. Res.* **2009**, *42*, 1910-1921.
- (2) Faunce, T.; Styring, S.; Wasielewski, M. R.; Brudvig, G. W.; Rutherford, A. W.; Messinger, J.; Lee, A. F.; Hill, C. L.; deGroot, H.; Fontecave, M.; MacFarlane, D. R.; Hankamer, B.; Nocera, D. G.; Tiede, D. M.; Dau, H.; Hillier, W.; Wang, L.; Amal, R. *Energy Environ. Sci.* **2013**, *6*, 1074-1076.
- (3) Nocera, D. G. *Acc. Chem. Res.* **2012**, *45*, 767-776.
- (4) Meyer, T. *Acc. Chem. Res.* **1989**, *22*, 163-170.
- (5) Gust, D.; Moore, T. A.; Moore, A. L. *Acc. Chem. Res.* **2009**, *42*, 1890-1898.

- (6) Frischmann, P. D.; Mahata, K.; Würthner, F. *Chem. Soc. Rev.* **2013**, *42*, 1847-1870.
- (7) Bard, A. J.; Fox, M. A. *Acc. Chem. Res.* **1995**, *28*, 141-145.
- (8) Concepcion, J. J.; House, R. L.; Papanikolas, J. M.; Meyer, T. J. *Proc. Natl. Acad. Sci.* **2012**, *109*, 15560-15564.
- (9) Yin, Q.; Tan, J. M.; Besson, C.; Geletii, Y. V.; Musaev, D. G.; Kuznetsov, A. E.; Luo, Z.; Hardcastle, K. I.; Hill, C. L. *Science* **2010**, *328*, 342-345.
- (10) Hu, S.; Shaner, M. R.; Beardslee, J. A.; Lichterman, M.; Brunschwig, B. S.; Lewis, N. S. *Science* **2014**, *344*, 1005-1009.
- (11) Panda, M. K.; Ladomenou, K.; Coutsolelos, A. G. *Coord. Chem. Rev.* **2012**, *256*, 2601-2627.
- (12) Li, L.-L.; Diao, E. W.-G. *Chem. Soc. Rev.* **2013**, *42*, 291-304.
- (13) Lv, H.; Geletii, Y. V.; Zhao, C.; Vickers, J. W.; Zhu, G.; Luo, Z.; Song, J.; Lian, T.; Musaev, D. G.; Hill, C. L. *Chem. Soc. Rev.* **2012**, *41*, 7572-7589.
- (14) Dolbecq, A.; Dumas, E.; Mayer, C. R.; Mialane, P. *Chem. Rev.* **2010**, *110*, 6009-6048.
- (15) Rausch, B.; Symes, M. D.; Chisholm, G.; Cronin, L. *Science* **2014**, *345*, 1326-1330.
- (16) Matt, B.; Fize, J.; Moussa, J.; Amouri, H.; Pereira, A.; Artero, V.; Izzet, G.; Proust, A. *Energy Environ. Sci.* **2013**, *6*, 1504-1508.
- (17) Lv, H.; Song, J.; Zhu, H.; Geletii, Y. V.; Bacsa, J.; Zhao, C.; Lian, T.; Musaev, D. G.; Hill, C. L. *J. Catal.* **2013**, *307*, 48-54.
- (18) Fu, H.; Qin, C.; Lu, Y.; Zhang, Z.-M.; Li, Y.-G.; Su, Z.-M.; Li, W.-L.; Wang, E.-B. *Angew. Chem. Int. Ed.* **2012**, *51*, 7985-7989.

- (19)Lv, H.; Guo, W.; Wu, K.; Chen, Z.; Bacsa, J.; Musaev, D. G.; Geletii, Y. V.; Lauinger, S. M.; Lian, T.; Hill, C. L. *J. Am. Chem. Soc.* **2014**, *136*, 14015-14018.
- (20)Geletii, Y. V.; Yin, Q.; Hou, Y.; Huang, Z.; Ma, H.; Song, J.; Besson, C.; Luo, Z.; Cao, R.; O'Halloran, K. P.; Zhu, G.; Zhao, C.; Vickers, J. W.; Ding, Y.; Mohebbi, S.; Kuznetsov, A. E.; Musaev, D. G.; Lian, T.; Hill, C. L. *Isr. J. Chem.* **2011**, *51*, 238-246.
- (21)Fateeva, A.; Chater, P. A.; Ireland, C. P.; Tahir, A. A.; Khimyak, Y. Z.; Wiper, P. V.; Darwent, J. R.; Rosseinsky, M. J. *Angew. Chem. Int. Ed.* **2012**, *51*, 7440-7444.
- (22)Fu, Y.; Sun, D.; Chen, Y.; Huang, R.; Ding, Z.; Fu, X.; Li, Z. *Angew. Chem. Int. Ed.* **2012**, *51*, 3364-3367.
- (23)Wang, J.-L.; Wang, C.; Lin, W. *ACS Catal.* **2012**, *2*, 2630-2640.
- (24)Xamena, F. X. L. i.; Corma, A.; Garcia, H. *J. Phys. Chem.* **2007**, *111*, 80-85.
- (25)Corma, A.; Garc á, H.; Llabr és i Xamena, F. X. *Chem. Rev.* **2010**, *110*, 4606-4655.
- (26)Gascon, J.; Corma, A.; Kapteijn, F.; Llabr és i Xamena, F. X. *ACS Catal.* **2013**, *4*, 361-378.
- (27)Pope, M. T.; Müller, A. *Angew. Chem.* **1991**, *103*, 56-70.
- (28)Sadakane, M.; Dickman, M. H.; Pope, M. T. *Inorg. Chem.* **2001**, *40*, 2715-2719.
- (29)Proust, A.; Thouvenot, R.; Gouzerh, P. *Chem. Commun.* **2008**, 1837-1852.
- (30)Neumann, R.; Khenkin, A. M. *Chem. Commun.* **2006**, 2529-2538.
- (31)Rhule, J. T.; Hill, C. L.; Judd, D. A.; Schinazi, R. F. *Chem. Rev.* **1998**, *98*, 327-357.
- (32)Guo, W.; Luo, Z.; Lv, H.; Hill, C. L. *ACS Catal.* **2014**, *4*, 1151-1161.

- (33) Biboum, R. N.; Njiki, C. P. N.; Zhang, G.; Kortz, U.; Mialane, P.; Dolbecq, A.; Mbomekalle, I. M.; Nadj, L.; Keita, B. *J. Mater. Chem.* **2011**, *21*, 645-650.
- (34) Miras, H. N.; Yan, J.; Long, D.-L.; Cronin, L. *Chem. Soc. Rev.* **2012**, *41*, 7403-7430.
- (35) Cronin, L.; Muller, A. *Chem. Soc. Rev.* **2012**, *41*, 7333-7334.
- (36) Miras, H. N.; Cooper, G. J. T.; Long, D.-L.; Bögge, H.; Müller, A.; Streb, C.; Cronin, L. *Science* **2010**, *327*, 72-74.
- (37) Hill, C. L. *Nature* **1999**, *401*, 436-437.
- (38) *Special Thematic Issue on Polyoxometalates*; Hill, C. L., Ed., 1998; Vol. 98, No. 1.
- (39) Hill, C. L. *Chem. Rev.* **1998**, *98*, 1-2.
- (40) Aiken, J. D., III; Finke, R. G. *J. Am. Chem. Soc.* **1999**, *121*, 8803-8810.
- (41) Oezkar, S.; Finke, R. G. *J. Am. Chem. Soc.* **2002**, *124*, 5796-5810.
- (42) Finke, R. G. In *Metal Nanoparticles*; Feldheim, D. L., Foss, C. A., Jr., Eds.; Marcel Dekker, Inc., New York, N. Y.: 2002, p 17-54.
- (43) Wang, Y.; Weinstock, I. A. *Chem. Soc. Rev.* **2012**, *41*, 7479-7496.
- (44) Mandal, S.; Selvakannan, P.; Pasricha, R.; Sastry, M. *J. Am. Chem. Soc.* **2003**, *125*, 8440-8441.
- (45) Hsu-Yao, T.; Browne, K. P.; Honesty, N.; Tong, Y. J. *Phys. Chem. Chem. Phys.* **2011**, *13*, 7433-7438.
- (46) Xing, X.; Liu, R.; Yu, X.; Zhang, G.; Cao, H.; Yao, J.; Ren, B.; Jiang, Z.; Zhao, H. *J. Mater. Chem. A* **2013**, *1*, 1488-1494.
- (47) Wang, C.; Xie, Z.; deKrafft, K. E.; Lin, W. *J. Am. Chem. Soc.* **2011**, *133*, 13445-13454.
- (48) Wang, C.; deKrafft, K. E.; Lin, W. *J. Am. Chem. Soc.* **2012**, *134*, 7211-7214.

- (49)Sun, D.; Fu, Y.; Liu, W.; Ye, L.; Wang, D.; Yang, L.; Fu, X.; Li, Z. *Chem. Eur. J.* **2013**, *19*, 14279-14285.
- (50)Zhou, T.; Du, Y.; Borgna, A.; Hong, J.; Wang, Y.; Han, J.; Zhang, W.; Xu, R. *Energy Environ. Sci.* **2013**, *6*, 3229-3234.
- (51)Nohra, B.; El Moll, H.; Rodriguez-Albelo, L. M.; Mialane, P.; Marrot, J. é; Mellot-Draznieks, C.; O’Keeffe, M.; Ngo Biboum, R.; Lemaire, J.; Keita, B.; Nadjo, L.; Dolbecq, A. *J. Am. Chem. Soc.* **2011**, *133*, 13363-13374.
- (52)Eddaoudi, M.; Kim, J.; Rosi, N.; Vodak, D.; Wachter, J.; O’Keeffe, M.; Yaghi, O. M. *Science* **2002**, *295*, 469-472.
- (53)Yaghi, O. M.; O’Keeffe, M.; Ockwig, N. W.; Chae, H. K.; Eddaoudi, M.; Kim, J. *Nature* **2003**, *423*, 705-714.
- (54)Yaghi, O. M.; Li, H.; Davis, C.; Richardson, D.; Groy, T. L. *Acc. Chem. Res.* **1998**, *31*, 474-484.
- (55)Britt, D.; Tranchemontagne, D.; Yaghi, O. M. *Proc. Natl. Acad. Sci.* **2008**, *105*, 11623-11627.
- (56)Rowsell, J. L. C.; Yaghi, O. M. *Microporous and Mesoporous Mater.* **2004**, *73*, 3-14.
- (57)Zhang, Z.-M.; Zhang, T.; Wang, C.; Lin, Z.; Long, L.-S.; Lin, W. *J. Am. Chem. Soc.* **2015**, *137*, 3197-3200.
- (58)Zhu, Q.-L.; Xu, Q. *Chem. Soc. Rev.* **2014**, *43*, 5468-5512.
- (59)Sun, C.-Y.; Liu, S.-X.; Liang, D.-D.; Shao, K.-Z.; Ren, Y.-H.; Su, Z.-M. *J. Am. Chem. Soc.* **2009**, *131*, 1883–1888.
- (60)Ma, F.-J.; Liu, S.-X.; Sun, C.-Y.; Liang, D.-D.; Ren, G.-J.; Wei, F.; Chen, Y.-G.; Su, Z.-M. *J. Am. Chem. Soc.* **2011**, *133*, 4178-4181.

- (61) Juan-Alcañiz, J.; Gascon, J.; Kapteijn, F. *J. Mater. Chem.* **2012**, *22*, 10102-10118.
- (62) Song, J.; Luo, Z.; Britt, D.; Furukawa, H.; Yaghi, O. M.; Hardcastle, K. I.; Hill, C. L. *J. Am. Chem. Soc.* **2011**, *133*, 16839-16846.
- (63) Dhakshinamoorthy, A.; Garcia, H. *Chem. Soc. Rev.* **2012**, *41*, 5262-5284.
- (64) Bromberg, L.; Hatton, T. A. *ACS Appl. Mater. Interfaces* **2011**, *3*, 4756-4764.
- (65) Bromberg, L.; Diao, Y.; Wu, H.; Speakman, S. A.; Hatton, T. A. *Chem. Mater.* **2012**, *24*, 1664-1675.
- (66) Maksimchuk, N. V.; Kovalenko, K. A.; Arzumanov, S. S.; Chesalov, Y. A.; Melgunov, M. S.; Stepanov, A. G.; Fedin, V. P.; Kholdeeva, O. A. *Inorg. Chem.* **2010**, *49*, 2920-2930.
- (67) Maksimchuk, N. V.; Kholdeeva, O. A.; Kovalenko, K. A.; Fedin, V. P. *Isr. J. Chem.* **2011**, *51*, 281-289.
- (68) Aijaz, A.; Karkamkar, A.; Choi, Y. J.; Tsumori, N.; Rönnebro, E.; Autrey, T.; Shioyama, H.; Xu, Q. *Journal of the American Chemical Society* **2012**, *134*, 13926-13929.
- (69) Bromberg, L.; Klichko, Y.; Chang, E. P.; Speakman, S.; Straut, C. M.; Wilusz, E.; Hatton, T. A. *ACS Appl. Mater. Interfaces* **2012**, *4*, 4595-4602.
- (70) Loiseau, T.; Serre, C.; Huguenard, C.; Fink, G.; Taulelle, F.; Henry, M.; Bataille, T.; Férey, G. *Chem. Eur. J.* **2004**, *10*, 1373-1382.
- (71) Palacios, E. G.; Juárez-López, G.; Monhemius, A. J. *Hydrometallurgy* **2004**, *72*, 139-148.
- (72) Kurihara, M.; Nishihara, H. *Coord. Chem. Rev.* **2002**, *226*, 125-135.
- (73) Liang, R.; Shen, L.; Jing, F.; Wu, W.; Qin, N.; Lin, R.; Wu, L. *Appl. Catal. B: Env.* **2014**, *162*, 245-251.

- (74)Zhang, K.-L.; Gao, H.-Y.; Qiao, N.; Zhou, F.; Diao, G.-W. *Inorg. Chim. Acta* **2008**, *361*, 153-160.
- (75)Han, Z.; Qiu, F.; Eisenberg, R.; Holland, P. L.; Krauss, T. D. *Science* **2012**, *338*, 1321-1324.
- (76)Hendrickson, J. B.; Cram, D. J.; Hammond, G. S. In *Organic Chemistry*; 3rd ed.; McGraw-Hill: New York, 1970; Vol. 3, p Chapter 8, pp 304-307.
- (77)Suzuki, K.; Tang, F.; Kikukawa, Y.; Yamaguchi, K.; Mizuno, N. *Angew. Chem. Int. Ed.* **2014**, *53*, 5356-5360.
- (78)Ewing, C. S.; Vesper, G.; McCarthy, J. J.; Johnson, J. K.; Lambrecht, D. S. *J. Phys. Chem. C* **2015**, *119*, 19934-19940.
- (79)Han, D.-D.; Liu, Z.-G.; Liu, J.-H.; Huang, X.-J. *RSC Adv.* **2015**, *5*, 38290-38297.
- (80)Ji, W.; Qi, W.; Tang, S.; Peng, H.; Li, S. *Nanomaterials* **2015**, *5*, 2203-2211.
- (81)Schrader, I.; Neumann, S.; Himstedt, R.; Zana, A.; Warneke, J.; Kunz, S. *Chem. Commun. (Cambridge, U. K.)* **2015**, *51*, 16221-16224.
- (82)Zhang, C.; Hwang, S. Y.; Peng, Z. *J. Mater. Chem. A* **2014**, *2*, 19778-19787.
- (83)Geletii, Y. V.; Gueletii, A.; Weinstock, I. A. *J. Mol. Catal. A: Chem.* **2007**, *262*, 59-66.
- (84)Park, H.; Choi, W. *J. Phys. Chem. B* **2003**, *107*, 3885-3890.
- (85)Pearson, A.; Jani, H.; Kalantar-zadeh, K.; Bhargava, S. K.; Bansal, V. *Langmuir* **2011**, *27*, 6661-6667.

Chapter 7.

Conclusions and Future Outlook

In summary, this dissertation has explored the structural features of several different POMs, developed POM-based catalysts for toxic compound decontamination and solar energy conversion. Specifically, POM-based catalysts have been developed for the aerobic formaldehyde oxidation, the oxidative removal of a mustard gas simulant, the hydrolytic removal of a wide range of CWAs as well as catalytic hydrogen production reactions. The versatile structures and properties of POMs make them attractive in these areas as well as in multiple others. To develop and investigate catalysts for the decontamination of toxic compounds (TICs and CWAs) and for the conversion of solar energy are of practical interest and importance, because our world is constantly changing with an urgent need for renewable energy, clean environments and peaceful living spaces. This work also illustrates the prospect of formulating POMs in multifunctional materials for practical applications including POM-based devices that absorb and purify indoor air pollutants, POM-based apparel that decontaminate CWAs and POM-based catalysts for water splitting systems. In addition, utilizing computation and simulation techniques also provide insightful information on the specific active sites for catalytic reactions as well as on the design of more efficient catalysts.